UNIVERSITÉ PARIS XI
UFR SCIENTIFIQUE D'ORSAY

THÈSE

Presentée

Pour obtenir

Le GRADE de DOCTEUR EN SCIENCES

DE L'UNIVERSITE DE PARIS XI ORSAY

Par

Bruno MARCOS

Etude des conditions initiales et de l'évolution linéaire des systèmes gravitationnels à N corps en cosmologie.

soutenue le 16 Décembre 2005 devant la commission d'examen

MM	Pierre BINETRUY	Examinateur
	Michael JOYCE	Directeur de thèse
	Dominique LEVESQUE	Examinateur
	William SASLAW	Rapporteur
	Joachim STADEL	Examinateur
	Pascal VIOT	Rapporteur

Contents

Remerciements

Premièrement, je tiens à remercier Pierre Binetruy pour avoir accepté d'être le président du jury de thèse. Je remercie aussi Pascal Viot et William Saslaw d'avoir eu la patiente de lire en détail cette thèse en tant que rapporteur et de m'avoir adressé de nombreux commentaires très pertinents. Je remercie Dominique Levesque et Joachim Stadel d'avoir accepté de faire partie de mon jury. Ce fut véritablement un plaisir de soutenir cette thèse devant un tel jury.

Je remercie profondément Michael Joyce de m'avoir offert la possibilité de travailler avec lui, et non seulement pour ses qualités scientifiques mais aussi humaines. Ce fut aussi vraiment un plaisir. Cette thèse est écrite dans un anglais à peu près convenable grâce à sa labeur éditoriale, que je ne peux que qualifier d'exceptionelle. Merci encore.

Je tiens à remercier Francesco Sylos Labini pour le dynamisme qu'il a su introduire dans le groupe et ses idées originales. Sans son influence cette thèse n'aurait sans doute jamais existée.

Je remercie aussi Andrea Gabrielli, spécialement pour tout ce qu'il m'a expliqué sur la théorie des champs de déplacements stochastiques. Sans le travail qu'il a réalisé et qu'il a mis si gentiment à ma disposition, cette thèse n'aurait pas pu voir le jour.

Je remercie une deuxième fois Dominique Levesque pour toute la patience qu'il a eu avec moi pour m'expliquer son code de Dynamique Moléculaire et de toutes ses explications sur l'OCP, qui m'on été réellement très utiles. Ce fut un plaisir pour moi d'écrire un article ensemble.

Je re-remercie aussi Pascal Viot pour son amabilité et ses explications sur les systèmes stochastiques et les simulations numériques. Je garde un très bon souvenir de l'article sur lequel nous avons collaboré ensemble.

Je remercie très vivement Thierry Baertschiger. L'effort que j'ai dû produire pour apprendre à écrire son nom n'a pu qu'être positif dans l'élaboration de ce travail. Ce fut une véritable joie de travailler avec lui mais aussi de l'avoir comme compagnon de cordée, de bar, de discussions, de «spremute» et j'en passe... Je le remercie aussi pour avoir relu avec patience une grande partie de ce travail, et corrigé les (très nombreuses) fautes d'ortographes des parties écrites en français.

Je ne saurais oublier Ruth Durrer qui m'a si gentiment accueilli deux fois au workshop "Facts and Fictions in Cosmology" dans les Alpes suisses. Je suis aussi débiteur de Norma Sanchez qui m'a donné la possibilité de travailler comme secrétaire scientifique dans les conférences qu'elle organise.

Je ne saurais oublier mes collègues du LPT, spécialement mes compagnons de bureau — Gregorio Herdoiza, Yacine Methar-Tani et Habib Aissaoui — pour les discussions sur la physique et pas que sur la physique. Je tiens a remercier Alain Barrat, Damir Beciveric, Philippe Boucaud (merci encore pour toute l'aide infor-

matique !), Martin Bucher, Jean-Michel Caillol, Christos Charmoussis, Emilian Dudas, Inyong Cho (non, je n'oublierai pas nos longues discussions...), Bernard Jancovici, Jean-Pierre Leroy, Yann Mambrini, Jihad Mourad, Renaud Parentani, Julien Serreau, Danielle Steer, Christina Timirgaziu, Emmanuel Trizac et Frederic Van-Wijlan. Et je n'oublie pas le staff administratif, qui a été toujours tellement aimable avec moi, en les personnes de Mireille Calvet, Patricia Flad, Mireille Geurts et Odile Heckenauer.

Il me faut aussi absolument remercier mes collègues étudiant (ou pas !) du LPNHE où j'ai passé le plus de temps pendant la thèse, c'est à dire (dans le désordre) : Guillaume Thérin (non, je n'oublierai jamais notre cohabitation !), Emmanuel Busato (mmm... !), Pietro Cavallieri (gracie per tutto !), Madgid Belkacem, Emmanuel Hornero (et sa passion communicative pour la programmation sur cartes graphiques), Jean-Roch Vlimant, Marc Dhellot, Richard Taillet, Julie Malcles, Gabriele Garavini, Julien Guy, Richard Randriatoamanana, Delphine Guide (ma correctrice orthographique... sauf pour la thèse, je la décharge de toute responsabilité !), Greg Sainton, Claire Juramy, Sébastien Gilles, Rui Pereira, Luz Guevara, Gian Piero Di Giovanni, Jónatan Piedra, Stephane Tourneur et Diego Terront (y las largas discusiones filosóficas...) — ces quatre dernier de l'équipe «dîner» lorsque j'écrivais cette thèse.

Je ne saurais oublier les historiques soirées passée en compagnie de Thi-Hanh N'Guyen, Jonathan Rocher, Guillaume Michel, Martino Trasinelli, Carlos Muñoz, Guillaume Thérin, Emmanuel Busato, Delphine Guide, Pietro Cavallieri, Yacine Mehtar-Tani (si, si, ils on droit a deux citation !), Marie Legendre, Sahra Guirshick, Dusko Cakara, François Limousin (et aussi nos inoubliables voyages à vélo), Perrine Royole-Degieux, Laurence Perotto, Thorsten Bruentje, Fréderic Jugeau et bien d'autres...

Je ne pourrais ne pas mentionner le club d'escalade d'Orsay, et très spécialement Mathieu Guinault, José Picheral, Nicolas Guillemet, William Herpson, Cyrille Thominiaux et Anne-Soisig Steunou.

Et je ne peux oublier Luis Marcos et Geneviève Dezeuze pour leur appui constant et sans faille...

Et je m'excuse pour tout ceux que j'ai oublié (momentanément !) en écrivant ces lignes...

Chapitre 1

Résumé en français

La compréhension précise de la formation des grandes structures dans l'univers (amas de galaxies, super-amas, etc.) est l'un des problèmes non résolus le plus important en cosmologie. Dans les modèles actuels, la matière est décrite théoriquement par un fluide continu. Son évolution sous l'action de sa propre gravité n'est pas comprise analytiquement et est donc étudiée en utilisant des simulations numériques. Pour réaliser ces simulations, le fluide est discrétisé sous forme de particules, appelées «N-corps». Dans cette thèse nous avons étudié les effets discrets introduits par l'usage de ces simulations à N-corps. C'est un sujet très important car beaucoup de prédiction théoriques — qui peuvent être comparées avec un nombre croissant d'observations précises — sont obtenues en utilisant ces simulations.

1.1 Le cadre de travail

Aujourd'hui l'univers apparaît très inhomogène, caractérisé par une collection de structures hiérarchiques de galaxies : amas de galaxies, super-amas, filaments, etc. Cependant, à partir de l'observation de la radiation du Fond Diffus Cosmologique, il s'avère que l'univers était dans le passé très homogène avec de petites fluctuations de densité. Pour expliquer cela, ainsi qu'un grand nombre d'autres observations, il est postulé que l'univers est constitué essentiellement par de la matière qui n'intéragit que faiblement (mais néamoins gravitationellement couplée), appelée *Matière Noire*. Aux échelles cosmologiques, l'interaction dominante est la gravité. Nous sommes intéressés en cosmologie à des échelles suffisamment petites pour pouvoir traiter le problème avec la mécanique Newtonienne. L'évolution du système peut être donc calculée en appliquant l'équation de Newton à un système de particules interagissant gravitationellement :

$$\frac{d^2\mathbf{r}_i}{dt^2} = -G\sum_{j\neq i}\frac{\mathbf{r}_i - \mathbf{r}_j}{|\mathbf{r}_i - \mathbf{r}_j|^3}, \tag{1.1}$$

où $\mathbf{r}_i$ est la position de la particule i. Cela donne un système de N équations différentielles couplées, où N est le nombre de particules. Dans la pratique, cependant, cette approche n'est pas réalisable en raison du nombre élevé de particules de matière noire dans l'univers : environs 10^{70} selon les estimations actuelles.

On emploie donc une approche statistique, qui sous certaines approximations justifiée conduit à l'équation de Boltzmann. Cette équation décrit l'évolution de la densité de probabilité de trouver une particule à une certaine position. Malgré cette simplification par rapport au problème de départ, il n'est toujours pas possible de résoudre l'équation de Boltzmann en général. Une approche analytique est uniquement possible avec des simplifications supplémentaires, qui mène à des équations d'un fluide. Dans ce formalisme, les variables sont la densité $\rho(\mathbf{r})$ et la vitesse $v(\mathbf{r})$ du fluide en chaque point. Il est alors possible d'écrire un développement perturbatif des équations du fluide pour le *contraste de densité* :

$$\delta\rho(\mathbf{r}) = \frac{\rho(\mathbf{r})}{\rho_0} - 1, \tag{1.2}$$

où ρ_0 est la densité moyenne de l'univers. Ce développement est valable uniquement dans la limite $\delta\rho \ll 1$. Lorsque cette condition n'est plus satisfaite, l'équation de Boltzmann doit alors être résolue numériquement. Une résolution numérique directe est problématique en raison de l'apparition de singularités à petites échelles dues au caractère attractif de la gravité. Une méthode très utilisée pour éviter ce problème consiste à *estimer* la solution de l'équation de Boltzmann en utilisant une méthode à N-corps. La distribution continue de densité est «échantillonnée» avec des particules (des N-corps) dont l'évolution est calculée avec l'équation (2.1) Il est important de remarquer, cependant, que le nombre de N-corps est beaucoup plus petit que le nombre de particules de Matière Noire. L'évolution des particules de Matière Noire noire déterminée par l'équation (2.1) et celles des N-corps (calculée avec la même équation) seront donc intrinsèquement différentes. Il est cependant clair que dans la limite telle qu'un N-corps correspond à une particule de Matière Noire, l'évolution des deux systèmes sera identique, mais dans tout autre cas elle sera différente.

1.2 Le sujet

Nous nous sommes concentré sur la différence entre l'évolution d'un système continu et celle d'une discrétisation particulière de ce même système (en utilisant des N-corps). Par système continu, nous nous référons à la Matière Noire, puisque aux échelles cosmologiques elle peut être approximée par un tel système. Dans le système à N-corps, de nouvelles échelles apparaissent qui peuvent induire des effets inexistant dans l'évolution du système continu. Par exemple, considérons un système continu parfaitement homogène, avec une densité ρ_0 constante en tout point. Une discrétisation sous forme de N-corps de masse m peut être, par exemple, un réseau simple avec une distance entre les particules $\ell = (m/\rho_0)^{1/3}$. Si le système est infini, ni le système continu ni le système discret n'évoluent sous l'effet de la gravité car la force est nulle en tout point du système. Si la distribution continue est légèrement perturbée, elle évoluera sous l'effet de la gravité, ainsi que sa discrétisation. Il est clair qu'à petite échelle (c'est a dire à des échelles de l'ordre de la distance entre les particules ℓ), ils évolueront d'une façon très différente. D'autre part, pour des échelles beaucoup plus grande que la distance entre les particules ℓ, nous nous attendons que dans ce régime (et nous avons effectivement vérifié que c'est le cas) les effets discrets sont négligeables.

1.3 Résultats connus et originalité de la thèse

La littérature existante traitant de la formation de structures en cosmologie suit deux directions : l'étude de solutions analytiques des équations du fluide (valables dans le régime linéaire et quasi-linéaire) et l'estimation de la solution de l'équation de Boltzmann en utilisant des simulations à N-corps dans le régime hautement non linéaire. La méthode des N-corps peux être vérifiée en faisant des simulations avec un nombre diffèrent de particules. Cependant, cette procédure ne peux donner une mesure quantitative des effets discrets : il est possible de considerer seulement un intervalle limité du nombre N. D'autre part, les simulations à N-corps peuvent être aussi comparées avec des solutions analytiques dans le régime linéaire. Cependant, en utilisant cette procédure, il est difficile de faire la différence entre les effets discrets et les effets non linéaires, qui sont présents dans la simulations à N-corps et non dans la théorie linéaire. En résumé, les résultats actuels traitant de la formations des structures sont essentiellement obtenus, soit en utilisant une théorie perturbative valable dans ce régime, soit en utilisant des simulations à N-corps avec des techniques numériques très élaborées. Cependant, un lien complet et rigoureux entre ces deux approches n'existe pas.

L'originalité de cette thèse réside dans le fait que nous avons commencé un programme d'analyse détaillé et quantitative des effets discrets dans les simulations à N corps. Jusqu'à maintenant, comme nous venons de l'expliquer, les simulations à N corps étaient validée, soit en comparant différentes simulations (essentiellement en changeant le nombre de particules) soit en les comparant avec une solution perturbative des équations du fluide. La principale innovation de ce travail est de comparer les deux approches d'une façon essentiellement analytique. Cette méthode permet de différencier exactement les effets discrets des effets non linéaire dans une approche perturbative.

Nous avons étudié dans un premier temps les conditions initiales des simulations à N-corps en cosmologie, en nous concentrant sur les différences entre les corrélations à deux points du système à N-corps et celles de la distribution continue qu'elle modélise. Des études antérieures sur ce sujet avaient calculé numériquement les corrélations à deux points dans le système à N corps et les avaient comparé avec celles du système continu. Notre approche est qualitativement différente, car nous calculons les corrélations directement dans la moyenne d'ensemble. Nous calculons certaines intégrales numériquement pour obtenir le résultat final, mais notre approche est essentiellement analytique et nos résultats «exacts». Cela est particulièrement important pour les fonctions de corrélations dans l'espace réel, où le rapport signal sur bruit est généralement très faible à grande échelles.

Évidemment, le calcul des effets discrets dans les conditions initiales ne permet pas de déterminer leur propagation pendant l'évolution (même si cette étude peux donner une idée générale de la situation). Dans l'état actuel des connaissances de la résolution des équations d'un fluide autogravitant, il est uniquement possible, comme nous l'avons expliqué plus haut, de les résoudre perturbativement. Au lieu de comparer des simulations numériques à N-corps avec cette théorie perturbative, nous avons développé une théorie perturbative pour le système discret à N-corps, analogue à celle du fluide. Cela est très utile pour deux raisons : nous pouvons comparer des quantités équivalentes et nous obtenons une solution «exacte» du problème à N-corps pour faire des com-

paraisons précises. Évidemment, notre approche du problème à N-corps peux être aussi utilisé pour étudier un ensemble de particules soumis à l'interaction gravitationnelle, sans connexion avec une théorie du fluide.

1.4 Résumé des résultats

Ci-dessous nous donnons un bref résumé des principaux résultats de la thèse :

1. Lorsque nous étudions les effets discrets il est instructif de le faire autant en espace réel qu'en espace de Fourier. Même s'ils contiennent en principe la même information (il est possible de passer d'une description à une autre par une transformation mathématique), ils soulignent des propriétés différentes du système discret comparé avec celle du système continu. L'accord entre le système continu et le système discret peut être très bon dans un espace sur une grande gamme d'échelle mais très mauvais dans l'autre à toute les échelles. Cela est dû essentiellement à ce que les transformées de Fourier ne sont pas locales. Une différence localisée dans un espace peut être complètement délocalisée dans l'autre.
2. La méthode standard utilisée pour générer les conditions initiales donne un excellent accord pour les corrélations en espace de Fourier entre le système discret et la distribution continue jusqu'à la fréquence de Nyquist. Cependant, dans certain cas, les corrélations dans l'espace réel du système discret peuvent être dominées à toutes les échelles par les effets discrets «délocalisés» venant d'échelles au dessus de la fréquence de Nyquist en espace de Fourier.
3. Nous avons développé une nouvelles méthode pour générer les conditions initiales. Elle distribue mieux les effets discrets entre l'espace réel et l'espace de Fourier. Elle a aussi l'avantagede propduire des configurations statistiquement isotropes et homogènes.
4. A partir de notre étude de l'évolution linéaire d'un système à N-corps nous pouvons conclure que :
   - La limite du fluide auto-gravitant est effectivement obtenue a des échelles plus grandes que la distance moyenne entre les particules.
   - Les petites échelles sont fortement affectées par les effets discrets. Ils se manifestent, par exemple, par un ralentissent de l'évolution et par de l'anisotropie.
   - Les effets discrets augmentent avec le temps. Ils peuvent même être arbitrairement grands si la simulations commence à des décalages vers le rouge arbitrairement petits. Il s'ensuit que le décalage vers le rouge de départ de la simulation est un paramètre essentiel, non considérée à ce jour, dans la caractérisation des effets discrets.
   - La réseau simple cubique généralement employé pour générer les conditions initiales présente des modes oscillatoires induit par la discrétisation. Un réseau bcc ne présente pas ces modes et est peux être une meilleure alternative pour générer les conditions initiales.

Chapter 2

Introduction

The accurate understanding of the origin of large scale structure in the universe (cluster of galaxies, superclusters, etc.) is one of the major unsolved questions in cosmology. In current models, at the scales of relevance, the matter is well described theoretically as a continuous fluid. The computation of its evolution under the action of gravity is not understood analytically and is done using very large numerical simulations. To perform such simulations, the fluid is discretized in particles ("N-bodies"). The focus of the work of this thesis is on the discretization effects introduced in these N-body simulations. This is a very important subject because very many theoretical predictions – to be compared with the rich and growing number of observations in cosmology – are obtained using such simulations.

2.1 The framework

Today the universe appears to be very inhomogeneous, characterized by a collection of hierarchical structures of galaxies: cluster of galaxies, superclusters, voids, filaments, etc. (see Fig. 2.1 on page 14). However, it is inferred from observations of the Cosmic Microwave Background (CMB) radiation that the universe was in the past very homogeneous with tiny density fluctuations. To explain these and many other observations, it is postulated that the matter in the universe is constituted mainly by a kind of very weakly interacting matter (but gravitationally coupled, see chapter 4), called *Dark Matter*. It is not well understood how the primordial homogeneous distribution of dark matter – combined with the small portion of visible matter – evolves under the action of gravity to form the current observed structures. If we knew precisely this evolution, it would be possible, for example, from the visible matter in galaxies, to infer much about the nature of the dark matter, which is one of the major problems in cosmology (see e.g. [DMS05]).

It is in principle relatively easy to compute the evolution of the dark matter. At cosmological scales, the relevant interaction in this system is gravity and we are interested in sufficiently small scales to apply Newtonian physics, which simplify greatly the treatment of the problem. Therefore, the evolution of this system can be computed applying Newton's equation to a system of particles in

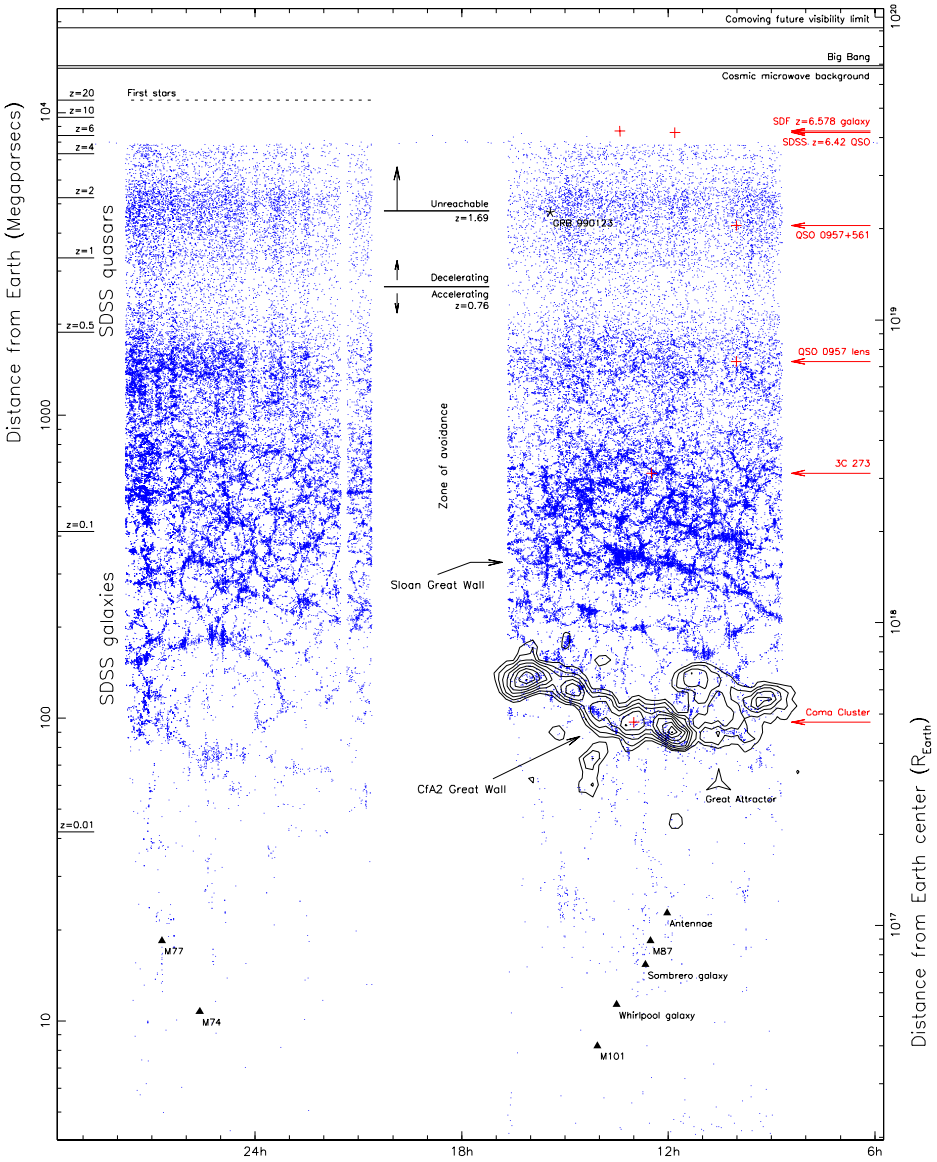

Figure 2.1: Map the the large scale structure of the universe made with the largest survey in date, SDSS.

gravitational interaction[1]:

$$\frac{d^2\mathbf{r}_i}{dt^2} = G\sum_{j\neq i}\frac{\mathbf{r}_i - \mathbf{r}_j}{|\mathbf{r}_i - \mathbf{r}_j|^3}, \tag{2.1}$$

where $\mathbf{r}_i$ is the position of the particle i. This gives N vectorial coupled differential equations, where N is the number of particles. In practice, this approach is completely unworkable because of the huge number of Dark Matter particles in the universe: around 10^{70}, for a typical Dark Matter particle candidate.

Therefore a statistical approach is employed. Instead of considering the *deterministic* position of each particle, we consider the *probability* to have each particle at some location. Despite the conceptual difference between the two approaches, the complexity of the equations is the same. The great advantage of the statistical method is that we can simplify the problem if we reduce the amount of information we want to know about the system. For example, we may be interested only in the probability $f_1(\mathbf{r}_1)$ to have a particle (any particle) at the position $\mathbf{r}_1$, or the joint probability $f_2(\mathbf{r}_1, \mathbf{r}_2)$ to have any particle at position $\mathbf{r}_1$ and at position $\mathbf{r}_2$ simultaneously, etc. Clearly using this procedure we loose information but, in most cases, it will be sufficient for our purposes. We will see (chapter 5) that for sufficiently large scales, in the cosmological context, it is possible to write an equation that is a very good approximation involving only the probability density f_1. The equation obtained is called the collision-less Boltzmann equation because it describes particles that do not suffer collisions, large regions mutually interacting as in a fluid. Solving this equation we would obtain the probability, as a function of time, to have a particle at some position (disregarding the position of all the other particles).

Despite the huge simplification involved in the Boltzmann equation, it is not possible either to solve it analytically in general. An analytic approach becomes feasible only with the further simplification of a truncation procedure, leading to a set of fluid equations. In this formalism the relevant variables are the matter density $\rho(\mathbf{r})$ and velocity $\mathbf{v}(\mathbf{r})$ of the fluid at each point. It is possible to write a perturbative expansion of the fluid equations in the *density contrast*

$$\delta\rho(\mathbf{r}) = \frac{\rho(\mathbf{r})}{\rho_0} - 1, \tag{2.2}$$

where ρ_0 is the average density of the universe. It is possible to find then a perturbative solution of the fluid equations, valid for $\delta\rho \ll 1$. When the density contrast starts to be larger than unity this treatment breaks down[2]. A numerical resolution of the Boltzmann equation has to be employed. A direct numerical resolution is problematic because of the apparition of singularities at sub-resolution scale: it is necessary to discretize the space with a finer and finer grid as times evolves. A very common method to avoid this problem is to estimate[3] the solution of the Boltzmann equation using a N-body method. The

[1] This simplified equation should be trivially modified to take into account the expansion of the universe, see chapter 4.

[2] This is Eulerian perturbation theory. In Lagrangian perturbation theory the expansion is in different variables and the regime of validity is slightly extended compared to Eulerian theory (see chapter 5).

[3] We will see in chapter 5 that actually N-body methods are not a rigorous approximation scheme to solve Boltzmann equation.

continuous density distribution is sampled by "tracer" particles (N-bodies) and their evolution computed by pure gravity, i.e. Eq. (2.1). Note however, that the number of N-bodies is much smaller than the number of Dark Matter particles. Therefore the evolution of the Dark Matter particles through Eq. (2.1) and the evolution of the N-bodies (through the same equation) will be intrinsically different. Of course, in the limit in which an N-body corresponds to a Dark Matter particle the two systems will be the same, but otherwise the evolution will be different.

2.2 The subject

We have focused our work on the difference between the evolution of a continuous system and a particular (N-body) discretization of it. By continuous system, we mean the Dark Matter one because, at the scales we are interested, it can be considered as such. In the N-body system new physical scales are introduced which can modify strongly, at some scales and in some regimes, the evolution. For example, consider a perfectly homogeneous continuous distribution with density ρ_0. A discretization of it with N-bodies of mass m can be, for example, a simple lattice with interparticle distance $\ell = (m/\rho_0)^{1/3}$. Clearly neither the continuous or discrete distribution evolve under gravity because the force is zero everywhere. If the continuous distribution is slightly perturbed, it will evolve under the effect of gravity as well as its discretization. But it is clear that at small scales (i.e. of order of the interparticle distance scale ℓ) they will do so in a very different way. On the other hand, for scales much larger than ℓ, we expect that in this regime (and we will see that it is the case) the discreteness effects are irrelevant.

The problem can be illustrated using the following analogy. Consider a set of N identical particles connected by an harmonic oscillator with coupling constant K (see Fig. 2.2). Numbering by n the particles in the linear chain, the position of a particle with label n is

$$x = na + u(na), \tag{2.3}$$

where na is the equilibrium position of the n-th particle and $u(na)$ its displacement from this position. Therefore the equation of motion for the n particle is:

$$m\ddot{u}(na) = -K\left[2u(na) - u([n-1]a) - u([n+1]a)\right], \tag{2.4}$$

where the double dots indicate a double derivative with respect to time. A solution of the Eq. (2.4) is (see e.g. [AM76])

$$u(na,t) \propto cos(kna - \omega t) \tag{2.5}$$

with

$$k = \frac{2\pi}{a}\frac{n}{N}, \quad n \text{ integer} \qquad \omega(k) = 2\sqrt{\frac{K}{m}}\left|\sin\frac{1}{2}ka\right|. \tag{2.6}$$

We can take the continuous limit of this system by sending $a \to 0$, $m \to 0$ keeping Km/a^2 fixed. In this limit Eq. (2.4) becomes

$$\ddot{u}(na) = K\frac{a^2}{m}u''(na), \tag{2.7}$$

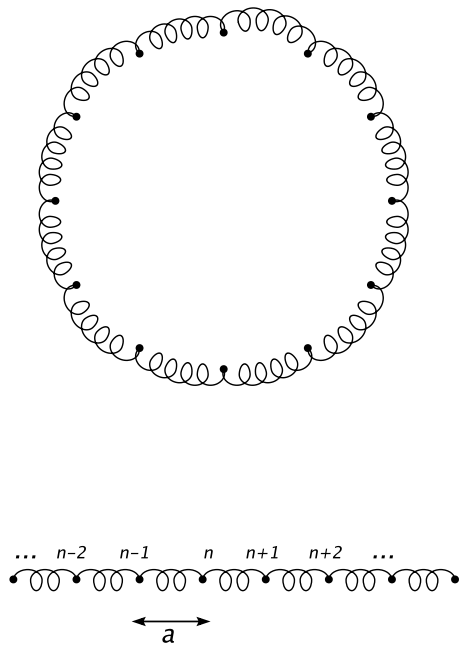

Figure 2.2: Up: linear chain with periodic (Born-von Karman) periodic boundary conditions and down the numbering convention.

where $''$ indicates double derivative with respect to position. Eq. (2.7) is a wave equation the solution of which is also given by the Eq. (2.5) but with dispersion relation

$$\omega(k) = a\sqrt{\frac{K}{m}}|k|. \tag{2.8}$$

With an N-body method we would model the latter continuous system with the former discrete one. In Fig. 2.3 we see how, as expected, the dispersion relation coincides in both cases for large scales (small k) compared with the scale ℓ introduced in the discretization, but not for smaller scales. The problem we address in the context of structure formation is far more complicated but the essential ideas are illustrated in this example. The most important difference is the fact that gravitational clustering is a highly unstable process. At large times, even if the initial distribution is homogenous (and therefore with a clearly defined discreteness scale given by the average interparticle distance), there are clusters and voids over a large range of scales. Then it is not clear which is the discreteness scale (and indeed whether this scale is unique). It is also highly non-linear and coupling between scales can introduce more complicated discreteness effects. And this list is far from being exhaustive... This thesis is centered on the study of the initial conditions and the early time evolution (i.e. when perturbative theory applies) of N-body systems and its similarities –and differences– with the corresponding continuous system. This has to be considered as a first step, before studying the discreteness effects in the non-linear regime in future work.

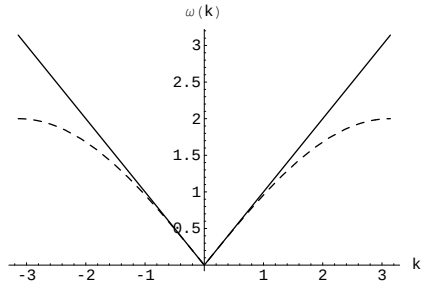

Figure 2.3: Dispersion relation for the continuous model (full line) and its discretization (dashed lines). We have taken $a = 1$, $K = 1$ and $m = 1$.

2.3 Previous well-known results and originality of this work

The literature on structure formation is mainly focused in two directions: the study of analytical solutions of the fluid equations (and therefore in the linear or quasi-linear regime) and the estimation of the solution of the Boltzmann equation using N-body simulations in the highly non-linear regime. The N-body scheme as a discretization of a continuous model can be checked by performing simulations with differing numbers of particles. This procedure cannot give a quantitative measurement of the discreteness effects: it is possible to explore only a very limited range of N, and one relies on qualitative judgments about what constitutes an agreement. As observational data becomes more and more precise, the theoretical models have to be also more and more accurate. On the other hand, the N-body discretization can be also checked by comparing the result of a simulation with analytical solutions in the linear regime. However, using this procedure, it is very difficult to differentiate, for example, the effects that come from discretization and non-linear effects, which are of course present in the N-body simulation and not in the linear fluid theory. In summary, the results in structure formation are essentially derived, on one hand from linear and perturbative (at the lowest orders) fluid theory and, on the other hand, from N-body simulations using very elaborate techniques. However, a full and rigorous link between these two approaches, and more specifically a quantification of the discreteness effects introduced by the N-body simulations is still lacking.

The originality of this thesis is to start a program of detailed and quantitative study of the discreteness effects in cosmological N-body simulations. Up to now, as explained above, the N-body simulations were validated either in checking different numerical simulations against one another or with a perturbative solution of the fluid equations. The main innovation of this work is to compare both approaches in an essentially analytical way. This allows one to differentiate, for example, the discreteness effects from the non-linear effects in a perturbative approach.

We have studied first of all the initial conditions for cosmological N-body simulations focusing on the differences between the two-point correlation properties of the N-body system and the continuous distribution it modelizes. As

mentioned above, previous studies about this subject computed numerically the correlations in the N-body system and compared them with those of the continuous one. Our approach is qualitatively different, as one computes the correlation properties directly in the ensemble average. We compute certain integrals numerically to obtain the final results but our approach is essentially analytic and our results "exact". This is especially important for the correlation function in real space where for typical available computer power, the ratio of signal to noise can be very low.

Of course the determination of the discreteness effects in the initial conditions does not allows one to conclude about their propagation during the evolution (even if it can give some insights about this question). In the current state-of-the-art of the resolution of the fluid system, we know only, as explained above, how to solve analytically in a perturbative approach. Instead of comparing numerical simulations with this perturbative theory, we have developed an exactly analogous perturbative theory of the discrete N-body problem. This is very useful for two reasons: it allows one to compare equivalent quantities and to have an "exact" solution of the N-body problem in this regime to make precise comparisons. Evidently, our treatment of the N-body problem can also be used when studying a set of particles in gravitational interaction, without any necessary connexion with a fluid theory.

2.4 Overview of the results

We give a brief summary of the most important results of our study:

1. When studying the effects of discreteness it is instructive to do so in both real and Fourier space. Even if they carry in principle the same information (it is possible to pass from one to the other description by a mathematical transformation) they highlight different properties of the discrete system compared to the continuous one. The agreement between the continuous system and its discretization can be very good in a wide range of scales in one space but very poor at all scales in the other one. This is essentially because the Fourier transform is a non-local transformation. A disagreement that was localized in one space may be completely delocalized in the other one.

2. The standard used method to set up initial conditions in N-body simulations gives an excellent agreement in correlations in Fourier space between the N-body and continuous distribution up to the "Nyquist" frequency. However, in certain cases, the real space correlation properties of the N-body system can be dominated at all scales by discreteness "delocalized" from scales above the Nyquist frequency in Fourier space.

3. We have developed a new method to set up initial conditions. It has the feature that it distributes more equally between real and Fourier space the effects of discreteness. It also has the advantage that the configurations are statistically isotropic.

4. From our study of the early time evolution of an N-body system we can conclude that:

- The limit of a self-gravitating fluid is indeed recovered at scales much larger than the average interparticle distance.
- Small scales are strongly affected by discreteness effects. They manifest themselves particularly by a slowing down of the evolution and anisotropic effects.
- The discreteness effects increase as a function of time. Indeed they can be arbitrarily large if the simulation is started at arbitrarily early times. Therefore the starting time of a simulation is an essential parameter, unconsidered until now, in the characterization of discreteness effects.
- The simple cubic lattice usually used to set up initial conditions in cosmological simulations has spurious oscillating modes. A bcc lattice does not present such behavior and may be a better alternative solution to set up initial conditions.

2.5 Organization of the thesis

The thesis is divided into two parts: the first one is devoted to giving the background necessary to develop the results that are presented in the second one. The first part can seem quite long to some readers but it has to be taken into account the interdisciplinarity of this thesis and the variety of methods used in the work. The manuscript is addressed to the two communities, whose methods and problems are relevant, the cosmological and the statistical physics one. I've attempted to be sufficiently pedagogical and self-contained in order that a researcher of one field should be able to follow presentation of the subject matter of the other field.

The first chapter treats the formalism, from statistical physics, of stochastic fields applied to cosmology. In it are defined the quantities necessary to treat statistically a continuous or discrete distribution, and specifically density distributions. Basic concepts such as correlation function, power spectrum, variance of the mass are introduced and they are used to distinguish different kind of distributions. We will see that the large scale structure in the universe, as described in current models, and the distribution of ions in a plasma present great similarities. We will study then the effect of applying a stochastic displacement field (with some specific statistical properties) to a given distribution, discrete or continuous. This is important because the canonical method to generate initial conditions for N-body simulations (i.e. to create a N-body distribution with "almost" the same statistical properties as a continuous one) uses a procedure of this kind.

The second chapter is devoted to the "minimal basics" of the problem of structure formation in cosmology. It starts as much as possible from first principles in an attempt to be comprehensible to a condensed matter physicist. The next chapter treats kinetic and fluid theory in different contexts, such as the ideal gas, Coulombian plasmas and also cosmology. We use the study of these different systems to understand better the different approximations that can be made to solve the kinetic equations in different contexts. This is particularly useful to study different systems because the approximations that can be used in the gravitational case are still very unclear. The Boltzmann equation and the

BBGKY hierarchy are derived from first principles. We present also the little used in cosmology, but powerful, Klimontovich formalism borrowed from plasma physics. Then we discuss the different approximations that lead to fluid equations (easier to solve analytically) and again the approximations and methods to solve them in different contexts and specially in the cosmological one. Finally, in the fourth chapter of this introductory part, we present the fundamentals of the physics of Coulombian plasma systems. To describe them quantitatively we derive the perturbative cluster expansion and present the principle results in the literature. We will use this to develop in the second part an alternative method to generate initial condition for the N-body simulations. In addition, it is very interesting to study more advanced methods to describe a Coulombian plasma to try to apply them in the future (as other authors have done) for gravity.

In the second part are contained the results of our work. First of all in chapter 7, we present our results on the quantification of discreteness effects in the initial conditions of cosmological N-body simulations, generated with the standard method which uses a stochastically perturbed lattice[4]. Chapter 8 reports our work on the development of an alternative method to generate initial condition for N-body simulations.[5] In chapter 9 we study the early time evolution of a gravitational N-body system and we compare it with the evolution of a self-gravitating fluid to extract discreteness effects[6]. Finally, in a short conclusion we review our work and give some perspectives. Some appendixes at the end explain some concrete physical and mathematical methods.

[4]This chapter is based on [JM04].

[5]Based on [JLM05].

[6]This is an extended treatment of results published in a recent letter [JMG+05], which is included in appendix I.

Part I

Background

Chapter 3

Stochastic density fields

Density fields[1] in cosmology are usually treated as a mean background positive density with small positive and negative stochastic fluctuations. In this chapter we will introduce the concept of stochastic distribution and the most important quantities that characterize them. We will see that a classification of this processes can be related with the kind of physical process that can produce such distribution. For example, particles interacting through a short range distribution in a gas at high temperature produce an (almost) uncorrelated Poisson distribution. On the other hand, if the interaction is long ranged, it may result a much more "uniform" distribution with spatial fluctuations more rapidly decaying with scale. We will also study the general difference between continuous and discrete density fields. This is an important point, because when studying gravitational clustering, continuous distributions are usually modelized by discrete ones. It is the case of "N-body" cosmological simulations, described in section 5.7. It is the starting point in the study of discreteness discreteness effects inherent to such method, to which a large part of this thesis is devoted. We will also study the effect of a displacement field applied to a "uniform" (i.e. with weak statistical fluctuations) point distribution. We will see how it is possible, using this method, to generate a particle distribution with approximatively the same correlations than a continuous theoretical model. This is the standard method to generate initial condition for "N-body simulation".

3.1 Stochastic distributions

Let us consider a discrete random mass distribution represented by the microscopic density function $\rho(\mathbf{r})$. The quantity $\rho(\mathbf{r})dV$ represents the number of particles contained in the infinitesimal volume dV around the point $\mathbf{r}$. Assuming that the particles have unitary mass we can write

$$\rho(\mathbf{r}) = \sum_i \delta(\mathbf{r} - \mathbf{r}_i), \tag{3.1}$$

where $\mathbf{r}_i$ is the position vector of the particle i of the distribution and $\delta(\mathbf{r})$ is the Dirac delta function. The function $\rho(\mathbf{r})$ can be thought as a realization of a

[1] Also e.g. velocity fields.

stochastic process. It means that to any point $\mathbf{r}$ is associated a positive random variable $\hat{\rho}(\mathbf{r})$ whose "extracted" value is $\rho(\mathbf{r})$. The stochastic process is totally characterized by the *probability density functional* $\mathcal{P}[\rho(\mathbf{r})]$ of the density field $\rho(\mathbf{r})$, that gives the probability to have the particular realization $\rho(\mathbf{r})$ of the stochastic field $\hat{\rho}(\mathbf{r}, t)$. We will limit our analysis to *ordinary* or *regular* point processes, in which taking a small volume ΔV in an arbitrary point of the space, the probability to have more than one point in this volume is of higher order of ΔV.

We can compute the average value[2] of any function of the density $F[\rho(\mathbf{r})]$ in function of the probability density functional:

$$\langle F \rangle = \int \mathcal{D}\rho(\mathbf{r}) F[\rho(\mathbf{r})] \mathcal{P}[\rho(\mathbf{r})], \tag{3.2}$$

where we have used a functional integral (see in App. B).

We can smooth a discrete distribution to obtain a continuous one $\overline{\rho}$ by averaging over small volumes $\Delta V(\mathbf{r}_i)$ (centered around the position $\mathbf{r}$) but containing a large amount of particles:

$$\overline{\rho}(\mathbf{r}, t) = \frac{1}{\Delta V(\mathbf{r})} \int_{\Delta V(\mathbf{r}')} d^3 r \rho(\mathbf{r}', t). \tag{3.3}$$

Note that the density for discrete distributions (3.1) is a sum of distributions (and then non-smooth analytic functions) whereas the averaged density function defined in (3.3) is a smooth function.

In the probability density functional $\mathcal{P}[\rho(\mathbf{r})]$ all the information about the stochastic field is contained. In general, this information is much more than what one wants (and can) manipulate. For this reason, one focuses on the l-point correlation functions of the stochastic field defined as

$$\langle \hat{\rho}(\mathbf{r}_1) \hat{\rho}(\mathbf{r}_2) ... \hat{\rho}(\mathbf{r}_l) \rangle = \int \mathcal{D}\rho(\mathbf{r}) \mathcal{P}[\rho(\mathbf{r})] \hat{\rho}(\mathbf{r}_1) \hat{\rho}(\mathbf{r}_2) ... \hat{\rho}(\mathbf{r}_l). \tag{3.4}$$

The quantity (3.4), multiplied by $[dV]^l$, gives the *a priori* probability of finding simultaneously l particles, in a volume dV about the positions $r_1, ..., r_l$, independently of the position of the remaining particles. For example, the 1-point correlation function is simply the local density function $\langle \rho(\mathbf{r}) \rangle$.

3.1.1 Statistically homogeneous and isotropic distributions

A stochastic process is *statistically homogeneous* when the probability density functional $\mathcal{P}[\rho(\mathbf{r})]$ is invariant under spatial translations. The consequence is that the complete l-point correlation function has the property:

$$\langle \hat{\rho}(\mathbf{r}_1) \hat{\rho}(\mathbf{r}_2) ... \hat{\rho}(\mathbf{r}_l) \rangle = \langle \hat{\rho}(\mathbf{r}_1 + \mathbf{r}_0) \hat{\rho}(\mathbf{r}_2 + \mathbf{r}_0) ... \hat{\rho}(\mathbf{r}_l + \mathbf{r}_0) \rangle . \tag{3.5}$$

It therefore does not depend on l vector variables anymore but only on $l-1$ vector variables. For example, the large scale structure of the universe is assumed to be described by a stochastic density field which is statistically homogeneous, i.e. it is assumed that there is no privileged positions in the universe (this is

[2] We discuss the relation between the average of (a function of) a stochastic field and the notion of measurement in section 5.2.

the *Cosmological Principle*, see chapter 4). All the other statistical mechanical systems that we are going to consider in this thesis are also generically statistically homogeneous when no external fields are applied on them. This is the case of gases, plasmas, solids, etc.

A stochastic system is statistically isotropic if the probability density functional is invariant under rotations, in the sense that

$$\mathcal{P}[\rho(\mathbf{r})] = \mathcal{P}[\rho(\hat{R}\mathbf{r})], \tag{3.6}$$

where $\hat{R}$ is any rotation. In the case of the universe, the Cosmological Principle assumes *statistical isotropy* (more details in chapter 4). Statistical isotropy is a quite general feature of systems that are not in a solid state (i.e. that have not crystallized in some definitive configuration, as the system we will treat in chapter 9).

The working hypothesis of the current cosmological models are therefore to assume statistically homogeneity and isotropy. In this case, the 1-point correlation function does not depend on the position:

$$\langle \hat{\rho}(\mathbf{r}) \rangle = \rho_0. \tag{3.7}$$

We will also suppose, when the average is performed in an infinite volume, that $\rho_0 > 0$, what is called *homogeneity* or *uniformity*[3]. It is distinct from the concept of statistical homogeneity or translational invariance discussed above. *Homogeneity* or *uniformity* means that if a local average density is performed in a *finite* volume, the result does not depend on the volume. Current observations indicate homogeneity on large scales in cosmology (see chapter 4). Using this hypothesis, we define the 2-point *reduced* correlation function as

$$C_2(r_{12}) = \langle (\hat{\rho}(\mathbf{r}_1) - \rho_0)(\hat{\rho}(\mathbf{r}_2) - \rho_0) \rangle \tag{3.8}$$

where $r_{12} = |\mathbf{r}_1 - \mathbf{r}_2|$. The *complete* 2-point correlation function can be written as a function of the *reduced* 2-point correlation function as:

$$\langle \hat{\rho}(\mathbf{r}_1)\hat{\rho}(\mathbf{r}_2) \rangle = \rho_0^2 + C_2(r_{12}). \tag{3.9}$$

A continuous[4] distribution is called *uncorrelated* when the probability to find two particles at distance r_{12} factorizes, i.e.

$$\langle \hat{\rho}(\mathbf{r}_1)\hat{\rho}(\mathbf{r}_2) \rangle = \langle \hat{\rho}(\mathbf{r}_1) \rangle \langle \hat{\rho}(\mathbf{r}_2) \rangle \tag{3.10}$$

The reduced correlation function C_{12} (also called *covariance* function) gives the non-trivial part of this probability. It is usual to normalize the correlation function for density field as

$$\xi(r_{12}) = \frac{C_2(r_{12})}{\rho_0^2}. \tag{3.11}$$

[3] If the average density is $\rho = 0$ (in an infinite volume), the distribution is fractal (see e.g. [GSLJP05] for further discussion about non-homogeneous distributions).

[4] This is not true in the case of discrete distribution where a divergence always appear in $C_2(r_{12})$, even if the distribution is uncorrelated. See section 3.1.4.

3.1.2 The Power Spectrum

In Cosmology and Statistical Physics it is very usual to characterize distribution in Fourier space rather than in real space. In Cosmology a particular emphasis is placed on this representation because it is mathematically much easier to modelize theoretically the evolution of structures in Fourier space[5]. We define the Fourier transform (hereafter FT) of a function $f(\mathbf{r})$, in a cubic volume of size L ($V = L^d$), where d is the spatial dimensions as:

$$\tilde{f}(\mathbf{k}) = \int_V d^d\mathbf{r} f(\mathbf{r}) e^{-i\mathbf{k}\cdot\mathbf{r}}. \tag{3.12}$$

The inverse transform is therefore

$$f(\mathbf{r}) = \frac{1}{V}\sum_{\mathbf{k}} \tilde{f}(\mathbf{k}) e^{-i\mathbf{k}\cdot\mathbf{r}}, \tag{3.13}$$

where the sum over the discrete $\mathbf{k}$ is restricted to those with components $k_i = 2m\pi/L$ with $m \in \mathbb{Z}$. In the limit of infinite d-dimensional Euclidean space the direct and inverse FT are defined as:

$$\tilde{f}(\mathbf{k}) = FT[f(\mathbf{r})] = \int_{\mathbb{R}^d} d^d r f(\mathbf{r}) e^{-i\mathbf{k}\cdot\mathbf{r}} \tag{3.14a}$$

$$f(\mathbf{r}) = FT^{-1}[\tilde{f}(\mathbf{k})] = \frac{1}{(2\pi)^d}\int_{\mathbb{R}^d} d^d k f(\mathbf{k}) e^{-i\mathbf{k}\cdot\mathbf{r}}, \tag{3.14b}$$

From now on, for simplicity, we will denote by $\rho(\mathbf{r})$ both the stochastic density field $\hat{\rho}(\mathbf{r})$ and any realization of it. We define the fluctuation of the density field $\delta_\rho(\mathbf{r})$ as

$$\delta_\rho(\mathbf{r}) = \rho(\mathbf{r}) - \rho_0. \tag{3.15}$$

Its Fourier transform in a volume V is

$$\delta_\rho(\mathbf{k}; V) = \int_V d^d r \delta_\rho(\mathbf{r}) e^{-i\mathbf{k}\cdot\mathbf{r}}. \tag{3.16}$$

Because $\delta_\rho(\mathbf{r})$ is real, $\delta_\rho(\mathbf{k}; V) = \delta_\rho^*(-\mathbf{k}; V)$, where "$*$" denotes "complex conjugate". We define the *structure factor* (SF)[6] as

$$S(\mathbf{k}) = \frac{\left\langle |\delta_\rho(\mathbf{k}; V)|^2 \right\rangle}{V}. \tag{3.17}$$

It is obviously a positive-definite quantity. In the thermodynamic limit, one takes $V \to \infty$ (with constant ρ_0). The brackets $\langle\cdot\rangle$ in Eq. (3.17) indicate an average over realizations. In Cosmology the SF is called Power Spectrum (PS) and it is defined as the infinite volume limit of the SF:

$$P(\mathbf{k}) = \lim_{V\to\infty} \frac{\left\langle |\delta_\rho(\mathbf{k}; V)|^2 \right\rangle}{V}. \tag{3.18}$$

[5] We will see in chapter 4 that the perturbative treatment of the evolution of a self-gravitating systems involves linear differential equations, the solution of which is much simpler in Fourier space.

[6] In Statistical Physics $S(\mathbf{k})$ has an additional factor $V/N = 1/\rho_0$, we have chosen the normalization used in Cosmology.

If we assume statistical homogeneity, it is simple to show from their respective definitions that the 2-point correlation function and the SF are FT pairs:

$$S(\mathbf{k}) = FT[C_2(\mathbf{r})] \tag{3.19a}$$

$$P(\mathbf{k}) = \rho_0^2 FT[\xi(\mathbf{r})]. \tag{3.19b}$$

If we assume statistical isotropy an additional average over vectors $\mathbf{k}$ with the same modulus can be performed, the SF depending then only on $k = |\mathbf{k}|$.

In observational cosmology it is not possible to average over different realizations and then *only* spatial averages can be performed. It is therefore necessary to make the assumption of *ergodicity*. It this context it means that it is possible to replace the average of a function $F[\rho(\mathbf{r})]$ over realizations (Eq. (3.2)) by the following spatial average:

$$\overline{F} = \lim_{V\to\infty} \frac{1}{V} \int_V d^3 r_0 F(\rho(\mathbf{r}_1 + \mathbf{r}_0), \rho(\mathbf{r}_2 + \mathbf{r}_0), \dots). \tag{3.20}$$

This is also known as the *self-averaging*. This is the reason of the definition of the PS as the infinite volume limit of the SF.

There is an important theorem in the theory of stochastic processes related with the PS. This is basically the Wiener-Khinchin theorem (see e.g. [GSLJP05]), which states that, given a two-point correlation function $C_2(r)$, it exists a statistically homogeneous continuous stochastic stationary process with this correlation, if, and only if, its PS is integrable and non negative for all $\mathbf{k}$, i.e. $FT[C_2(\mathbf{r})] > 0$. In the case of a point distribution this condition is only *necessary*. A corollary of this theorem is the property:

$$\xi(0) \geq \xi(\mathbf{r}). \tag{3.21}$$

Its proof is straightforward: the correlation function $\xi(\mathbf{r})$ if the FT of the PS

$$\xi(\mathbf{r}) = \frac{1}{(2\pi)^d} \int_{\mathbb{R}^d} P(\mathbf{k}) e^{i\mathbf{k}\cdot\mathbf{r}} d^d k. \tag{3.22}$$

Since, by definition, $P(\mathbf{k}) \geq 0$ and $\|\exp(i\mathbf{k}\cdot\mathbf{r})\| \leq 1$, the inequality (3.21) is evident.

3.1.3 Mass variance

Another convenient way to characterize stochastic distributions is via the fluctuations of mass in d-dimensional regions that we will denote $\mathcal{L}$. The normalized mass variance is defined as

$$\sigma^2(\mathcal{L}) = \frac{\langle M(\mathcal{L})^2 \rangle - \langle M(\mathcal{L}) \rangle^2}{\langle M(\mathcal{L}) \rangle^2}. \tag{3.23}$$

The average amount of mass in the region $\mathcal{L}$ is

$$\langle M(\mathcal{L}) \rangle = \int_{\mathbb{R}^d} W_{\mathcal{L}}(\mathbf{r}) \langle \rho(\mathbf{r}) \rangle \, d^d r, \tag{3.24}$$

where we have introduced the window function $W_{\mathcal{L}}(\mathbf{r})$

$$W_{\mathcal{L}}(\mathbf{r}) = \begin{cases} 1 & \text{if } \mathbf{r} \in \mathcal{L}; \\ 0 & \text{otherwise.} \end{cases}$$

Further, the average of the square of the mass in the same region is

$$\left\langle M(\mathcal{L})^2 \right\rangle = \int \int_{\mathbb{R}^d} d^d r_1 d^d r_2 W_{\mathcal{L}}(\mathbf{r}_1) W_{\mathcal{L}}(\mathbf{r}_2) \left\langle \rho(\mathbf{r}_1)\rho(\mathbf{r}2) \right\rangle . \tag{3.25}$$

Using the above formulae and the definition of correlation function (3.11) we can write

$$\sigma^2(\mathcal{L}) = \frac{1}{V^2} \int \int_{\mathbb{R}^d} d^d r_1 d^d r_2 W_{\mathcal{L}}(\mathbf{r}_1) W_{\mathcal{L}}(\mathbf{r}_2) \xi(|\mathbf{r}_1 - \mathbf{r}_2|), \tag{3.26}$$

where V is the volume of the region $\mathcal{L} = \int d^d r W_{\mathcal{L}}(\mathbf{r})$. Performing the FT of (3.26) we obtain

$$\sigma^2(\mathcal{L}) = \frac{1}{(2\pi)^d} \int d^d k P(\mathbf{k}) |\tilde{W}_{\mathcal{L}}(\mathbf{k})|^2, \tag{3.27}$$

where $\tilde{W}_{\mathcal{L}}(\mathbf{k})$ is the FT of $W_{\mathcal{L}}(\mathbf{r})$. Very often the natural choice of volume $\mathcal{L}$ in which to compute the fluctuations is a sphere. It is simple to find that the FT of the window function is, in three dimensions,

$$\tilde{W}_{\mathcal{L}}(\mathbf{k}) = \frac{3}{(kR)^3} (\sin kR - kR \cos kR). \tag{3.28}$$

3.1.4 Discrete versus continuous distributions

When performing numerical simulations in cosmology, a continuous fields is usually modelized using a N-body discretization of it. The evolution of the continuous field is then computed evolving the discrete N-body distribution (see section 5.7). In this context it is evidently very important to understand the main differences between continuous and discrete distributions.

Discreteness introduces a kind of fluctuations that does not appear in continuous distributions. For example, it is possible to construct a continuous distribution with zero fluctuations, i.e. with $C_{12}(\mathbf{r}) = 0$ for all $\mathbf{r}$ (we assume statistical homogeneity). This is simply a distribution with constant density everywhere. In the case of discrete distributions there is always a fluctuation introduced by discreteness: a particle is correlated with itself, which introduces a singularity in $C_{12}(\mathbf{r})$. We can see that studying the uncorrelated (discrete) Poisson distribution.

The Poisson distribution

We work for simplicity in $d = 3$ dimensions. We divide the three-dimensional real space in $n = V/dV$ infinitesimal cells of volume dV and we define the stochastic density field in each cell as

$$\hat{\rho}(\mathbf{r}) = \begin{cases} \frac{1}{dV} & \text{with probability } \rho dV; \\ 0 & \text{with probability } 1 - \rho dV. \end{cases}$$

The average density (the 1-point correlation function) is trivially

$$\langle \hat{\rho}(\mathbf{r}) \rangle = \frac{n(1/dV)\rho_0 dV + n \cdot 0 \cdot (1 - \rho_0 dV)}{n} = \rho_0. \tag{3.29}$$

The 2-point correlation function is:

$$\langle \hat{\rho}(\mathbf{r}_1)\hat{\rho}(\mathbf{r}_2)\rangle = \langle \hat{\rho}(\mathbf{r})\rangle^2 = \rho_0^2, \quad \text{if } \mathbf{r}_1 \neq \mathbf{r}_2 \tag{3.30}$$

and

$$\langle \hat{\rho}(\mathbf{r}_1)\hat{\rho}(\mathbf{r}_2)\rangle = \frac{n(1/dV)^2\rho_0 dV + n\cdot 0^2\cdot(1-\rho_0 dV)}{n} = \frac{\rho_0}{dV}, \quad \text{if } \mathbf{r}_1 = \mathbf{r}_2. \tag{3.31}$$

Therefore, in the limit $dV \to 0$ we obtain:

$$C_2(r_{12}) = \langle \hat{\rho}(\mathbf{r}_1)\hat{\rho}(\mathbf{r}_2)\rangle - \rho_0^2 = \rho_0\delta(\mathbf{r}_1 - \mathbf{r}_2). \tag{3.32}$$

The discreteness of the distribution introduces a singularity in the correlation function $C_{12}(r)$ at $r = 0$ (and indeed for all l-point correlation functions). The density has an infinite discontinuity around any particle with finite mass, which is mathematically represented by a delta function in the correlation function. Note that this result is general for any *particle* distribution and not only for a Poisson (uncorrelated) distribution. The correlation function of a correlated particle distribution can be written therefore as the sum of two pieces:

$$C_{12}(\mathbf{r}) = \delta(\mathbf{r}) + \rho_0^2 h(\mathbf{r}), \tag{3.33}$$

where $\delta(\mathbf{r})$ is the singularity introduced by discreteness and $h(\mathbf{r})$ is a smooth function[7].

Asymptotic behavior

It is important for what follows to know the permitted asymptotic behavior of the correlation function. The general condition to be a *continous* stochastic process well defined are

- The distribution is no singular with regions with infinite density, i.e.

$$\int_\epsilon n_0(1+\xi(r))dV < \infty, \tag{3.34}$$

  where the integration is performed in any arbitrary small region ϵ. It implies that if we consider a power-law behavior of the correlation function at small scales, we have

$$\lim_{r\to 0}\xi(r) \sim r^\alpha, \qquad \alpha > -d. \tag{3.35}$$

- Regions at a infinite distance are not correlated. Therefore for

$$\lim_{r\to\infty}\xi(r) \sim r^\beta, \qquad \beta < 0. \tag{3.36}$$

In the case of a discrete distribution the situation is very similar. At large scales, the correlation function remains unchanged and therefore condition (3.36) holds. At small scales, the divergence introduced by the discreteness

[7] In statistical physics, it is called the *pair correlation function* (up to a normalization factor)

(see Eq. (3.33)) give rise only to a finite contribution and the condition (3.35) has to be fulfilled now by the smooth function $h(r)$.

From above properties for the correlation function, it is simple to deduce the analogous permitted asymptotic behaviour of the PS. From Eq. (3.35), for a continuous distribution, we have the condition

$$\lim_{k\to\infty} P(k) = 0, \tag{3.37}$$

which implies that, if $P(k \to \infty) \sim k^\gamma$, $\gamma < 0$. If, moreover, the stochastic process has finite variance (i.e. $\xi(0) < \infty$), then

$$\lim_{k\to\infty} k^d P(k) = 0 \tag{3.38}$$

and then $\gamma < -d$. For a point-particle distribution, using Eq. (3.33), and the condition (3.35) for the function $h(r)$, we have the constraint

$$\lim_{k\to\infty} \left| P(k) - \frac{1}{\rho_0} \right| = 0, \tag{3.39}$$

i.e. if

$$\left| P(k) - \frac{1}{\rho_0} \right| \sim k^\gamma \tag{3.40}$$

then $\gamma < 0$. The small k asymptotic behaviour of the PS is, from condition (3.36), if

$$P(k \to 0) \sim k^\delta, \tag{3.41}$$

then $\delta > -d$.

3.2 Classification of stochastic processes

It is clear that the two distributions shown in Figs. 6.8 and 6.9 (pages 113, 114) are different. The first distribution is a Coulombian plasma, where the interaction is long range. The second one is a gas at hight temperature, where the interactions are short range. We see therefore the usefulness in classificate the stochastic processes: it can give us information about the nature of the physical processes involved in these distributions.

In our analysis we are going to assume that the average density $\langle \hat{\rho}(\mathbf{r}) \rangle$ is positive. These particular kind of distributions with zero mean density are called *fractals* (e.g. [GSLJP05]). Current observations suggest that the universe, at sufficiently large scale, is not a fractal. This is the reason why we are going to restrict ourselves to distributions with defined positive density.

A way to differentiate into classes distributions of this type is in terms of the *correlation length* r_c. It gives a characteristic scale r_c up to which the system is correlated. In a system with finite r_c it is possible to show a *fluctuation-dissipation* theorem that links the fluctuations and the response of the system through the integral of $\xi(\mathbf{r})$ [GSLJP05]. This allows the following classification depending on the behavior of the correlation function at large r:

- Infinite correlation length for $\xi(r) \sim r^{-\gamma}$ with $0 < \gamma \leq d$. The response of a small localized perturbation will be felt in the whole system.

- Finite correlation length for $\gamma > d$ or $\xi(r) \sim \exp(-r/r_*)$ or any function that decays faster than any power law. In this case the response of a small localized perturbation is felt in only a region of size r_c[8].

A possible definition of the correlation length that embodies the above features is[9]:

$$r_c = \frac{\int_{\mathbb{R}^d} d^d r r^2 |\xi(\mathbf{r})|}{\int_{\mathbb{R}^d} d^d r |\xi(\mathbf{r})|}. \tag{3.42}$$

This suggest that an useful classification of stochastic systems can be expressed in terms of the value of the integral of the correlation function, i.e. in terms of the PS at $k = 0$

$$P(k=0) = \int_{\mathbb{R}}^{3} d^3 r \xi(r). \tag{3.43}$$

Depending if it is finite or infinite, one has a similar classification to that just given above. Given that $\xi(r)$ is assumed to be integrable at $r = 0$, this classification depends only of the behavior of the correlation function $\xi(r)$ at large r. However if the integral (3.43) vanishes (i.e. $P(0) = 0$) it gives a stronger *global* constraint on the system, where correlations and anti correlations cancels globally in an exact manner. We will study in detail such systems in chapter 6, an example of a correlation function of such a system appear in Fig. 6.12. The balance between correlations and anti-correlations gives fluctuations which decay at a faster rate than in a Poisson distribution (an explicit configuration of such systems is shown in Fig. 6.9, compared to a Poisson distribution).

We can quantify how the density fluctuations are spatially distributed by computing, for example, the behavior of the normalized variance in the mass computed in spheres of different radius. More the normalized variance decays faster, more the system will be regularly distributed, at least at sufficiently large scale. We will do first the computation in three dimensions and then we will generalize it to any dimension. Using Eqs. (3.27) and (3.28) we obtain the expression:

$$\sigma^2(R) = \frac{1}{2\pi^2} \int_0^\infty dk \frac{9}{(kR)^6} (\sin kR - kR \cos kR)^2 k^2 P(k), \tag{3.44}$$

for the normalized variance in a sphere of radius R. We will consider a simple PS that behaves, at large scales (small k) as

$$P(k) = A k^n e^{-k/k_c}, \tag{3.45}$$

with $n > -3$ to ensure integrability (i.e. that follows the condition on the PS explained above). Substituting Eq. (3.45) in (3.44) and rescaling variables we obtain:

$$\sigma^2(R) = \frac{9A}{2\pi^2} \frac{1}{R^{3+n}} \int_0^\infty dx (\sin x - x \cos x)^2 x^{n-4} e^{-x/x_c}, \tag{3.46}$$

where $x_c = k_c R$. Clearly Eq. (3.46) has two different behaviors depending on whether $n > 1$ or $n < 1$. If $n > 1$, the integral will be dominated by the cutoff

[8] This is only rigorously true for systems at thermal equilibrium, as in liquids,, considered in chapter 6.

[9] Note that this with definition of correlation length gives $r_c \to \infty$ for $\xi(r) \sim r^{-\gamma}$ with $3 < \gamma \leq 5$ and, as explained above, corresponds physically to a finite correlation length.

x_c and it can be approximated by

$$\int_0^\infty x^{n-2} e^{-x/x_c} \sim x_c^{n-1}, \tag{3.47}$$

so that one gets $\sigma^2(R) \sim 1/R^4$. For $n < 1$ the integral (3.46) does not need the cutoff to converge and its value can be evaluated to be

$$\begin{aligned} \int_0^\infty dx (\sin x - x\cos x)^2 x^{n-4} &= 2^{-n} \left[4\Gamma(n-3) + \Gamma(n-2) + \Gamma(n-1)\right] \\ &\times \sin\left(\frac{n\pi}{2}\right). \end{aligned} \tag{3.48}$$

so that $\sigma^2(R) \sim 1/R^{3+n}$. It is usual in cosmology to write for this case the variance as a function of the PS as

$$\sigma^2(R) \approx P(k)k^3|_{k=R^{-1}}, \tag{3.49}$$

up to a numerical factor of order unity. For the limiting case of $n = 1$ we approximate the integral (3.46) by

$$\int \frac{dx}{x} e^{-x/x_c} \sim \ln x_c \sim \ln R. \tag{3.50}$$

A summary of the variance as a function of the exponent n is therefore:

$$\sigma^2(R) \sim \begin{cases} R^{-(3+n)} & \text{for } -3 < n < 1 \\ R^{-4} \ln R & \text{for } n = 1 \\ R^{-4} & \text{for } n > 1. \end{cases} \tag{3.51}$$

These three kind of distributions have a different convergence rate, with scale, to the average density. This is apparent by recalling that, by definition, the density contrast, averaged over the sphere R, is equal to the variance at this same scale:

$$\left\langle \delta^2 \right\rangle (R) \equiv \sigma^2(R). \tag{3.52}$$

Note that this do not imply that at some scale any of these distributions have larger or smaller fluctuations because this is also function of the amplitude of the correlations.

An example of the first kind of distributions in the classification (3.51) are systems at the critical point of a second order phase transition. The systems with $P(k) \sim k^n$ and index $n = 0$ can be called *substantially Poisson*, because, despite they are not all truly Poisson distributions, they have the same rate of fluctuations decreasing with scale. A large number of systems have such behavior, for example a gas in thermodynamic equilibrium at sufficiently high temperature. A distribution with index $n > 0$ will have fluctuations more suppressed with scale than a Poisson one. It corresponds, for example, to a Coulombian plasma, in which the global constraint in the correlation function produces spatially ordered distributions as shown in Fig. 6.8. In this kind of distributions, it is interesting to note that, regardless their index $n(> 1)$, they have the same scaling behaviour of the variance with R. Indeed, there is a theorem which states that there does not exist, in any dimension, any statistically homogeneous and isotropic distribution with a mass variance which decays faster than $1/R^{d+1}$, where d is the dimension of the system (see [GSLJP05] for references).

3.2.1 Generalization to any dimensional space

In the second part of this thesis we will work in spaces of arbitrary dimensions. For example, there are computations that cannot be performed analitycally in three dimensions but only in one dimension. We will see that, despite the reduction of the number of dimensions, we retain the essential physical elements of the problem. The classification of stochastic systems (3.51) is easily generalized to

$$\sigma^2(R) \sim \begin{cases} R^{-(d+n)} & \text{for } -d < n < 1 \\ R^{-(d+1)} \ln R & \text{for } n = 1 \\ R^{-(d+1)} & \text{for } n > 1. \end{cases} \tag{3.53}$$

3.3 Stochastic displacement fields

In cosmology, as discussed in chapter 5, we are interested to generate a point distribution that have (approximatively) the same correlations that a continuous field. This is necessary to set up the initial conditions of N-body simulations that are employed to model the evolution a self-gravitating *fluid*. In this section we will describe the resulting fluctuations of a distribution when a stochastic displacement field is applied. We will also outline how initial conditions are set-up; a complete description appears in chapter 8. What it is presented here is based on the original work [Gab04] (see also [GSLJP05]).

3.3.1 A first approximation to the effect of displacements fields

Before going into the exact mathematical treatment of the effect of a displacement field we are going to give an intuitive argument. First of all, consider a distribution of particles with "sufficiently low fluctuations", $\rho_{in}(\mathbf{r})$. Then, we apply to this distribution a displacement field $\mathbf{u}(\mathbf{r})$, i.e. a particle at $\mathbf{r}$ is displaced by the vector $\mathbf{u}(\mathbf{r})$. For infinitesimally small displacements we can write the continuity equation

$$\rho(\mathbf{r}) - \rho_{in}(\mathbf{r}) + \nabla \cdot [\rho_{in}(\mathbf{r})\mathbf{u}(\mathbf{r})] = 0. \tag{3.54}$$

If the fluctuations of the initial distribution can be neglegted (we will specify below what this requires), we can write $\rho_{in} \simeq \rho_0 (> 0)$. Then Eq. (3.54) can be written as

$$\rho(\mathbf{r}) - \rho_0 + \rho_0 \nabla \cdot \mathbf{u}(\mathbf{r}) = 0. \tag{3.55}$$

Using the definitions (3.15) and (3.16), we thus obtain

$$|\delta_\rho(\mathbf{k})|^2 = |\mathbf{k} \cdot \tilde{u}(\mathbf{k})|^2 , \tag{3.56}$$

where $\tilde{u}(\mathbf{k}) = FT[\mathbf{u}(\mathbf{r})]$. If the displacement field is isotropic, we can infer, using Eq. (3.18), that

$$P_\rho(\mathbf{k}) \simeq k^2 P_{\mathbf{u}}(k), \tag{3.57}$$

i.e. the PS of the final distribution is approximatively the PS of the displacement field multiplied by k^2. Note that (i) we have neglected the discreteness of the initial (and therefore final) distribution and (ii) the result is valid only for $k \to 0$ because Eq. (3.54) is only true for infinitisimally small displacements. In the next subsection we are going to study the general result without these two approximations.

3.3.2 Exact treatment of the effect of displacement fields

Let's consider a set of N particles described by the stochastic density field $\rho_{in}(\mathbf{r})$. To this distribution we apply a displacement field $\mathbf{u}(\mathbf{r})$ described itself as a stochastic process. We assume that both have a well defined probability density functional. After applying the displacement field, the resultant density field will be

$$\rho(\mathbf{r}) = \sum_i \delta(\mathbf{r} - \mathbf{r}_i - \mathbf{u}_i), \tag{3.58}$$

where the sum i is over all the particles of the system. The displacement field $\mathbf{u}(\mathbf{r})$ can be treated mathematically as continuous, even if in Eq. (3.58) it is evaluated only at the positions where there is a particle $\mathbf{r}_i$. Moreover, we will assume that it is spatially stationary and that it is statistically independent of the initial density $\rho_{in}(\mathbf{r})$. With these hypotheses we are going to compute the one and two-point statistical properties of the distribution (3.58).

Computing statistical quantities we have two different averages over the distribution (3.58). First, an average over initial realizations of the density $\rho_{in}(\mathbf{r})$ field and, then, another average over the displacement field $\mathbf{u}(\mathbf{r})$. The average over the initial realization is defined as in Eq. (3.4) and denoted by $\langle\cdot\rangle$. The average over displacements is realized in the same manner, substituting the probability density functional of the density field in Eq. (3.4) by the one of the displacement field. In practice, consider a function A that depends only on the displacements $\{\mathbf{u}_1, \ldots, \mathbf{u}_N\}$, applied respectively to a set of spatial points $\{\mathbf{r}_1, \ldots, \mathbf{r}_N\}$. The average of A over all the possible realizations of $\mathbf{u}(\mathbf{r})$ is (in d spatial dimensions):

$$\overline{A} = \int \left[\prod_{j=1}^{N} d^d u_j\right] f(\mathbf{u}_1, \ldots, \mathbf{u}_N) A(\mathbf{u}_1, \ldots, \mathbf{u}_N), \tag{3.59}$$

where $f_N\{\mathbf{u}_i\}$ is the joint probability density function (hereafter PDF) for all the displacements applied to the particles of the initial distribution, defined as

$$f_N(\mathbf{u}_1, \ldots, \mathbf{u}_N) = \int \mathcal{D}[\mathbf{u}(\mathbf{r})]\mathcal{P}[\mathbf{u}(\mathbf{r})] \prod_{i=1}^{N} \delta(\mathbf{u}(\mathbf{r}_i) - \mathbf{u}_i). \tag{3.60}$$

In the case of a statistically stationary displacement field, $f_N\{\mathbf{u}_i\}$ depends only on the separation vectors between all the couples of points of the set $\{\mathbf{r}_1, \ldots, \mathbf{r}_N\}$. Note that because of the hypothesis of independence of the displacement field of the initial distribution, the order in which these average are performed does not matter. We are now going to compute the exact result of the 1-point and 2-point correlation functions of the resulting distribution.

3.3.3 The one-point correlation function

We assume the initial distribution has the well defined average:

$$\langle \rho_{in}(\mathbf{r}) \rangle = \rho_0. \tag{3.61}$$

It is evident that the density does not change when applying the displacement field because it does not create or destroy particles and we have assumed spatial

stationarity of the displacement field. Explicitly it is shown as follows. The average over displacements is:

$$\overline{\rho(\mathbf{r})} = \sum_i \int d^d u_i f_1(\mathbf{u}_i)\delta(\mathbf{r} - \mathbf{r}_i - \mathbf{u}_i) = \sum_i f_1(\mathbf{r} - \mathbf{r}_i) \tag{3.62}$$

where $f_1(\mathbf{u}_i)$ is obtained integrating over all the $\mathbf{u}_j$, $j \neq i$ of the PDF f_N, and we have used that the spatial stationarity to infer that it does not depend on the point of application of the displacement. Averaging over realizations we obtain

$$\langle \rho(\mathbf{r}) \rangle = \left\langle \int d^d r' f_1(\mathbf{r}') \sum_i \delta(\mathbf{r}' - \mathbf{r} + \mathbf{r}_i) \right\rangle = \rho_0 \int d^d r' f_1(\mathbf{r}') = \rho_0, \tag{3.63}$$

where we have used the statistical spatial stationarity of $\rho_{in}(\mathbf{r})$ and the normalization condition on the one-displacement PDF $f_1(\mathbf{u})$.

3.3.4 The two-point correlation function

The computation of the 2-point correlation function follows exactly the same procedure as the 1-point one described in the precedent subsection. We wish to compute the two averages of the quantity

$$\rho(\mathbf{r})\rho(\mathbf{r}') = \sum_{i,j} \delta(\mathbf{r} - \mathbf{r}_i - \mathbf{u}_i)\delta(\mathbf{r}' - \mathbf{r}'_j - \mathbf{u}_j). \tag{3.64}$$

As for the case of the one-point correlation function we do not need all the information contained in the PDF f_N but only the joint two-displacements PDF $f_2(\mathbf{u}, \mathbf{v})$, obtained by integrating over all the $\mathbf{u}_i$ of f_N but two. Using the hypothesis of spatial stationarity, $f_2(\mathbf{u}, \mathbf{v})$ depends only parametrically on the separation vector $\mathbf{r}$ between these two points. For this reason, we will write $f_2(\mathbf{u}, \mathbf{v}; \mathbf{r})$ for the probabibility to have a displacement $\mathbf{u}$ at the point $\mathbf{r}'$ and a displacement $\mathbf{v}$ at the point $\mathbf{r}''$ with $\mathbf{r}' - \mathbf{r}'' = \mathbf{r}$. Moreover, this PDF satisfies the following limit conditions on $\mathbf{r}$:

$$f_2(\mathbf{u}, \mathbf{v}; 0) = \delta(\mathbf{u} - \mathbf{v}) f_1(\mathbf{u}) \tag{3.65a}$$

$$\lim_{\mathbf{r}\to\infty} f_2(\mathbf{u}, \mathbf{v}; \mathbf{r}) = f_1(\mathbf{u}) f_1(\mathbf{v}). \tag{3.65b}$$

The first condition is trivial and the second one states that displacements at two points infinitely separated must be uncorrelated. Let us compute first the average over the displacement field:

$$\begin{aligned} \overline{\rho(\mathbf{r})\rho(\mathbf{r}')} &= \sum_{i,j} \int d^d u_i d^d u_j f_2(\mathbf{u}_i, \mathbf{u}_j : \mathbf{r}_{ij}) \delta(\mathbf{r} - \mathbf{r}_i - \mathbf{u}_i)\delta(\mathbf{r}' - \mathbf{r}_j - \mathbf{u}_j) \\ &= \sum_{i,j} f_2(\mathbf{r} - \mathbf{r}_i, \mathbf{r}' - \mathbf{r}_j; \mathbf{r}_{ij}), \end{aligned} \tag{3.66}$$

where $\mathbf{r}_{ij} = \mathbf{r}_i - \mathbf{r}_j$ and we have used (3.65a) not to separate the contribution from $i = j$ and $i \neq j$. Let us now compute the average over the initial particle

configurations using the following mathematical trick:

$$\begin{aligned}
\left\langle \overline{\rho(\mathbf{r})\rho(\mathbf{r}')} \right\rangle &= \left\langle \sum_{i,j} f_2(\mathbf{r}-\mathbf{r}_i, \mathbf{r}'-\mathbf{r}_j; \mathbf{r}_{ij}) \right\rangle \qquad (3.67)\\
&= \left\langle \int d^d r_a d^d r_b f_2(\mathbf{r}-\mathbf{r}_a, \mathbf{r}'-\mathbf{r}_b; \mathbf{r}_{ab}) \sum_{ij} \delta(\mathbf{r}_a-\mathbf{r}_i)\delta(\mathbf{r}_b-\mathbf{r}_j) \right\rangle \\
&= \int d^d r_a d^d r_b f_2(\mathbf{r}-\mathbf{r}_a, \mathbf{r}'-\mathbf{r}_b; \mathbf{r}_{ab}) \left\langle \sum_{ij} \delta(\mathbf{r}_a-\mathbf{r}_i)\delta(\mathbf{r}_b-\mathbf{r}_j) \right\rangle \\
&= \int d^d r_a d^d r_b f_2(\mathbf{r}-\mathbf{r}_a, \mathbf{r}'-\mathbf{r}_b; \mathbf{r}_{ab}) \left\langle \rho_{in}(\mathbf{r}_a)\rho_{in}(\mathbf{r}_b) \right\rangle .
\end{aligned}$$

Using the definition of the pair correlation function (of the initial distribution) (3.33) (with definition (3.11) and (3.9)) we have finally:

$$\left\langle \overline{\rho(\mathbf{r})\rho(\mathbf{r}')} \right\rangle = \int d^d r_a d^d r_b f_2(\mathbf{r}-\mathbf{r}_a, \mathbf{r}'-\mathbf{r}_b; \mathbf{r}_{ab})[\rho_0^2 + C_{2,in}(\mathbf{r}_a-\mathbf{r}_b)]. \qquad (3.68)$$

This expression can be rewritten as

$$\begin{aligned}
\left\langle \overline{\rho(\mathbf{r})\rho(\mathbf{r}')} \right\rangle &= \rho_0 \delta(\mathbf{x}-\mathbf{y}) \qquad (3.69)\\
&+ \rho_0^2 \int d^d r_a d^d r_b f_2(\mathbf{r}-\mathbf{r}_a, \mathbf{r}'-\mathbf{r}_b; \mathbf{r}_{ab})[1 + h_{in}(\mathbf{r}_a-\mathbf{r}_b)].
\end{aligned}$$

With Eq. (3.68), and the knowledge of the two-point displacements function f_2 and the two-point pair correlation function h_{in} of the initial distribution it is possible (at least numerically) to compute the two-point properties of the final distribution.

3.3.5 Independent displacements

Let us first study the simpler case in which the displacements are independent, i.e., the displacement field applied to the points $\mathbf{r}$ and $\mathbf{r}'$, with $\mathbf{r} \neq \mathbf{r}'$, is not correlated. The N-point displacements PDF can then be factorized:

$$f_N(\mathbf{u}_1, \ldots, \mathbf{u}_N) = \prod_{i=1}^{N} p(\mathbf{u}_i). \qquad (3.70)$$

Therefore the two-point displacements PDF can be written as

$$f(\mathbf{u}, \mathbf{v}; \mathbf{r}) = \begin{cases} \delta(\mathbf{u}-\mathbf{v}) f_1(\mathbf{u}) & \text{for } \mathbf{r} = 0 \\ f_1(\mathbf{u}) f_1(\mathbf{v}) & \text{for } \mathbf{r} \neq 0 \end{cases} \qquad (3.71)$$

Using (3.71), the two-point correlation (3.68) is simplified to

$$\left\langle \overline{\rho(\mathbf{r})\rho(\mathbf{r}')} \right\rangle = \rho_0^2 + \rho_0 \delta(\mathbf{r}-\mathbf{r}') + \rho_0^2 \int d^d r_a d^d r_b f_1(\mathbf{r}-\mathbf{r}_a) h_{in}(\mathbf{r}_a-\mathbf{r}_b) f_1(\mathbf{r}'-\mathbf{r}_b). \qquad (3.72)$$

In Fourier space, a very simple local expression for the SF (definition (3.17)) is obtained:

$$S(\mathbf{k}) = \rho_0(1 - |\hat{f}_1(\mathbf{k})|^2) + |\hat{f}_1(\mathbf{k})|^2 S_{in}(\mathbf{k}), \qquad (3.73)$$

where $\hat{f}_1(\mathbf{k})$ is the characteristic function of the one-displacement PDF

$$\hat{f}_1(\mathbf{k}) = FT[f_1(\mathbf{u})], \tag{3.74}$$

and $S_{in}(\mathbf{k})$ is the structure factor of the initial distribution. Observe that if the initial distribution is Poissonian,

$$S_{in}(\mathbf{k}) = \rho_0 \tag{3.75}$$

and then $S(\mathbf{k}) = S_{in}(\mathbf{k})$. This is because the uncorrelated displacements cannot introduce correlations in the system and, because the Poisson distribution is uncorrelated, the final distribution can be only also a Poisson distribution.

Small k behavior of $S(\mathbf{k})$

It is interesting to study the large scale correlations of the resulting distribution. It permits, for example, to determinate the kind of resulting distribution, attending to the classification given in section 3.2. We can do so computing the small k behavior of the PS. It is sufficient to know the large scale behavior of the 1-point displacements PDF. Let us consider that it behaves at large $\mathbf{u}$ as

$$f_1(\mathbf{u}) = A\frac{1}{u^{\alpha+d}} + o\left(\frac{1}{u^{\alpha+d}}\right), \tag{3.76}$$

where $\alpha > 0$ to ensure integrability of $f_1(\mathbf{u})$. Using App. A we conclude that the behavior of the characteristic function $\hat{f}_1(\mathbf{k})$ at small k is

$$\hat{f}_1(\mathbf{k}) = 1 - Bk^{\beta} \text{ with} \begin{cases} \beta = \alpha & \text{if } 0 < \alpha \leq 2 \\ \beta = 2 & \text{if } \alpha > 2, \end{cases} \tag{3.77}$$

where $B > 0$. For the first case

$$B = A\int d^d x x^{-\alpha}\left(1 - e^{-ikx\cos\theta}\right), \tag{3.78}$$

where θ is the angle between $\mathbf{x}$ and any of the coordinate axis and, for the second case,

$$B = \frac{\overline{u^2}}{2}. \tag{3.79}$$

Note that the main difference between the first and second case is that in the first one the variance of displacements is infinite whereas in the second is finite. The small k behavior of the resulting SF is, using Eq. (3.73),

$$S(\mathbf{k} \to 0) = S_{in(\mathbf{k})} + 2B\rho_0 k^{\beta}. \tag{3.80}$$

It is instructive to compare this result with the approximative solution (3.57). The exact result (at small k) (3.80) includes a term –which can be important– of the initial SF. Moreover, the intuitive treatment do not consider the case in which the variance of displacements is not finite, i.e. when $0 < \alpha \leq 2$.

3.3.6 The lattice with uncorrelated displacements

We are going to study the correlation properties of a lattice with uncorrelated displacements. It is simple to check (e.g. [GJSL02]) that the structure function of a lattice (the initial distribution) is (in d dimensions)

$$S_{lat}(\mathbf{k}) = (2\pi)^d \rho_0^2 \sum_{\mathbf{h}\neq 0} \delta(\mathbf{k}-\mathbf{H}), \tag{3.81}$$

where the sum runs over all the *reciprocal lattice* (more details in chapter 9). For example, in the case of a *simple cubic lattice*, $\mathbf{h} = k_N \mathbf{m}$, where k_N is the *Nyquist frequency* $k_N = 2\pi/\ell$ (ℓ is the lattice spacing) and $\mathbf{m}$ a triple non-zero integer. Using Eq. (3.73), the final SF is

$$S(\mathbf{k}) = \rho_0 \left(1 - |\hat{f}_1(\mathbf{k})|^2\right) + (2\pi)^d \rho_0^2 \sum_{\mathbf{h}\neq 0} |\hat{f}_1(\mathbf{h})|^2 \delta(\mathbf{k}-\mathbf{h}). \tag{3.82}$$

The first term of the r.h.s. of (3.82) gives the small k behavior of the SF (up to the Nyquist frequency). The second term of the r.h.s is a sum of peaks modulated by the characteristic function.

An example: the shuffled lattice

Let us consider the case of the one-dimensional lattice to which are applied random displacements of a given amplitude, called "shuffled lattice". The one-point displacements probability is:

$$f_1(x) = \text{ with} \begin{cases} 1/a & \text{if } |x| \leq a/2 \\ 0 & \text{if } |x| > a/2 \end{cases} \tag{3.83}$$

The characteristic function is

$$\hat{f}_1(k) = \int_{-a/2}^{a/2} dx f_1(x) e^{-ikx} = \frac{1}{a}\int_{-a/2}^{a/2} dx e^{-ikx} = \frac{2}{ka}\sin\left(\frac{ka}{2}\right), \tag{3.84}$$

which has the correct normalization $\hat{f}_1(0) = 1$. Using Eqs. (3.82) and (3.84) we obtain the final SF:

$$S(\mathbf{k}) = \rho_0 \left(1 - \frac{4}{k^2}\sin^2\left(\frac{ka}{2}\right)\right) + (2\pi)^d \rho_0^2 \sum_{\mathbf{h}\neq 0} \frac{4}{h^2}\sin^2\left(\frac{ha}{2}\right)\delta(\mathbf{k}-\mathbf{h}) \tag{3.85}$$

If the shuffling is small, i.e. $a \ll \ell$, then $k_N a \ll 1$. Therefore a development in Taylor series around $k = 0$ of the first term of the r.h.s. of (3.85) will be valid up to a few times the Nyquist frequency. The small k behavior is

$$S(\mathbf{k} \to 0) = 2\rho_0 a^4 k^2, \tag{3.86}$$

proportional to k^2 because the displacements have finite variance (as we have seen above). The second term of the r.h.s. contributes only from the Nyquist frequency, as peaks with an envelope $4\sin^2(ka/2)/ka$. The SF for this distribution is shown in Fig. 3.1.

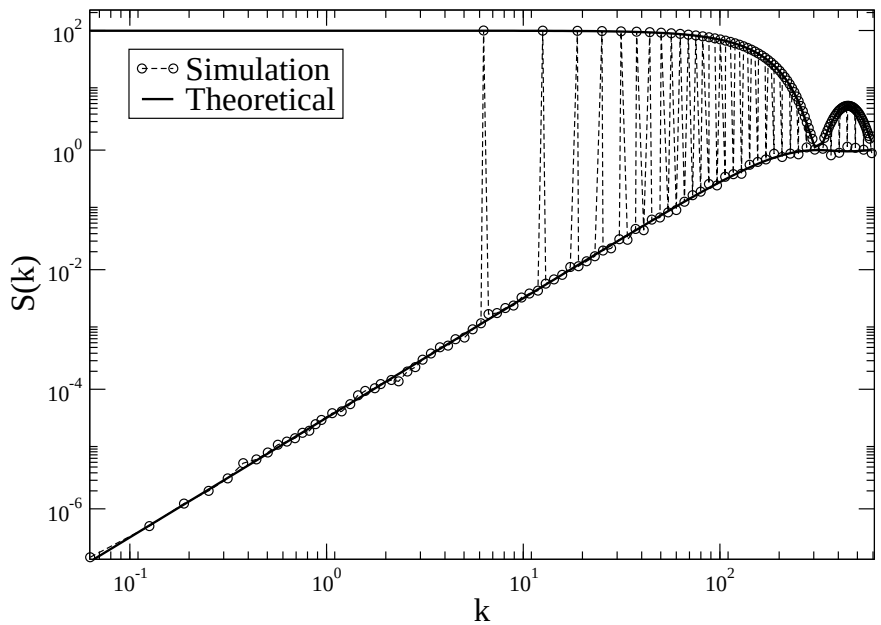

Figure 3.1: SF of a shuffled lattice in $d = 1$ dimension with shuffling $a = \ell/50$. It is shown both the theoretical calculation (3.85) and a numerical simulation.

3.3.7 Correlated displacements

If the displacements are correlated the calculation is slightly more complicated because $f_2(\mathbf{u}, \mathbf{v}, \mathbf{x})$ cannot be factorized as in the uncorrelated case. However, this case is much more interesting because *it can create spatial correlations*.

It is simpler to compute the SF rather than the correlation function in real space (the correlation function can be obtained by FT over the SF). Noting that

$$\langle \rho(\mathbf{r})\rho(\mathbf{r}')\rangle = \rho_0^2 + C_2(\mathbf{r} - \mathbf{r}'), \tag{3.87}$$

and using, the definition of SF, it follows that

$$\int d^d r d^d r' e^{-i(\mathbf{k}\cdot\mathbf{r}+\mathbf{k}'\cdot\mathbf{r}')} C_2(\mathbf{r} - \mathbf{r}') = (2\pi)^d \delta(\mathbf{k} + \mathbf{k}') S(\mathbf{k}). \tag{3.88}$$

Then

$$\begin{aligned} (2\pi)^d \delta(\mathbf{k} + \mathbf{k}') S(\mathbf{k}) &= \int d^d r d^d r' e^{-i(\mathbf{k}\cdot\mathbf{r}+\mathbf{k}'\cdot\mathbf{r}')} C_2(\mathbf{r} - \mathbf{r}') \\ &= \int d^d r d^d r' e^{-i(\mathbf{k}\cdot\mathbf{r}+\mathbf{k}'\cdot\mathbf{r}')} \langle \rho(\mathbf{r})\rho(\mathbf{r}')\rangle \\ &\quad -\rho_0^2 \int d^d r d^d r' e^{-i(\mathbf{k}\cdot\mathbf{r}+\mathbf{k}'\cdot\mathbf{r}')}. \end{aligned} \tag{3.89}$$

Introducing the expression for $\langle \rho(\mathbf{r})\rho(\mathbf{r}')\rangle$ (3.68) in Eq. (3.89), a simple calculation gives:

$$S(\mathbf{k}) = \int d^d r e^{-i\mathbf{k}\cdot\mathbf{r}} \hat{f}_1(\mathbf{k}, -\mathbf{k}; \mathbf{r})[\rho_0^2 + C_{2,in}(\mathbf{r})] - (2\pi)^d \rho_0^2 \delta(\mathbf{k}), \tag{3.90}$$

where we have defined

$$\hat{f}_1(\mathbf{k},\mathbf{k}';\mathbf{r}) = \int d^d u d^d v e^{-i(\mathbf{k}\cdot\mathbf{u}+\mathbf{k}'\cdot\mathbf{v})} f_1(\mathbf{u},\mathbf{v};\mathbf{r}). \tag{3.91}$$

The characteristic function $f_1(\mathbf{k},-\mathbf{k};\mathbf{r})$ depends only on a single k-vector because of the stationarity of the displacement field assumed in the derivation of (3.68). Let us define $s(\mathbf{w};\mathbf{r})$ as the PDF that two points, separated by the distance vector $\mathbf{r}$, undergo a relative displacement $\mathbf{w}$. It is related with f_1 through the relation

$$s(\mathbf{w};\mathbf{r}) = \int d^d u d^d v f_1(\mathbf{u},\mathbf{v};\mathbf{r})\delta(\mathbf{w}-\mathbf{u}+\mathbf{v}). \tag{3.92}$$

The FT with respect to $\mathbf{w}$ of (3.92) is

$$\hat{s}(\mathbf{k};\mathbf{r}) = \hat{f}_1(\mathbf{k},-\mathbf{k};\mathbf{r}). \tag{3.93}$$

Substituting Eq. (3.93) in (3.90) we obtain finally the equation:

$$S(\mathbf{k}) = \int d^d r e^{-i\mathbf{k}\cdot\mathbf{r}} \hat{s}(\mathbf{k};\mathbf{r})[\rho_0^2 + C_{2,in}(\mathbf{r})] - (2\pi)^d \rho_0^2 \delta(\mathbf{k}). \tag{3.94}$$

In Eq. (3.94) there is all the information necessary to compute the SF. The difficulty consists in computing the two-point characteristic function $\hat{s}(\mathbf{k};\mathbf{r})$. Before showing an example of a Gaussian correlated displacement field, let us study the small k behavior of $S(\mathbf{k})$.

Small k behavior of $S(\mathbf{k})$

In the same way as for uncorrelated displacements, we first to calculate the small k behavior of the characteristic function $\hat{s}(\mathbf{k};\mathbf{r})$. Let us assume that the variance between differences of the displacements $\overline{w^2} = \overline{(u-v)^2}$ is finite, which is the case of practical interest for what follows[10]. Then we can write the characteristic function as:

$$\hat{s}(\mathbf{k};\mathbf{r}) = \int d^d w s(\mathbf{w};\mathbf{r}) e^{-i\mathbf{k}\cdot\mathbf{w}} = 1 - i\mathbf{k}\cdot\overline{\mathbf{w}(\mathbf{r})} - \frac{1}{2}\overline{[\mathbf{k}\cdot\mathbf{w}(\mathbf{r})]^2} + o(k^2), \tag{3.95}$$

where $\overline{\mathbf{w}(\mathbf{r})}$ is the average on the relative displacements. We define the two-displacement correlation matrix as

$$g_{\mu\nu}(\mathbf{r}-\mathbf{r}') = \overline{(u_\mu(\mathbf{r}) - \overline{u}_\mu)(u_\nu(\mathbf{r}') - \overline{u}_\nu)}, \tag{3.96}$$

where u_μ is the μ-th component of the displacement $\mathbf{u}$. Using this definition, and supposing symmetry by space inversion or rotation (and hence $\overline{\mathbf{w}(\mathbf{r})} = 0$ and $g_{\mu\nu}(\mathbf{r}) = g_{\mu\nu}(-\mathbf{r})$), we have

$$\begin{aligned} \overline{[\mathbf{k}\cdot\mathbf{w}]^2} &= k_\mu k_\nu \overline{(u_\mu(\mathbf{r}) - u_\mu(0))(u_\nu(\mathbf{r}) - u_\nu(0))} \\ &= 2k_\mu k_\nu [g_{\mu\nu}(0) - g_{\mu\nu}(\mathbf{r})]. \end{aligned} \tag{3.97}$$

[10] If the variance between different displacements is not finite, we have to perform an analogous analysis than the one performed for the case of uncorrelated displacements.

Then we can write the first two terms of a small k expansion of (3.94) as

$$S(\mathbf{k}) = S_{in}(\mathbf{k}) + k_\mu k_\nu \left\{ \rho_0^2 \tilde{g}_{\mu\nu}(\mathbf{k}) + \int \frac{d^d q}{(2\pi)^d} \tilde{g}_{\mu\nu}(\mathbf{q}) [S_{in}(\mathbf{k}-\mathbf{q}) - S_{in}(\mathbf{k})] \right\}, \tag{3.98}$$

where

$$\tilde{g}_{\mu\nu}(\mathbf{k}) = FT[g_{\mu\nu}(\mathbf{r})] \tag{3.99}$$

and we have used that

$$g_{\mu\nu}(0) = \int \frac{d^d q}{(2\pi)^d} \tilde{g}_{\mu\nu}(\mathbf{q}). \tag{3.100}$$

If the displacements are not correlated between different directions $g_{\mu\nu}(\mathbf{r}) = g(\mathbf{r})\delta_{\mu\nu}$. In addition, if the displacement field is isotropic, i.e. $g(\mathbf{r}) = g(r)$, we can write (3.98) in a form that simplifies the analysis of the different terms:

$$S(\mathbf{k}) = S_{in}(\mathbf{k}) + k^2 \left\{ \rho_0^2 \tilde{g}(k) + \int \frac{d^d q}{(2\pi)^d} \tilde{g}(q) [S_{in}(\mathbf{k}-\mathbf{q}) - S_{in}(\mathbf{k})] \right\}. \tag{3.101}$$

Depending on the large scale (small k) behavior of the displacement fields and on the initial SF, the final SF will be determined by the former or the latter. Neglecting the contribution of the integral in Eq. (3.101) and choosing as initial distribution a lattice we have:

$$S(\mathbf{k}) = \rho_0^2 k^2 \tilde{g}(k), \qquad k < k_N, \tag{3.102}$$

because $S_{lat} = 0$ for $k < k_N$. The expression (3.102) is used to set up initial conditions for N-body simulation. If we want to obtain a distribution with SF $S_{theo}(k)$ we should apply a displacement field with the correlations:

$$\tilde{g}(k) = \frac{S_{theo}(k)}{k^2 \rho_0^2}. \tag{3.103}$$

We will obtain the desired PS at small k compared with the inverse average displacements. We will discuss extensively this method in chapter 7.

3.3.8 Correlated Gaussian displacement field

In this section we treat the important case of Gaussian displacement fields. A Gaussian field is totally determined by its two first moments, its average and its variance. It is important for (at least) two reasons: first, it is simple to treat and to compute quantities (generally through Gaussian integrals, that can be solved analytically). Second, the primordial fluctuations in cosmology (and the initial conditions for the N-body simulations) are Gaussian, as good (first) approximation[11]. The normalized probability density functional for a Gaussian field is

$$\mathcal{P}[\mathbf{u}(\mathbf{r})] = \frac{1}{\mathcal{N}} \exp\left[-\frac{1}{2} \int_{\mathbb{R}^d} d^d r d^d r' u_\alpha(\mathbf{r}) \mathcal{K}_{\alpha\beta}(|\mathbf{r}-\mathbf{r}'|) u_\beta(\mathbf{r}') \right], \tag{3.104}$$

[11] Moreover, it is possible to show that when we know only the two first moments of some field (and they are finite), the probability to be a Gaussian field is maximum [GSLJP05]. The proof is very simple, based on the in the *central limit theorem*.

where the explicit value of the normalization $\mathcal{N}$ is not relevant here, a calculation of it is given in App. B. It is useful to rewrite Eq. (3.104) using the FT of the displacement field as[12]:

$$\mathcal{P}[\mathbf{u}(\mathbf{r})] = \frac{1}{\mathcal{N}} \exp\left[-\frac{1}{2(2\pi)^3}\int_{\mathbb{R}^d} d^d k\, \tilde{u}_\alpha(\mathbf{k})\tilde{u}^*_\beta(\mathbf{k})\tilde{\mathcal{K}}_{\alpha\beta}(\mathbf{k})\right], \tag{3.105}$$

where we have used that $\mathcal{K}(\mathbf{r})$ is real and symmetric (and hence $\mathcal{K}(\mathbf{k})$ is also real and symmetric) and $\mathbf{u}(\mathbf{r})$ is real (and therefore $\tilde{\mathbf{u}}(-\mathbf{k}) = \tilde{\mathbf{u}}^*(\mathbf{k})$). Note that performing the FT we have *diagonalized* the matrix $\mathcal{K}$ in the space represented by the indices $\mathbf{r}, \mathbf{r}'$. To make the expression (3.105) more transparent it is convenient to discretize[13] the integral in the exponent of (3.105) in the same way it is done in App. B :

$$\mathcal{P}[\mathbf{u}(\mathbf{r})] = \lim_{n\to\infty} \frac{1}{\mathcal{N}} \prod_{i=1}^{n} \exp\left[-\frac{1}{2V}(\tilde{u}_i)_\sigma(\tilde{u}^*_i)_\nu(\tilde{\mathcal{K}}_i)_{\sigma\nu}\right], \tag{3.106}$$

where discretizing we have introduced the volume V (the limit $V \to \infty$ is taken at the end). The two-point correlation function reads:

$$g_{\alpha\beta}(\mathbf{r}) = \overline{u_\alpha(\mathbf{r}+\mathbf{r}')u_\beta(\mathbf{r}')} = \int \mathcal{D}[\mathbf{u}(\mathbf{r})]u_\alpha(\mathbf{r}+\mathbf{r}')u_\beta(\mathbf{r}')\mathcal{P}[\mathbf{u}(\mathbf{r})]. \tag{3.107}$$

The FT of the correlation function, $S_{\alpha\beta}(\mathbf{k}) \equiv \mathrm{FT}[g_{\alpha\beta}(\mathbf{r})]$ is easier to compute. Computing the FT of Eq. (3.107) we have formally:

$$(\tilde{g}_j)_{\alpha\beta} = \lim_{V\to\infty} \frac{1}{V} \int \mathcal{D}[\mathbf{u}(\mathbf{r})]u_\alpha(\mathbf{k})u^*_\beta(\mathbf{k})\mathcal{P}[\mathbf{u}(\mathbf{r})], \tag{3.108}$$

Discretizing the functional integral of Eq. (3.108) and inserting in it Eq. (3.106) we get:

$$(\tilde{g}_j)_{\alpha\beta} = \lim_{V,n\to\infty} \frac{1}{\mathcal{N}V} \int \left[\prod_{i=1}^{n} d^d\tilde{u}_i\right] (\tilde{u}_j)_\alpha(\tilde{u}^*_j)_\beta \prod_{k=1}^{n} \exp\left[-\frac{1}{2V}(\tilde{u}_k)_\sigma(\tilde{u}^*_k)_\nu(\tilde{\mathcal{K}}_k)_{\sigma\nu}\right] \tag{3.109}$$

where we have changed coordinates $\mathbf{u}(\mathbf{r}) \to \tilde{\mathbf{u}}(\mathbf{k})$, whose Jacobian is unity. It is always possible to integrate analytically Eq. (3.109) – performing another rotation – but the result is not simple because, in general, the matrix $\tilde{\mathcal{K}}_k$ in the exponential is non-diagonal. Nevertheless, in one dimension (or when $\tilde{\mathcal{K}}_k$ is diagonal) the result is simple[14]:

$$\tilde{g}(k) = \lim_{V,n\to\infty} \frac{1}{\mathcal{N}V} \int \left[\prod_{i=1}^{n} d\tilde{u}_i\right] |\tilde{u}_j|^2 \prod_{k=1}^{n} \exp\left[-\frac{1}{2V}|\tilde{u}_k|^2\tilde{\mathcal{K}}_k\right] = \frac{1}{\tilde{\mathcal{K}}(k)}, \tag{3.110}$$

where in the last step we have used the explicit calculation (B.10) for the normalization $\mathcal{N}$ and we have returned to the continuum. Eq. (3.110) gives a very

[12] We assume that we are in an infinite space and then we use the set of equations (3.14), otherwise we use (3.12).

[13] This discretization comes naturally in a finite periodic system, i.e with Born–Von Karman boundary conditions.

[14] Using that $\int_{-\infty}^{+\infty} dx x^2 \exp(-a^2x^2/2) = \sqrt{2\pi}/a^3$.

clear illustration of what a Gaussian field is, in one dimension: each mode in k-space is independent[15] with a Gaussian PDF given by the exponential of Eq. (3.110). In more than one dimension, the same is almost true except that there can be correlations between different directions of the same mode[16].

To compute the SF of the final distribution we need to compute the function $\hat{s}(\mathbf{k},\mathbf{r})$ defined in Eq. (3.93):

$$\begin{aligned}\hat{s}(\mathbf{k};\mathbf{r}) &= \int d^d v d^d v' d^d w \mathcal{D}[\mathbf{u}(\mathbf{r})]\mathcal{P}[\mathbf{u}(\mathbf{r})]e^{-i\mathbf{k}\cdot\mathbf{w}} \\ &\times \delta(\mathbf{v}(\mathbf{r}+\mathbf{r}')-\mathbf{u}(\mathbf{r}))\delta\left(\mathbf{v}'(\mathbf{r}')-\mathbf{u}(\mathbf{r})\right)\delta(\mathbf{w}-\mathbf{v}+\mathbf{v}') \\ &= \int \mathcal{D}[\mathbf{u}(\mathbf{r})]\mathcal{P}[\mathbf{u}(\mathbf{r})]e^{-i\mathbf{k}\cdot\left[\mathbf{u}(\mathbf{r}+\mathbf{r}')-\mathbf{u}(\mathbf{r}')\right]}.\end{aligned} \tag{3.111}$$

Using for a Gaussian field Eq. (3.104) we obtain:

$$\hat{s}(\mathbf{k};\mathbf{r}) = e^{-k_\mu k_\nu [g_{\mu\nu}(\mathbf{0})-g_{\mu\nu}(\mathbf{r})]}, \tag{3.112}$$

where the sum is implicit over the labels μ and ν. Substituting Eq. (3.112) in (3.94) we have finally:

$$S(\mathbf{k}) = e^{-k_\mu k_\nu g_{ij}(0)} \int_{\mathbb{R}^d} d^d r e^{-i\mathbf{k}\cdot\mathbf{r}+k_\mu k_\nu g_{\mu\nu}(\mathbf{r})}\left[\rho_0^2 + C_{2,in}(\mathbf{r})\right] - (2\pi)^d\delta(\mathbf{k}). \tag{3.113}$$

We will make extensive use of this result in chapter 7.

[15] Moreover, the *real* and *imaginary* part of each mode are also independent.
[16] In this case the matrix $\mathcal{K}$ is not diagonal.

Chapter 4

Structure formation in Cosmology

In this chapter we review the basics of the standard cosmological model, focusing on the formation of large scale structure. This is the only chapter of the first part of the thesis strictly devoted to cosmology and it gives the context for the work. We will start briefly listing the main observations underpinning the standard cosmological model. In the second part of the thesis we will see that the matter distribution of the universe is assumed to be homogeneous at large scales (i.e. with constant matter density), with small density fluctuations. Using this hypothesis, we will describe the Friedmann – Robertson – Walker model of a perfectly homogeneous and isotropic universe (i.e. exactly constant spatial density). We will outline the paradigm for formation of structures in terms of the evolution of perturbations to this model. We will use the results explained to determine which cosmological initial conditions should be taken for the N-body simulations in chapters 7 and 8. We will also use some of the results given here in chapter 9, where we will compare the linear theory of a self-gravitating fluid with gravitational N-body linear theory, in order to quantify discreteness effects.

4.1 Homogeneity and isotropy of the universe

The basic hypothesis used to construct the standard cosmological model is given by the *Cosmological Principle*. One way to state it is:

"Viewed on sufficiently large distance scales, the universe is homogeneous and isotropic".

Homogeneity means that the universe looks the same from all points and isotropy means that the universe looks the same in all directions[1]. For a long time, there was no clear observational evidences for this statement. It had the status of a *postulate*, in the same manner as, for example, Einstein's Principle of Relativity[2].

[1] Note the difference with the concept of *statistical homogeneity* and *statistical isotropy* defined in chapter 3.

[2] For a review about the subject see e.g. [Pee80].

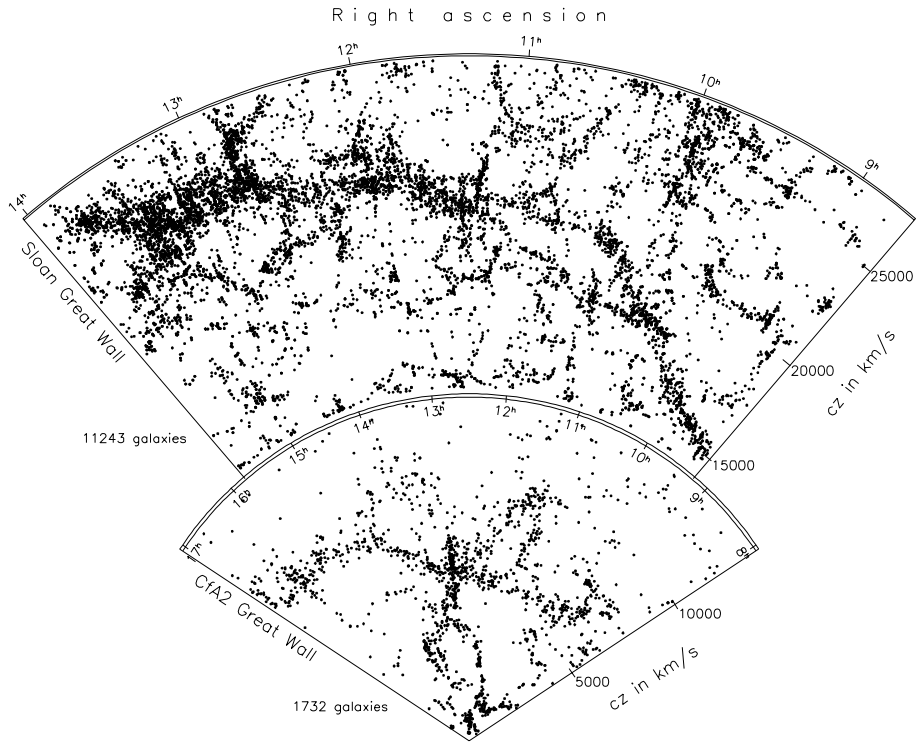

Figure 4.1: Slices of the 2dF and SDSS surveys. Observe how at small scales (small redshift) the galaxies are highly clustered, forming walls, filaments, etc.

The Cosmological Principle, stated as above, is a strong hypothesis. There is another version of it, called the *conditional* cosmological principle, which hypothesis are only *statistical isotropy* and *statistical homogeneity*. This is a much weaker assumption, which allows one to admit the possibility of a fractal distribution of matter, in which the density averaged in an infinite volume is zero.

An indication to support the hypothesis of strict homogeneity and isotropy at large scales is the fact that the model based on it – which we will study in the next section – describes remarkably well the large scale dynamics of the observed universe, given by the Hubble law. In addition, the dynamics is isotropic about our point of observation, which suggests that it could be isotropic from any point of view in the universe. Another indirect indication is the isotropy of the temperature of the Cosmic Microwave Background (hereafter CMB) radiation, which pervades the universe [PW65]. Indeed it took more than two decades after its discovery to detect the fluctuations of the temperature as a function of the angle of observation, which are at a level of about one in ten thousand [BKH$^+$94]. However all these observations do not constitute, of course, a direct test of the hypothesis.

The only direct current observation which directly probes the homogeneity of the universe is that provided by 3-dimensional surveys constraining the distribution of visible matter, notably galaxy and cluster surveys. Given that

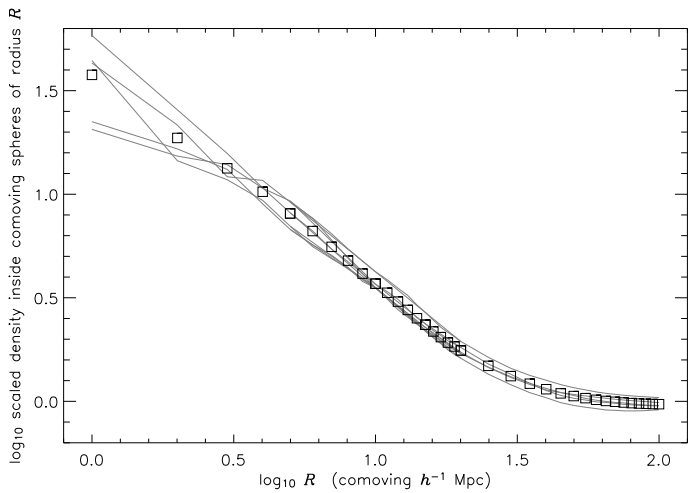

Figure 4.2: (From [H$^+$05]), the average comoving density (i.e. number counted divided by expected from an homogeneous distribution) as function of a comoving sphere of radius R. Observe how at $\log_{10} R \approx 1.5$ the density stabilizes, which means that observed at scales larger than this one the universe is homogeneous.

current cosmological model describes a universe in which 80% of the matter is non visible "dark matter", this is, of course, an incomplete test of homogeneity. However, it is plausible to suppose that the visible matter trace the dark one and therefore these kind of observations are a good probe of homogeneity. In Fig. 4.1 we show a slice of the largest galaxy survey to date. It is apparent that at small scales the distributions of galaxies is very inhomogeneous, with complex structures as cluster of galaxies, voids, walls, etc. However, at large scale, there is an evidence that the distribution of galaxies reaches a definitive (non-zero) density. This is shown in Fig. 4.2, in which the density in function of the scale is shown. For large scales, the density presents a crossover to a constant density, i.e. to homogeneity.

In the rest of the chapter, we will assume isotropy and homogeneity on large scales, as the standard model does. This allows one to construct it in two steps. First, because the universe is homogeneous and isotropic at sufficiently large scales, we construct an exactly homogeneous (equal density everywhere) and isotropic model. This is called the Friedmann – Robertson – Walker model. This model gives the large scale dynamics of the universe. Then, it is perturbed by matter and energy fluctuations, which are the seeds for the formation of structures. The (small) temperature fluctuations in the CMB can be related with these fluctuations, which give us therefore information about the initial fluctuations for the formation of structures.

4.2 The Friedmann-Robertson-Walker universe

The standard cosmological model is constructed by first considering a perfectly homogeneous (i.e with equal density everywhere) and isotropic universe. We work within the framework of the theory of General Relativity. The distance between two infinitesimally close events (in space and time) is given by the metric:

$$ds^2 = g_{ij}(x)dx^i dx^j, \tag{4.1}$$

where the time is represented by $x^0 = t$ and the space coordinates by (x^1, x^2, x^3). The tensor $g_{ij}(x)$ is called the *metric tensor*. It is a generalization of the interval of special relativity (without gravity) in which the metric is simply

$$ds^2 = dt^2 - d\mathbf{l}^2, \tag{4.2}$$

where we have chosen units in which the speed of light is unity and $d\mathbf{l}^2 = (dx^1)^2 + (dx^2)^2 + (dx^3)^2$. Because of the *Principle of Equivalence*[3] it is always possible to choose *locally* a reference frame in which the metric takes the form (4.2), i.e. that *locally* erases the effect of the gravitational field. These reference frames are free falling frames. The magnitude $d\tau = ds$ is called *proper time* because it is the time measured by an observer moving with a particle. The expressions (4.1) and (4.2) contain all the kinematic information about the space-time.

In General Relativity ds^2 is invariant with respect to change to *any* reference frame (in Special Relativity only with respect to *inertial frames*). Given its expression it is possible (in principle) to compute the trajectories of any test particle in the universe. To determine this, we *just* need a relation between the metric $g_{ij}(x)$ and the sources of the gravitational field, namely the massive bodies and the energy. It is given by the Einstein equation:

$$G_{ij}(x) = -8\pi G T_{ij}(x) - \Lambda g_{ij}(x), \tag{4.3}$$

where the term G_{ij} is the Einstein tensor, which is a linear combination of second derivatives of $g_{ij}(x)$. The stress-energy tensor T_{ij} is the source term for the mass and the energy (for a derivation, see e.g. [LL66]). Λ is the other source term, called the "cosmological constant", that corresponds to a vacuum energy which may arise from particle physics. The Eq. (4.3) is analogous to the Poisson equation, that relates the gravitational field to the distribution of matter in the Newtonian framework.

Given the assumption of homogeneity and isotropy of spatial sections, it can be shown that the most general permitted form of T_{ij} is that of a perfect fluid (e.g. [Wei72]). It is characterized by the density $\rho(t)$ and pressure $p(t)$, both measured in the frame in which the fluid is at rest. In such system of coordinates the stress-energy tensor of the fluid is [Pee93]

$$T_{ij} = \begin{pmatrix} \rho & 0 & 0 & 0 \\ 0 & p & 0 & 0 \\ 0 & 0 & p & 0 \\ 0 & 0 & 0 & p \end{pmatrix}. \tag{4.4}$$

[3] It has been experimentally verified, up to an uncertainty of 10^{-12} [E+04], that the *inertial mass* is the same that appears in the expression of the gravitational force, the *gravitational mass*.

Actually, in a sufficiently small region of spacetime (with not too high mass density) it is possible to use a weak field approximation, derived from Eqs. (4.3) and (4.4). It gives rise to the modified Poisson equation

$$\nabla^2_{\mathbf{r}}\Phi(\mathbf{r}) = 4\pi G\left(\rho(\mathbf{r}) + 3p\right) - \Lambda, \tag{4.5}$$

where $\Phi(\mathbf{r})$ is related to the Newtonian gravitational potential (see Eq. (4.63)) and $\mathbf{r}$ is a small distance about a free-falling observer. The pressure p which appears in Eq. (4.5) has different expressions depending on the kind of fluid assummed:

1. For an ideal gas of particles with $v \ll 1$ (where we have chosen unities in which the speed of light is unity), we have the standard relation $p = \rho\left\langle v^2\right\rangle/3$, where $\left\langle v^2\right\rangle$ is the r.m.s. particle velocity. Because $\left\langle v^2\right\rangle \sim \left\langle |v|\right\rangle^2$ (e.g. [Hua87]) it follows that $\rho \gg p$ and we obtain the standard Poisson equation (for $\Lambda = 0$).

2. For relativistic particles (e.g. photons), the pressure is equal to $p = \rho/3$ (e.g. [Wei72]). Therefore the corrections to the Newtonian Poisson equation are important, giving a factor of 2 in the source term.

It is possible to derive simply [Pee93] a conservation equation that relates the rate of change of the density with the density itself and the pressure. Let us consider a sphere of matter whose volume V changes slowly with time. The Einstein relation $U = m$ (e.g. [LL66]) gives that the energy density of the sphere can be expressed, neglecting the gravitational binding energy, as

$$U = \rho V. \tag{4.6}$$

Differentiating (4.6) with to respect to t, and using that $\partial U/\partial t = -p\partial V/\partial t$, we have

$$-p\frac{\partial V}{\partial t} = \rho\frac{\partial V}{\partial t} + V\frac{\partial \rho}{\partial t}, \tag{4.7}$$

and rearranging terms we obtain finally

$$\frac{\partial \rho}{\partial t} = -(\rho + p)\frac{\partial \ln V}{\partial t}. \tag{4.8}$$

We will use this relation when studying solutions of the Friedmann equation.

4.3 The Friedmann-Robertson-Walker metric

Using the homogeneity and isotropy of the spatial sections, it is possible to write (e.g. [Wei72]) the spatial part of the metric in coordinates in which it takes the form:

$$d\mathbf{l}^2 = \frac{dr^2}{1 + \varkappa\frac{r^2}{A^2(t)}} + r^2(\sin^2\theta d\phi^2 + d\theta^2). \tag{4.9}$$

The parameter $\varkappa$, that defines the *curvature*, can take three different values, associated to three different possible geometries of the universe[4]:

[4] We have chosen the units of r in such a way that $\varkappa$ is normalized to unity. For the geometry of the universe what is of relevance is only the sign of $\varkappa$ and not its magnitude.

- $\varkappa = 0$, corresponding to *flat space*.
- $\varkappa = 1$, corresponding to a *closed space*.
- $\varkappa = -1$ corresponding to an *open space*.

It is convenient to make the following change of variables in the metric (4.9):

$$r = A \sin\chi \qquad \text{with } \chi \in [0, \pi], \text{ for } \varkappa = 1 \tag{4.10a}$$
$$r = A\chi \qquad \text{with } \chi \in [0, \infty[, \text{ for } \varkappa = 0 \tag{4.10b}$$
$$r = A \sinh\chi \qquad \text{with } \chi \in [0, \infty[, \text{ for } \varkappa = -1. \tag{4.10c}$$

In these new coordinates, the metric (4.9) is:

$$d\mathbf{l}^2 = A^2(t) \left[d\chi^2 + \left\{ \begin{array}{c} \sin^2\chi \\ \chi^2 \\ \sinh^2\chi \end{array} \right\} (\sin^2\theta d\phi^2 + d\theta^2) \right], \tag{4.11}$$

for $\varkappa = 1$, $\varkappa = 0$ and $\varkappa = -1$ respectively. Two things are important in this choice of coordinates to write the metric. First of all, we have chosen a metric which is explicitly isotropic at each point of the universe. Secondly, it is simple [Pee93] to show that $\chi =$ constant is a solution of the equation of motion, i.e., a piece of matter will move with $r(t) = A(t)$. This is the phenomenon of *expansion* (if $\dot{A}(t) > 0$) or *contraction* (if $\dot{A}(t) < 0$). The universe is currently in a phase of expansion, but it is not excluded that in the future it might enters a phase of contraction.

4.4 The Friedmann equation

To derive the evolution of the universe from the FRW metric computed above (for each case of a flat, closed and open universe), we need to determine the evolution of the scale factor $A(t)$. The evolution is described by the Einstein equation (4.3) substituting the appropriate expression for G_{ij} in terms of the function $A(t)$, density ρ and pressure p. This gives the two equations:

$$\left(\frac{\dot{A}}{A}\right)^2 = \frac{8\pi G\rho}{3} - \frac{\varkappa}{A^2} \tag{4.12a}$$

$$2\frac{\ddot{A}}{A} + \left(\frac{\dot{A}}{A}\right) + \frac{\varkappa}{A^2} = -8\pi G p. \tag{4.12b}$$

The first equation (4.12a) is the "Friedmann equation". In both equations we have incorporated the cosmological constant Λ in the energy density ρ. Combining both equations we obtain

$$\frac{\ddot{A}}{A} = -\frac{4\pi G}{3}(\rho + 3p). \tag{4.13}$$

This last equation can in fact be obtained from the "modified Poisson equation" (4.5), i.e. from Newtonian physics, modulo the pressure term that has a relativistic origin. Indeed integrating again Eq. (4.13) we obtain the Friedmann

equation (4.12a) where $\varkappa$ acts as an integration constant. The curvature of the universe $\varkappa$ is fixed by the matter content of the universe. Let us show this explicitly. We define the Hubble constant[5] $H(t)$ as

$$H(t) = \frac{\dot{A}(t)}{A(t)}, \tag{4.14}$$

and the critical density ρ_c as the density that, for a given rate of expansion, corresponds to a flat universe, i.e,

$$\rho_c = \frac{3H^2}{8\pi G}. \tag{4.15}$$

We define the density parameter Ω_T as the ratio between the total density and the critical density. Using (4.12a) we have therefore

$$\Omega_T(t) = \frac{\rho(t)}{\rho_c(t)} = \frac{8\pi G\rho(t)}{3H(t)^2}. \tag{4.16}$$

At $t = t_0$, the Friedmann equation (4.12a) takes the form

$$\frac{\varkappa}{A_0^2} = \frac{8\pi G\rho(t_0)}{3H_0^2} - H_0^2 = H_0^2(\Omega_T - 1), \tag{4.17}$$

where $A_0 = A(t_0)$, $H_0 = H(t_0)$ and $\Omega_T = \Omega(t_0)$ are the values of these parameters at the present time. From Eq. (4.17) it follows that the sign of $\varkappa$ depends on the density parameter Ω_T. Finally, we can write Friedmann equation (4.12a) as

$$\left(\frac{\dot{a}}{a}\right)^2 = \frac{8\pi G\rho}{3} + H_0^2(1 - \Omega_T)a^{-2}, \tag{4.18}$$

where we have defined the adimensional scale factor $a = A/A_0$.

4.4.1 Evolution of the density with time

The density ρ can be of different types, with different possible evolution during the expansion. We can derive this different behavior using the conservation equation (4.8). Considering that $V \sim a^3$ and therefore $\partial \ln V/\partial t = 3\dot{a}/a$, we have the equation

$$\frac{\partial \rho}{\partial t} = -3(\rho + p)\frac{\dot{a}}{a}. \tag{4.19}$$

It is straightforward to solve Eq. (4.19) for the following cases:

- Non-relativistic matter ($p \ll \rho$): its density will decay (as expected) in proportion to the inverse of the volume i.e.

$$\rho_M(a) = \rho_M(a_0)a^{-3}. \tag{4.20}$$

- Relativistic matter (radiation, $\rho + p = 2\rho$). The density decays more rapidly than for the case of non-relativistic matter, i.e.

$$\rho_R(a) = \rho_R(a_0)a^{-4}. \tag{4.21}$$

[5] It is actually not a constant but a function of time.

This is because photons, or more generally massless particles, loose energy by the "stretching" of their wavelength λ during the expansion (see the discussion of the redshift, section 4.4.5). Through the De Broglie relation, it follows $E \propto 1/\lambda \sim 1/a$.

- Vacuum energy density does not vary with time ($\rho = -pc^2$) and

$$\rho_\Lambda(a) = \rho_\Lambda(a_0). \tag{4.22}$$

We can write the Friedmann equation (4.18) in the very convenient form[6]

$$\left(\frac{\dot{a}}{a}\right)^2 = H_0^2 \left[\Omega_M a^{-3} + \Omega_R a^{-4} + \Omega_\Lambda + (1 - \Omega_T) a^{-2}\right], \tag{4.23}$$

where the Ω_i are defined as

$$\Omega_i = \frac{\rho}{\rho_c} \frac{\rho_i(a_0)}{3H_0^2/8\pi G}, \tag{4.24}$$

where ρ_c is the critical density defined above in Eq. (4.15). The different density parameters are computed at the current time. Ω_M corresponds to non-relativistic matter, Ω_R to relativistic one (radiation) and Ω_Λ cosmological constant. Ω_T is the total density at the current time, i.e.,

$$\Omega_T = \Omega_M + \Omega_R + \Omega_\Lambda. \tag{4.25}$$

They are the so called *cosmological parameters* which characterize the evolution of the FRW universe. A great effort in contemporary cosmology is devoted to their determination. Their current values, measured by a combination of experiments[7], correspond to a flat universe with

$$\begin{aligned} \Omega_T &= 1.02 \pm 0.02 \\ \Omega_M &= 0.27 \pm 0.04 \\ \Omega_\gamma &= (4.9 \pm 0.5) \times 10^{-5} \\ \Omega_\nu &< 0.015 \\ \Omega_\Lambda &= 0.73 \pm 0.04, \end{aligned} \tag{4.26}$$

where Ω_γ corresponds to photons, Ω_ν to neutrinos and hence

$$\Omega_R = \Omega_\gamma + \Omega_\nu. \tag{4.27}$$

More than 80% of the matter content (i.e. the energy given by Ω_M) consists of "dark matter", non-baryonic, non-visible and still of undetermined composition. Inspecting Eq. (4.23) it is clear that at some sufficiently early time the Universe was dominated by the radiation. The moment at which the radiation density

[6] This expression neglects the fact that particles that were relativistic in the past (e.g. neutrinos, that have a very small mass) have lost energy with the expansion (and thus velocity) and may therefore be at a later time non-relativistic.

[7] Essentially measures of the anisotropies on the CMB, observations of large scale structure (2dF, SDSS) and supernovae. For a review see [E$^+$04].

and matter density was equal is referred to as "time of equality" t_{eq}. The correspondent scale factor is called "a of equality" and, for the parameters (4.26) it is

$$a_{eq} = \frac{\Omega_R}{\Omega_M} \approx 5000. \tag{4.28}$$

Analogously, we define the moment at which the cosmological constant Λ dominates the matter by $t_{c\Lambda}$. The correspondent scale factor is

$$a_{c\Lambda} = \left(\frac{\Omega_M}{\Omega_\Lambda}\right)^{1/3} \approx 0.7. \tag{4.29}$$

4.4.2 Some solutions of the Friedmann equation

It is possible to solve Eq. (4.23) analytically, to obtain a solution in a parametric form, i.e. $t = t(a)$ (but not $a = a(t)$). However, in the case of a flat universe ($\Omega_T = 1$), it is possible to derive simple analytic solutions for matter-dominated universes ($\Omega_T = \Omega_M$), radiation-dominated ($\Omega_T = \Omega_R$) (both with zero cosmological constant), and universes dominated by the cosmological constant ($\Omega_T = \Omega_\Lambda$). We have:

- Flat matter dominated without cosmological constant, known as the Einstein – de Sitter (EdS) universe ($\Omega_M = \Omega_T = 1$, $\Omega_R = 0$, $\Omega_\Lambda = 0$). The solution is simply

$$a(t) = \left(\frac{t}{t_0}\right)^{2/3} \qquad \frac{9}{4}H_0^2 t_0^2 = 1. \tag{4.30}$$

- Flat radiation dominated ($\Omega_M = 0$, $\Omega_R = \Omega_T = 1$, $\Omega_\Lambda = 0$). The solution is

$$a(t) = \left(\frac{t}{t_0}\right)^{1/2} \qquad 4H_0^2 t_0^2 = 1. \tag{4.31}$$

- Flat dominated by the cosmological constant ($\Omega_M = 0$, $\Omega_R = 0$, $\Omega_\Lambda = \Omega_T = 1$). The solution is an exponential expansion

$$a(t) = e^{H_0 \Omega_\Lambda^{1/2}(t-t_0)}. \tag{4.32}$$

4.4.3 The Age of the universe

We can compute the current age t_0 of the Universe using the Friedmann equation (4.18):

$$\begin{aligned} t_0 &= \int_0^{t_0} dt = \int_0^{a_0} \frac{da}{\dot{a}} \\ &= \frac{1}{H_0}\int_0^1 \frac{da}{a\left[\Omega_M a^{-3} + \Omega_R a^{-4} + \Omega_\Lambda + (1-\Omega_T)a^{-2}\right]^{1/2}}. \end{aligned} \tag{4.33}$$

We can neglect the time during the radiation-dominated era because it is comparatively very short. The integral can be only computed for simple cases. For

example, for a flat matter-dominated universe with zero cosmological constant, we have

$$t_0 = t_H \int_0^1 da\, a^{1/2} = \frac{2}{3} t_H, \tag{4.34}$$

where we have defined the Hubble time as

$$t_H = \frac{1}{H_0}. \tag{4.35}$$

In general, the Hubble time at any scale factor a is:

$$t_H(a) = \frac{a}{\dot{a}} = a^2 \left[\Omega_M a + \Omega_R + \Omega_\Lambda a^4 + (1-\Omega_T)a^2\right]^{-1/2}. \tag{4.36}$$

The age of the universe is always of the order of the Hubble time, except if (4.33) diverges, for example if $\Omega_\Lambda = 1$. The age of the universe will be then a function of a_{eq}, if finite. A realistic numerical computation with the parameters of (4.26) gives

$$t_0 \approx 0.6 t_H. \tag{4.37}$$

4.4.4 Photon propagation and the size of the horizon

Let us compute the path travelled by a photon emitted from the position $r = 0$ (and therefore $\chi = 0$, c.f. Eq. (4.9)). Photons propagate with $ds^2 = 0$. Using the metric (4.9) (and considering that the photon propagates in the direction $\phi = 0 = \theta$, which is always possible due to the spherical symmetry of the metric), we have:

$$d\chi = \frac{dt}{A(t)}. \tag{4.38}$$

Therefore

$$\begin{aligned} \chi &= \frac{1}{A_0} \int_{t_1}^{t_0} \frac{dt}{a(t)} = \int_{a_1}^{a_0} \frac{da}{a\dot{a}} \\ &= \frac{d_H}{A_0} \int_{\frac{a_1}{a_0}}^{1} \frac{da}{a^2 \left[\Omega_M a^{-3} + \Omega_R a^{-4} + \Omega_\Lambda + (1-\Omega_T)a^{-2}\right]^{1/2}}, \end{aligned} \tag{4.39}$$

where d_H is the *Hubble distance* defined as $d_H = ct_H$. Depending on the geometry of the Universe, the physical distance r will be, using (4.10),

$$r = A_0 \times \begin{cases} \chi & \text{for a flat universe} \\ \sin\chi & \text{for a closed universe} \\ \sinh\chi & \text{for an open universe.} \end{cases} \tag{4.40}$$

A very important quantity is the size of the *horizon*. The horizon is the maximal distance χ_{hor} which can be traveled by a photon that has been emitted at the beginning of the Universe, i.e. when $a \to 0$. The size of the horizon thus indicates which scales have had time to interact during the history of the Universe. From (4.39), the present size of the horizon can be computed as

$$\chi_{hor} = \frac{d_H}{A_0} \int_0^1 \frac{da}{a^2 \left[\Omega_M a^{-3} + \Omega_R a^{-4} + \Omega_\Lambda + (1-\Omega_T)a^{-2}\right]^{1/2}}. \tag{4.41}$$

The obvious generalization of (4.41) for the size of the horizon at any time is

$$\chi_{hor}(a) = \frac{d_H}{A_0} \int_0^{a/a_0} \frac{da}{a^2 \left[\Omega_M a^{-3} + \Omega_R a^{-4} + \Omega_\Lambda + (1-\Omega_T) a^{-2}\right]^{1/2}}. \tag{4.42}$$

The corresponding physical distance today is given by (4.40) replacing a_0 by $a(t)$. From (4.40) and (4.39) we conclude that the horizon for the different epochs is (for a flat universe)

$$r_{hor} = A_0 \times \begin{cases} a\chi_{hor}(a) \sim a^2 & \text{for radiation-dominated} \\ a\chi_{hor}(a) \sim a^{3/2} & \text{for matter-dominated} \\ a\chi_{hor}(a) \to \infty & \Lambda\text{-dominated.} \end{cases} \tag{4.43}$$

where we have assumed that the photons can travel freely through the Universe[8]. The size of the horizon is of great physical importance also because it gives the scales up to which a Newtonian description is valid. Using Eq. (4.39), it is simple to see that the size of the horizon is proportional to the Hubble length $d_H(a)$ for the radiation-dominated and matter dominated era. The case of Λ-dominated era is different because the integral (4.39) diverges, and therefore the size of the horizon depends on a model dependent cutoff.

The horizon problem

At early times the universe was ionized, i.e. the electrons and protons existed as free charges. The number of electrons was sufficiently high so that the interaction rate of Compton scattering ($e^- + \gamma \longrightarrow e^- + \gamma$) was so large that the mean free path of the photons was very small. The universe was thus opaque for the electromagnetic radiation. With the expansion, the universe cooled off up to a moment in which the electrons and protons could combine to form neutral Hydrogen. This is called *recombination*. Therefore, at this time, the number of free electrons dropped and consequently, also the reaction rate of Compton scattering. This is called *decoupling*. The mean free path of the photons became of the order of the Hubble radius and thus the universe became transparent of the radiation. There are these photons that we observe today in the CMB.

Photons that come from opposite directions on the sky were not causally connected at decoupling because at this time they were separated by a distance greater than the Hubble radius. Therefore the isotropy observed in the CMB cannot be produced by a causal process, given the model we have described. The principal proposed explanations for this large scale homogeneity are based on modifications of the FRW model. Currently the most popular such model is *inflation*. The basic idea in such models is to modify the nature of the density (by particle physics processes that we are not going to detail) to increase dramatically the size of the horizon at early times. The essential idea (e.g. [Ric01]) can be given by considering a Λ-dominated universe for $a \to 0$ (or, equivalently, $\rho(a) = constant$ in the same limit). We have seen above that for these kind of models the size of the horizon can be made arbitrarily large.

[8] This is not the case in the radiation epoch in a realistic model.

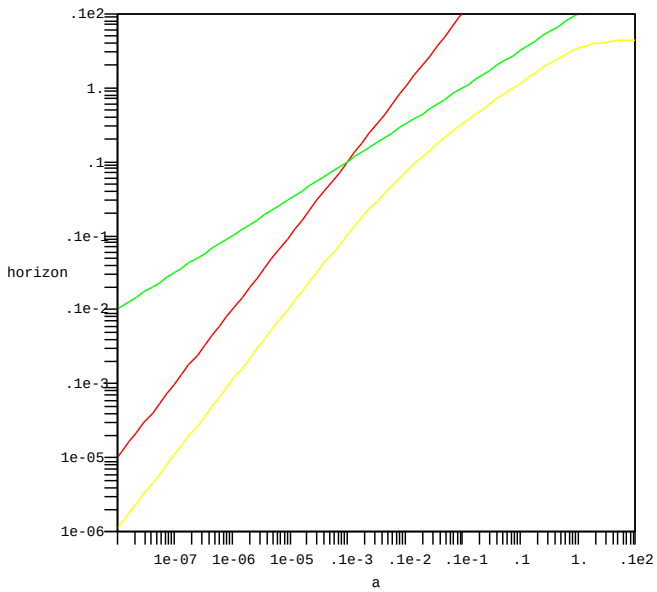

Figure 4.3: Size of the horizon (clear line, in units of d_H) as a function of the scale factor $a(t)$, normalized to the scale factor today for the cosmological parameters (4.26). The two power-law lines are $\sim a$ and $\sim a^{1/2}$. Observe how the horizon follows the behavior $\sim a$ for the radiation-dominated era, then $\sim a^{1/2}$ for the matter-dominated era and finally turning over a constant in the Λ-dominated era.

4.4.5 Hubble law and redshift

From Eq. (4.40) it is possible to write a simple relation between the distance and the recession velocity of a galaxy (measured at the current time):

$$v = \dot{A}_0 \times \begin{cases} \chi & \text{for a flat universe} \\ \sin\chi & \text{for a closed universe} \\ \sinh\chi & \text{for an open universe.} \end{cases} \tag{4.44}$$

If the galaxy is close to the observer, the geometry of the universe can always be considered flat (i.e. if $\chi \ll 1$ then $\sin\chi \simeq \chi \simeq \sinh\chi$). Then (4.44) can be approximated by

$$v = \dot{A}_0 \chi = H_0 d, \tag{4.45}$$

where d is the distance of the galaxy. The relation (4.45) is called *Hubble's law*. One way to check this relation and measure H_0 is by the observation of the shifts in frequency of light emitted by distant sources, such as galaxies. Consider a light pulse that have been emmited at time t_1 by a galaxy at χ_1. The crest of the pulse follows $ds^2 = 0$, and then using the metric (4.11) (with Eq. (4.2)) we have:

$$\chi_1 = \int_{t_0}^{t_1} \frac{dt}{A(t)}. \tag{4.46}$$

A typical galaxy that follows the Hubble flow has constant χ. Hence, the next wave crest leaves χ_1 at time $t_1 + \delta t_1$ and will arrive at the observer at time $t_0 + \delta t_0$. Then:

$$\chi_1 = \int_{t_0+\delta t_0}^{t_1+\delta t_1} \frac{dt}{A(t)}. \tag{4.47}$$

Subtracting (4.46) from (4.47), and taking into account that $A(t)$ changes very little during the period of a light signal, we have

$$\frac{\delta t_0}{A(t_0)} = \frac{\delta t_1}{A(t_1)}. \tag{4.48}$$

The frequency ν_0 observed is thus related by the emmited one ν_1 by the relation

$$\frac{\nu_0}{\nu_1} = \frac{\delta t_1}{\delta t_0} = \frac{A(t_1)}{A(t_0)}. \tag{4.49}$$

It is conventionally expressed in terms of the *redshift parameter* z, defined as

$$z = \frac{\nu_1}{\nu_0} - 1. \tag{4.50}$$

Then using Eq. (4.49) we obtain the relation

$$z = \frac{a(t_0)}{a(t_1)} - 1. \tag{4.51}$$

For close galaxies $\chi \sim d \to 0$ and $t_0 \to t_1$. We can therefore write

$$z \simeq \frac{\dot{A}(t_0)(t_0 - t_1)}{A(t_0)} \simeq \dot{A}(t_0)\chi \simeq H_0 d, \tag{4.52}$$

which gives the relation of the measured redshift of a galaxy with its distance. This relation is used to compute H_0 from the observations. The distance of the galaxies has to be measured directly. For example, a powerful method to determine H_0 at large scales, make use of *supernovae*, which have typically the same luminosity irrespective the galaxy in which they are observed.

4.5 Perturbing the FRW model: structure formation

Up to now we have described a universe constituted by an exactly homogeneous and isotropic distribution of radiation and matter. In reality, the universe is highly inhomogeneous, containing galaxies organized in clusters, voids, filaments, walls, etc. We will discuss the mechanism of the formation of these structures. Observations of the CMB indicate that the universe, at the epoch of recombination, was very homogeneous, with fluctuations in the density of about 10^{-5}. It is then natural to consider a perturbation of the FRW metric and to study its evolution. As we have noted in the previous section, general relativistic effects are appreciable only for scales comparable to or larger than the Hubble distance. Therefore we consider the problem in two limiting cases:

1. For scales larger than d_H we use general relativistic perturbation theory.

2. For scales smaller than the horizon[9], we use simply Newtonian gravity.

4.5.1 Perturbation theory in the Newtonian limit

The natural way to obtain a Newtonian fluid theory is to take the weak field limit of the Einstein equations (4.3) (e.g. [Pee80]). However, it is much simpler to start directly from the fluid equations for a self-gravitating fluid (e.g. [LL79]). This system is described by a continuity equation, the Euler equation and the Poisson equation:

$$\frac{\partial \rho}{\partial t} + \nabla_{\mathbf{r}} \cdot (\rho \mathbf{v}) = 0 \tag{4.53a}$$

$$\frac{\partial \mathbf{v}}{\partial t} + (\mathbf{v} \cdot \nabla_{\mathbf{r}})\mathbf{v} = -\frac{1}{\rho}\nabla_{\mathbf{r}} p - \mathbf{g} \tag{4.53b}$$

$$\nabla_{\mathbf{r}} \times \mathbf{g} = \mathbf{0} \tag{4.53c}$$

$$\nabla_{\mathbf{r}} \cdot \mathbf{g} = -4\pi G\rho. \tag{4.53d}$$

The symbol $\nabla_{\mathbf{r}}$ makes explicit that the derivative is with respect to the variable $\mathbf{r}$. The velocity $\mathbf{v}$ is expressed in an inertial frame. The gravitational acceleration $\mathbf{g}$ is connected with the gravitational potential Φ defined in Eq. (4.5) by

$$\mathbf{g} = -\nabla_{\mathbf{r}}\Phi. \tag{4.54}$$

The Eqs. (4.53) are in *Eulerian coordinates*. In this formulation of fluid theory, the variables are the local density $\rho(\mathbf{r})$ and the local velocity $\mathbf{v}(\mathbf{r})$. Another formulation is the *Lagrangian* fluid theory, in which the evolution of the system is expressed in terms of displacements of volume elements of the fluid (see section 5.5).

It is convenient to write Eqs. (4.53) in *comoving* coordinates, i.e. in coordinates that follow the expansion of the background model. We define the comoving coordinates $\mathbf{x}$ as:

$$\mathbf{r} = a(t)\mathbf{x}, \tag{4.55}$$

[9] Remember that the size of the horizon changes, in general, with time.

where $\mathbf{r}$ is the (physical) coordinate of a piece of fluid about the observer and $a(t)$ the scale factor (whose time dependence is known through Friedmann equation (4.12a)). The change of coordinates (4.55) implies the following relations between derivatives with respect to physical and comoving coordinates:

$$\nabla_{\mathbf{x}} = a(t)\nabla_{\mathbf{r}} \tag{4.56a}$$

$$\left(\frac{\partial f}{\partial t}\right)_r = \left(\frac{\partial f}{\partial t}\right)_x - \frac{\dot{a}}{a}\left(\mathbf{x}\cdot\nabla_{\mathbf{x}}\right) f. \tag{4.56b}$$

We define the *peculiar velocity* $\mathbf{v}_{\mathrm{pec}}$ as the velocity of a particle with respect to the expanding background (which is usually called the *Hubble flow*):

$$\mathbf{v} = \dot{\mathbf{r}} = \dot{a}\mathbf{x} + \mathbf{v}_{\mathrm{pec}}(\mathbf{x}, t), \tag{4.57}$$

The peculiar velocity $\mathbf{v}_{\mathrm{pec}}$ is therefore the physical velocity $\mathbf{v}$ with the Hubble flow subtracted:

$$\mathbf{v}_{\mathrm{pec}} = \dot{\mathbf{r}} - H\mathbf{r} = a\dot{\mathbf{x}}. \tag{4.58}$$

The physical acceleration can be expressed in terms of comoving coordinates as

$$\ddot{\mathbf{r}} = a\ddot{\mathbf{x}} + 2\dot{a}\dot{\mathbf{x}} + \ddot{a}\mathbf{x}. \tag{4.59}$$

The peculiar gravitational acceleration is defined as the physical acceleration subtracting the acceleration of the background:

$$\mathbf{g}_{\mathrm{pec}} = \ddot{\mathbf{r}} - \ddot{a}\mathbf{x} = \ddot{\mathbf{r}} - \frac{\ddot{a}}{a}\mathbf{r} = a\left[\ddot{\mathbf{x}} + 2H\dot{\mathbf{x}}\right]. \tag{4.60}$$

The peculiar gravitational acceleration obeys a modified Poisson equation (4.5). Using Eq. (4.54) and Eq. (4.60), we have

$$\mathbf{g}_{\mathrm{pec}} = -\nabla_{\mathbf{r}}\Phi - \ddot{a}\mathbf{x}. \tag{4.61}$$

We can rewrite Eq. (4.61) in comoving coordinates, using the transformation (4.56b), as

$$\mathbf{g}_{\mathrm{pec}}(\mathbf{x}, t) = -\frac{1}{a}\nabla_{\mathbf{x}}\left[\Phi(\mathbf{x}, t) - \frac{2}{3}\pi G\rho_0(t)x^2\right] \tag{4.62}$$

where we have used Eq. (4.13) (with $\rho \gg p$) to substitute the value of $\ddot{a}$. We define the new potential $\phi(\mathbf{x}, t)$ as

$$\phi(\mathbf{x}, t) = \Phi(\mathbf{x}, t) - \frac{2}{3}\pi G\rho_0(t)x^2, \tag{4.63}$$

and therefore Eq. (4.62) can be simply rewritten as

$$\mathbf{g}_{\mathrm{pec}}(\mathbf{x}, t) = -\frac{1}{a}\nabla_{\mathbf{x}}\phi(\mathbf{x}, t). \tag{4.64}$$

The Poisson equation (4.53d) for the peculiar gravitational field is, using Eq. (4.62):

$$-\nabla_{\mathbf{x}}\cdot\mathbf{g}_{\mathrm{pec}}(\mathbf{x}, t) = 4\pi G\left[\rho(\mathbf{x}, t) - \rho_0\right]. \tag{4.65}$$

We see that the expansion introduces a negative background in the Poisson equation, which is analogous to the negative background introduced by the electro-neutrality in a plasma (see chapter 6).

We want now to perturb the set of equations (4.53) around the FRW solution i.e. with mean density of the universe $\rho_0(t)$ (that depends only on time). Let's therefore define the fluctuations $\delta(\mathbf{x}, t)$ as

$$\rho = \rho_0(t)\left(1 + \delta(\mathbf{x}, t)\right). \tag{4.66}$$

In comoving coordinates it is then straightforward (using also Eq. (4.65)) to show that Eqs. (4.53) become:

$$\frac{\partial \delta}{\partial t} + \frac{1}{a}\nabla_{\mathbf{x}} \cdot \left(\mathbf{v}_{\mathrm{pec}}(1+\delta)\right) = 0 \tag{4.67a}$$

$$\frac{\partial \mathbf{v}_{\mathrm{pec}}}{\partial t} + \frac{\dot{a}}{a}\mathbf{v}_{\mathrm{pec}} + \frac{1}{a}\left(\mathbf{v}_{\mathrm{pec}} \cdot \nabla_{\mathbf{x}}\right)\mathbf{v}_{\mathrm{pec}} = \frac{1}{a}\mathbf{g}_{pec} - \frac{1}{\rho a}\nabla_{\mathbf{x}} p \tag{4.67b}$$

$$\nabla_{\mathbf{x}} \times \mathbf{g}_{\mathrm{pec}} = \mathbf{0} \tag{4.67c}$$

$$\nabla_{\mathbf{x}} \cdot \mathbf{g}_{\mathrm{pec}} = -4\pi G a \rho_0 \delta. \tag{4.67d}$$

4.5.2 Evolution of fluctuations in the linear regime

It is not possible to solve analytically the set of equations (4.67). As the fluctuations are small at early time, we perform a series expansion in powers of δ. Formally we write [GBRW86] as:

$$\delta(\mathbf{x}, t) = \sum_{n=1}^{\infty} \epsilon^n \delta^{(n)}(\mathbf{x}, t), \quad \mathbf{v}_{\mathrm{pec}}(\mathbf{x}, t) = \sum_{n=1}^{\infty} \epsilon^n \mathbf{v}_{\mathrm{pec}}^{(n)}(\mathbf{x}, t) \tag{4.68}$$

where $\epsilon \ll 1$ is a parameter we set to 1 at the end of the calculation. The expansion (4.68) assumes that both fluctuations in the density and the velocities are small[10]. Multiplying (4.67a) by ρ and (4.67b) by v, taking the divergence of the result and keeping terms linear in the density contrast and the peculiar velocity we obtain:

$$\frac{\partial^2 \delta}{\partial t^2} + 2\frac{\dot{a}}{a}\frac{\partial \delta}{\partial t} = \frac{\nabla^2 p}{\rho_0 a^2} + 4\pi G \rho_0 \delta, \tag{4.69}$$

where we have used Eq. (4.67d) to eliminate the gravitational field. The characteristic time t_G of a pure gravitational collapse (i.e. with $p = 0$ and with no expansion) is given by the only combinations of the remaining physical quantities with dimensions of time, $t_G \sim (G\rho_0)^{-1/2}$. Explicitly, setting $a = 1$, $\dot{a} = 0$ and $p = 0$ in Eq. (4.69), the solution of this partial differential equation is a combination of two exponentials (a growing and decaying solution)

$$\delta(\mathbf{x}, t) = A(x) e^{\sqrt{4\pi G \rho_0}(t - t_i))} + B(x) e^{-\sqrt{4\pi G \rho_0}(t - t_i)}, \tag{4.70}$$

with the coefficients $A(x)$ and $B(x)$ fixed by the density fluctuations at the initial time, $\delta(\mathbf{x}, t_i)$ and $\dot{\delta}(\mathbf{x}, t_i)$. Indeed one can rewrite (4.70) in the simple

[10] Let us give a quantitative idea of what is a *small* fluctuation. Consider an homogeneous background with density ρ_0 and a spherical region of radius R_0 with a tiny over-density, sufficient to cause this region to collapse. The relation between the density $\rho_0 + \delta\rho$ and the new radius R of the over-density region is $|R_0/R|^3 = (1 + \delta\rho)$. What's the new radius of the sphere as a function of the over-density? If we assume a small fluctuation in the density, e.g., $\delta = 0.1$, the new radius will be $R_0/R \approx 1.03$. When the fluctuations start to be large, e.g. $\delta = 1$, the new radius will be $R_0/R \approx 1.26$.

form

$$\delta(\mathbf{x},t) = \delta(\mathbf{x},t_i)\cosh\left[\sqrt{4\pi G\rho_0}(t-t_i)\right] + \frac{\dot{\delta}(\mathbf{x},t_i)}{\sqrt{4\pi G\rho_0}}\sinh\left[\sqrt{4\pi G\rho_0}(t-t_i)\right]. \tag{4.71}$$

4.5.3 Eulerian linear fluid theory without pressure

Let us solve first Eq. (4.69) without pressure in an EdS universe. Using Eqs. (4.20) and (4.30) in Eq. (4.69) we obtain:

$$\frac{\partial^2\delta}{\partial t^2} + \frac{4}{3t}\frac{\partial\delta}{\partial t} = \frac{2}{3t^2}\delta, \tag{4.72}$$

of which the solution is:

$$\begin{aligned}\delta(\mathbf{x},t) &= \frac{3}{5}\left(\delta(\mathbf{x},t_i) + \dot{\delta}(\mathbf{x},t_i)t_i\right)\left(\frac{t}{t_i}\right)^{2/3} \\ &+ \frac{1}{5}\left(2\delta(\mathbf{x},t_i) - 3\dot{\delta}(\mathbf{x},t_i)t_i\right)\left(\frac{t}{t_i}\right)^{-1}.\end{aligned} \tag{4.73}$$

The solution is also (as in (4.70)) a combination of growing and decaying modes, but the expansion has the effect of slowing down the growth or decay. The velocity field is found noting that it obeys, using the continuity equation (4.67a), the potential form

$$\nabla\cdot\mathbf{v}_{\rm pec} = -a\frac{\partial\delta}{\partial t}, \tag{4.74}$$

whose solution is

$$\mathbf{v}_{\rm pec}(\mathbf{x},t) = -a\int d^3x'\frac{\partial\delta(\mathbf{x}',t)}{\partial t}\frac{(\mathbf{x}-\mathbf{x}')}{|\mathbf{x}-\mathbf{x}'|^3}, \tag{4.75}$$

where we have used that in the linear approximation $\nabla\times\mathbf{v}_{\rm pec} = \mathbf{0}$ because of Eqs. (4.67b) and (4.67c). Therefore, in the EdS universe, using solution (4.73), the velocity field scales with time as

$$\begin{array}{ll}\mathbf{v}_{\rm pec}\sim t^{1/3} & \text{for the growing mode} \\ \mathbf{v}_{\rm pec}\sim t^{-4/3} & \text{for the decaying mode.}\end{array} \tag{4.76}$$

Moreover it is possible to find a simple relation between $\mathbf{v}_{\rm pec}$ and $\mathbf{g}_{\rm pec}$. From (4.67b) (in the linear approximation) we know that $\mathbf{v}_{\rm pec}\propto\mathbf{g}_{\rm pec}$. Then using (4.67a) and the Poisson equation (4.67d) we obtain

$$\mathbf{v}_{\rm pec} = \frac{1}{4\pi G\rho_0\delta}\frac{\partial\delta}{\partial t}\mathbf{g}_{\rm pec}. \tag{4.77}$$

4.5.4 Eulerian linear fluid theory with pressure

We include now the pressure term in the treatment of the problem. To close the system of equations, we need an explicit model for the pressure, i.e., the dependence of the pressure on the density and the velocity field. We will discuss different possibilities (and their physical origin) in chapter 5 and for the moment

we will suppose that the pressure depends only on the density. At linear order we can then write the pressure as

$$p(\rho) = p(\rho_0) + c_s^2 \rho_0 \delta, \tag{4.78}$$

where $c_s^2 \equiv \partial p/\partial \rho$, and c_s is the sound speed in the medium. Therefore Eq. (4.69) is now

$$\frac{\partial^2 \delta}{\partial t^2} + 2\frac{\dot{a}}{a}\frac{\partial \delta}{\partial t} = \left(\frac{c_s}{a}\right)^2 \nabla^2 \delta + 4\pi G \rho_0 \delta. \tag{4.79}$$

To solve this equation it is convenient to go to Fourier space[11], looking for solutions of the form

$$\delta(\mathbf{x}, t) = \frac{1}{(2\pi)^3} \int d^3k \tilde{\delta}(\mathbf{k}, t) e^{i\mathbf{k}\cdot\mathbf{x}}, \quad \lambda = 2\pi a(t)/k, \tag{4.80}$$

where λ is the *physical wavelength*, i.e. the wavelength in physical coordinates (in contrast to k which is in *comoving* coordinates). Therefore, taking the Fourier transform of (4.79) we have

$$\frac{\partial^2 \tilde{\delta}}{\partial t^2} + 2\frac{\dot{a}}{a}\frac{\partial \tilde{\delta}}{\partial t} = \left(4\pi G \rho_0 - \left(\frac{c_s k}{a}\right)^2\right) \tilde{\delta}. \tag{4.81}$$

The r.h.s. term of equation (4.81) vanishes at the *Jeans length* λ_J

$$\lambda_J = c_s (\pi/G\rho_0)^{1/2}. \tag{4.82}$$

In the limit of wavelengths much larger than the Jeans length, i.e., $\lambda_J \ll 1/k$, the first term on the r.h.s. of (4.81) can be neglected. Its solution in an EdS universe (i.e. flat matter dominated without cosmological constant) is a combination of two decaying plane waves

$$\begin{aligned} \delta(\mathbf{x}, t) &= \delta(\mathbf{x}, t_i) \cos\left[3c_s k \left(\frac{t}{6\pi G\rho_0}\right)^{1/3}\right] \left(\frac{t}{t_i}\right)^{-1/3} \\ &+ \dot{\delta}(\mathbf{x}, t_i) \sin\left[3c_s k \left(\frac{t}{6\pi G\rho_0}\right)^{1/3}\right] \left(\frac{t}{t_i}\right)^{-1/3} \end{aligned} \tag{4.83}$$

The equation (4.81), for EdS universes, with a polytropic equation of state ($p(\rho) = A\rho^\gamma$), has a general solution in term of Bessel functions [MT01, TSM+02]. Without entering into the details of the solution, it is simple to see that wavelengths smaller than λ_J (small scales, large k) will oscillate as sound waves because the pressure dominates the dynamics. For large scales (small k) the pressure will be negligible and the modes will grow[12]. This behavior can be understood by the fact that a periodic perturbation of wavelength λ needs a time $\sim \lambda/c_s$ to be dispersed (that is the only characteristic time in Eq. (4.81) neglecting gravity). On the other hand, we have seen that the characteristic

[11] We assume that we are in an infinite space. In a periodic space, one applies the recipes discussed in chapter 3.

[12] To be totally rigorous, the borderline between oscillations and growth is not exactly at λ_J because of the effects of the expansion. For exact expressions see the references cited in the text.

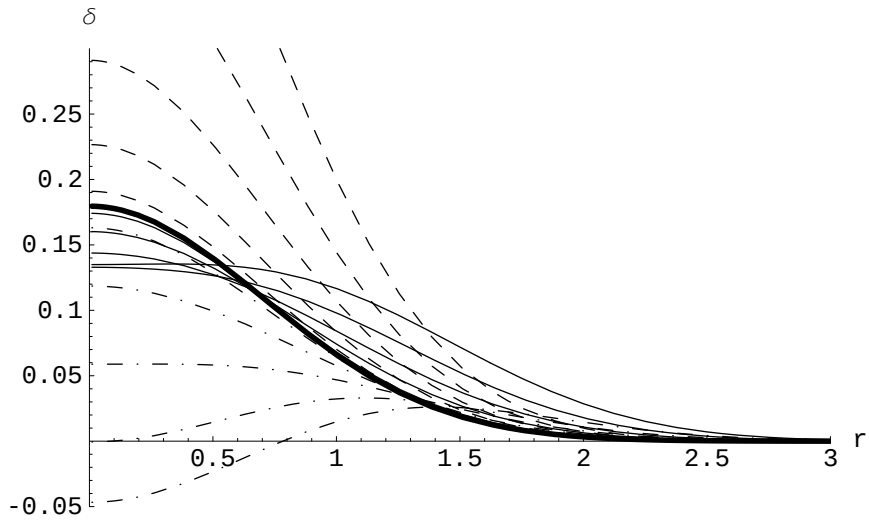

Figure 4.4: Evolution of a perturbation in a non-expanding universe. The parameters are chosen so that $G\rho_0 = 1$ and $c_s = 3$. The initial conditions are $\delta(r, 0) = \exp(-r)$. The thick full line is the initial perturbation. The evolution is given by the full lines. Pure gravitational evolution (i.e. $c_s = 0$) is plotted with dashed lines. Pure pressure evolution $G = 0$, $c_s \neq 0$ in dashed-dotted lines. The times are $t = 0$, 0.1, 0.2, 0.3, 0.4, 0.5 in units of $G\rho_0$. For discussion see the text.

time for clustering is $t_G \sim (\rho_0 G)^{-1/2}$. Demanding that the two timescales are comparable gives the order of magnitude of the Jeans length.

In Fig. 4.4 we show the linear evolution of a perturbation with initial Gaussian density profile with time in a non-expanding universe. The limiting case of pure gravitational evolution shows a rapid growth in the density contrast. The pure pressure evolution shows an oscillating behavior that destroys the initial over density. The case that includes both effects presents an intermediate behavior. At small scales, the growth is suppressed in comparison with the pure gravitational evolution whereas it is amplified at large scales.

4.5.5 Linear theory in general relativity

To describe the growth of perturbations at scales comparable and larger than d_H, or for relativistic particles, at any scale, we need to use general relativity. We are not going to derive here the general relativistic perturbation theory but just give the essential results. The evolution of a perturbation of matter or radiation, in an universe in which it is the dominant species (i.e. radiation perturbations in a radiation-dominated era or matter perturbations in a matter-dominated universe) is given by the expression [Pad93]:

$$\ddot{\tilde{\delta}} + [2 - 3(2\nu - c_s^2)]H\dot{\tilde{\delta}} - \frac{3H^2}{2}(1 - 6c_s^2 + 8\nu - 3\nu^2)\tilde{\delta} = -\frac{k^2}{a^2}c_s^2\tilde{\delta}, \qquad (4.84)$$

where $\nu \equiv p/\rho$. For a radiation-dominated epoch we have $\nu = c_s^2 = 1/3$ and therefore (4.84) is:

$$\ddot{\tilde{\delta}} + H\dot{\tilde{\delta}} + \frac{2H^2}{3}\tilde{\delta} = -\frac{k^2}{a^2}c_s^2\tilde{\delta}, \tag{4.85}$$

and for a matter dominated universe $\nu = c_s^2 \approx 0$ and therefore we have

$$\ddot{\tilde{\delta}} + 2H\dot{\tilde{\delta}} - \frac{3H^2}{2}\tilde{\delta} = -\frac{k^2}{a^2}c_s^2\tilde{\delta}, \tag{4.86}$$

which coincides with the expression found in the Newtonian limit.

Perturbation of radiation in a radiation-dominated universe, $\lambda \gg d_H$

In Eq. (4.85) the pressure is negligible because

$$H^2 \gg \frac{k^2}{a^2}c_s^2. \tag{4.87}$$

Then:

$$\tilde{\delta} \sim \begin{cases} t \propto a^2 & \text{for the growing mode} \\ t^{-1/2} \propto a & \text{for the decaying mode.} \end{cases} \tag{4.88}$$

Perturbation of radiation in a radiation-dominated universe, $\lambda \ll d_H$

In this case the pressure term will dominate because in a radiation-dominated universe, $\lambda_J \sim d_H$. Therefore we will have an oscillatory solution similar to the non-relativistic case illustrated in Fig. 4.4.

Perturbations of matter in a radiation-dominated universe

Here the situation is more complicated because we have to treat a system with different components. In the case of the kind of initial fluctuations currently favored by cosmologists, for scales larger than t_H, the evolution of the matter is driven by the radiation. In the case of scales smaller than d_H the fluctuations in the matter are almost constant because the characteristic time of expansion (for radiation) is much shorter than the characteristic time of clustering for matter. We can compute simply this behavior in the pressure-less Newtonian limit ($\lambda_J \ll \lambda \ll d_H$)

$$\ddot{\tilde{\delta}}_{DM} + 2\frac{\dot{a}}{a}\dot{\tilde{\delta}}_{DM} \approx 4\pi G\rho_{DM}\tilde{\delta}_{DM}, \tag{4.89}$$

where on the r.h.s. of Eq. (4.89) we have neglected the contribution of the fluctuation of the radiation because, as we have seen in the previous case, it oscillates and therefore, on average, it is not a source for clustering. Note that the behavior of the scale factor in (4.89) is given by:

$$\frac{\dot{a}^2}{a^2} = \frac{8\pi G}{3}(\rho_R + \rho_{DM}). \tag{4.90}$$

It is convenient to use the new variable $x \equiv a/a_{\rm eq}$ to rewrite Eq. (4.69) (with the help of (4.90)) as

$$2x(1+x)\frac{d^2\tilde{\delta}_{DM}}{dx^2} + (2+3x)\frac{d\tilde{\delta}_{DM}}{dx} = 3\tilde{\delta}_{DM}, \tag{4.91}$$

whose growing solution behaves as

$$\tilde{\delta}_{DM} = 1 + \frac{3}{2}x, \tag{4.92}$$

which for $a \ll a_{eq}$, is constant, and behaves like the previous growing mode (i.e. $\propto a$ for $a \gg a_{eq}$).

4.5.6 The evolution of initial perturbations

With what we have reviewed above we are in a position to calculate the evolution of fluctuations (in the linear regime). These fluctuations are assumed be generated by some physical process (inflation, for example) that we are not going to study here. We are going to consider a Cold Dark Matter (hereafter CDM) model, the currently most favored by observation. It is a model in which the universe is dominated by non-relativistic massive particles. It is very simple to predict the linear evolution of a perturbation in Fourier space. The evolution depends mainly on two things:

1.– The epoch in which the universe is at a given time. We have seen that generically the growth rate depends on the epoch considered.

2.– The size of the perturbation compared with the size of the horizon *at a given time*. It increases approximately as the scale factor of the universe (i.e. it grows with a) and it can be characterized by its physical wavelength λ at any time. The size of the horizon grows faster, as $\sim a^2$ for a radiation-dominated universe and $\sim a^{3/2}$ for a matter-dominated one. This implies that a perturbation that has a wavelength greater than the horizon at a given time will "enter" the horizon at some time later and, consequently, its growth rate will change. It is therefore important to identify the time of which a perturbation enters the horizon. We will call this moment $a_{\rm ent}(k)$.

Preliminaries

Let us consider a perturbation of initial physical wavelength $\lambda_i(a_i)$ associated with the comoving wavenumber k_i, where $a_i = a(t_i)$:

$$\lambda_i = \frac{2\pi}{k_i} a_i. \tag{4.93}$$

In the linear regime, the size of the perturbation will follow the expansion of the universe

$$\lambda(a) = \lambda_i \frac{a}{a_i}. \tag{4.94}$$

The horizon size is approximately given by the Hubble radius (Eq. (4.36)):

$$d_H(a) = c\, a^2 \left[\Omega_M a + \Omega_R + \Omega_\Lambda a^4 + (1-\Omega_T) a^2\right]^{-1/2}. \tag{4.95}$$

When the mode λ_i enters the horizon we have

$$\lambda_i \frac{a}{a_i} \simeq d_H(a_{\rm ent}). \tag{4.96}$$

Using Eq. (4.93) we can write Eq. (4.96) as

$$\frac{2\pi}{k_i} a \simeq d_H(a_{ent}). \tag{4.97}$$

Eq. (4.97) gives the scale factor a at which the perturbation with initial length λ_i, denoted by the comoving wavenumber k_i through Eq. (4.93), enters the horizon. Perturbations with large k_i enter the horizon earlier, in the radiation-dominated epoch ($a_{ent} < a_{eq}$). Then, using Eqs. (4.95) and (4.97), we have:

$$a_{ent} = H_0 \frac{2\pi}{k_i} \Omega_R^{1/2}. \tag{4.98}$$

Perturbations with small k_i enter the horizon later, in the matter-dominated epoch ($a_{ent} > a_{eq}$). Therefore,

$$a_{ent} = H_0 \left(\frac{2\pi}{k_i}\right)^2. \tag{4.99}$$

The borderline between long and short wavelengths is given by the equality time a_{eq}. The modes which enters the horizon at this moment have comoving wave number denoted k_{eq}.

The Harrison-Zeldovich PS

It is natural to assume that there is no characteristic scale above the horizon and that the primordial PS is has power-law:

$$P(k_i < k_{ent}) \sim k^n. \tag{4.100}$$

Actually, we are going to assume the particular index $n = 1$. This is called the "scale-invariant" or "Harrison-Zeldovich" spectrum (hereafter HZ spectrum). It was proposed for theoretical reasons (which we will outline below) and it has since been observed to be highly consistent with the observations of the CMB. It has the property that the PS when entering the Hubble radius is $\propto 1/k_i^3$. We can see this explicitly using the equations we have derived above. For large wavenumbers ($a_{ent} < a_{eq}$) we have, using Eq. (4.98):

$$P(k, a_{\rm ent}) \simeq P(k_i) \left(\frac{a_{\rm ent}}{a_i}\right)^4 \sim k_i \left(\frac{2\pi}{k_i}\right)^4 \sim \frac{1}{k_i^3}. \tag{4.101}$$

(remember that $P(k) \sim \delta^2$). For small wavevenumbers ($a_{ent} < a_{eq}$) we obtain, using Eq. (4.99):

$$P(k, a_{\rm ent}) \simeq P(k_i) \left(\frac{a_{eq}}{a_i}\right)^4 \left(\frac{a_{\rm ent}}{a_{\rm eq}}\right)^2 \sim k_i \left(\frac{2\pi}{k_i}\right)^4 \sim \frac{1}{k_i^3}. \tag{4.102}$$

This behavior of the PS implies that the variance of the density fluctuations, independently of the moment at which they enter the horizon, have almost the same variance of mass, according to Eq. (3.49) (for a discussion about the applicability of this equation for a spectrum with exactly $n = 1$ see [GSLJP05]):

$$\sigma^2(R) \approx P(k_i) k_i^3|_{k_i = R^{-1}}. \tag{4.103}$$

If the index in the spectrum of (4.100) is $n < 1$, then the variance of the fluctuations with small k_i is larger than that of those with large k_i. As small k_i enters the horizon later than large k_i, it means that the variance of the perturbation when entering the horizon would be larger and larger with time. When the fluctuations enter the horizon, causal physics starts to act, and this situation would lead, at some scale, to a universe which is no longer a perturbed FRW one. In the case in which $n > 1$, the variance of the density fluctuations would have been very large in the past, leading to a high density of collapsed objects like black holes, which we do not observe. These are the reasons for which the HZ spectrum was originally theoretically favored.

Evolution of the initial PS

It is simple to compute the asymptotic behavior of the evolved PS. Small scale perturbations ($k_i \gg k_{eq}$) enter the horizon very early in the radiation epoch. They do not grow during this period as shown in Eq. (4.92). Therefore they grow only in the matter epoch. Considering as initial PS the HZ one, the evolved PS at the time a for these scales is:

$$P(k,a) \sim \frac{1}{k^3}\left(\frac{a}{a_{eq}}\right)^2 \sim \frac{1}{k^3}. \tag{4.104}$$

Large scales enter the horizon in the matter epoch. Then, for these scales:

$$P(k,a) \sim \frac{1}{k^3}\left(\frac{a}{a_{ent}}\right)^2 \sim \frac{1}{k^3}\left(\frac{k}{2\pi}\right)^4 \sim k \tag{4.105}$$

where we have used (4.99) for a_{ent}. Therefore in this case it conserves the initial HZ PS. We can conclude then that the evoluted PS in a CDM model follows a dependence with $\sim k$ at small k and $\sim 1/k^3$ at large k. To improve this calculation refining the intermediate k, it is necessary to enter into details of the physics in the radiation epoch (see e.g. [BE84]). An adequate parameterization of a realistic CDM spectrum is (see e.g. [J+98]):

$$P(k) = \frac{\mathcal{N}(z)k}{\left(1 + (aq + (bq)^{3/2} + (cq)^2)^\nu\right)^{2/\nu}} \tag{4.106}$$

where $q = k/\Lambda$ is a rescaling of k by a dimensionless parameter Λ which depends on the parameters of the CDM model ($\Lambda = 0.21$ for "standard" CDM). In units of h^{-1} Mpc, where h is the Hubble constant today in units of 100 km/s/Mpc, one has $a = 6.4$, $b = 3$ and $c = 1.7$ and $\nu = 1.13$. The factor $\mathcal{N}(z)$ gives the overall normalization of the PS, which is a function of the initial red-shift z (for a red-shift chosen in the matter dominated era, during which the fluctuations are, to a very good approximation, simply amplified in the same way at all scales.) It is in principle fixed by the amplitude of fluctuations measured in the cosmic micro-wave background (CMB), and is often expressed as a value for σ_8, the normalized mass variance in a sphere of radius $8h^{-1}$ Mpc calculated from the PS when the model is extrapolated linearly to today. The PS (4.106) is the spectrum we will use when studying realistic initial conditions for N-body simulations in chapters 7 and 8.

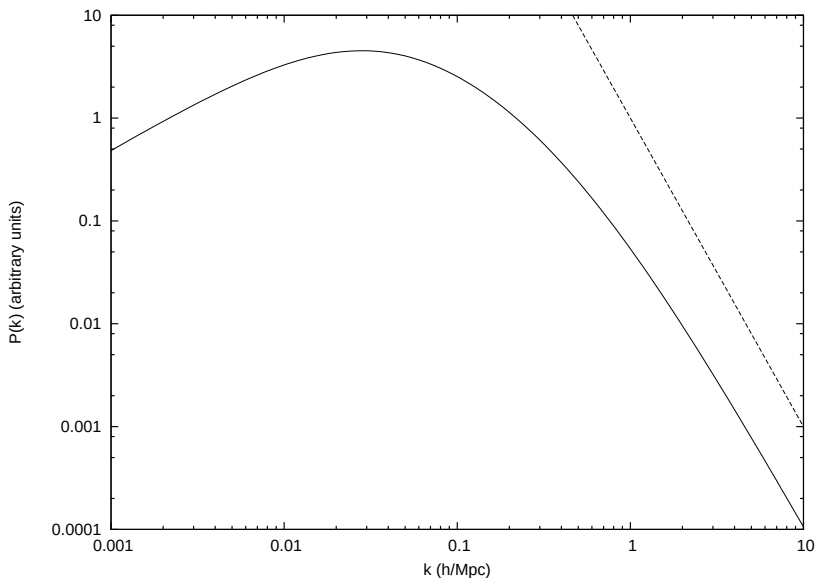

Figure 4.5: PS of a CDM model given by Eq. (4.106). The dashed lines are $\propto 1/k^3$.

Chapter 5

Kinetic and Fluid Theory

In this chapter we present some methods to describe the non-equilibrium evolution of a system of particles. This is a key subject because it will permit us to justify the fluid formalism of chapter 4 and understand the approximations we made. It is also one of the starting points to develop the statistical physics of Coulomb systems in chapter 6. We will start reviewing the basics of kinetic theory, i.e. the (in general) non-equilibrium evolution of a system of interacting particles. To do so, we will study the well known Boltzmann equation. Then, we will introduce the standard concept in statistical physics of *ensemble* (due to Gibbs) that will permit us to generalize the Boltzmann equation into the BBGKY hierarchy. We will discuss briefly the motivation of some *closures* of this hierarchy. Then, we will introduce the Klimontovich formalism of kinetic theory. It is equivalent to the BBGKY hierarchy and mainly used in the context of plasma physics. It is not widely used in cosmology but it is very useful to understand the approximations made in the derivation of a fluid theory from the kinetic one. We will study these approximations and we will introduce another method than in chapter 4 to solve (perturbatively) the fluid equation: Lagrangian fluid theory. It is in general better than Eulerian one. We will compare both methods. We will finish the chapter describing numerical methods to "solve" the Boltzmann equation, and in particular N-body methods.

5.1 The Boltzmann Transport Equation

Let us suppose[1] that we have a system of N particles in a volume V with, for simplicity, the same mass m. We will consider that the temperature is sufficiently high and the density sufficiently small so that it may be considered as a *classical* system. In this case each particle is a localized wave packets with defined position and momenta. This condition will be realized if the uncertainty in the position of the particles, given by the De Broglie wavelength

$$\lambda_B = \left(\frac{2\pi\hbar^2}{mk_BT}\right)^{\frac{1}{2}} \tag{5.1}$$

(where $\hbar$ is the reduced Planck constant and k_B the Boltzmann constant) is much smaller than the average interparticle separation $\ell \simeq \rho^{1/3}$ i.e. $\lambda_B \ll \ell$.

[1] This section follows essentially the treatment of [Hua87].

With this conditions we will consider also that the particles are *distinguishable*. We will also suppose that the boundaries of the box are perfect in the sense that particles are reflected elastically on them. We are not interested in the trajectory of *each* particle in detail but in the distribution function $f(\mathbf{r}, \mathbf{p}, t)$ defined so that

$$f(\mathbf{r}, \mathbf{p}, t) d\mathbf{r} d\mathbf{p} \tag{5.2}$$

is the number of particles that are contained in the real-space (infinitesimal) volume $d\mathbf{r}$ about $\mathbf{r}$ and in the momentum-space volume $d\mathbf{p}$ about $\mathbf{p}$. The real-space element has to be sufficiently large to contain a large number of particles, but small enough compared to the whole system[2]. The distribution function has to satisfy the normalization condition[3]

$$\int_V d\mathbf{r} \int_{\Omega_p} d\mathbf{p} f(\mathbf{r}, \mathbf{p}, t) = N, \tag{5.3}$$

where the integration is performed over the volume V of the box and the infinite momentum-space volume Ω_p. The six-dimensional space constituted by $(\mathbf{r}, \mathbf{p})$ for each particles is called μ space. If we determine the evolution of the distribution function $f(\mathbf{r}, \mathbf{p}, t)$ with time, for each point of in real-space and momentum-space, we have all the macroscopic information we need about the system.

Let us first derive the equation describing the evolution of the system, supposing that the particles do not undergo collisions[4] with one another inside the volume $d\mathbf{r}$. We suppose that an external mean field $\mathbf{F}(\mathbf{r})$ may act on the particles in the volume $d\mathbf{r}$. A particle with coordinate $(\mathbf{r}, \mathbf{p})$ at the instant t will have coordinates $(\mathbf{r} + \mathbf{v}\delta t, \mathbf{p} + \mathbf{F}\delta t)$ at the instant infinitesimally after, $t + \delta t$, where $\mathbf{v} = \mathbf{p}/m$ is the particle velocity. Then all the particles that at the instant t are in the volume $d\mathbf{r}d\mathbf{p}$ about $(\mathbf{r}, \mathbf{p})$ are at $t + \delta t$ in the volume $(\mathbf{r}', \mathbf{p}')$ about $(\mathbf{r} + \mathbf{v}\delta t, \mathbf{p} + \mathbf{F}\delta t)$. Therefore we can write, in the absence of collisions, the so-called *Vlasov equation*:

$$f(\mathbf{r} + \mathbf{v}\delta t, \mathbf{p} + \mathbf{F}\delta t, t + \delta t) = f(\mathbf{r}, \mathbf{p}) \tag{5.4}$$

where we have used that the volume elements are constant with time $d\mathbf{r}d\mathbf{p} = d\mathbf{r}', d\mathbf{p}'$[5]. If we now allow for collisions, we will lose (or gain) some particles in the infinitesimal volume and Eq. (5.4) is modified to:

$$f(\mathbf{r} + \mathbf{v}\delta t, \mathbf{p} + \mathbf{F}\delta t, t + \delta t) = f(\mathbf{r}, \mathbf{v}) + \left(\frac{\partial f}{\partial t}\right)_{\text{coll}} \delta t, \tag{5.5}$$

which defines $(\partial f/\partial t)_{\text{coll}}$. Expanding (5.5) up to first order in δt we obtain the distribution function for $\delta t \to 0$:

$$\left(\frac{\partial}{\partial t} + \frac{\mathbf{p}}{m} \cdot \nabla_{\mathbf{r}} + \mathbf{F} \cdot \nabla_{\mathbf{p}}\right) f(\mathbf{r}, \mathbf{p}, t) = \left(\frac{\partial f}{\partial t}\right)_{\text{coll}}. \tag{5.6}$$

[2]. The quantitative criteria is that it needs to be sufficiently large to have macroscopically defined properties but sufficiently small compared to the box size to be considered as a point.

[3] Note that strictly speaking the integral over real space of (5.3) would be a sum over finite volumes $d\mathbf{r}$ but, as it was said above, $d\mathbf{r}$ can be considered as a point and the integral is justified.

[4] We neglect collision between particles that are at the boundaries of two adjacent infinitesimal volumes $d\mathbf{r}$.

[5] This is true only if $(\mathbf{r}, \mathbf{p})$ are canonical conjugate coordinates at all time.

The collision term can be evaluated from its definition. During the time elapsed between t and $t+\delta t$ the collisions can produce two things: particles that were in the volume $d\mathbf{r}d\mathbf{p}$ about $(\mathbf{r},\mathbf{p})$ suffer a collision and are ejected from this volume, not longer in the volume $(\mathbf{r}+\mathbf{v}\delta t, \mathbf{p}+\mathbf{F}\delta t)$ at the time $t+\delta t$ (we suppose the volume element to be so small that one collision produce automatically an ejection from it). Let's assume that we have $R\delta t d\mathbf{r}d\mathbf{p}$ collisions of this kind, R being a parameter that depends of nature of the system. On the other hand, collisions in a volume close to $(\mathbf{r},\mathbf{p})$ (but outside the volume $d\mathbf{r}d\mathbf{p}$) can cause that some particles to enter the volume $d\mathbf{r}d\mathbf{p}$ about $(\mathbf{r}+\mathbf{v}\delta t, \mathbf{p}+\mathbf{F}\delta t)$. Let's suppose in this case that we have $\overline{R}\delta t d\mathbf{r}d\mathbf{p}$ collisions of this kind. Then we can write the collision term as

$$\left(\frac{\partial f}{\partial t}\right)_{\text{coll}} \delta t = (\overline{R}-R)\delta t \tag{5.7}$$

and the final equation that we get is

$$\left(\frac{\partial}{\partial t} + \frac{\mathbf{p}}{m}\cdot\nabla_{\mathbf{r}} + \mathbf{F}\cdot\nabla_{\mathbf{p}}\right) f(\mathbf{r},\mathbf{p},t) = \overline{R}-R \tag{5.8}$$

This is in fact a very simple equation: it is a kind of continuity equation, with a source term on the r.h.s. The only hypothesis we have made is that the force $\mathbf{F}(\mathbf{r})$ that is such that it conserves the six-dimensional volume of the space $d\mathbf{r}d\mathbf{p}$. Nevertheless, the collision term (r.h.s.) of (5.8) is in practice very difficult to evaluate. For dilute systems, only binary collisions may be considered (the probability to have ternary collisions is very small) and it can be computed in terms of the cross section of interaction.

In the astrophysical community the Vlasov equation (5.4) is usually called the *collisionless Boltzmann equation*. The force term is the gravitational force created by the particles outside the volume $d\mathbf{r}d\mathbf{p}$. Particles in the same infinitesimal volume are considered to be affected by the same force given by the Poisson equation:

$$\nabla^2\Phi(\mathbf{r},t) = 4\pi G\rho(\mathbf{r},t) = 4\pi G m \int_\Omega f(\mathbf{r},\mathbf{v},t)d\mathbf{r}, \tag{5.9}$$

where $\Phi(\mathbf{r},t)$ is the gravitational potential in a volume $d\mathbf{r}$ around $\mathbf{r}$ and $\rho(\mathbf{r},t)$ the mean density in the same volume. Note that the force is thus treated in a kind of mean-field approximation.

5.2 The Gibbs ensemble and the BBGKY hierarchy

Let us now describe the same physical phenomena as in the precedent section (the evolution of the probability density function of a set of interacting particles within a box) but using a more general and powerful framework. A key concept is the *Gibbs ensemble*. A state of a system of N particles can be totally specified by its $3N$ canonical coordinates $q_1,...,q_{3N}$ and their conjugate momenta $p_1,...,p_{3N}$. The $6N$-dimensional space of these coordinates is called phase-space and denoted by Γ. A point in the $6N$-dimensional Γ space is called a *representative point*. Note that the difference between the phase space and the

6-dimensional μ space defined in the precedent section. Given a macroscopic system, a very large number of states are compatible with the measurement of a macroscopic magnitude of the system. When we speak about a macroscopic state of the system, we are not considering a points in the Γ space, but a collection (maybe infinite) of point in this space compatible with the macroscopic state. Gibbs call this collection of identical microscopical states an *ensemble*. It is represented in Γ space as a distribution of points, usually continuous. It is described by the density function $\rho(p,q,t)$ where (p,q) is an abbreviation for $(p_1,...,p_{3N};q_1,...,q_{3N})$ and

$$\rho(p,q,t)d^{3N}d^{3N}q \tag{5.10}$$

is the number of representative points that at the time t are contained in the infinitesimal volume $d^1p...d^{3N}pd^1q...d^{3N}q$ of Γ about (p,q). An ensemble is totally specified by the density function $\rho(p,q,t)$. Further, if it is known at a time t it is possible, through the equations of motion of the particles, to compute it at any time t'. The concept of ensemble is closely related with the notion of measurement. A realistic measurement takes a certain amount of time. The measurement of the observable O can be considered as the time average

$$\langle O\rangle = \frac{1}{\tau}\int_{t_0}^{t_0+\tau} O(P(t))dt, \tag{5.11}$$

where $P(t)$ is a representative point of the system at time t and τ the time required to perform the measurement, which has to be much greater than the relaxation time, i.e. the time that need the macroscopic quantities to change. Under certain conditions it is possible to prove an *ergodic theorem* which states that average over *time* can substituted by averages over *ensembles*. Then the observable can be computed using

$$\langle O\rangle = \frac{\int d^{3N}pd^{3N}qO(p,q)\rho(p,q,t)}{\int d^{3N}pd^{3N}q\rho(p,q,t)}, \tag{5.12}$$

All the systems we are going to treat are assumed to obey this theorem, further discussion can be found in, for example, [Isi71].

Let's suppose that the system is governed by the Hamiltonian

$$\mathcal{H}(p_1,...,p_{3N};q_1,...,q_{3N}). \tag{5.13}$$

The evolution of the canonical variables is given by the Hamilton's equations:

$$\dot{p}_i = -\frac{\partial\mathcal{H}}{\partial q_i} \qquad (i=1,...,3N) \tag{5.14a}$$

$$\dot{q}_i = \frac{\partial\mathcal{H}}{\partial p_i} \qquad (i=1,...,3N) \tag{5.14b}$$

In the case of the systems we will consider, the number of systems is conserved in an ensemble. Through the evolution of the system they simply change their position in Γ space[6]. In this case, the density function does not change with time

$$\frac{d\rho}{dt} = 0. \tag{5.15}$$

[6] For example, if the number of particles in the system is not conserved this is not true.

Using Hamilton's equations (5.14), we obtain the continuity equation in Γ space

$$\frac{\partial \rho}{\partial t} + \sum_{i=1}^{3N} \left(\frac{\partial \rho}{\partial p_i} \dot{p}_i + \frac{\partial \rho}{\partial q_i} \dot{q}_i \right) = 0, \tag{5.16}$$

that can be rewritten in terms of the Hamiltonian using the Poisson brackets:

$$\frac{\partial \rho}{\partial t} + \{\rho, \mathcal{H}\} = 0. \tag{5.17}$$

This equation is the *Liouville* equation. It describes totally the evolution of the system.

5.2.1 BBGKY hierarchy

Let's now change the notation for greater simplicity. We will use as coordinates in the Γ-space the Cartesian coordinates $(\mathbf{r}_i, \mathbf{p}_i)$ (where the subscript i denotes the particles) and let's use the abbreviation $\mathbf{x}_i = (\mathbf{r}_i, \mathbf{p}_i)$ for the particle's position and $d\mathbf{x} = d\mathbf{r}d\mathbf{p}$ for the volume elements. Then the density function is denoted by $\rho(\mathbf{x}_1, ..., \mathbf{x}_N; t)$. If we normalize the density function to unity, i.e.,

$$\int d\mathbf{x}_1 ... d\mathbf{x}_N \rho(\mathbf{x}_1, ..., \mathbf{x}_n; t) = 1 \tag{5.18}$$

then the density function $\rho(\mathbf{x}_1, ..., \mathbf{x}_N; t)$ represents the probability of finding the particles of the system at the positions $(\mathbf{x}_1, ..., \mathbf{x}_N)$ at the time t. With this notation we rewrite Eq. (5.17) as

$$\frac{\partial \rho}{\partial t} = \sum_{i=1}^{N} \left(\nabla_{\mathbf{p}_i} \rho \cdot \nabla_{\mathbf{r}_i} \mathcal{H} - \nabla_{\mathbf{r}_i} \rho \cdot \nabla_{\mathbf{p}_i} \mathcal{H} \right). \tag{5.19}$$

The Liouville equation contains a huge amount of information for large N and it is very difficult to solve it. Fortunately, we are not in general interested in practice in the full density function but only in some subset of the information contained in it. Let's define the n-point density $f^{(n)}$ function

$$f^{(n)}(\mathbf{x}_1, ..., \mathbf{x}_n; t) = \frac{N!}{(N-n)!} \int d\mathbf{x}_{n+1} d\mathbf{x}_N \rho(\mathbf{x}_1, ..., \mathbf{x}_N; t), \tag{5.20}$$

which represents the probability of finding n particles at the coordinates $(\mathbf{x}_1, ..., \mathbf{x}_n)$ at time t regardless of the position of the other $N - n$ particles. The 1-point density function $f^{(1)}(\mathbf{x}_1)$ is just the distribution function that obeys the Boltzmann equation. The combinatorial pre-factor comes from the fact that we are dealing with distinguishable particles.

We now derive from the Liouville equation an equation for the n-point densities. We will see that to have a solution of $f^{(1)}$ it is necessary to know $f^{(2)}$, for $f^{(2)}$ the knowledge of $f^{(3)}$ and so on. This is an N-hierarchy, and it is called the BBGKY hierarchy[7]. We need first to assume the form of the Hamiltonian of the system to introduce it in (5.19). Throughout this thesis we will assume that there is no external force acting on the system (as an external magnetic

[7] Acronym for the physicists Bogoliubov-Born-Green-Kirkwood-Yvon.

field) and the particles interact by a central pair potential. Therefore we can write the Hamiltonian as

$$\mathcal{H} = \sum_{i=1}^{N} \frac{\mathbf{p}^2}{2m} + \sum_{i<j} v_{ij} \tag{5.21}$$

where the potential is central

$$v_{ij} = v_{ji} = v(|\mathbf{r}_i - \mathbf{r}_j|) \tag{5.22}$$

and the force is defined as the gradient of the potential:

$$\mathbf{F}_{ij} = -\nabla_{r_i} v(|\mathbf{r}_i - \mathbf{r}_j|). \tag{5.23}$$

We write the Liouville equation (5.19) as

$$\left[\frac{\partial}{\partial t} + h_N(\mathbf{x}_1, ..., \mathbf{x}_N)\right] \rho(\mathbf{x}_1, ..., \mathbf{x}_N) = 0 \tag{5.24}$$

where

$$h_N(\mathbf{x}_1, ..., \mathbf{x}_N) = \sum_{i=1}^{N} S_i + \frac{1}{2} \sum_{i \neq j=1}^{N} P_{ij} \tag{5.25a}$$

$$S_i = \frac{\mathbf{p}_i}{m} \cdot \nabla_{r_i} \tag{5.25b}$$

$$P_{ij} = \mathbf{F}_{ij} \cdot (\nabla_{p_i} - \nabla_{p_j}). \tag{5.25c}$$

Using the Liouville equation (5.24) and the definition of n-point density function we obtain the equation of motion:

$$\frac{\partial}{\partial t} f^{(n)} = \frac{N!}{(N-n)!} \int d\mathbf{x}_{n+1} ... d\mathbf{x}_N \frac{\partial}{\partial t} \rho = -\frac{N!}{(N-n)!} \int d\mathbf{x}_{n+1} ... d\mathbf{x}_N h_N \rho \tag{5.26}$$

We isolate the terms involving the coordinates $\mathbf{x}_1 ... \mathbf{x}_n$ in the function h_N:

$$h_N(\mathbf{x}_1, ..., \mathbf{x}_N) = h_n(\mathbf{x}_1, ..., \mathbf{x}_n) + h_{N-n}(\mathbf{x}_{n+1}, ..., \mathbf{x}_N) + \sum_{i=1}^{n} \sum_{j=n+1}^{N} P_{ij}. \tag{5.27}$$

Assuming that the density function vanishes at the boundaries of the box, applying the divergence theorem and using the explicit form of the function h_{N-n} (5.25a) we have

$$\int d\mathbf{x}_{n+1} ... d\mathbf{x}_N h_{N-n}(\mathbf{x}_{n+1}, ..., \mathbf{x}_N) \rho(\mathbf{x}_1, ..., \mathbf{x}_N) = 0. \tag{5.28}$$

Introducing Eq. (5.27) in (5.26) and using the property (5.28) we obtain:

$$\left(\frac{\partial}{\partial t} + h_n\right) f^{(n)}(\mathbf{x}_1, ..., \mathbf{x}_n) = -\sum_{i=1}^{n} \int d\mathbf{x}_{n+1} P_{i,n+1} f_{n+1}(\mathbf{x}_1, ..., \mathbf{x}_{n+1}). \tag{5.29}$$

Expliciting the P_{ij} term from Eq. (5.25) and using again the divergence theorem to eliminate its second term we get finally:

$$\left(\frac{\partial}{\partial t} + h_n\right) f^{(n)}(\mathbf{x}_1, ..., \mathbf{x}_n) = -\sum_{i=1}^{n} \int d\mathbf{x}_{n+1} \mathbf{F}_{i,n+1} \cdot \nabla_{p_i} f_{n+1}(\mathbf{x}_1, ..., \mathbf{x}_{n+1}). \tag{5.30}$$

This is the BBGKY set of N (coupled) equations. They contain precisely the same information as the Liouville equation. The BBGKY has the great advantage that it can approximated using an appropriate closure at some n. We will see that if we adopt a suitable closure we obtain the collision-less Boltzmann equation (5.4). First of all we are going to write the two first equation of the hierarchy to understand the relative contribution of each term and determine which can be neglected:

$$\left(\frac{\partial}{\partial t} + \frac{\mathbf{p}_1}{m} \cdot \nabla_{r_1}\right) f^{(1)}(\mathbf{x}_1, t) = -\int d\mathbf{x}_2 \mathbf{F}_{12} \cdot \nabla_{p_1} f^{(2)}(\mathbf{x}_1, \mathbf{x}_2, t) \tag{5.31a}$$

$$\left(\frac{\partial}{\partial t} + \frac{\mathbf{p}_1}{m} \cdot \nabla_{r_1} + \frac{\mathbf{p}_2}{m} \cdot \nabla_{r_2} + \frac{1}{2}\mathbf{F}_{12} \cdot (\nabla_{p_1} - \nabla_{p_2})\right) f^{(2)}(\mathbf{x}_1, \mathbf{x}_2, t) \tag{5.31b}$$

$$= -\int d\mathbf{x}_3 (\mathbf{F}_{13} \cdot \nabla_{p_1} + \mathbf{F}_{23} \cdot \nabla_{p_2}) f^{(3)}(\mathbf{x}_1, \mathbf{x}_2, \mathbf{x}_3, t)$$

5.2.2 Closures of the BBGKY hierarchy

Depending on the system considered it is possible to find a truncation of the BBGKY hierarchy that leads to suitable approximations. In general, if the density of the system is sufficiently low, the collisions that involve more and more particles are less and less probable. This makes possible to truncate the BBGKY set of equations at some level in the hierarchy.

Low density systems

Let us consider a system of particles (typically a gas or a dilute plasma[8]). Let us write the two-point correlation function, without any loss of generality, as:

$$f^{(2)}(\mathbf{x}_1, \mathbf{x}_2, t) = f^{(1)}(\mathbf{x}_1, t) f^{(2)}(\mathbf{x}_2, t) + g^{(2)}(\mathbf{x}_1, \mathbf{x}_2, t). \tag{5.32}$$

The first term on the r.h.s. of (5.32) represents the trivial correlations (Poisson-type) related to the density around $\mathbf{x}_1$ and $\mathbf{x}_2$: the greater is the product of the densities of both regions, the greater is the probability to find a particle. The second term on the r.h.s. corresponds to non-trivial correlations. This function goes to zero as $|\mathbf{r}_1 - \mathbf{r}_2| \to \infty$, i.e. we assume there are no non-trivial correlations between two points separated by an infinite distance. Substituting Eq. (5.32) in (5.31a) we obtain:

$$\left(\frac{\partial}{\partial t} + \frac{\mathbf{p}_1}{m} \cdot \nabla_{r_1} + \langle \mathbf{F}(\mathbf{r}, t) \rangle \cdot \nabla_{p_1}\right) f^{(1)}(\mathbf{x}_1, t) = -\int d\mathbf{x}_2 \mathbf{F}_{12} \cdot \nabla_{p_1} g^{(2)}(\mathbf{x}_1, \mathbf{x}_2, t) \tag{5.33}$$

where

$$\langle \mathbf{F}(\mathbf{r}_1, t) \rangle = \int d\mathbf{x}_2 \mathbf{F}_{12} f^{(1)}(\mathbf{x}_2, t). \tag{5.34}$$

The equation (5.33) is exact. Let us study the time scales involved in it to find a suitable closure:

$$\mathbf{F} \cdot \nabla_p \sim \frac{1}{\tau_f} \tag{5.35a}$$

$$\frac{\mathbf{p}}{m} \cdot \nabla_r \sim \frac{1}{\tau_s} \tag{5.35b}$$

[8] For more details about plasma see chapter 6.

where τ_f is the typical duration of a collision and τ_s is the time for a particle to traverse a distance in which the $f^{(1)}$ varies significantly. There are two possible closures in function of the respective value of these characteristic times:

- If the particles cross the system with very low probability of collisions[9] it means that $\tau_f \gg \tau_s$. The dynamics is therefore driven by the "streaming" of the mean field and the r.h.s. of the Eq. (5.33) can be neglected. This is the collision-less Boltzmann or Vlasov equation.

- On the contrary, if the streaming time scale is much smaller than the collision one (this is the case in a gas with short range interaction) then $\tau_f \ll \tau_s$. The variation of $f^{(2)}$ is driven by the collision time-scale whereas the characteristic variation of $f^{(1)}$ is given by the "streaming" with time-scale τ_s. It is therefore not possible to neglect the r.h.s. of Eq. (5.33) and we have now a collision term that depends on $g^{(2)}$. In the approximation of low densities it is possible to compute the function $g^{(2)}$ through Eq. (5.31b). On the l.h.s. as well as on the r.h.s. of this equation there is a term with time scale τ_f. but the r.h.s. is $\rho_0 r_0^3$ times smaller, where r_0 is the range of the interaction. Therefore a good approximation is the systems of Eq. (5.31a) and Eq. (5.31b) with r.h.s. set equal to zero, i.e. truncating the hierarchy considering only the first two equations.

5.3 The Klimontovich-Dupree equation

We now derive the kinetic equation in another way, following [MB04] and [BD05]. We will use a formalism originally developed by Y. Klimontovich in the context of Plasma Physics. The Klimontovich density in the one-particle phase space is defined as:

$$f_K(\mathbf{r}, \mathbf{p}, t) = \sum_{i=1}^{N} \delta(\mathbf{r} - \mathbf{r}_i)\delta(\mathbf{v} - \mathbf{v}_i), \tag{5.36}$$

where i labels each of the N particles. The system of N particles is specified deterministically at each time t (the time is implicit in the positions $\mathbf{r}(t)$ and velocities $\mathbf{v}(t)$). Let's suppose that the particle dynamics obey the Hamiltonian (5.21). The Klimontovich density follows a Liouville-like conservation equation as in the Gibbsian ensemble (Eq. (5.16)), the Klimontovich-Dupree equation:

$$\frac{\partial f_K}{\partial t} + \mathbf{v}(\mathbf{r}, t) \cdot \frac{\partial f_K}{\partial \mathbf{r}} + \mathbf{F}_K(\mathbf{r}, t) \cdot \frac{\partial f_K}{\partial \mathbf{v}} = 0, \tag{5.37}$$

where

$$\frac{d\mathbf{r}}{dt} = \mathbf{v}(\mathbf{r}, t) \tag{5.38a}$$

$$\frac{d\mathbf{v}}{dt} = \mathbf{F}_K(\mathbf{r}, t) = \frac{1}{4\pi} \int d\mathbf{r}' d^{\mathbf{p}} \frac{f_K(\mathbf{r} - \mathbf{r}', \mathbf{p}, t)}{|\mathbf{r}' - \mathbf{r}|^3} (\mathbf{r} - \mathbf{r}'). \tag{5.38b}$$

This equation is derived computing the total derivative of the Klimontovich density explicitly (Eq. (5.36)) and using some properties of the Dirac delta

[9] This is case in a dilute plasma[LP81] or in a gravitational system with a very large number of particles[BT87].

functions[10]. The Klimontovich-Dupree equation (5.37) and (5.16) contain very different physical information despite their formal resemblance. The former contains *all* the information of the system in a deterministic manner (i.e. in a single realization) whereas the latter contains the *maximum* information but in a statistically manner (in the framework of a Gibbs ensemble). To convert the Klimontovich-Dupree equation to a "statistical equation", we consider a very large number of systems described by the Klimontovich density and to define the 1-point density function as:

$$\langle f_K(\mathbf{x},t)\rangle = f^{(1)}(\mathbf{x},t) \tag{5.39}$$

and the 2-point density function as

$$\langle f_K(\mathbf{x}_1,t) f_K(\mathbf{x}_2,t)\rangle = \delta(\mathbf{x}_1-\mathbf{x}_2) f^{(1)}(\mathbf{x}_1,t) + f^{(2)}(\mathbf{x}_1,\mathbf{x}_2,t), \tag{5.40}$$

where $x \equiv (\mathbf{r},\mathbf{p})$, as in the previous sections. The Dirac delta which appears in Eq. (5.40) corresponds to the case when two particles coincide at the same position. The 3-point density function is defined in an analogous manner to (5.40), with two Dirac deltas for $\mathbf{x}_1 = \mathbf{x}_2 = \mathbf{x}_3$ and one for $\mathbf{x}_1 = \mathbf{x}_2$, $\mathbf{x}_1 = \mathbf{x}_3$ and $\mathbf{x}_2 = \mathbf{x}_3$. Note that while the Klimontovich density is not a smooth function, its average $\langle f_K(\mathbf{x},t)\rangle$ is. It is possible to derive the BBGKY hierarchy noting that, if $df_K/dt = 0$, then $d(f_K)^m/dt = 0$ for $m > 0$. This implies the existence of a Klimontovich-Dupree like equation (5.37) not only for f_K but also for any positive integer power of it. We derive the first equation of the hierarchy(5.31a) averaging Eq. (5.37) over an ensemble of realizations:

$$\left\langle \frac{\partial f_K}{\partial t}\right\rangle + \left\langle \mathbf{v}(\mathbf{r},t)\cdot\frac{\partial f_K}{\partial \mathbf{r}}\right\rangle + \left\langle \mathbf{F}_K(\mathbf{r},t)\cdot\frac{\partial f_K}{\partial \mathbf{v}}\right\rangle = 0. \tag{5.41}$$

We define the average over realizations of the quantity $A(x)$ as

$$\langle A(x)\rangle = \int d\mathbf{x} A(\mathbf{x}) f_K(\mathbf{x},t). \tag{5.42}$$

Using Eqs. (5.39), (5.40), (5.41), (5.42), we obtain exactly the first equation of the BBGKY hierarchy (5.31a).

Instead of averaging the Klimontovich density over a Gibbs ensemble it is possible to take instead a single realization of the system and perform a coarse-graining of it (the philosophy adopted in the derivation of the Boltzmann equation in the first section of this chapter). Following [BD05], we define a coarse graining of the Klimontovich density as

$$f(\mathbf{r},\mathbf{v},t) = \int \frac{d\mathbf{r}'}{\mathcal{L}^3}\frac{d\mathbf{v}'}{\mathcal{V}^3} W_{\mathcal{L}}\left(\frac{\mathbf{r}-\mathbf{r}'}{\mathcal{L}}\right) W_{\mathcal{V}}\left(\frac{\mathbf{v}-\mathbf{v}'}{\mathcal{V}}\right) f_K(\mathbf{r}',\mathbf{v}',t), \tag{5.43}$$

where $W_{\mathcal{L}}$ and $W_{\mathcal{V}}$ are rotationally symmetric coarsening window functions for positions and velocities respectively. Introducing Eq. (5.43) in the Klimontovich-Dupree equation (5.37) we obtain:

$$\frac{\partial f}{\partial t} + \mathbf{v}(\mathbf{r},t)\cdot\frac{\partial f}{\partial \mathbf{r}} + \langle \mathbf{F}(\mathbf{r},t)\rangle\cdot\frac{\partial f}{\partial \mathbf{v}} = -\frac{\partial}{\partial \mathbf{r}}\cdot\mathbf{S}^{(v)} - \frac{\partial}{\partial \mathbf{v}}\cdot\mathbf{S}^{(g)} \tag{5.44}$$

[10] These properties are: $\mathbf{r}\delta(\mathbf{r}-\mathbf{r}_i) = \mathbf{r}_i\delta(\mathbf{r}-\mathbf{r}_i)$, $\mathbf{v}\delta(\mathbf{v}-\mathbf{v}_i) = \mathbf{v}_i\delta(\mathbf{v}-\mathbf{v}_i)$, $(\partial/\partial t)\delta[\mathbf{r}-\mathbf{r}_i(t)] = -d\mathbf{r}_i/dt\cdot(\partial/\partial\mathbf{r})\delta[\mathbf{r}-\mathbf{r}_i(t)]$ and $(\partial/\partial t)\delta[\mathbf{v}-\mathbf{v}_i(t)] = -d\mathbf{v}_i/dt\cdot(\partial/\partial\mathbf{v})\delta[\mathbf{v}-\mathbf{v}_i(t)]$.

with the average force defined as

$$\langle \mathbf{F}(\mathbf{r},t)\rangle = \int d\mathbf{x}_2 \mathbf{F}_{12} f(\mathbf{x}_2,t) \tag{5.45}$$

and the "collision terms"

$$\mathbf{S}^{(v)}(\mathbf{r},\mathbf{v},t) = \int \frac{d\mathbf{r}'}{\mathcal{L}^3}\frac{d\mathbf{v}'}{\mathcal{V}^3} W_{\mathcal{L}}\left(\frac{\mathbf{r}-\mathbf{r}'}{\mathcal{L}}\right) W_{\mathcal{V}}\left(\frac{\mathbf{v}-\mathbf{v}'}{\mathcal{V}}\right)(\mathbf{v}-\mathbf{v}') f_K(\mathbf{r}',\mathbf{v}',t) \tag{5.46}$$

and

$$\begin{aligned}\mathbf{S}^{(g)}(\mathbf{r},\mathbf{v},t) &= \int \frac{d\mathbf{r}'}{\mathcal{L}^3}\frac{d\mathbf{v}'}{\mathcal{V}^3} W_{\mathcal{L}}\left(\frac{\mathbf{r}-\mathbf{r}'}{\mathcal{L}}\right) W_{\mathcal{V}}\left(\frac{\mathbf{v}-\mathbf{v}'}{\mathcal{V}}\right) \\ &\times \quad (\mathbf{F}(\mathbf{r}',t) - \langle \mathbf{F}(\mathbf{r},t)\rangle) f_K(\mathbf{r}',\mathbf{v}',t). \end{aligned} \tag{5.47}$$

If we compare Eq. (5.44) with the Boltzmann equation (5.6), we see that the r.h.s. of (5.44) is the collision term $(\partial f/\partial t)_{coll}$. We see how erasing some information about the knowledge of the system we obtain a source term in the "Liouville" equation. This is in fact well known, the original idea being due to Gibbs (see e.g. [Sas00] for a discussion). The source term in the Liouville-like equations is the responsible for the increase of entropy.

5.4 Macroscopic quantities: fluid equations

The description we have given up to now is *microscopic*. For example, Eqs. (5.6), (5.33) or (5.44) gives a description of how each point of the system varies with time. It is convenient (when possible) to simplify the problem to a set of *fluid equations* which give a less detailed (but sufficiently accurate, in most cases) description of the system. The approach we are going to describe is valid when the macroscopic properties of the system (temperature, density, velocity, etc) vary sufficiently slowly compared with some characteristic scale as the interparticle distance. We will therefore be able to describe the system with this approach at scales much larger than the mean free path. We are going to follow mostly the "*à la* Klimontovich" derivation of the precedent subsection given in [BD05] (we will follow also [LP81]).

We define the *mass density* and the *mean fluid velocity* from the velocity moments of $f(\mathbf{r},\mathbf{v},t)$:

$$\rho(\mathbf{r},t) = m\int d\mathbf{v} f(\mathbf{r},\mathbf{v},t) = \frac{m}{\mathcal{L}^3}\sum_{i=1}^{N} W_{\mathcal{L}}\left(\frac{\mathbf{r}-\mathbf{r}_i}{\mathcal{L}}\right) \tag{5.48a}$$

$$\rho\overline{\mathbf{v}}(\mathbf{r},t) = m\int d\mathbf{v} f(\mathbf{r},\mathbf{v},t) = \frac{m}{\mathcal{L}^3}\sum_{i=1}^{N} W_{\mathcal{L}}\left(\frac{\mathbf{r}-\mathbf{r}_i}{\mathcal{L}}\right)\mathbf{v}_i(\mathbf{r},t). \tag{5.48b}$$

The evolution of these two fields can be directly computed from Eqs. (5.44-5.47) by integrating Eq. (5.44) and $v_\mu \cdot$ (5.44), giving:

$$\frac{\partial \rho}{\partial t} + \nabla\cdot(\rho\langle v\rangle) = 0 \tag{5.49a}$$

$$\frac{\partial\langle v\rangle}{\partial t} + (\langle v\rangle\cdot\nabla)\langle v\rangle = \langle F(\mathbf{r},t)\rangle + \frac{1}{\rho}(\mathcal{F} - \nabla\cdot\mathcal{P}), \tag{5.49b}$$

where we have introduced the two new fields:

$$\mathcal{F}_\mu(\mathbf{r},t) = m\int d\mathbf{v} S_\mu^{(g)}(\mathbf{r},\mathbf{v},t) = \sum_{i=1}^{N} W_{\mathcal{L}}\left(\frac{\mathbf{r}-\mathbf{r}_i}{\mathcal{L}}\right)\left[F_\mu(\mathbf{r}_i,t) - \langle F\rangle_\mu(\mathbf{r},t)\right] \tag{5.50a}$$

$$\begin{aligned}\mathcal{P}_{\mu\nu}(\mathbf{r},t) &= m\int d\mathbf{v}\Big\{[v_\mu - \langle v\rangle_\mu(\mathbf{r},t)][v_\nu - \langle v\rangle_\nu(\mathbf{r},t)]f(\mathbf{r},\mathbf{v},t) \\ &\quad + [v_\nu - \langle v\rangle_\nu(\mathbf{r},t)]S_\mu^{(v)}(\mathbf{r},\mathbf{v},t)\Big\} \qquad (5.50b)\\ &= \sum_{i=1}^{N} W_{\mathcal{L}}\left(\frac{\mathbf{r}-\mathbf{r}_i}{\mathcal{L}}\right)\left[v_\mu(\mathbf{r}_i,t)v_\nu(\mathbf{r}_i,t) - \langle v\rangle_\mu(\mathbf{r},t)\langle v\rangle_\nu(\mathbf{r},t)\right]\end{aligned}$$

The equation (5.49) and (5.50) are *exact*, provided the averages (5.48) are finite. The expression (5.49a) is just a matter density conservation equation and the equation (5.49b) contains the dynamics. To have a well defined problem, another equation is required relating the density with the force. In the case of electrodynamics and gravity, this is the Poisson equation. The second term on the r.h.s. of (5.49b) are corrections to the *mean fields* $\langle F\rangle$ and $\langle v\rangle$. The mean fields can be understood as a *monopole* approximation of the physics that occurs at scales below the coarse graining scale. Neglecting the corrections implies to loose all the details of the physics beyond these scales. The correction (5.50a) is related with the *fluctuations* in the force and the corrections of Eq. (5.50b) are related with the dispersion of velocities. The tensor $\mathcal{P}$ is thus related with pressure. An important difference between these two terms is that, because we have averaged over $\mathbf{v}$ and not over $\mathbf{r}$, dispersion in the velocities survives even if the $S^{(v)}$ term is neglected[11]. If we had averaged over the position $\mathbf{r}$, the opposite would have happened.

In principle it is possible to solve the set of equations (5.49) and (5.50) (plus an equation that relates the density field and the force) but it is extremely complicated. For example, if we compute dynamical equations for the fields $\mathcal{F}$ and $\mathcal{P}$, new fields will appear, exactly in the same manner than in the BBGKY hierarchy. To be able to handle the problem some well-motivated closure (approximation) needs to be found.

5.4.1 Zero-order approximation: the ideal fluid

If the mean free path of the particles is much smaller than the other (macroscopic) characteristic lengths, it is possible to neglect the r.h.s. of Eq. (5.37). Then Eq. (5.49) is simplified to

$$\frac{\partial\rho}{\partial t} + \nabla\cdot(\rho\langle v\rangle) = 0 \tag{5.51a}$$

$$\frac{\partial\langle v\rangle}{\partial t} + (\langle v\rangle\cdot\nabla)\langle v\rangle = \langle F(\mathbf{r},t)\rangle - \frac{1}{\rho}\nabla\cdot\mathcal{P}^{(0)}, \tag{5.51b}$$

where

$$\mathcal{P}_{\mu\nu}^{(0)}(\mathbf{r},t) = \rho(\langle v_\mu(\mathbf{r},t)v_\nu(\mathbf{r},t)\rangle - \langle v\rangle_\mu\langle v\rangle_\nu). \tag{5.52}$$

[11] Except in the case of a system with zero pressure.

The Eq. (5.51) describes an *ideal incompressible fluid* with a pressure that comes only from the dispersion of velocities and not from the degrees of freedom lost in the coarse graining procedure. Note that it is possible to compute a dynamical equation for (5.52) by integrating $v_\mu v_\nu \cdot$ (5.44), which leads to an extra (unknown) field, depending on the third moment of the velocity [BD98]:

$$\frac{\partial \mathcal{P}^{(0)}_{\mu\nu}}{\partial t} + \langle v \rangle_\sigma \frac{\partial \mathcal{P}^{(0)}_{\mu\nu}}{\partial \mathbf{r}_\sigma} + \frac{\partial \langle v \rangle_\sigma}{\partial r_\sigma} \mathcal{P}^{(0)}_{\mu\nu} + \frac{\partial \langle v \rangle_\nu}{\partial r_\sigma} \mathcal{P}^{(0)}_{\mu\sigma} + \frac{\partial \langle v \rangle_\nu}{\partial r_\sigma} \mathcal{P}^{(0)}_{\mu\sigma} = -\frac{\partial \mathcal{L}_{\mu\nu\sigma}}{\partial r_\sigma}, \quad (5.53)$$

where the new function $\mathcal{L}$ is

$$\mathcal{L}_{\mu\nu\sigma}(\mathbf{r},t) = \rho \left\langle (v_\mu(\mathbf{r},t) - \langle v \rangle_\mu)(v_\nu(\mathbf{r},t) - \langle v \rangle_\nu)(v_\sigma(\mathbf{r},t) - \langle v \rangle_\sigma) \right\rangle . \quad (5.54)$$

This is a BBGKY-type (infinite) hierarchy. In what follows we are going to outline some possible closures for it.

5.4.2 Hydrodynamical-type closure

Let's consider a system in which the mean free path is small compared with the other characteristic lengths. This is the case, for example, in a gas at sufficiently high temperature and with short-ranged interaction. In this situation the particles make a large number of collisions in a small characteristic volume, given e.g. by the average interparticle distance. Therefore, they reach very rapidly equilibrium and it is reasonable to suppose that they obey locally an equilibrium distribution (at all times). In the case of a gas it is natural to suppose that the particles obey the Maxwell-Boltzmann distribution [Hua87]. Instead of considering such distribution, we are going to consider a general distribution with the two assumptions below. We will see that the result does not depend (strongly) on the explicit form of the distribution function. The assumptions are:

1. The distribution depends only on the difference between the mean velocity and the velocity of the particle considered.

2. The distribution is isotropic.

This is the case of the Maxwell-Boltzmann distribution given in Eq. (6.4):

$$f_{MB}(\mathbf{v},t) = \left(\frac{\beta(\mathbf{r},t)m}{2\pi} \right)^{3/2} e^{-\beta(\mathbf{r},t)\frac{m|\mathbf{v}-\langle \mathbf{v} \rangle|^2}{2}}, \quad (5.55)$$

where we assume that the variables $\rho(\mathbf{r},t)$, $\mathbf{v}(\mathbf{r},t)$ and $\beta(\mathbf{r},t)$ are slowly varying functions of $\mathbf{r}$ and t (if not, the hypothesis of local equilibrium is not fulfilled). Instead of Eq. (5.55) we will use the generalized (normalized) distribution:

$$f(\mathbf{v},t) = f_{gen}\left(-\beta(\mathbf{r},t), |\mathbf{v} - \langle \mathbf{v} \rangle|\right) \quad (5.56)$$

The tensor $P_{\mu\nu}$ is

$$\begin{aligned} \mathcal{P}^{(0)}_{\mu\nu}(\mathbf{r},t) &= \rho(\mathbf{r},t) \int d\mathbf{v} (v_\mu(\mathbf{r},t) v_\nu(\mathbf{r},t) - \langle v \rangle_\mu \langle v \rangle_\nu) f_{gen}\left(-\beta(\mathbf{r},t), |\mathbf{v} - \langle \mathbf{v} \rangle|\right) \\ &= \delta_{\mu\nu} \rho(\mathbf{r},t) h(m,\beta)) \equiv p(\mathbf{r},t)\delta_{\mu\nu}, \end{aligned} \quad (5.57)$$

where the non-diagonal part is zero by symmetry and h is a function of the mass m and the inverse temperature β. This equation gives an *equation of state*, with the isotropic pressure p related to the temperature β. For example, in the case of a Boltzmann distribution, we obtain the equation of state of an ideal gas:

$$p(\mathbf{r},t) = \frac{1}{3}\rho(\mathbf{r},t)\left(\frac{\beta m}{2\pi}\right)^{3/2}\int d\mathbf{V}V^2 e^{-\beta\frac{V^2}{2m}} = \frac{\rho(\mathbf{r},t)}{m\beta}, \tag{5.58}$$

where $V \equiv |\mathbf{v} - \langle\mathbf{v}\rangle|$. By symmetry also, the function $\mathcal{L}_{\mu\nu\sigma}$ which appears in the r.h.s. of Eq. (5.53) is zero. The Eq. (5.53), using Eq. (5.51a) to eliminate the density ρ, can be written as:

$$\frac{\partial h}{\partial t} + (\langle\mathbf{v}\rangle\cdot\nabla)h + \frac{2}{3}h\nabla\cdot\mathbf{v} = 0. \tag{5.59}$$

Summing the continuity equation (5.51a) with (5.59) we have:

$$\left(\frac{\partial}{\partial t} + \langle\mathbf{v}\rangle\cdot\nabla\right)\left(\rho h^{-3/2}\right) = 0. \tag{5.60}$$

Using now the equation of state (5.57) we obtain the result

$$p(\mathbf{r},t) = \varsigma(\mathbf{r})\rho(\mathbf{r},t)^{5/3}, \tag{5.61}$$

along a *streamline*, i.e., along paths followed by "volume elements"[12]. The parameter ς is positive definite. This last result is the condition for an adiabatic transformation of an ideal gas. This condition is naturally independent of the distribution of velocities taken, the only condition being the vanishing of the tensor $\mathcal{L}_{\mu\nu\sigma}$. This tensor is the responsible of heat flux between different parts of the system, which vanishes in an adiabatic transformation.

5.4.3 Closures for self-gravitating systems

In the case of a self-gravitating system, relevant to cosmology, it is much more difficult to find a suitable closure because there is not a situation of local equilibrium (it is not even clear if such a closure exists). This is because the interaction is attractive and long range, which produces clustering over larger and larger scales. There are different attempts to find a suitable closure in this context, which we will outline in what follows:

The "dust" closure

This model have been extensively applied in cosmology because it is the most simple and it gives good results for early times. Its assumptions are [BD05]: (i) small-scales inhomogeneities are irrevelevant (so that the gravitational mean-field gravity is dominant), and (ii) velocity dispersion is absent and small-scale kinetic degrees of freedom are subdominant. Therefore fluctuations in the gravitational force and in the velocities are neglected as well as the velocity dispersion. Then the r.h.s. of Eqs. (5.53) vanishes and the equations are very simple to solve (see chapter 4 and section 5.5 in this chapter).

[12] In the notation of the Lagrangian formulation of the fluid theory (see section 5.5), we would write this equation as $p(\mathbf{R},t) = \varsigma(\mathbf{R})\rho(\mathbf{R},t)^{5/3}$, where $\mathbf{R}$ is the Lagrangian coordinate that labels the particles. At $t = t_0$ we have $\mathbf{R} = \mathbf{r}$.

The adiabatic closure

This is a closure that gives a similar result to the one described in the hydrodynamic one but without using explicitly the assumption of local equilibrium. The basic assumptions [BD98] are :

1. The velocity dispersion is small. If we estimate the velocity dispersion as $|\mathbf{v}\langle\mathbf{v}\rangle| \sim \epsilon\langle\mathbf{v}\rangle$, with $\epsilon \ll 1$, then it implies that the pressure term is of order ϵ^2 and $\mathcal{L}_{\mu\nu\sigma}$ of order ϵ^3 and can be therefore neglected.

2. Isotropy.

With both assumptions we obtain again the adiabatic "equation of state" (5.61) (valid along a streamline). The main difference with respect to result (5.61) is that we do not have local equilibrium and therefore it is not guaranteed that the initial assumption of both small velocity dispersion and isotropy will remain valid with the evolution of the system.

5.5 Lagrangian perturbation theory

In this section we describe another formulation of the fluid theory, that presents, in general, more accurate solutions in the perturbative regime than the Eulerian picture, studied in chapter. 4. In section 5.6 we will explain why the Lagrangian approach is in general better than the Eulerian one. We will work in a cosmological expanding framework[13]. The fluid equation in Eulerian *physical* (not comoving) coordinates r, are:

$$\frac{\partial\rho}{\partial t} + \nabla_{\mathbf{r}}\cdot(\rho\mathbf{v}) = 0 \tag{5.62a}$$

$$\frac{\partial\mathbf{v}}{\partial t} + (\mathbf{v}\cdot\nabla_{\mathbf{r}})\mathbf{v} = \mathbf{g} \tag{5.62b}$$

$$\nabla_{\mathbf{r}}\times\mathbf{g} = 0 \tag{5.62c}$$

$$\nabla_{\mathbf{r}}\cdot\mathbf{g} = -4\pi G\rho(\mathbf{r},t) \tag{5.62d}$$

In this picture the system is determined at each time by the density $\rho(\mathbf{r},t)$ and the velocities $\mathbf{v}(\mathbf{r},t)$. The idea of the Lagrangian formulation is to follow the trajectories of infinitesimal fluid elements. The velocity is given by the velocity of these fluid elements and the density varies according with the convergence or the divergence of the fluid elements to each point. We define the Lagrangian coordinate $\mathbf{q}$ as the position of the fluid element at the initial time[14]. In an expanding universe, the physical position $\mathbf{r}$ of the fluid element is a function of its Lagrangian coordinate and time through the relation

$$\mathbf{r}(t) = a(t)(\mathbf{q} + \mathbf{u}(\mathbf{q},t)), \tag{5.63}$$

where $\mathbf{u}(\mathbf{q},t)$ is a "displacement field". This expression is actually a coordinate transformation between the coordinates $\mathbf{r}$ and $\mathbf{q}$; solving the evolution problem means finding this transformation.

[13] It is possible to recover the non-expanding case by setting $\dot{a} = 0$, $a = 1$.
[14] It can be view just as a "label" of the particle.

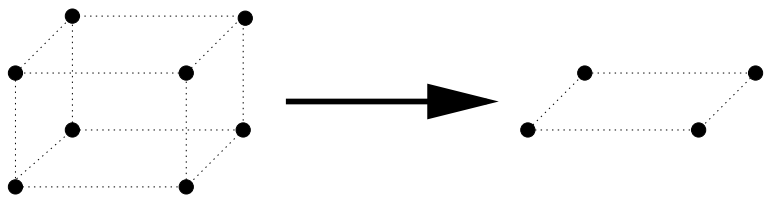

Figure 5.1: Evolution of a fluid which was initially a cube. Choosing the principal axis as coordinate system, it will be a parallelepipedic during the evolution. The moment in which it has collapsed into a plane is the *shell crossing*.

Let us rewrite the set of Eulerian fluid equations (5.62) in the Lagrangian framework. The continuity equation (5.62a) can be expressed using the conservation of mass in the coordinates transformation (5.63):

$$\rho(\mathbf{r}, t)\,\mathrm{d}\,\mathbf{r} = \rho(\mathbf{q})\,\mathrm{d}\,\mathbf{q}, \tag{5.64}$$

where $\rho(\mathbf{r}, t_0) = \rho(\mathbf{q})$. The densities are thus related by the Jacobian $\mathbf{J}$ of the transformation (5.63):

$$\rho(\mathbf{r}, t) = \rho(\mathbf{q})\frac{\mathrm{d}\,\beta 3q}{\mathrm{d}\,\mathbf{r}} = \frac{\rho(\mathbf{q})}{\det\left(\frac{\partial r_i}{\partial q_j}\right)} \equiv \rho(\mathbf{q})\mathbf{J}^{-1}. \tag{5.65}$$

With the evolution by the effect of gravity of the fuid element, it will be inevitably a time in which the Jacobian will be zero (see Fig. 5.1). It corresponds to the moment in which the fluid element has collapsed into a plane. This is called *shell crossing*. In Lagrangian coordinates the equation of continuity (5.62) can we written as:

$$\frac{\mathrm{d}}{\mathrm{d}\,t}\left[\rho\mathbf{J}\right] = 0, \tag{5.66}$$

where we have used the identity [Buc92]:

$$\frac{\mathrm{d}}{\mathrm{d}\,t}\mathbf{J} = \mathbf{J}\nabla_{\mathbf{r}} \cdot \mathbf{v}. \tag{5.67}$$

In Lagrangian coordinates the total derivative with respect to time reduces to a partial derivative with respect to time because of the time independence of $\mathbf{q}$ in Eq. (5.63):

$$\frac{\mathrm{d}}{\mathrm{d}\,t} = \left(\frac{\partial}{\partial t}\right)_r + \mathbf{v} \cdot \nabla_{\mathbf{r}} = \left(\frac{\partial}{\partial t}\right)_q. \tag{5.68}$$

Using Eqs. (5.68) and (5.63) we can write Eq. (5.62b) into Lagrangian coordinates as:

$$\mathbf{g} = \left(\frac{\partial \mathbf{v}}{\partial t}\right)_q = a\left(\ddot{\mathbf{u}} + 2\frac{\dot{a}}{a}\dot{\mathbf{u}} + \frac{\ddot{a}}{a}\mathbf{u} + \frac{\ddot{a}}{a}\mathbf{q}\right). \tag{5.69}$$

To summarize, we have transformed the set of Eulerian equations (5.62) in Lagrangian coordinates:

$$\rho(\mathbf{r},t) = \rho(\mathbf{q})\mathbf{J}^{-1} \tag{5.70a}$$

$$\mathbf{g} = a\left(\ddot{\mathbf{u}} + 2\frac{\dot{a}}{a}\dot{\mathbf{u}} + \frac{\ddot{a}}{a}\mathbf{u} + \frac{\ddot{a}}{a}\mathbf{q}\right) \tag{5.70b}$$

$$\nabla_{\mathbf{r}} \times \left(\ddot{\mathbf{u}} + 2\frac{\dot{a}}{a}\dot{\mathbf{u}} + \frac{\ddot{a}}{a}\mathbf{u} + \frac{\ddot{a}}{a}\mathbf{q}\right) = 0 \tag{5.70c}$$

$$a\nabla_{\mathbf{r}} \cdot \left(\ddot{\mathbf{u}} + 2\frac{\dot{a}}{a}\dot{\mathbf{u}} + \frac{\ddot{a}}{a}\mathbf{u} + \frac{\ddot{a}}{a}\mathbf{q}\right) = -4\pi G\rho(\mathbf{q})\mathbf{J}^{-1} \tag{5.70d}$$

In order to solve Eqs. (5.70c) and (5.70d) we need to find a relation between the derivatives with respect to r and q. It is simple to compute the derivative with respect to r_i as a function of the derivatives with respect to q_i through the formula (5.63). Nevertheless, we need the derivative with respect to q_i as a function of r_i. This relation can be obtained by inverting formally Eq. (5.63). However, we haven't yet determined the explicit form of the function $\mathbf{u}$. We can done this inversion perturbatively using Eq. (5.63):

$$\frac{\partial}{\partial q_i} = \frac{\partial r_j}{\partial q_i}\frac{\partial}{\partial r_j} = a\frac{\partial}{\partial r_i} + \frac{\partial p_j}{\partial q_i}\frac{\partial}{\partial r_j}, \tag{5.71}$$

and inverting this relation recursively up to $\mathcal{O}(p)$ (it can be done up to any desired order):

$$\frac{\partial}{\partial r_i} = \frac{1}{a}\frac{\partial}{\partial q_i} - \frac{1}{a}\frac{\partial p_j}{\partial q_i}\frac{\partial}{\partial q_j}. \tag{5.72}$$

Using that at $\mathcal{O}(p)$ the Jacobian can be expressed as $\mathbf{J} = a^3(1+\nabla_q \cdot \mathbf{u})$ and Eq. (5.72), we obtain then for Eqs. (5.70c) and (5.70d):

$$\nabla_q \times \left(\ddot{\mathbf{u}} + 2\frac{\dot{a}}{a}\dot{\mathbf{u}}\right) = 0 \tag{5.73a}$$

$$\nabla_q \cdot \left(\ddot{\mathbf{u}} + 2\frac{\dot{a}}{a}\dot{\mathbf{u}}\right) + 3\frac{\ddot{a}}{a} = -\frac{4\pi G\rho(\mathbf{q})(1-\nabla_q\mathbf{u})}{a^3} \tag{5.73b}$$

where in the last line we have used the Poisson equation (5.62d). We will consider that the configuration for $\mathbf{u} = 0$ corresponds to a homogeneous and isotropic EdS universe. Putting $\mathbf{u} = \mathbf{0}$ in Eq. (5.73b) we have:

$$3\frac{\ddot{a}}{a} = -\frac{4\pi G\rho_0}{a^3}, \tag{5.74}$$

which is Eq. (4.13) with $\rho \ll p$. Using this result and choosing an homogeneous and isotropic configuration $\rho(\mathbf{q}) = \rho_0$, we obtain finally the final set of equations:

$$\nabla_q \times \left(\ddot{\mathbf{u}} + 2\frac{\dot{a}}{a}\dot{\mathbf{u}}\right) = 0 \tag{5.75a}$$

$$\nabla_q \cdot \left(\ddot{\mathbf{u}} + 2\frac{\dot{a}}{a}\dot{\mathbf{u}} - \frac{4\pi G\rho_0}{a^3}\mathbf{u}\right) = 0, \tag{5.75b}$$

which determines the displacement field $\mathbf{u}$.

5.5.1 First order solution

We are going to look for a solution of Eqs. (5.70) at first order in the displacement field $\mathbf{u}$ in an EdS universe. We divide the displacements into a curl-free part, $\mathbf{u}_\parallel$ and a divergence-free part, $\mathbf{u}_\perp$:

$$\mathbf{u} = \mathbf{u}_\parallel + \mathbf{u}_\perp, \tag{5.76}$$

i.e. with $\nabla \times \mathbf{u}_\parallel = \mathbf{0}$ and $\nabla \cdot \mathbf{u}_\perp = 0$. Then Eqs. (5.73) are:

$$\ddot{\mathbf{u}}_\perp + \frac{4}{3t}\dot{\mathbf{u}}_\perp = \nabla\psi \tag{5.77a}$$

$$\Delta_{\mathbf{q}}\psi = 0$$

$$\ddot{\mathbf{u}}_\parallel + \frac{4}{3t}\dot{\mathbf{u}}_\parallel - \frac{2}{3t^2}\mathbf{u}_\parallel = \nabla \times \mathbf{K} \tag{5.77b}$$

$$\nabla_q \times (\nabla_q \times \mathbf{K}) = 0.$$

We impose boundary conditions such that $\nabla_q\psi = 0$ and $\nabla_q \times \mathbf{K} = 0$. We take the displacement field at $t = t_0$ as

$$\mathbf{u}_\perp(\mathbf{q}, t_0) \equiv \mathbf{u}_\perp(\mathbf{q}) \tag{5.78a}$$

$$\mathbf{u}_\parallel(\mathbf{q}, t_0) \equiv \mathbf{u}_\parallel(\mathbf{q}) \tag{5.78b}$$

and the initial velocity field:

$$\dot{\mathbf{u}}_\perp(\mathbf{q}, t_0) \equiv \mathbf{v}_\perp(\mathbf{q}) \tag{5.79a}$$

$$\dot{\mathbf{u}}_\parallel(\mathbf{q}, t_0) \equiv \mathbf{v}_\parallel(\mathbf{q}). \tag{5.79b}$$

With these boundary conditions we find as general solution of (5.77):

$$\mathbf{u}_\perp(\mathbf{q}, t) = \mathbf{u}_\perp(\mathbf{q}) + 3\mathbf{v}_\perp(\mathbf{q})t_0\left(1 - \left(\frac{t}{t_0}\right)^{-\frac{1}{3}}\right) \tag{5.80a}$$

$$\begin{aligned}\mathbf{u}_\parallel(\mathbf{q}, t) = {}& \mathbf{u}_\parallel(\mathbf{q})\left(\frac{3}{5}\left(\frac{t}{t_0}\right)^{\frac{2}{3}} + \frac{2}{5}\left(\frac{t}{t_0}\right)^{-1}\right) \\ &+ \mathbf{v}_\parallel(\mathbf{q})t_0\left(\frac{3}{5}\left(\frac{t}{t_0}\right)^{\frac{2}{3}} - \frac{3}{5}\left(\frac{t}{t_0}\right)^{-1}\right)\end{aligned} \tag{5.80b}$$

It is simple to derive an expresion for the peculiar gravitational accelaration in function of the displacements. Using the definition (4.60), we can write Eqs. (5.75) as

$$\nabla_q \times \mathbf{g}_{pec} = 0 \tag{5.81a}$$

$$\nabla_q \cdot \left(\frac{1}{a}\mathbf{g}_{pec} - \frac{4\pi G\rho_0}{a^3}\mathbf{u}_\parallel\right) = 0. \tag{5.81b}$$

Imposing the same boundary condition than in (5.77) we obtain:

$$\mathbf{g}_{pec}(\mathbf{q}, t) = \frac{4\pi G\rho_0}{a^2}\mathbf{u}_\parallel(\mathbf{q}, t) = \frac{2}{3t_0^2}\left(\frac{t}{t_0}\right)^{-4/3}\mathbf{u}_\parallel(\mathbf{q}, t). \tag{5.82}$$

Using the result (5.82) in the solution (5.80) we obtain finally:

$$\mathbf{u}_\perp(\mathbf{q},t) = \mathbf{u}_\perp(\mathbf{q}) + 3\mathbf{v}_\perp(\mathbf{q})t_0\left(1-\left(\frac{t}{t_0}\right)^{-\frac{1}{3}}\right) \tag{5.83a}$$

$$\begin{aligned}\mathbf{u}_\parallel(\mathbf{q},t) = {}& \mathbf{g}_{rel}(\mathbf{q},t_0)t_0^2\left(\frac{9}{10}\left(\frac{t}{t_0}\right)^{\frac{2}{3}} + \frac{3}{5}\left(\frac{t}{t_0}\right)^{-1}\right) \\ & + \mathbf{v}_\parallel(\mathbf{q})t_0\left(\frac{3}{5}\left(\frac{t}{t_0}\right)^{\frac{2}{3}} - \frac{3}{5}\left(\frac{t}{t_0}\right)^{-1}\right)\end{aligned} \tag{5.83b}$$

5.5.2 The Zeldovich approximation

For asymptotically large times the solution (5.83) is

$$\mathbf{u}(\mathbf{R},t) \simeq \frac{3}{5}t_0\left(\frac{t}{t_0}\right)^{2/3}\left[\frac{3}{2}\mathbf{g}(\mathbf{R},t_0)t_0 + \mathbf{v}_\parallel(\mathbf{R},t_0)\right]. \tag{5.84}$$

This solution, using Eqs. (4.60) and (4.57), gives the following simple relation between the displacements and the peculiar velocity with the peculiar acceleration at any time:

$$\mathbf{u}(\mathbf{R},t) = \frac{3}{2}\left(\frac{t}{t_0}\right)^{4/3}\mathbf{g}(\mathbf{R},t)t_0^2 \tag{5.85a}$$

$$\mathbf{v}(\mathbf{R},t) = \mathbf{g}(\mathbf{R},t)t. \tag{5.85b}$$

By imposing the initial conditions

$$\mathbf{u}_\perp(\mathbf{R},t_0) = \mathbf{0} = \mathbf{v}_\perp(\mathbf{R},t_0) \tag{5.86a}$$

$$\mathbf{v}_\parallel(\mathbf{R},t_0) = \mathbf{g}(\mathbf{R},t_0)t_0 = \frac{2}{3t_0}\mathbf{u}_\parallel(\mathbf{R},t_0). \tag{5.86b}$$

the relation (5.85) hold at any time and the evolution is simply given by Eqs. (5.85), which is the well known Zeldovich approximation, in which the decaying mode is zero from the initial time. The initial conditions (5.86) are usually imposed in N-body simulations.

5.6 Comparison between Lagrangian and Eulerian theory

There is an extensive literature about the accuracy of Eulerian and Lagrangian perturbative theory. Two kinds of test have been performed: comparison with N-body simulations (e.g. Melott, [BCHJ95]) or with exactly solvable models, essentially the plane-symmetric case (e.g. [Tat04] and references therein) and the spheroidal collapse ([MSS94, BCHJ95, YMM98, YMGM05]). The main result is that Lagrangian theory gives, at the same order in perturbation theory, better results than Eulerian one for the density field, and about the same results (or better) for the velocity field. Some reasons which can explain this apparent superiority of the Lagrangian approach are:

- The perturbative Lagrangian theory conserves mass at all orders. This is trivial because we compute the flow of fluid elements. The trajectories of these fluid elements will be only approximate, but they will not appear or disappear. The Eulerian theory does not. It is patent in the fact that the continuity equation is approximated.
- The Lagrangian theory (indeed the *Zeldovich approximation*) is exact in one dimension ([Buc89]).

The way in which they work is very different. The linear Eulerian equation is local: the growth of density fluctuations at a given point is related to the density fluctuation *at the same point*. Imagine, for simplicity, an non-expanding space. If there is an over-density in some region, it will grow indefinitely (or at least up to $\delta \sim 1$, after which the approximation breaks down). But it is possible that due to the attraction of a larger over-density, the whole over-density moves and this region of space remains empty of matter. However, if we are not interested in the exact position of the fluctuation (and we are not in general, we are only interested in statistics), the fluctuation will grow approximately with the right rate, but not in the right position. The Lagrangian approximation is dynamical, in the sense that the (approximated) flow of particles is computed. In what follows we are going to develop an oversimplified example inspired by what has been done in the literature to try to understand what the *linear* Lagrangian and Eulerian theory "really do".

5.6.1 Spherical collapse

Let us consider now the more physical example of spherical collapse. It has been treated extensively in the literature (e.g. [Pee80, SC95, Sas00]). We consider a spherical over-density of initial radius R_0 and density $\rho = \rho_0(1+\delta)$ embedded in an EdS universe with initial density ρ_0. Consider a shell of radius r_0 that contains initially (at $t = t_0$) a mass

$$M = \frac{4\pi}{3}\rho_0(1+\delta_0)r_0^3, \tag{5.87}$$

The equation of motion for this shell is

$$\frac{d^2r}{dt^2} = -\frac{GM}{r^2} = -\frac{4\pi}{3}\frac{G\rho_0(1+\delta_0)}{r^2}r_0^3, \tag{5.88}$$

where M is the mass contained in the sphere of radius r_0. We will consider that the sphere contracts homogeneously, i.e. that a shell has always the same amount of matter inside it, and different shells do not cross. It is very simple to solve Eq. (5.88) (e.g. [LL59a]). First we integrate Eq. (5.88) multiplying both sides by dr/dt. The result is

$$\left(\frac{dr}{dt}\right)^2 = \frac{8\pi}{3}\frac{G\rho_0(1+\delta_0)}{r}r_0^3 + 2E, \tag{5.89}$$

where the constant of integration E is the energy of the shell. To obtain the Friedmann equation (4.18) (with $\Omega_T = 1$) in the limit $\delta_0 = 0$ at $t = t_0$, we choose E so that:

$$\left(\frac{dr}{dt}\right)^2 = \frac{8\pi}{3}G\rho_0\left[\frac{(1+\delta_0)}{r}r_0^3 - r_0^2\delta_0\right]. \tag{5.90}$$

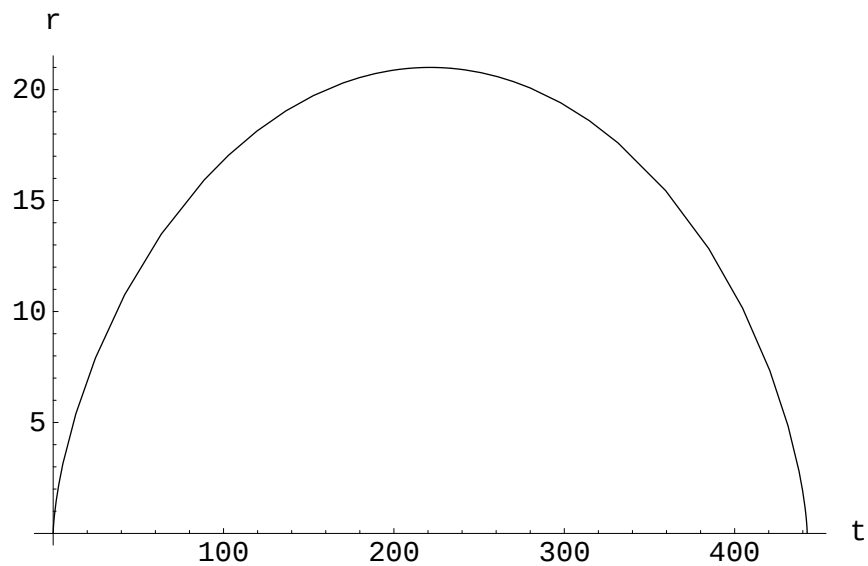

Figure 5.2: Evolution of a shell in the spherical collapse model. The parameters are $t_0 = 1$, $r_0 = 1$ and $\delta_0 = 0.05$. The time is in units of t_0.

We have therefore to integrate

$$t = \frac{1}{r_0\sqrt{\frac{8\pi G}{3}\rho_0}} \int \frac{dr}{\sqrt{\frac{(1+\delta_0)r_0}{r} - \delta_0}}. \tag{5.91}$$

Changing variables $r = (1+\delta_0)r_0(1-\cos\xi)/2\delta_0$ we find the parametric expression:

$$r = \frac{1+\delta_0}{2\delta_0} r_0 (1-\cos\xi) \tag{5.92a}$$

$$t = \frac{3}{4}\frac{1+\delta_0}{\delta_0^{3/2}} t_0 (\xi - \sin\xi), \tag{5.92b}$$

where we have used the definition of t_0 given in Eq. (4.30):

$$6\pi G \rho_0 t_0^2 = 1. \tag{5.93}$$

In Eq. (5.92b), the integration constant has been chosen in order to have only the growing mode at $t = t_0$. It can be checked with Eq. (5.92a) that $r(0) = 0$ and $r(t_0) = r_0$. The shell initially at r_0 collapses at $\xi = 2\pi$. This evolution can be seen in Fig. 5.2. The evolution of the density within the shell is given by:

$$\rho_s(t) = \frac{2\rho_0\delta_0}{1-\cos\xi}. \tag{5.94}$$

The evolution of the background, for an EdS universe (c.f. Eq. (4.30), is

$$\rho(t) = \rho_0 \left(\frac{t_0}{t}\right)^2. \tag{5.95}$$

The evolution of the density contrast is thus given by:

$$\delta(t) = \frac{\rho_s(t)}{\rho(t)} - 1 = \frac{9}{2}\frac{(\xi - \sin\xi)^2}{(1-\cos\xi)^3} - 1. \tag{5.96}$$

Eulerian perturbation theory

Let us expand Eq. (5.96) in power series of ξ at the dominant order:

$$\delta(\xi) = \frac{3}{20}\xi^2 + \mathcal{O}(\xi^4). \tag{5.97}$$

Expanding in series Eq. (5.92b) up to $\mathcal{O}(\xi^3)$ we find

$$t = \frac{t_0}{8\delta^{3/2}}\xi^3 + \mathcal{O}(\xi^5). \tag{5.98}$$

Solving for ξ we have:

$$\xi = 2\delta^{1/2}\left(\frac{t}{t_0}\right)^{1/3} + \mathcal{O}(t). \tag{5.99}$$

Substituting the result in Eq. (5.97), we get the expression for the density contrast:

$$\delta(t) = \frac{3}{5}\delta_0\left(\frac{t}{t_0}\right)^{2/3} + \mathcal{O}(t^{4/3}). \tag{5.100}$$

This is the result obtained using Eulerian linear theory (see Eq. (4.73)). We have chosen the initial conditions in such a way that only the growing mode is present at $t = t_0$. If we had expandes (5.96) around $t = t_0$ instead, we would have obtained both growing and decaying modes, as in Eq. (4.73).

Lagrangian perturbation theory

Let us now expand Eq. (5.96) in power series in a different way. We rewrite Eq. (5.96) as:

$$\delta(t) = \left[\left(\frac{9}{2}\right)^{-1/3}\frac{(1-\cos\xi)}{(\xi-\sin\xi)^{2/3}}\right]^{-3} - 1. \tag{5.101}$$

We expand the expression in brackets in power series of ξ and we use Eq. (5.98) to obtain:

$$\left(\frac{9}{2}\right)^{-1/3}\frac{(1-\cos\xi)}{(\xi-\sin\xi)^{2/3}} = 1 - \frac{\delta_0}{5}\left(\frac{t}{t_0}\right)^{2/3} + \mathcal{O}(t^{4/3}). \tag{5.102}$$

Therefore the density contrast is

$$\delta(t) = \left[1 - \frac{\delta_0}{5}\left(\frac{t}{t_0}\right)^{2/3} + \mathcal{O}(t^{4/3})\right]^{-3} - 1. \tag{5.103}$$

It is simple to check that this result corresponds to the linear order in Lagrangian perturbative theory. We use Eq. (5.83) without the decaying mode (and no initial velocities and divergence-free displacements) to get:

$$u(t) = g_{pec}(t_0)t_0^2\frac{9}{10}\left(\frac{t}{t_0}\right)^{2/3}, \tag{5.104}$$

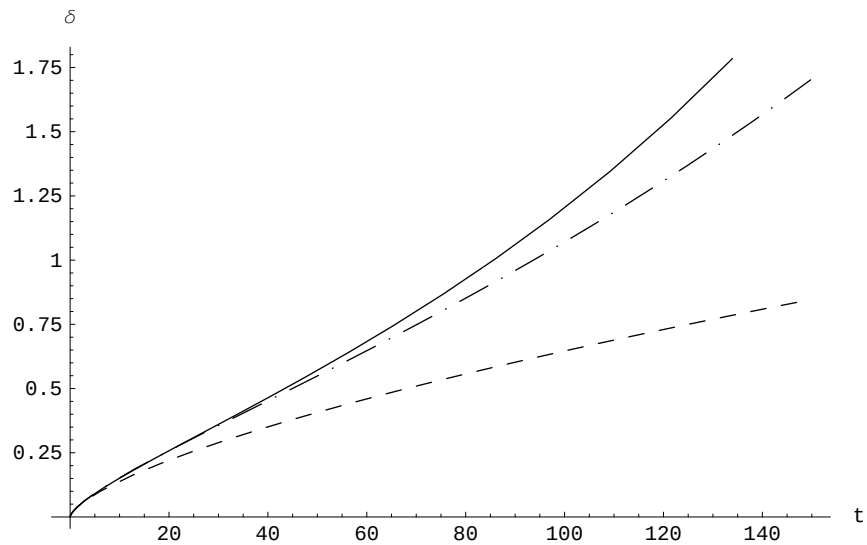

Figure 5.3: Comparison of the evolution of contrast density for exact spherical shell model (full lines), Eulerian approximation (dashed) and Lagrangian approximation (dashed-dotted). The parameters are $t_0 = 1$, $r_0 = 1$ and $\delta_0 = 0.05$. The time is in units of t_0.

where the initial gravitational field is:

$$g(t_0) = -\frac{4\pi}{3} G\rho_0\delta_0 = \frac{\delta_0}{t_0^2}\frac{2}{9}. \tag{5.105}$$

Using these expressions the evolution of the contrast is given by:

$$\delta(t) \simeq \left[1 - \frac{\delta_0}{5}\left(\frac{t}{t_0}\right)^{2/3}\right]^{-3} - 1, \tag{5.106}$$

i.e. Eq. (5.103). This confirms that the expression in brackets in Eq. (5.101) is the lagrangian displacement $u(t)$.

We see in Fig. 5.3 a plot of the exact solution, the Eulerian an Lagrangian approximation. The Lagrangian approximation is better. The reason is simple: Taylor expansion has been performed up to the same order, but not in the same variable. The result (5.106) is clearly more accurate than (5.100).

5.7 Numerical simulations of structure formation

Perturbation theory breaks down when the density contrast δ becomes too large. Computing the evolution of the initial perturbation using linear theory (see chapter 4) it is possible to estimate simply, at each time, the scale at which perturbation theory breaks down as a function of time. In Fig. 5.4 we show the linear evolution of the PS of density fluctuations for two different times (the amplitude grows with time). In practice, numerical simulations show that linear

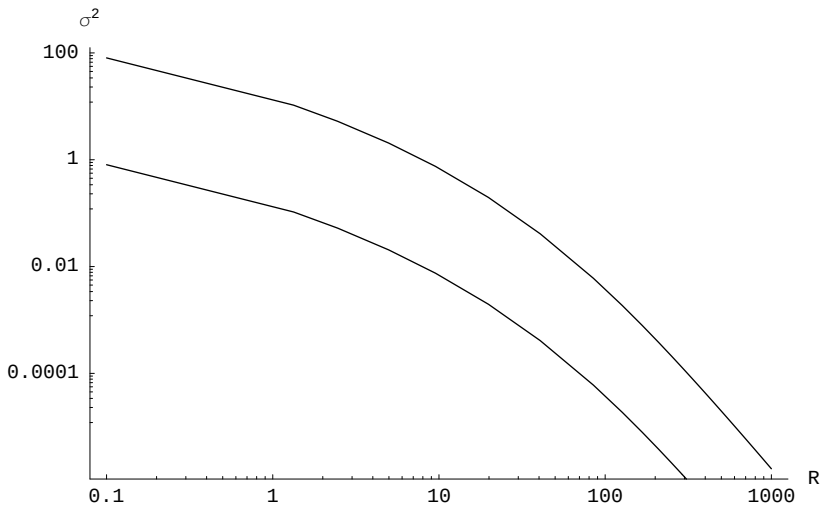

Figure 5.4: Variance in mass now for a CDM model with parameters given in section 4.5.6. The units of R are h^{-1}Mpc.

theory works reasonably well up to $\delta \approx 1$ (i.e. a bit later than in the spherical collapse we worked out in the previous section). Therefore, at the earlier time shown in the figure, the perturbative approach breaks down at scales larger than $R \approx 2\,h^{-1}$ Mpc whereas at the later time $R \approx 20\,h^{-1}$ Mpc. To compute the gravitational clustering at scales below these ones we might solve numerically the Vlasov-Poisson equation. The main problem in trying to solve this equation by brute force is that instabilities appear, because of non-linearities, at sub-resolution scales [HRWH04]. The most commonly used method which avoids these problems is N-body simulation. The idea is to sample the 6-dimensional phase space distribution $f(\mathbf{r}, \mathbf{p})$ of the Vlasov equation by "tracer" particles, because it is not possible to handle numerically the problem using the real number of CDM particles in a cosmological volume. Then, the position of the particles are evolved simply under Newtonian gravity, with the only modification that the expansion of the universe is included, as described in chapter 4, in a way analogous to that described in chapter 4. We emphasize that there is no rigorous derivation establishing the relation between this method and the exact solution of the Vlasov equation. Indeed for this reason it is not possible to quantify precisely the error introduced by using it.

5.7.1 N-body simulation

Let us outline the basics of how cosmological N-body simulations are performed. Gravity is an attractive force which produces, during the evolution, smaller and smaller structures. It implies the necessity to resolve the smallest possible scales. On the other hand, it is long range and distant parts of the system have influence on one another. Therefore, the combination of the necessity to resolve small scales in large regions implies the need to use the maximum number of particles. The direct calculation of the force is numerically costly —N^2

operations for N particles — and even a modest 10^4 particles simulation needs considerable computer resources (current simulations use up to 2046^3 particles). To solve this technical problem different approximations are used, such as the "Particle-Mesh" (PM) method, the "Particle-Particle+Particle-Mesh" method (P^3M) or "tree-codes" (for a review see e.g. [ama]). In short, the first one smooths the particle mass on a grid to allow the use FFT techniques, that speed up the computation. The P^3M method does almost the same but gains accuracy by computing directly ("particle-particle") the force from nearby particles. Tree-codes build a hierarchy between the particles that resembles a "tree". The gravitational force is calculated using the structure of the tree. The force between two close particles in the tree is computed almost exactly. The force between distant particles in the tree is computed using a whole branch as a single effective particle, as in a multipole expansion method. The N-body code GADGET that we will use in chapter 9 utilizes this latter method to compute the force (for the details see [SYW01]). Others refinements are used to improve the small scale resolution in the simulations. One of them is to use an adaptative mesh: in regions with higher density a mesh with more resolution is used, keeping a lower resolution in regions with small density. Another method is the technique of "re-simulation" (e.g. [P+03]: a first simulation is performed to localise regions with high density. Then, the simulation is performed again putting more particles in the region where the particles of the final high density regions were initially.

5.7.2 Initial conditions

An essential and delicate issue in the N-body simulations is how to set up initial conditions. The regime in which we study CDM (through the Vlasov equation) can be well approximated by a fluid equation. Therefore the problem is to approximate a fluid with given correlation properties by a system of particles with (almost) the same correlations. The most widely method employed uses the "displacement field" method outlined in chapter 3 (e.g. [EDWF85], [Ber95] and references therein): to a lattice is applied a small displacement field with some appropriate correlations (we will discuss extensively this method in chapter 7). It reproduces well the correlations up to the Nyquist frequency in Fourier space, but has the disadvantage that the initial conditions maintain the structure of a lattice (because the relative displacements are small compared with the interparticle distance) and it leads to strongly preferred directions on all scales, which can introduce artifacts in the modelization of an isotropic system. A variant of this method uses a "glass" as initial configuration (see [Whi94]) as an alternative to the perfect lattice to which displacements are applied. Particles are initially placed randomly in the simulations box and their evolution under *reversed* gravity computed (i.e. as in the OCP, see chapter 6). After a sufficiently long time, the distribution presents a "glass" structure in which the gravitational force is near zero at the particle positions. Then displacements are applied exactly as for the lattice. The advantage of this method is that it gives a much more isotropic initial configuration.

5.7.3 Discreteness effects in N-body simulations

"Solving" the Vlasov equation using N-body simulations involves a discretization, in which scales that are not in the original problem (mass of the "N-body" particles, average distance between them) are introduced. In chapter 7 we will give a detailed analysis of the discreteness effects in the *initial conditions* of the N-body simulations. In chapter 9 we will study the discreteness effects in the evolution of an N-body system in the *linear regime* by comparing the evolution of a self-gravitating fluid and its discretization into N-bodies.

Some studies of the issue of discreteness in N-body simulations can be found in [KMS96, MSS97, SMSS98, HYS01, BK02, P$^+$03, DMSK04, DMS04]. The main aspects of the problem discussed in these papers are:

1. Two-body relaxation. It consists of the scattering (i.e. close encounter) of two N-body particles. This is a process that clearly is not contained in the Vlasov equation, which is collision-less (there is no source term on its r.h.s.). In other words, the force in the Vlasov equation comes from large regions of the system producing a kind of mean field. Numerical studies show that the effects of the two-body relaxation decreases when increasing the number of particles following roughly a $N^{0.3}$ law [DMSK04]. This very slow decreasing with N of two-body relaxation can be explained by the fact that in a CDM model the clustering is hierarchical: the first objects to form have very few particles, independently of the resolution of the simulation, i.e. of N.

2. Breaking of isotropy. The Vlasov equation has no preferred direction. However, N-body simulations breaks its isotropy. This is discussed in [MSS97]. We will study this phenomenon at early times in chapter 9. The anisotropy comes simply from the fact that the initial configuration is not statistically isotropic when setting up initial conditions with a perturbed lattice. Therefore in some directions the collapse is faster than in others. Such effects may be minimized using a "glass" as initial configuration.

3. It has been observed that global properties of the final structures of N body simulations (e.g. correlation properties)[BJSL02] or halo profiles (e.g. [P$^+$03, DMS04, HRWH04]) do not depend on the number of particles. This suggest that the N body simulation are not fundamentally biased by the use of a finite N.

Chapter 6

Statistical physics of Coulomb systems

To set up initial conditions for N-body gravitational simulations, we will use in chapter 8 a modified Coulombian system at thermal equilibrium. In this chapter we are going to review the basics of these kind of systems. First, we will remind the concept of ensemble and partition function, essentially to fix notations. Then, we will introduce the diagrammatic expansion of partition functions in order to compute statistical quantities in a system of interacting particles at thermal equilibrium. We will apply these results to a gas with short range interactions as well as a Coulombian long-ranged system. We will use the technique of diagram ressumation to derive integral equations, that permits to study very fruitfully the correlation function in a wide class of systems. Then, we will study more precisely the one-component plasma, introducing the Debye-Huckel theory. We will refine the results of this theory using the integral equations mentioned above. We will also give some practical recipes how to use these equations as well as some techniques of Molecular Dynamics simulations, that permits to compute "exactly" the correlation function. All this chapter is written for people that does not have a previous knowledge of all these techniques, as a priori cosmologists. For this reason, the introduction of the cluster techniques is done step by step, which can seem very slowly for a specialist. What it is interesting, is that these techniques could be applied also in the context of gravitational clustering. We will outline some examples at the end of the chapter. All the material presented here has been mainly extracted from [LL59b, Isi71, HM76, BH80, Hua87, GT].

6.1 Ensembles in Statistical Physics

Equilibrium Statistical Physics is constructed using the concept of *ensembles*. An ensemble is a collection of systems subject to some boundary conditions. Depending the system to study, it is useful to use different kind of ensembles, i.e. subjects to different boundary conditions. In the next we will outline, for some ensembles, the most important results that are relevant for this chapter.

6.1.1 The micro-canonical ensemble

The micro-canonical ensemble consist of a collection of isolated systems of N particles with total energy between E and $E + \Delta E$. The basic assumption is the *a priori equiprobability* of all the accessible states of the system. It means that a all the configurations allowed by the dynamics (through, for instance, the Hamiltonian $\mathcal{H}$), have the same probability. Therefore, the micro-canonical distribution function can be written as

$$\rho(p,q) = const, \quad \mathcal{H}(p,q) \in (E, E+\Delta E) \tag{6.1a}$$

$$\rho(p,q) = 0, \quad \mathcal{H}(p,q) \notin (E, E+\Delta E), \tag{6.1b}$$

where $\rho(p,q)$ is defined in Eq. (5.10).

6.1.2 The canonical ensemble

The canonical ensemble consits in a collection of system of particles in a box of volume V in contact with a heat bath at temperature T, with which it can exchange energy. The equilibrium probability density[1] $f_0^{(N)}$ for finding a system with its N particles having precisely coordinates $\mathbf{r}^N$ and momenta $\mathbf{p}^N$ is:

$$f_0^{(N)}(\mathbf{r}^N, \mathbf{p}^N) = \frac{1}{N!}\frac{1}{h^{3N}}\frac{1}{Q_N(V,T)} \exp\left[-\beta\mathcal{H}(\mathbf{r}^N, \mathbf{p}^N)\right], \tag{6.2}$$

where h is the Planck's constant, the factor $N!$ appears because we consider the particles indistinguishable and $Q_N(V,T)$ is called the *partition function*:

$$Q_N(V,T) = \frac{1}{h^{3N}N!}\int_V e^{-\beta\mathcal{H}(\mathbf{p}^N,\mathbf{r}^N)} d\mathbf{p}^N d\mathbf{r}^N. \tag{6.3}$$

For example, the PDF of momenta of a single particle in an ideal gas is given by the *Boltzmann distribution* (e.g. [Isi71]):

$$\rho(p,q) = \frac{e^{-\beta\frac{p^2}{2m}}}{\int d^{3N}p e^{-\beta\frac{p^2}{2m}}} = \left(\frac{\beta m}{2\pi}\right)^{3/2} e^{-\beta\frac{p^2}{2m}}. \tag{6.4}$$

We are going to consider Hamiltonians that can be written as the sum of a kinetic part – that depends only on the momenta $\mathbf{p}^N$ — and a potential part — that depends only on the positions $\mathbf{r}^N$:

$$\mathcal{H}(\mathbf{p},\mathbf{r}) = \frac{\mathbf{p}^2}{2m} + V_N(\mathbf{r}^N), \tag{6.5}$$

where

$$V_N = \sum_{i<j} v(|\mathbf{r}_i - \mathbf{r}_j|) \tag{6.6}$$

and $v(\mathbf{r})$ is the interacting potential. Therefore integrating (6.3) over the variable $\mathbf{p}^N$ yields

$$Q_N(V,T) = \frac{Z_N(V,T)}{N!\lambda_B^{3N}} \tag{6.7}$$

[1] It is defined in Eq. (5.10) for non equilibrium in general, the subscript "0" here denotes equilibrium.

with the *configurational integral*

$$Z_N(V,T) = \int e^{-\beta V_N(\mathbf{r}^N)} d\mathbf{r}^N \tag{6.8}$$

and λ_B is the De Broglie wavelength defined in Eq. (5.1). Note that it is possible to write

$$Q_N(V,T) = Q_{ideal}(V,T)\frac{Z_N(V,T)}{V^N}, \tag{6.9}$$

where $Q_{ideal}(V,T)$ is the partition function of the ideal gas. From the partition function (6.3) it is possible to compute all the thermodynamic quantities. For example, the average energy is given by the formula

$$\begin{aligned} U \equiv \langle E \rangle &= \frac{1}{N! h^{3N} Q_N} \int \mathcal{H}(\mathbf{p}^N, \mathbf{r}^N) e^{-\beta \mathcal{H}(\mathbf{p}^N, \mathbf{r}^N)} d\mathbf{p}^N d\mathbf{r}^N \\ &= -\left[\frac{\partial}{\partial \beta} \ln Q_N(V,T)\right]_V = \left[\frac{\partial}{\partial T} \ln Q_N(V,T)\right]_V k_B T^2 \end{aligned} \tag{6.10}$$

and the pressure by

$$p = k_B T \left[\frac{\partial(\ln Q_N(V,T))}{\partial V}\right]_T. \tag{6.11}$$

It is simple to show (e.q. [Hua87]) that the partition function is related with the Helmholtz free energy in the way

$$Q_N(V,T) = \exp\left(-\beta F(V,T)\right). \tag{6.12}$$

Assuming an Hamiltonian of the form (6.5), the PDFto find, simultaneously, the particle 1 around $\mathbf{r}_1$, particle 2 around $\mathbf{r}_2$, etc., is given by:

$$\rho_N(\mathbf{r}^N) = \frac{1}{Z_N} e^{-\beta V_N(\mathbf{r}^N)}. \tag{6.13}$$

If we are interested only in the information about $n < N$ particles, we integrate over the other $N - n$ ones:

$$\rho_N^{(n)}(\mathbf{r}^n) = \frac{1}{Z_N} \frac{N!}{(N-n)!} \int e^{-\beta V_N(\mathbf{r}^N)} d\mathbf{r}_{n+1} \ldots d\mathbf{r}_N. \tag{6.14}$$

This is the n-particle density function, defined in the general non-equilibrium case in chapter 5. The combinatory pre-factor comes from the indistinguishability of the particles. The expression (6.14) can be obtained in an elegant way using functional derivatives (see chapter Appendix B). Introducing the auxiliary field $u(\mathbf{r}_i)$ in the configurational integral

$$Z_N(V,T) = \int \prod_{i<j}^{N} e^{-\beta v(\mathbf{r}_{ij})} \prod_k^N e^{u(r_k)} d\mathbf{r}_1 \ldots d\mathbf{r}_N, \tag{6.15}$$

it is trivial to check that

$$\rho_N^{(n)}(\mathbf{r}_1 \ldots \mathbf{r}_n) = \frac{N!}{(N-n)!} \frac{1}{Z_N} \lim_{u \to 0} \frac{\delta^{(n)} Z_N(\mathbf{u})}{\delta u(\mathbf{r}_1) \ldots \delta u(\mathbf{r}_n)}. \tag{6.16}$$

We define the function g as

$$g(\mathbf{r}_1, \mathbf{r}_2) = \frac{\rho^{(2)}(\mathbf{r}_1, \mathbf{r}_2)}{\rho^{(1)}(\mathbf{r}_1)\rho^{(1)}(\mathbf{r}_2)}. \tag{6.17}$$

For a statistically homogeneous and isotropic system we have

$$g(\mathbf{r}_1, \mathbf{r}_2) = g(|\mathbf{r}_1 - \mathbf{r}_2) \equiv g(r). \tag{6.18}$$

The function $g(r)$ is called the *radial distribution function*. It is the Fourier pair of the structure factor $S(k)$ defined in Eq. (3.17), i.e.

$$S(k) = 1 + n \int [g(r) - 1] e^{i\mathbf{k}\cdot\mathbf{r}} d\mathbf{r}. \tag{6.19}$$

We introduce also the function h defined as

$$h(\mathbf{r}_1, \mathbf{r}_2) = g(\mathbf{r}_1, \mathbf{r}_2) - 1. \tag{6.20}$$

It is easy to check that

$$h(\mathbf{r}_1, \mathbf{r}_2) = \frac{1}{\rho^{(1)}(\mathbf{r}_1)\rho^{(1)}(\mathbf{r}_2)} \lim_{u \to 0} \frac{\delta^{(2)} \ln Z_N(\mathbf{u})}{\delta u(\mathbf{r}_1)\delta u(\mathbf{r}_2)}. \tag{6.21}$$

It is possible to write the corrections to the ideal gas for the energy and the pressure as a function of $g(r)$. From the definitions (6.9), (6.10) (6.16) and (6.20), it is simple to show that the correction to the ideal gas are (for a statistically homogeneous and isotropic system):

$$\frac{U_c}{N} = 2\pi\rho \int_0^\infty g(r) v(r) r^2 dr \tag{6.22a}$$

$$\left(\frac{\beta P}{\rho}\right)_c = -\frac{2}{3}\pi\beta\rho \int_0^\infty g(r) r^3 \frac{dv(r)}{dr} dr. \tag{6.22b}$$

6.1.3 The grand canonical ensemble

The grand canonical ensemble consists in a collection of systems with the same boundary conditions than the canonical ensemble (fixed volume V, interaction with a heat bath that maintains a fixed temperature T) but it can exchange, in addition, particles with the heat bath. To describe such situation, the chemical potential of the specie i, μ_i is introduced, which is the thermodynamic variable conjugate to the number of particles of the same specie. The equilibrium probability density of the grand canonical ensemble is a generalization of Eq. (6.2):

$$f_0^{(N)}(N, \mathbf{r}^N, \mathbf{p}^N) = \frac{1}{N!} \frac{1}{h^{3N}} \frac{1}{\Xi_N(z, V, T)} \exp[\beta N \mu] \exp\left[-\beta \mathcal{H}(\mathbf{r}^N, \mathbf{p}^N)\right] \tag{6.23}$$

Eq. (6.23) represents the probability of finding a system with N particles with positions $\mathbf{r}^N$ and momenta $\mathbf{p}^N$. The normalization factor Ξ is the *grand canonical partition function*:

$$\Xi(z, V, T) = \sum_{N=0}^{\infty} \left(\frac{z^N}{N!}\right) Z_N(V, T), \tag{6.24}$$

for the grand canonical partition function, where Z_N is given by Eq. (6.8) and we have used the *fugacity*, defined as

$$z = \frac{e^{\beta\mu}}{\lambda_B^3}. \tag{6.25}$$

In an analogous manner than with the canonical ensemble, it is possible to compute the thermodynamic quantities (e.g. the pressure, average energy, average number of particles, etc.) by derivation about the convenient variable of the grand canonical partition function (6.24).

Assuming an Hamiltonian of the form (6.5), the n-point probability density function is

$$\begin{aligned} \rho^{(n)}(\mathbf{r}^n) &= \frac{1}{\Xi}\sum_{N\geq n}^{\infty}\frac{z^N}{(N-n)!}\int e^{-\beta V_N(\mathbf{r}^N)}d\mathbf{r}_{n+1}\ldots d\mathbf{r}_N \\ &= \frac{1}{\Xi}\sum_{N\geq n}^{\infty}\frac{z^N}{N!}\rho_N^{(n)}(\mathbf{r}^n), \end{aligned} \tag{6.26}$$

where the last expression gives the relation with the canonical equation (6.14). In an analogous way to what we did in that case, we introduce the external field $\mathbf{u}(\mathbf{r})$ and we write the grand canonical function as

$$\Xi(z^*, V, T) = \sum_{N=0}^{\infty}\frac{1}{N!}\int\prod_{i=1}^{N}z^*(\mathbf{r}_i)\prod_{i<j}^{N}e^{-\beta v(\mathbf{r}_i-\mathbf{r}_j)}d\mathbf{r}_{n+1}\ldots d\mathbf{r}_N, \tag{6.27}$$

where

$$z^*(\mathbf{r}) = ze^{\beta u(\mathbf{r})}. \tag{6.28}$$

The n-point correlation function (6.26) can be written as

$$\rho^{(n)}(\mathbf{r}^n) = \frac{1}{\Xi}\prod_{i=1}^{n}z^*(\mathbf{r}_i)\frac{\delta^n\Xi}{\prod_{i=1}^{n}\delta z^*(\mathbf{r}_i)}. \tag{6.29}$$

6.2 Classical cluster expansion and HNC equation

Once we have computed the partition function we can compute all the thermodynamic quantities of interest. However, the main difficulty is precisely to compute the partition function. It is easy to see that for an arbitrary interaction it is an impossible task. We are going to describe a perturbative method to compute the partition function by a series expansion. Let us consider the canonical configurational integral (6.8). We rewrite it as follow

$$Z_N(V,T) = \int\prod_{i<j}^{N}e(\mathbf{r}_{ij})d\mathbf{r}^N, \tag{6.30}$$

where $\mathbf{r}_{ij} \equiv \mathbf{r}_i - \mathbf{r}_j$ and $e(\mathbf{r}_{ij}) = \exp(-\beta v(\mathbf{r}_{ij}))$. Let us define the Mayer f function as

$$f(\mathbf{r}_{ij}) = e^{-\beta v(\mathbf{r}_{ij})} - 1. \tag{6.31}$$

We can then write the partition function (6.30) as

$$Z_N = \int \prod_{i<j}^{N} [f(\mathbf{r}_{ij}) + 1]\, d\mathbf{r}^N. \tag{6.32}$$

For the moment we assume that (6.32) is convergent. For a potential which decreases as a function of distance as $f(r) \simeq -\beta v(r)$ for $r \to \infty$, It is therefore natural to expand Eq. (6.32) in powers of f. Then, up to order f^2 we have:

$$Z_N \simeq \int \left(1 + \sum_{i<j}^{N} f(\mathbf{r}_{ij})\right) d\mathbf{r}^N = V^N + \frac{N(N-1)}{2} V^{N-1} \int f(\mathbf{r}_{12}) d\mathbf{r}_{12}, \tag{6.33}$$

where we have assumed translational invariance. We can write:

$$Z(V,T) \simeq Z_{ideal} \left(1 - \rho \frac{N-1}{2} I_2\right) \tag{6.34}$$

where $\rho = N/V$ and I_2 is the integral of (6.33). Clearly something strange happens in Eq. (6.34)! In the thermodynamic limit the expression seems to diverge (assuming that I_2 is non-zero). The problem is that we have eliminated some terms in the product (6.32) that makes (6.34) infinite in this limit. This is what we are going to study in the next subsection but we can already anticipate that the right expression is

$$\beta Z(V,T) = Z_{ideal} \left(1 - \rho \frac{N-1}{2} I_2\right) \simeq Z_{ideal} \left(1 - \rho I_2/2\right)^N = Z_{ideal} e^{-\rho I_2/2}, \tag{6.35}$$

for small densities.

6.2.1 Cumulant expansion

The quantity we really want to compute is the logarithm of the partition function. We will see that computing it instead of the partition function we will not have the problems that appeared above. Let us then write the configurational integral (6.8) as

$$Z_N(V,T) = V^N \left\langle e^{-\beta v} \right\rangle_0, \tag{6.36}$$

where$\langle \cdots \rangle_0$ means "average over the PDF of the ideal gas":

$$\langle \cdots \rangle_0 = \frac{1}{V^N} \int \cdots d\mathbf{r}^N. \tag{6.37}$$

The Helmholtz potential can be therefore written as

$$F(V,T) = F_{ideal}(V,T) - k_B T \ln \left\langle e^{-\beta v} \right\rangle_0. \tag{6.38}$$

We know how to expand (6.36) in powers of f. We can relate this expansion with the one on the r.h.s. of Eq. (6.38) in the following way. Let us consider the function $\phi(t)$ defined through the following average over the PDF $p(x)$:

$$\phi(t) \equiv \left\langle e^{tx} \right\rangle = \int \sum_{n=0}^{\infty} \frac{(tx)^n}{n!} p(x) dx \equiv \sum_{n=0}^{\infty} \frac{t^n}{n!} \left\langle x^n \right\rangle. \tag{6.39}$$

We want also to calculate

$$\ln \phi(t) = \ln \left\langle e^{tx} \right\rangle = \sum_{n=1}^{\infty} \frac{t^n M_n(x)}{n!}, \tag{6.40}$$

where the $M_n(x)$ are called cumulants or Thiele semi-invariants. It is easy to calculate them comparing, order by order of t , the Eqs. (6.39) and (6.40). The first cumulants are:

$$\begin{aligned} M_1(x) &= \langle x \rangle \\ M_2(x) &= \left\langle x^2 \right\rangle - \langle x \rangle^2 \\ M_3(x) &= \left\langle x^3 \right\rangle - 3 \langle x \rangle \left\langle x^2 \right\rangle + 2 \langle x \rangle^3 \\ M_4(x) &= \left\langle x^4 \right\rangle - 4 \left\langle x^3 \right\rangle \langle x \rangle - 3 \left\langle x^2 \right\rangle^2 - 6 \langle x \rangle^4 . \end{aligned} \tag{6.41}$$

For what follows, it is important to note that all cross terms in M_n vanish, i.e.

$$M_n(x+y) = M_n(x) + M_n(y), \tag{6.42}$$

where x and y are two independent variables. We are now able to write the high-temperature and low-density expansion of the Helmholtz function.

6.2.2 High temperature expansion

Let us write the corrections to the ideal gas of the Helmholtz function as

$$-\beta F_c(V,T) = \sum_{n=1}^{\infty} \frac{(-\beta)^n}{n!} M_n(v) . \tag{6.43}$$

We can write the first cumulants using their definition (6.41) and Eqs. (6.32) and (6.36):

$$M_1(V,T) = \sum_{i<j} \langle v_{ij} \rangle_0 = \frac{1}{V^N} \int d\mathbf{r}^N \sum_{i<j} v_{ij} = \frac{1}{2} \frac{N(N-1)}{V^2} \int d\mathbf{r}_1 d\mathbf{r}_2 v_{12} \tag{6.44}$$

In the limit $N \to \infty$ and assuming statistical homogeneity and isotropy, we obtain

$$\frac{M_1}{N} = \frac{\rho}{2} \int d\mathbf{r} u(r). \tag{6.45}$$

Note that (6.45) is an extensive quantity, as it should be. Let us compute now the second cumulant:

$$M_2 = \sum_{i<j} \sum_{j} \sum_{k<l} \sum_{l} \langle v_{ij} v_{kl} \rangle_0 - \sum_{i<j} \sum_{j} \langle v_{ij} \rangle_0 . \tag{6.46}$$

It is extremely useful to write the integral appearing in Eq. (6.46) in a diagrammatic form. Each index of the potential is written as a vertex (a black circle) and a "bond" (a dotted line) between each vertex. Studying the first term of Eq. (6.46) we are going to identify different kind of diagrams:

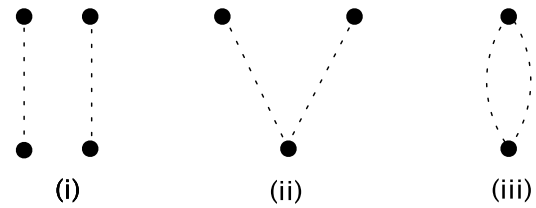

Figure 6.1: Mayer diagrams, (i) disconnected, (ii) reducible and (iii) irreducible.

1. If $i \neq j \neq k \neq l$, and therefore $\langle v_{ij} v_{kl} \rangle_0 = \langle v_{ij} \rangle_0 \langle v_{kl} \rangle_0$. These diagrams are called *disconnected*. Using property (6.42) (or just doing the calculation explicitly) these diagrams cancel each to another. Note that they produce a bad dependence of F_c on N, making this magnitude non-extensive.

2. Diagrams with $i = k$ and $j \neq l$ or $i \neq k$ and $j = l$. In this case $\langle v_{ij} v_{jl} \rangle_0 = \langle v_{ij} \rangle_0 \langle v_{jl} \rangle_0$. They are called *reducible* diagrams because removing a vertex two disconnected diagrams appear. By property (6.42) they also vanish.

3. Diagrams $i = k$ and $j = l$. Then the average is $\langle v_{ij}^2 \rangle_0$. They are called *irreducible* and they are the only ones which contribute to F_c.

In Fig. 6.1 we give the three king of diagrams corresponding to $\langle v^2 \rangle_0$. We can therefore write

$$M_2 = \sum_{i<j} \left[\langle v_{ij}^2 \rangle_0 - \langle v_{ij} \rangle_0^2 \right] \tag{6.47}$$

It is possible to simplify more Eq. (6.47) by noting that, in the thermodynamic limit $N \to \infty$

$$\langle v_{ij}^2 \rangle_0 = \frac{1}{V} \int v_{ij}^2 d\mathbf{r}_{ij} \sim \frac{1}{V} \sim \frac{\rho}{N} \tag{6.48a}$$

$$\langle v_{ij} \rangle_0^2 = \left(\frac{1}{V} \int v_{ij} d\mathbf{r}_{ij} \right)^2 \sim \frac{1}{V^2} \sim \frac{\rho^2}{N^2} \tag{6.48b}$$

Therefore we can conclude that, in the thermodynamic limit (and assuming that the above integrals converge), that (6.48a) dominates (6.48b). We will write finally

$$M_2 = \sum_{i<j} \langle v_{ij}^2 \rangle_0 , \tag{6.49}$$

and therefore

$$\frac{M_2}{N} = \frac{\rho}{2} \int v^2(\mathbf{r}) d\mathbf{r}. \tag{6.50}$$

Its diagrammatic representation is given in graph (iii) of Fig. 6.1. An example of the diagrammatic representation of M_3 is given in Fig. 6.2. The corresponding integrals are:

$$\frac{M_3}{N} = \frac{\rho}{2} \int v^3(\mathbf{r}) d\mathbf{r} + \rho^2 \int v_{12} v_{23} v_{31} d\mathbf{r}_{12} d\mathbf{r}_{23}. \tag{6.51}$$

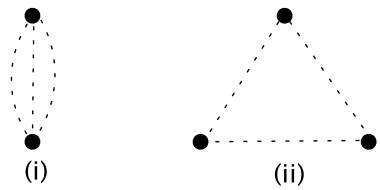

Figure 6.2: Irreducible Mayer diagrams for M_3.

6.2.3 Density expansion

In the above section we have derived the high temperature expansion of the Helmholtz free energy. We have shown that each power in β^n is accompanied by the cumulant M_n. Each order n contains terms with different powers in the density ρ. If we want to construct a density expansion we should group the diagrams which have the same dependence in the density. This can be achieved noting that the power m of the density (i.e. ρ^m) corresponds to the number of bonds, plus one, of the diagrams (see the example (6.51)). Let us write then the density expansion of F_c as

$$-\beta\frac{F_c}{N} = \sum_{p=1}^{\infty}\frac{b_p\rho^p}{p+1}. \tag{6.52}$$

It is simple to find the coefficients b_p by comparing Eq. (6.52) with (6.43):

$$b_p = \frac{p+1}{N}\sum_{n=1}^{\infty}\frac{(-\beta)^n}{n!}M_n(\text{all the irreducible diagrams with } p+1 \text{ vertices}). \tag{6.53}$$

Let us compute the term b_1. All the diagrams with two bonds are written in Fig. 6.3. Then

$$\begin{aligned} b_1 &= \rho\sum_{n=1}^{\infty}\frac{(-\beta)^n}{n!}\int v^n(\mathbf{r})d\mathbf{r} = \rho\int\left(e^{-\beta v(\mathbf{r})}-1\right)d\mathbf{r} \\ &= \rho\int f(\mathbf{r})d\mathbf{r}. \end{aligned} \tag{6.54}$$

The meaning of the full line in the resummed diagram of Fig. 6.3 (on the right) represents an "f-bond" instead of a "v-bond" (represented by a dotted line). The first few diagrams for b_2 are given in Fig. 6.4. The correspondent coefficient is:

$$b_2 = \frac{1}{2!}\int f_{12}f_{23}f_{31}d\mathbf{r}_{12}d\mathbf{r}_{23}. \tag{6.55}$$

In general (e.g. [Isi71]), it can be shown that

$$b_p = \frac{1}{p!}\sum\int\prod f_{ij}d\mathbf{r}^p, \tag{6.56}$$

where the sum is over all *the irreducible topologically distinct diagrams among* $p+1$ *vertices*. To summarise, the practical rule to build a density expansion is:

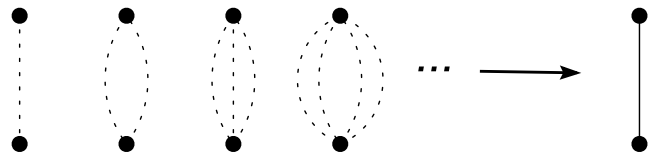

Figure 6.3: First diagrams that gives contributions proportional to b_1.

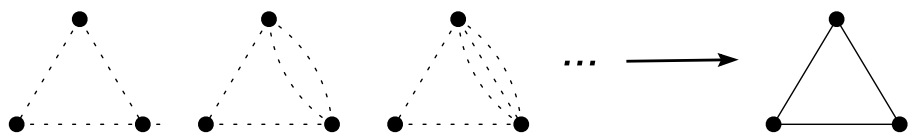

Figure 6.4: First diagrams that gives contributions proportional to b_2.

1. Write the expression (6.32) of the canonical partition function Z_N in function of f functions.

2. Expand in powers of f. One can write a set of (in general) *uncorrelated* diagrams.

3. Take the logarithm. If one groups the diagrams in function of the number of vertices, only *irreducible diagrams* survive. One has therefore a density expansion of $\ln Z_N$ where the number of vertices represent the power of the density. The contribution of each graph is given by *the number of topologically non-equivalent graphs* one can build from it.

6.2.4 An application: computation of distribution functions

Using the diagrammatic machinery we have outlined it is possible to write a diagrammatic expansion of the pair correlation function. Using the partition function with external field (6.15) and Eqs. (6.20) and (6.21) we can write:

$$g(r) = e^{-\beta v(r)} \sum_{n=0}^{\infty} \rho^n y_n(r). \tag{6.57}$$

The Boltzmann factor comes from the f-functions that are not integrated because of the action of the functional derivative. An functional representation of $y_n(r)$ can be found in analogy with the density expansion (e.g. [HM76]). We can derive the diagrammatic representation of $y_n(r)$ knowing the representation of $\ln Z_N$. Two vertices are taken to be the position of the particles, $\mathbf{r}_1$ and $\mathbf{r}_2$ (where $r = |\mathbf{r}_1 - \mathbf{r}_2|$), denoted commonly by a white point[2]. The diagrams are obtained by replacing two black-circles in the diagrams of $\ln Z_N$ by two white-circles for $y_n(r)$ (some diagrams have to be eliminated, see [HM76]). The

[2] We have used in our representation a white dot with a cross in.

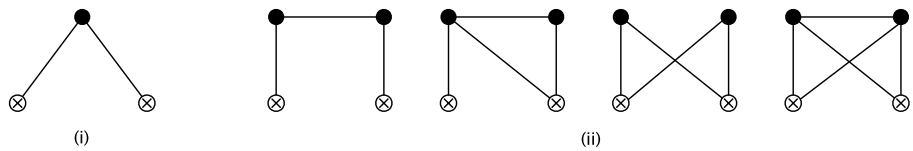

Figure 6.5: Diagrams contributing to (i) $y_1(r)$ and (ii) $y_2(r)$.

diagrams contributing for $y_1(r)$ and $y_2(r)$ are given in Fig. 6.5, which explicit expressions are:

$$y_1(r) = \int f(\mathbf{r}_{13}) f(\mathbf{r}_{23}) d\mathbf{r}_{23} \tag{6.58a}$$

$$\begin{aligned} y_2(r) =& \frac{1}{2} \int [2 f(\mathbf{r}_{13}) f(\mathbf{r}_{34}) f(\mathbf{r}_{42}) + 4 f(\mathbf{r}_{13}) f(\mathbf{r}_{34}) f(\mathbf{r}_{42}) f(\mathbf{r}_{32}) \\ &+ f(\mathbf{r}_{13}) f(\mathbf{r}_{42}) f(\mathbf{r}_{32}) f(\mathbf{r}_{14}) + f(\mathbf{r}_{13}) f(\mathbf{r}_{34}) f(\mathbf{r}_{42}) f(\mathbf{r}_{32}) f(\mathbf{r}_{14})] d\mathbf{r}_3 d\mathbf{r}_4. \end{aligned} \tag{6.58b}$$

Finally, note that the radial correlation function is for asymptotically small densities

$$g(r) \sim e^{-\beta v(r)}. \tag{6.59}$$

The limit (6.59) is also the *weak coupling* limit. A consequence of that is also the behaviour of the radial correlation function at large distance, where the coupling is weak.

6.2.5 Formal theory in the grand canonical ensemble

We have been working up to now in the canonical ensemble because the canonical partition is slightly simpler than the grand canonical one. However, for some calculations it is much simpler to use the latter one (we will see the reasons below). On the basis of what we have studied in the canonical ensemble, we are going to outline the diagrammatic expansion in the grand canonical ensemble using the formalism of functional analysis.

We use the grand partition function with an external field as in Eq. (6.27). As we did for the canonical partition function, we can write it as a function of the f function (6.31) and expand it in powers of f:

$$\Xi(z^*, V, T) = \sum_{N=0}^{\infty} \frac{1}{N!} \int \prod_{i=1}^{N} z^*(\mathbf{r}_i) \prod_{i<j}^{N} [f(\mathbf{r}_i, \mathbf{r}_j) + 1] \, d\mathbf{r}^N. \tag{6.60}$$

Writing the grand-canonical partition function as a function of the canonical one (Eq. (6.24)), it is simple to perform an expansion in terms of f functions. It is clear that the diagrammatic representation of the grand partition function is the one given in Fig. 6.6, where the points represent now "z^*-circles" and the full lines are f-bonds. If we compute the $\ln \Xi$ it is simple to show [HM76] that only the *connected* diagrams in Fig. 6.6 survive. Clearly from this diagram we have obtained an expansion of $\ln \Xi$ in powers of z: the power of z corresponds to the number of z^*-circles of the diagram. In the same way as in the canonical case, the *reducible* diagrams disappear in a density expansion: reducible diagrams that

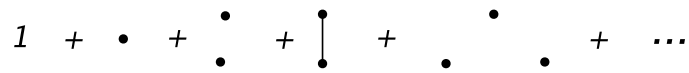

Figure 6.6: First diagrams that gives contributions proportional to Ξ.

contribute at different order in the diffusivity cancel when they are grouped in a density expansion. It is possible to write the activity in function of the density and then write the partition function solely as a function of powers in the density (for details [HM76]).

6.2.6 The Ornstein-Zernike equation

Let us define the *direct correlation function* as

$$c(\mathbf{r}_1, \mathbf{r}_2) = \frac{\delta \ln[\rho^{(1)}(\mathbf{r}_1)/z^(\mathbf{r}_1)]}{\delta \rho^{(1)}(\mathbf{r}_2)}. \tag{6.61}$$

This function is a measure of the *direct* correlation between two particles at the position $\mathbf{r}_1$ and $\mathbf{r}_2$. We will explain better the meaning of this statement below. It is simple to check that

$$-\beta \frac{\delta u(\mathbf{r}_1)}{\delta \rho^{(1)}(\mathbf{r}_2)} = \frac{\delta \ln z^*(\mathbf{r}_1)}{\delta \rho^{(1)}(\mathbf{r}_2)} = \frac{1}{\rho^{(1)}(\mathbf{r}_1)} \delta(\mathbf{r}_1 - \mathbf{r}_2) - c(\mathbf{r}_1, \mathbf{r}_2). \tag{6.62}$$

On the other hand, let us compute the quantity

$$\begin{aligned} \frac{1}{-\beta} \frac{\delta \rho^{(1)}(\mathbf{r}_1)}{\delta u(\mathbf{r}_2)} &= \frac{\delta \rho^{(1)}(\mathbf{r}_1)}{\delta \ln z^*(\mathbf{r}_2)} = z^*(\mathbf{r}_1) \frac{\delta}{\delta z^*(\mathbf{r}_2)} \left[\frac{z^*(\mathbf{r}_1)}{\Xi} \frac{\delta \Xi}{\delta z^*(\mathbf{r}_1)} \right] \\ &= \rho^{(1)}(\mathbf{r}_1) \delta(\mathbf{r}_1 - \mathbf{r}_2) + \rho^{(1)}(\mathbf{r}_1) \rho^{(1)}(\mathbf{r}_2) h(\mathbf{r}_1, \mathbf{r}_2), \end{aligned} \tag{6.63}$$

where $h(\mathbf{r}_1, \mathbf{r}_2)$ is called the *total correlation function* defined as

$$h(\mathbf{r}_1, \mathbf{r}_2) = \frac{\rho^{(2)}(\mathbf{r}_1, \mathbf{r}_2)}{\rho^{(1)}(\mathbf{r}_1) \rho^{(1)}(\mathbf{r}_2)} - 1. \tag{6.64}$$

The expression (6.63) gives the change of the one-point density when an external field is applied to the system. By the property (B.6) of functional integration we have that

$$\int \frac{\delta u(\mathbf{r}_1)}{\delta \rho^{(1)}(\mathbf{r}_3)} \frac{\delta \rho^{(1)}(\mathbf{r}_3)}{\delta u(\mathbf{r}_2)} d\mathbf{r}_3 = \delta(\mathbf{r}_1 - \mathbf{r}_2). \tag{6.65}$$

This expression shows that c and h are almost functional inverses. Substituting in this expression the explicit quantities of the integrand, Eqs. (6.62) and (6.63), we obtain the Ornstein-Zernike (OZ) equation:

$$h(\mathbf{r}_1, \mathbf{r}_2) = c(\mathbf{r}_1, \mathbf{r}_2) + \int \rho^{(1)}(\mathbf{r}_3) c(\mathbf{r}_1, \mathbf{r}_3) h(\mathbf{r}_3, \mathbf{r}_2) d\mathbf{r}_3. \tag{6.66}$$

This relation clarifies the meaning of the direct correlation function. Eq. (6.66) can be rewritten as a function of c in the following infinite series:

$$\begin{aligned} h(\mathbf{r}_1, \mathbf{r}_2) &= c(\mathbf{r}_1, \mathbf{r}_2) + \int \rho^{(1)}(\mathbf{r}_3) c(\mathbf{r}_1, \mathbf{r}_3) c(\mathbf{r}_3, \mathbf{r}_2) d\mathbf{r}_3 \\ &+ \int \rho^{(1)}(\mathbf{r}_3) \rho^{(1)}(\mathbf{r}_4) c(\mathbf{r}_1, \mathbf{r}_3) c(\mathbf{r}_3, \mathbf{r}_4) c(\mathbf{r}_4, \mathbf{r}_4 2) d\mathbf{r}_3 d\mathbf{r}_4 + \ldots \end{aligned} \tag{6.67}$$

Equation (6.67) can be understood in term of collisions. In a low density medium, the main contribution to the probability of interaction ("collision") between particle situated at $\mathbf{r}_1$ and $\mathbf{r}_2$ comes from direct collision between these particles. The next contribution comes from a particle 3 colliding with the 1 and then entering in collision with 2 and so on... Of course the picture of collision only holds for a short range interaction but the idea remains the same even for a long-range one. For a statistically homogeneous and isotropic medium Eq. (6.67) takes the simpler form:

$$h(r) = c(r) + \rho \int c(|\mathbf{r} - \mathbf{r}'|)h(\mathbf{r}')d\mathbf{r}'. \tag{6.68}$$

The practical utility of the OZ equation is mainly in Fourier space. Taking the FT of (6.68) and using the convolution theorem we have

$$\tilde{h}(k) = \frac{\tilde{c}(k)}{1 - \tilde{c}(k)}, \tag{6.69}$$

where $\tilde{h}(k)$ and $\tilde{c}(k)$ are the FT of $h(r)$ and $c(r)$ respectively.

The Ornstein-Zernike relation can only be derived in the grand canonical ensemble[3]. In the grand canonical ensemble, using Eqs. (6.17) and (6.26), it is simple to show that the integral of the radial correlation function is, for an homogeneous sytem:

$$1 + \rho \int [g(r) - 1]d\mathbf{r} = \frac{\langle N^2 \rangle - \langle N \rangle^2}{\langle N \rangle}. \tag{6.70}$$

The r.h.s. of (6.70) is proportional to the compressibility of the system. In the canonical ensemble, the number of particles cannot fluctuate and therefore the compressibility is zero. There is therefore the constraint:

$$1 + \rho \int [g(r) - 1]d\mathbf{r} = 0, \tag{6.71}$$

which is equivalent to have $S(k = 0) = 0$. Therefore the canonical ensemble modelize, by construction, only super-homogeneous systems (see chapter 3). The constraint (6.71) is incompatible with the OZ equation (6.68), which justifies the necessity to work in the grand canonical ensemble.

6.3 The One Component Plasma

The OCP (for a review, see [BH80]) is a system of positive charged point particles ("ions") interacting through a Coulomb (i.e. repulsive $1/r$) potential, and embedded in a uniform (rigid, non-dynamical) negatively charged background. The latter gives overall charge neutrality, and a high degree of stability to the system. The system exhibits two phases at thermal equilibrium, a fluid phase and a solid phase. We will treat it always at densities and temperatures where it is in the fluid phase. In this range of densities and temperature it can be considered as completely classical.

[3] Althought it is possible to a find an "Ornstein-Zernike like" equation in the canonical ensemble, see [WV01].

The equilibrium thermodynamics of the OCP is determined by a single parameter, and not by its temperature and density independently. Because of the scale-free nature of the power-law interaction potential, there are only two characteristic length scales. One is specified by the number density, and is conventionally taken to be the "ion-sphere" radius a defined by[4]

$$a = \left(\frac{3}{4\pi n}\right)^{1/3} \tag{6.72}$$

where $n = N/V$ is the number density of the N points in a volume V. The other scale is given by the distance at which the potential is of order the mean thermal kinetic energy. It is the dimensionless ratio of these two scales which parametrises the one dimensional phase space of the system at thermal equilibrium. Conventionally this parameter is taken to be

$$\Gamma = \beta(Ze)^2/a. \tag{6.73}$$

where $\beta = 1/(k_B T)$ and Ze is the ionic charge. It is referred to as the "plasma parameter" (or simply "coupling constant").

6.3.1 Asymptotic correlation properties

The diagrammatic expansion in powers of density is not valid in the case of long-ranged potentials. This is evident when trying to compute the coefficients b_p of the expansion of F_c: the coefficients diverge for an interaction that decays slower than $1/r^3$ at large scales. This is apparent already from Eq. (6.30), that can be evaluated, if the integral is dominated by large r by

$$Z_N \sim \int \frac{1}{r^N} d\mathbf{r}^N \sim \int \lim_{r\to\infty} (\ln r)^N \to \infty. \tag{6.74}$$

However, the phenomena of *screening* of the interaction permits to obtain finite results. It can be simply explained by the Debye-Huckel theory. The version we give in what follows have been extracted from [LL59b].

The OCP is made by two species of particles with opposite charges, typically ions and electrons. Let us call the mass density of ions $n_1(\mathbf{r})$ and the density of electron $n_2(\mathbf{r})$. The total charge density is then

$$\rho(\mathbf{r}) = en_1(\mathbf{r}) - en_2(\mathbf{r}). \tag{6.75}$$

By the condition of electro-neutrality the average density of each species is equal in magnitude with different sign[5]:

$$en_0 \equiv \frac{e}{V}\int n_1(\mathbf{r})d\mathbf{r} = -\frac{e}{V}\int n_2(\mathbf{r})d\mathbf{r}. \tag{6.76}$$

We will assume that the plasma deviates slightly from the ideal gas. To ensure that, the mean energy of Coulomb interaction of two ions needs to be small compared with their mean kinetic energy:

$$n_0 \ll \left(\frac{1}{\beta e^2}\right)^3. \tag{6.77}$$

[4] Do not confuse the ion-sphere radius a — used in this chapter and in the following one to follow the usual notation in statistical physics — with the scale factor a used in cosmology.

[5] We have assumed that the ions are simply ionised Ageneralisation is straightforward.

The ions, by their charge, create around them an inhomogeneously charged electron cloud (but on average spherically symmetrical). The density distribution of ions around an ion at $\mathbf{r} = 0$ is given by the Boltzmann factor

$$n_1(\mathbf{r}) = n_0 e^{-e\beta\psi(\mathbf{r})}, \tag{6.78}$$

where $\psi(\mathbf{r})$ is the *average* potential around $\mathbf{r} = 0$. We can use the Poisson equation to find –self-consistently – the average potential:

$$\nabla^2\psi(\mathbf{r}) = -4\pi e\left[\delta(\mathbf{r}) - n_0 + n_0 e^{-e\beta\psi(\mathbf{r})}\right], \tag{6.79}$$

where the first term on the r.h.s. represents the point charge of the ion, the second one the uniform background of electrons and the third one the density of ions. Using the hypothesis (6.77) in Eq. (6.79), the Poisson equation is simplified:

$$\left[\nabla^2 - \kappa^2\right]\psi(r) = -4\pi e\delta(r), \tag{6.80}$$

where

$$\kappa = \sqrt{4\pi\beta n_0 e^2} \tag{6.81}$$

is called *Debye-Hückel screening constant*. It is simple to show that the solution of Eq. (6.80) is

$$\psi(r) = e^2\frac{e^{-\kappa r}}{r}. \tag{6.82}$$

The potential is screened by the electron cloud at a typical distance $\lambda_D = 1/\kappa$ called *Debye length*. Observe how the typical distance of screening depends on the temperature (at higher temperature the screening is less efficient because the particles have more kinetic energy) and on the density (at lower density λ_D increases because there are less electrons to screen the ions). The Debye-Hückel model does not take into account the size of the ions. Doing so, the effective potential (6.82) potential is modified and a van der Waals type potential[6] is obtained [VGM]. The density of the ions (6.78) reads

$$n_1(\mathbf{r}) = \delta(\mathbf{r}) + n_0\exp\left[-e^2\beta\frac{e^{-\kappa r}}{r}\right]. \tag{6.83}$$

It is usual to rewrite Eq. (6.83) using the "plasma parameters" (6.72) and (6.73):

$$n_1\left(\frac{\mathbf{r}}{a}\right) = \delta(\mathbf{r}) + n_0\exp\left[-\Gamma\frac{e^{-\sqrt{3\Gamma}r/a}}{r/a}\right] \simeq \delta(\mathbf{r}) + n_0\left(1 - \Gamma\frac{e^{-\sqrt{3\Gamma}r/a}}{r/a}\right). \tag{6.84}$$

In Fig. 6.7 it is shown the density around an ion for different values of Γ. Observe how the exclusion volume decreases with temperature.

To compute the correlation function in general, the following property[7] of the direct correlation function is invoked [HM76, BH80]:

$$c(r) \simeq -\beta v(r), \qquad r \to \infty. \tag{6.85}$$

[6] A van der Waals potential is repulsive at short distance, then attractive and repulsive again at large distances.

[7] But, at my knowledge, never rigorously shown.

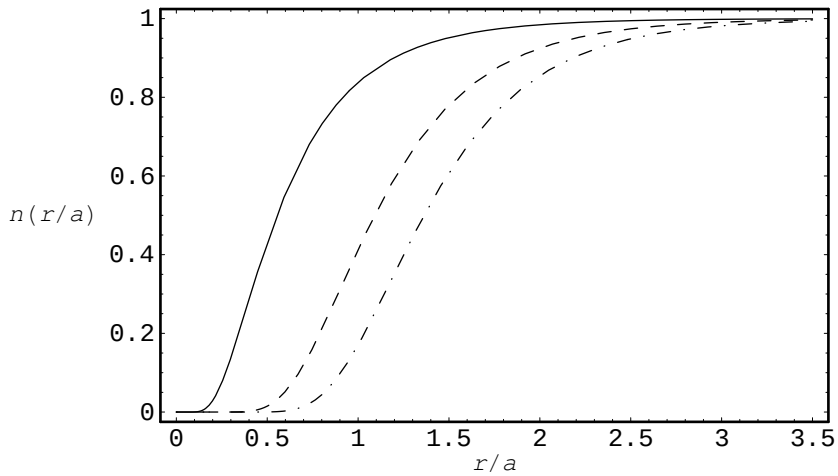

Figure 6.7: Ion density in the Debye-Hückel approximation for different temperatures. Note that the radial correlation function (6.86) has the same functional dependence.

Instead of starting from this property, let us follow another route. Using (6.59), we can guess (we will check this assumption below) that the radial correlation function, at low density, is given by

$$g(r) \simeq \exp(-e\beta\psi(r)) = \exp\left[-e^2\beta\frac{\exp(-\kappa r)}{r}\right] \simeq 1 - e^2\beta\frac{e^{-\kappa r}}{r}, \tag{6.86}$$

where we have made the replacement of the interaction potential by the effective screened one (and we have used also the dilute approximation (6.77)). Using Eq. (6.19) we can compute the structure factor as

$$S(k) = 1 + n\int[g(r)-1]e^{i\mathbf{k}\cdot\mathbf{r}}d\mathbf{r} = 1 - \kappa^2\int\frac{e^{-\kappa r}}{r}d\mathbf{r} = \frac{k^2}{\kappa^2+k^2}. \tag{6.87}$$

The large scale correlations of the system are given by $S(k \to 0)$. Expanding (6.87) in powers of k we have:

$$S(k) \simeq \frac{k^2}{\kappa^2}\left[1 + \ldots\right]. \tag{6.88}$$

The conclusion is that the structure factor is zero for $k \to 0$. Recalling the discussion in chapter 3 we conclude that the OCP corresponds to a *super-homogeneous* distribution. Therefore the variance in spheres of the number of particles will decrease slowly, with the surface of the sphere. This is a consequence of the long range of the interaction combined with the electroneutrality. In Fig. 6.8 appears a typical configuration of the ions. The excluded region is denoted by a dashed circle. The fluctuations in the number of particles come only from the last shell. In Fig. 6.9 appears a comparison between the OCP and a Poisson (uncorrelated) distribution. Using the asymptotic result (6.88) we can

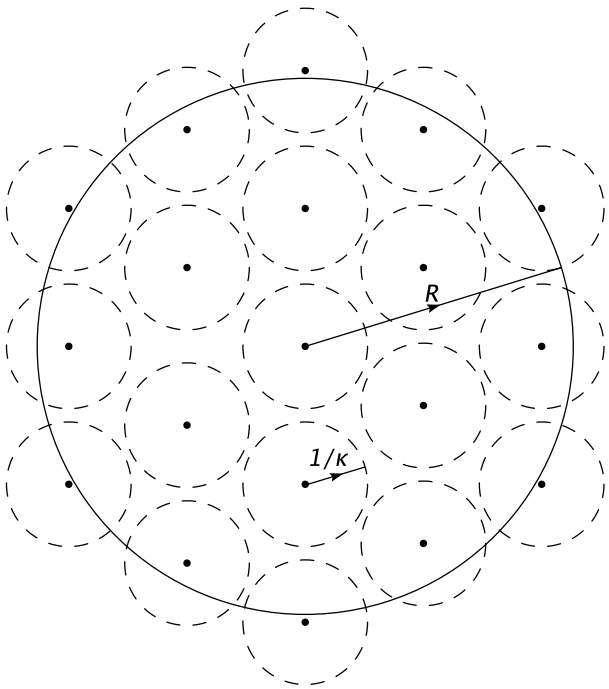

Figure 6.8: Configuration of the OCP. The excluded region of radius λ_D is denoted by a dashed circle. The variance of particles is measured in the sphere of radius R.

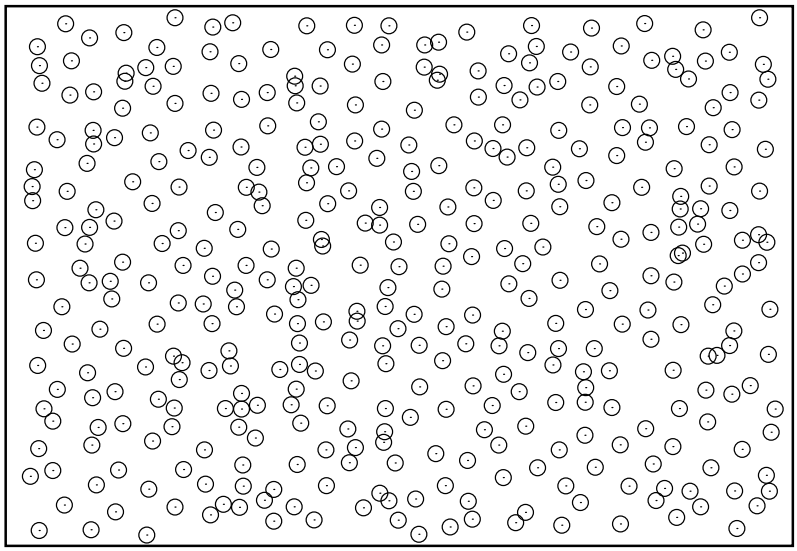

(i)

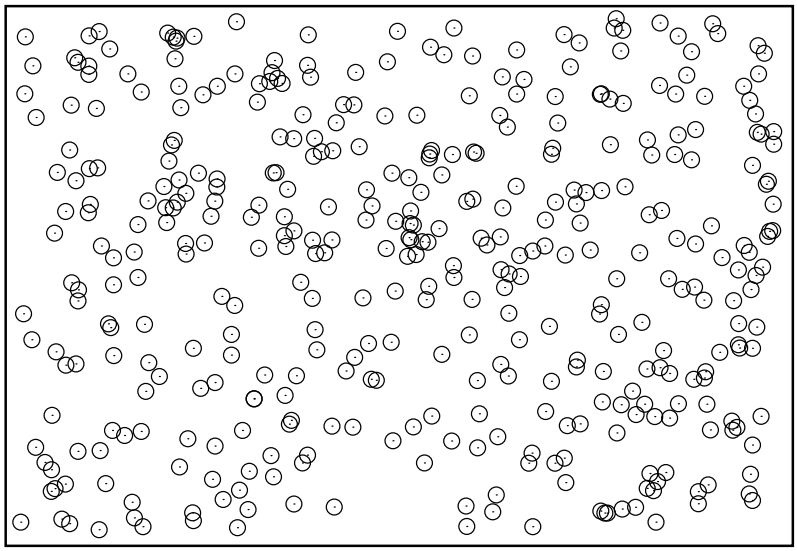

(ii)

Figure 6.9: (i) Configuration of an OCP system. The figure shows a projection of a slice of the 1/20-th of system (ii) a Poissonian distribution with the same number of particles.

compute the asymptotic behaviour of the direct correlation function. Using the OZ equation (6.69) we obtain

$$\tilde{c}(k) = 1 - \frac{1}{S(k)} \simeq 1 - \frac{\kappa^2}{k^2} + \dots . \tag{6.89}$$

Using Eq. (6.88) we see that $\tilde{c}(k)$ is divergent for $k \to 0$. This is a consequence of the non-integrability of $c(r)$ (see Eq. (6.85)). Note that taking the FT of (6.89) we obtain the ansatz (6.85). In practice – for example to perform numerical computations, see section 6.4 — the direct correlation function is divided in a short-range and a long range part:

$$\tilde{c}(k) = -\frac{\kappa^2}{k^2} + \tilde{c}_s(k), \tag{6.90}$$

with $\tilde{c}_s(k) = \tilde{c}(k) + \kappa^2/k^2$. Note that, even if $\tilde{c}(k)$ is divergent, $\tilde{h}(k)$ is convergent (as follows from (6.86)). The physical reason is that $h(r)$ "feels" the screening whereas $c(r)$ not. The asymptotic behaviour of the direct correlation function is always equal to the interactive potential, as in Eq. (6.85).

To conclude this subsection let us verify (and generalise) our guess (6.86). Following [G$^+$03a], let us apply to the OCP an external infinitesimal charge density of very long wavelength:

$$\rho_{ext} = \epsilon\, e^{i\mathbf{k}\cdot\mathbf{r}}, \qquad \epsilon \ll 1. \tag{6.91}$$

Let us consider the general central interaction in the OCP (not necessarily Coulombian) $v(r)$. Therefore the charge creates an electric potential

$$\phi(\mathbf{r}) = \int \rho_{ext}(\mathbf{r}')v(|\mathbf{r}-\mathbf{r}'|d\mathbf{r} = \epsilon\tilde{v}(k)e^{i\mathbf{k}\cdot\mathbf{r}}, \tag{6.92}$$

where $\tilde{v}(k)$ is the FT of $v(r)$. This creates a perturbation in the "potential" part of the Hamiltonian, that we call

$$V_{ext} \simeq \int \rho(\mathbf{r})\phi(\mathbf{r})\mathbf{r} = \epsilon\tilde{v}(k)\int \rho(\mathbf{r})e^{i\mathbf{k}\cdot\mathbf{r}}d\mathbf{r}, \tag{6.93}$$

where $\rho(\mathbf{r})$ is the density of the unperturbed system and we have neglected terms of order ϵ^2. Assuming linear response of the charge (C.7)

$$\langle\delta\rho(\mathbf{r})\rangle = -\beta\,\langle\rho(\mathbf{r})\delta V(\mathbf{r})\rangle \tag{6.94}$$

(where the average is over the unperturbed states), and assuming that the applied charge is perfectly screened (i.e. $\langle\delta\rho(\mathbf{r})\rangle = -\rho_{ind}(\mathbf{r})$), we can write, in the limit $k \to 0$):

$$\epsilon\, e^{i\mathbf{k}\cdot\mathbf{r}} \sim \epsilon\tilde{v}(k)\int \langle\rho(\mathbf{r}')\rho(\mathbf{r})\rangle\, e^{i\mathbf{k}\cdot\mathbf{r}'}d\mathbf{r}'. \tag{6.95}$$

We conclude therefore that, for $k \to 0$,

$$S(k) \sim \frac{1}{\beta n_0^2}\frac{1}{\tilde{v}(k)}, \tag{6.96}$$

exactly as in (6.88) for the Coulomb case.

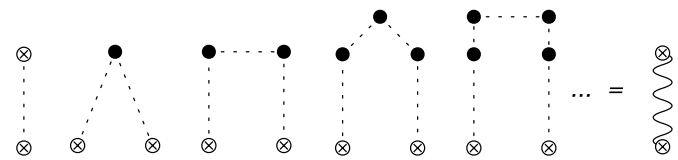

Figure 6.10: Fist chain-diagram contribution to $g(r)$ for the OCP. Note that the bonds are $v = e/r$ bonds.

6.3.2 Diagrammatic expansion and HNC equation

To study the OCP in greater detail than given by the asymptotic properties which we have reviewed in the precedent subsection we need to go beyond the mean field approximation. To do so, we are going to exploit the diagrammatic techniques that we have outlined above. First of all, we must emphasise that an expansion in integer powers of the density has no physical meaning for long-ranged forces. For example, if we compute the corrections to the energy in the Debye-Hückel approximation we find (using Eq. (6.22a)):

$$\frac{E_c}{N} = 2\pi n \int_0^\infty [g(r) - 1] v(r) r^2 dr = -\frac{2\pi n e^2 \beta}{\kappa} \propto n^{1/2}, \tag{6.97}$$

which is not proportional to an integer power of n. We are going to study how to construct a diagrammatic expansion for long-ranged potentials. The starting point of the density expansion (subsection 6.2.3) is valid but we have to sum the diagrams in a different order to obtain sensible results. At the end of this subsection we will work out an example to show how it works. Following the idea of (6.57) and (6.86) it is natural to write the correlation function as

$$g(\mathbf{r}_1, \mathbf{r}_2) = e^{-\beta v(\mathbf{r}_1, \mathbf{r}_2)} e^{w(\mathbf{r}_1, \mathbf{r}_2)}. \tag{6.98}$$

where $w(\mathbf{r}_1, \mathbf{r}_2)$ is the logarithm of the sum of Eq. (6.57) (which has to be rearranged to obtain a finite result). Expression (6.98) is exact. Using the OZ equation (6.67) it is clear that the diagrams of $c(\mathbf{r}_1, \mathbf{r}_2)$ are a subset of the ones of $h(\mathbf{r}_1, \mathbf{r}_2)$. We can write then

$$h(\mathbf{r}_1, \mathbf{r}_2) = c(\mathbf{r}_1, \mathbf{r}_2) + b(\mathbf{r}_1, \mathbf{r}_2). \tag{6.99}$$

The diagrams belonging to $b(\mathbf{r}_1, \mathbf{r}_2)$ are frequently called "series" diagrams. Obviously these diagrams also belong to the set of $w(\mathbf{r}_1, \mathbf{r}_2)$. Then

$$w(\mathbf{r}_1, \mathbf{r}_2) = b(\mathbf{r}_1, \mathbf{r}_2) + d(\mathbf{r}_1, \mathbf{r}_2), \tag{6.100}$$

where $d(\mathbf{r}_1, \mathbf{r}_2)$ are called "bridge" diagrams. Combining Eqs. (6.98), (6.99) and (6.100) we obtain the *exact* relation:

$$h(\mathbf{r}_1, \mathbf{r}_2) - c(\mathbf{r}_1, \mathbf{r}_2) - \ln\left[h(\mathbf{r}_1, \mathbf{r}_2) + 1\right] = \beta v(\mathbf{r}_1, \mathbf{r}_2) - d(\mathbf{r}_1, \mathbf{r}_2). \tag{6.101}$$

A very good approximation for Coulomb systems consist in neglecting the bridge diagrams in Eq. (6.101):

$$h(\mathbf{r}_1, \mathbf{r}_2) - c(\mathbf{r}_1, \mathbf{r}_2) - \ln\left[h(\mathbf{r}_1, \mathbf{r}_2) + 1\right] = \beta v(\mathbf{r}_1, \mathbf{r}_2). \tag{6.102}$$

This is the *Hypernetted Chain Equation* (HNC). For statistically homogenous and isotropic systems and central interactions, it takes the simpler form:

$$h(r) = c(r) + \ln\left[h(r) + 1\right] + \beta v(r). \tag{6.103}$$

Note how an expansion expansion at first order in $h(r)$ of the logarithm gives the asymptotic value of $c(r)$ (6.85). Studies about the behaviour of the bridge function in the OCP [II83, PAD88] have shown that it is essentially a short-ranged function. In a Coulomb system it is crucial to modelize well the long-range correlations in (6.101), it explains why neglecting them it is a good approximation. For the same reason it is not such a very good approximation for short-ranged interactions. Combining Eq. (6.103) for an homogeneous system with the OZ equation (6.66) gives a closed set of integral equations. We will study below how to solve this equation numerically. Note that it is possible to derive the HNC equation from a functional expansion of the partition function [HM76]. The idea is similar to that used between Eqs. (6.91)–(6.96) to derive the large-scale behaviour of the correlation function. An external field is applied to the OCP, which creates an induced charge distribution $\delta\rho(\mathbf{r})$. Expanding the function

$$\ln\left[\frac{\rho^{(1)^*}(\mathbf{r})}{z^*(\mathbf{r})}\right] \tag{6.104}$$

in terms of the perturbation $\delta\rho$ up to first order one recovers the HNC equation. This alternative derivation gives further insight about the nature of the approximation.

We are going to conclude this subsection with an explicit computation of the radial correlation function using a sum of diagrams. It is possible to show (e.g. [HM76]) that the most divergent diagrams are the least connected ones. This is physically reasonable because the Coulomb interaction is a long-ranged force and the processes involving a lot of particles should be dominant. The summation process consists in two steps: first, sum all the chain diagrams of Fig. 6.10. Then, sum over all the the possible multi-lines of the chain graph (Fig. 6.11). The sum over the diagrams of Fig. 6.10 gives [I$^+$99]:

$$\begin{aligned} -\beta\psi(r) &= -\beta v(r) + n\int[-\beta v(r_{13})][-\beta v(r_{32})]d\mathbf{r}_3 \\ &+ n^2\int[-\beta v(r_{13})][-\beta v(r_{34})][-\beta v(r_{42})]d\mathbf{r}_3 d\mathbf{r}_4 \ldots \end{aligned} \tag{6.105}$$

The sum (6.105) is simply performed going to Fourier space and using the convolution theorem:

$$-\beta\tilde{\psi}(k) = -\beta\tilde{v}(k) + n[-\beta\tilde{v}(k)]^2 + n^2[-\beta\tilde{v}(k)]^3 + \cdots = -\beta\frac{4\pi e^2}{k^2+\kappa^2}. \tag{6.106}$$

where $\tilde{\psi}(k)$ is the FT of $\psi(r)$. Note that we have obtained for $v(r)$ in Eq. (6.82).. Now we sum the diagrams of Fig. 6.11:

$$g(r) = 1 + \psi(r) + \frac{1}{2!}[\psi(r)]^2 + \frac{1}{3!}[\psi(r)]^3 + \cdots = e^{\psi(r)} = \exp\left[e^2\beta\frac{e^{-\kappa r}}{r}\right], \tag{6.107}$$

i.e. the result (6.86).

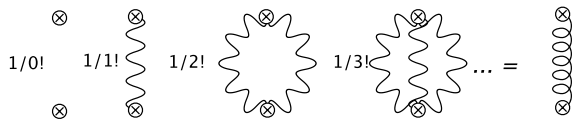

Figure 6.11: Multi-lines of the chain graph.

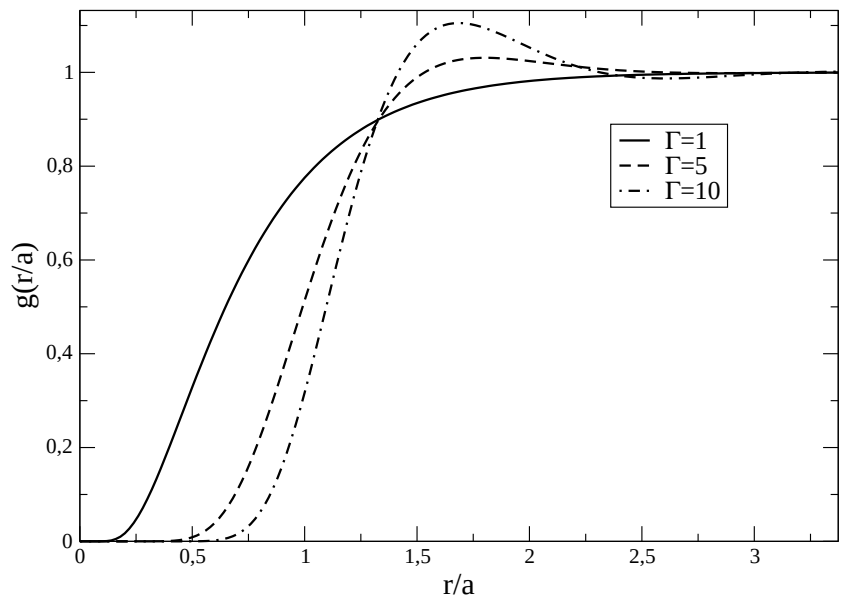

Figure 6.12: Correlation function of the OCP with Coulomb interaction for different temperatures (recall that $\Gamma \sim 1/T$).

6.3.3 Correlations in the strong coupling regime

The HNC equation allows one to compute reliably the correlation properties of the OCP for a very large field of "normal" plasma parameters, despite its breakdown at low temperatures (very strong coupling) and at temperatures above the coexistence region between gas and liquid gases [VGM]. However, the results of the HNC should always be checked with numerical simulations. The correlation function $g(r)$ and SF $S(k)$ are shown in Figs. 6.12 and 6.13 for different values of the coupling Γ. The computation has been done using the HNC equation and the result checked by a molecular dynamics simulation (not shown). We can see that at high temperature (low Γ) the behaviour predicted with the Debye-Hückel theory. At larger values of Γ (i.e. lower temperature/higher density) one sees that the correlation function develops a "bump" at small scales, indicating that the first neighbour is becoming increasingly localised. As Γ increases further several "bumps" develop (corresponding to first, second, third neighbours) which give to the correlation function and PS an oscillatory structure, fore-shadowing the transition to the ordered solid phase at $\Gamma \approx 180$ (for more details, see [SDS90]).

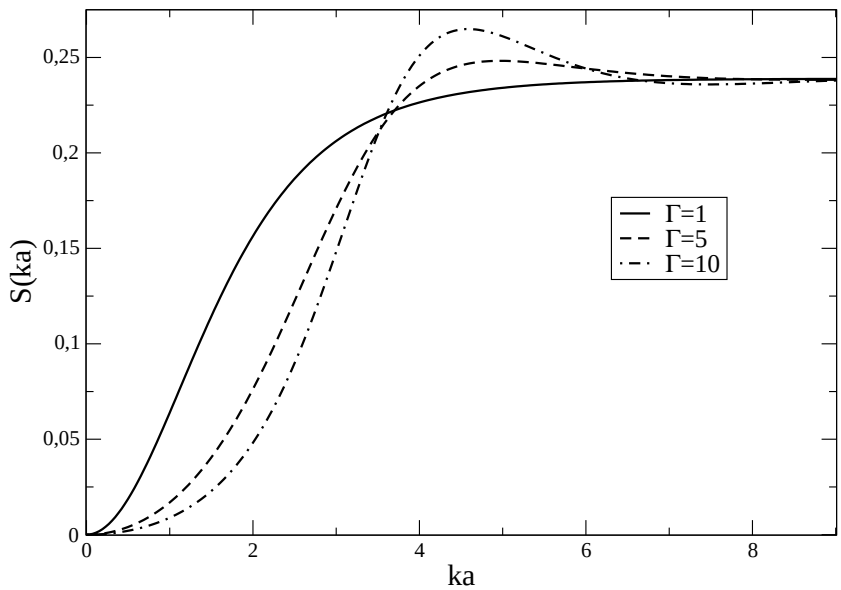

Figure 6.13: Power spectrum of the OCP with interacting Coulomb potential.

6.4 Practical determination of $h(r)$ using the HNC equation

We consider here now the determination of the correlation function using the HNC equation. Given the potential $v(r)$, the OZ equation (6.68) and HNC equation (6.103) give a closed set of equations for the correlation function $h(r)$, which can be solved by iteration as follows. It is convenient to define $\gamma(r) = h(r) - c(r)$, of which the FT $\tilde{\gamma}(k)$ is given in terms of $\tilde{c}(k)$ as (Eq. (6.69))

$$\tilde{\gamma}(k) = \frac{\tilde{c}(k)}{1 - n\tilde{c}(k)} - \tilde{c}(k). \tag{6.108}$$

We start with a first guess for $c(r)$, denoted $c_0(r)$. One can take $c_0(r) = 0 \ \forall r$, or, its asymptotic value (6.85), $c_0(r) \simeq -\beta v(r)$. We can then use a Fast Fourier transform (FFT) to calculate $\tilde{c}_0(k)$, which then gives $\tilde{\gamma}_0(k)$ through (6.108). With an inverse FFT we find $\gamma_0(r)$, and then use the HNC equation Eq. (6.103) to compute $c_1(r)$ (using $\gamma_0(r)$ in the exponent to obtain $c_1(r) + \gamma_0(r)$ on the left hand side). The iteration process then proceeds with the computation of $\gamma_i(k)$ with (6.108). To ensure convergence, successive approximations on $\gamma(r)$ need to be taken, so the ith input is mixed linearly with the precedent one:

$$\gamma_i'(r) = \alpha\gamma_{i-1}(r) + (1-\alpha)\gamma_i(r) \tag{6.109}$$

where $0 < \alpha < 1$. The new $\gamma_i'(r)$ is substituted in equation (6.108) to get $c_{i+1}(r)$ and so on. In all the numerical resolutions we did we took $\alpha = 0.5$ which gives rapid convergence (less than one hundred iterations were necessary in all cases). If there are problems with convergence (which can occur e.g. at larger densities) a value of α closer to 1 is taken.

There is one additional elaboration of this method which is necessary when the potential is long-range, as it is for the case of the standard OCP [Coo73]. Since

$$\tilde{c}(k) = \frac{\tilde{h}(k)}{1 + n\tilde{h}(k)} = \frac{1}{n}\left(1 - \frac{1}{n_0 S(k)}\right) \tag{6.110}$$

we have that $\tilde{c}(k)$ diverges for $k \to 0$, which is problematic numerically. This is dealt with in an analogous manner to that described in the Sect. 6.5 below for the calculation of the force by the Ewald sum. One breaks $c(r)$ into the sum of a short-range part $c_s(r)$ (see Eq. (6.90)), with an analytic FT at $k = 0$, and a long part $f(r)$, which contains the divergence in the FT. A typical long range part is $v(r)\mathrm{erf}(\eta r)$ or $v(r)(1 - \exp(-\eta r))$, where η is a free positive parameter (on which the final result does not depend). The total correlation function $h(r)$ has no divergence, and thus $\gamma(r)$ is divided in the same way, $\gamma(r) = \gamma_s(r) + f(r)$, with $\gamma_s(r) = h(r) - c_s(r)$. The potential likewise is separated into a short and long range part $\beta v_s(r) = v(r) + f(r)$, so that the HNC reads

$$h(r) = \exp[-\beta v_s(r) + \gamma_s(r)] - 1. \tag{6.111}$$

When we compute Eq.(6.108) we use the FT of the long-range part of the potential:

$$\tilde{\gamma}_s(k) = \frac{\tilde{c}_s(k) + \tilde{f}(k)}{1 - n(\tilde{c}_s(k) + \tilde{f}(k))} - \tilde{c}_s(k). \tag{6.112}$$

All the computations are then done as described above but with $c_s(r)$ and $\gamma_s(r)$ instead of $c(r)$ and $\gamma(r)$, and using Eq. (6.112) instead of Eq.(6.108).

6.5 Determination of the thermal equilibrium properties using molecular dynamics

The two numerical methods used widely in statistical physics to study systems at thermal equilibrium are molecular dynamics and Monte Carlo simulations. We will discuss some aspects of the former method, in which one evolves numerically the $3N$ classical coupled equations of motions of a system of N interacting particles in a volume V (for a review about numerical techniques in Statistical Physics, e.g. [Vio]). Finite-size effect are treated using periodic-type boundary conditions.

6.5.1 Discretisation of the Newton equations

To discretise the equations of motion we use the Verlet algorithm. Performing a Taylor expansion of the position of a particle at times $t + \Delta t$ and $t - \Delta t$ about its position at time t, the position of the *i-th* particle is given to order $\mathcal{O}((\Delta t)^4)$ by:

$$\mathbf{r}_i(t + \Delta t) = 2\mathbf{r}(t) - \mathbf{r}(t - \Delta t) + \frac{(\Delta t)^2}{m} \sum_{i=1}^{N} \mathbf{F}_{ij}(t)\,. \tag{6.113}$$

This algorithm, which is historically one of the earliest ones, has three important properties: it conserves energy very well, it is reversible (as the Newton equations), and it is symplectic (i.e. it conserves the phase space volume). More

refined algorithms have been proposed and used, but they often have less good conservation of energy at large times. Furthermore, the rapidity of the execution of the program is not determined by the computation of the new positions but by the calculation of the forces.

6.5.2 Force calculation using the Ewald sum

In our simulations N particles are placed in a cubic box of size L. To compute the interaction between the particles we apply the *image* method to minimize boundary effects: an infinite number of copies of the system is supposed and the potential is computed considering not only the particles situated in the original box but also the particles of all the copies. Then if the particle i has coordinate $\mathbf{r}_i$, its copies will have coordinates $\mathbf{r}_i + \mathbf{n}L$, where $\mathbf{n}$ is a vetor with integer components. For a power-law interaction potential $v(r) = r^{-\alpha}$ the potential is then

$$\phi(\mathbf{r}_i) = \sum_{j,\mathbf{n}}^{*} \frac{q_j}{|\mathbf{r}_{ij} + \mathbf{n}L|^{\alpha}}, \tag{6.114}$$

where q_j is the charge of the particles and the asterisk denotes that the sum $\mathbf{n} = 0$ does not include the term $i = j$. In a numerical calculation the infinite sum Eq.(6.114) must be truncated. For $\alpha > 3$ the potential is short-range and the approximation to compute the interaction potential between the i and j particles by taking only the interaction between i and the closest image of j is very good. When the potential is long-range ($\alpha < 3$) this approximation is no longer good, and indeed the sum appears to be formally divergent. For the case of the Coulomb potential, the presence of the neutralising uniform background ensures that the potential of the infinite periodic system is well defined. A natural way of writing the sum in an explicitly convergent way taking this regularisation into account is to separate the potential into a short range and long range part by introducing a parameter-dependent damping function $f(\mathbf{r}; \alpha)$:

$$\phi(\mathbf{r}_i) = \sum_{j,\mathbf{n}}^{*} q_j \left(\frac{f(\mathbf{r}_{ij} + \mathbf{n}L; \alpha)}{|\mathbf{r}_{ij} + \mathbf{n}L|^{\alpha}} + \frac{1 - f(\mathbf{r}_{ij} + \mathbf{n}L; \alpha)}{|\mathbf{r}_{ij} + \mathbf{n}L|^{\alpha}} \right). \tag{6.115}$$

The first term on the r.h.s of Eq.(6.115) is short-range and the second term is long-range. The procedure used in the Ewald summation method is to compute the first term in real space and the second in Fourier space. If the parameter α is appropriately chosen the real part converges well taking only the sum over the closest image, and the part of the sum in Fourier part is rapidly convergent. Physically the first term corresponds to a smearing of the original distribution, and the second term to the original point distribution surrounded by a countercharge smeared distribution. Of course the sum of the two terms yields the original particle distribution. We write the potential energy then as:

$$\phi = \phi_{\mathbf{r}}^{(s)} + \phi_{\mathbf{k}}^{(l)}. \tag{6.116}$$

Further it is convenient to separate out the zero mode in the long range part, writing

$$\phi_{\mathbf{k}}^{(l)} = \phi_{\mathbf{k}=0}^{(l)} + \phi_{\mathbf{k}\neq 0}^{(l)}. \tag{6.117}$$

The function $f(\mathbf{r};\alpha)$ is chosen in the Ewald summation so that $\phi^{(s)}_{\mathbf{r}}$ and $\phi^{(l)}_{\mathbf{k}\neq 0}$ are both rapidly convergent, and with a known analytical expression for its Fourier transform. The value of the term $\mathbf{k}=0$ depends on how precisely the infinite sum in Eq.(6.114) is defined, and, as we will see further in particular examples, it is equal to zero in the presence of the background because of the charge neutrality. This method of evaluating the potential energy using the Ewald Sum has been generalised for generic $r^{-\alpha}$ potentials [Wu01], and for a Yukawa potential [SC00]. In principle it may be used for other potentials. Note in particular that the Ewald method is applied to sum the long-range part of the potential: it remains valid if one introduces any additional short-range potential which can be absorbed in $\phi^{(s)}_{\mathbf{r}}$ without modification of $\phi^{(l)}_{\mathbf{k}}$. We now give more detail first on its implementation for the standard OCP, we will modify it in chapter 8.

The $f(\mathbf{r};\alpha)$ function is usually chosen to be

$$f(\mathbf{r};\alpha) = \mathrm{erfc}(\alpha|\mathbf{r}+\mathbf{n}L|) \tag{6.118}$$

where erfc is the complementary error function, $\mathrm{erfc}(x) \equiv 1-2/\sqrt{\pi}\int_0^x dt\,\exp(-t^2)$. It is equivalent to smearing the charge distribution to obtain

$$\rho(\mathbf{r}) = \sum_{j=1}^{N}\sum_{\mathbf{n}} q_j \exp\left(-\alpha|\mathbf{r}-(\mathbf{r}_j+\mathbf{n}L)|^2\right) \tag{6.119}$$

and introducing in Fourier space the original distribution plus the opposite smeared distribution. With this choice the short-range interaction energy is given by

$$\phi^{(s)}_{\mathbf{r}}(\mathbf{r}_i) = \sum_{j=1}^{N}\sum_{\mathbf{n}} q_j \frac{\mathrm{erfc}(\alpha|\mathbf{r}_{ij}+\mathbf{n}L|)}{|\mathbf{r}_{ij}+\mathbf{n}L|}\,, \tag{6.120}$$

and the long-range part by

$$\phi^{(l)}_{\mathbf{k}\neq 0}(\mathbf{r}_i) = \frac{4\pi}{L^3}\sum_{j=1}^{N}\sum_{\mathbf{k}\neq 0} q_j \frac{1}{k^2}\exp\left(\frac{-k^2}{4\alpha^2}\right)\cos(\mathbf{k}\mathbf{r}_{ij}). \tag{6.121}$$

The $\mathbf{k}=0$ term is zero for a neutral distribution is only well defined in the presence of the negative background that ensure neutrality:

$$\lim_{k\to 0}\phi^{(l)}_{\mathbf{k}=0}(\mathbf{r}_i) = \frac{4\pi}{L^3}\lim_{k\to 0}\frac{1}{k^2}\sum_{j=1}^{N} q_j. \tag{6.122}$$

In the case of electroneutrality the sum in the limit is identically zero. An appropriate choice of α is $\alpha \sim 5.6/L$, where L is the size of the box. This gives good convergence in both (6.120) and (6.121), i.e. it includes only the first term $\mathbf{n}=0$ in the first equation and not too many $\mathbf{k}$ in the second.

Part II

Results

Chapter 7

Initial conditions of N-body simulations: a study of their correlation properties

In chapter 5 we have seen that it is very difficult to solve numerically the Vlasov equation. Instead of doing so, a simulation of N bodies (i.e. particles) evolving under their self gravity is performed. We have underlined that there is no rigorous established connexion between the Vlasov equation and the N-body model. Experience says that the N-body method works reasonably well (see section 5.7 and references therein) but there are still many open and fundamental open questions.

When one runs an N-body simulation, the first step is to generate adequate initial conditions (hereafter IC) with the correlations specified by some theoretical model, such as the PS given by Eq. (4.106). One of the most widely used methods to generate such IC uses correlated displacements of particles initially placed on a lattice. The correlations of the "displacement field" are determined to be such as to obtain a final distribution that has, approximately, the desired correlation properties. The principles of this method has been outlined in the second part of chapter 3.

In this chapter we are simply going to analyze the differences between the correlation properties of the continuous and the N-body model in the IC, i.e. at the initial time. Of course, this analysis does not allow one to conclude about the importance of the discreteness effects *during the gravitational evolution*, which is what we are really interested in. This analysis is a "first step" (or rather just a "zero-th step") in quantifying the discreteness effects introduced in N-body simulations. However, as we will see, it is a very instructive analysis because it gives insight about the limitations of discretization process and the advantages and disavantadges of a given discretization scheme compared with another. When discretizing, one loses information but this information can be lost in different ways. One has to choose the best one for the particular problem considered. We will see that generating IC from a perturbed lattice, there is almost no information lost in the PS for scales below the Nyquist frequency k_N (corresponding to the interparticle distance). The discreteness (i.e. the information lost) is therefore localized, in the PS, at modes larger than k_N.

However, the counterpart is that, in real space, the discreteness effects can be totally delocalized, and present at all scales[1]. If the dynamics depends only on the PS at scales below k_N –we will return to this point in chapter 9 where we discuss the evolution for these IC – this kind of IC is appropriate. However, if real space properties are important, this way to set up IC will be problematic.

We begin this chapter by explaining in detail the standard method to generate IC with correlated displacements on an initial distribution. Using the formalism studied in chapter 3 we will derive exact analytical expressions for the correlation functions of the resulting distribution, in real and Fourier space. We will then consider them in one dimension, where the numerical integration is straightforward.

By comparing the correlation function of the particle distribution with the underlying theoretical (fluid) model, we will be able to study quantitatively the discreteness effects. Depending on the spectrum considered – indeed if there is a good agreement in the PS – we will see that the differences in real space can be very significant.

This detailed study of IC has been motivated by a series of papers [BSL02, DK03, DK02, BSL03] where analogous *numerical* studies to the one presented here have been considered. Both set of authors agree about the properties of the IC in Fourier space, but not those in real space. One of the reasons for this discrepancy was the limitation in the resolution introduced by the noise of the *estimators* of the correlation functions, i.e. by the fact that they were using a numerical estimate of the correlations. The advantage of this study is that one works with analytical expressions; our results can be therefore considered as *exact*. An improvement would be perform the calculation in three dimensions, instead of one, which demands greater computer power than that to which we had access. However, as we will see in the chapter, a qualitative generalization to three dimensions is quite straightforward[2]

7.1 Generation of IC using the Zeldovich approximation

The method which is used canonically for the generation of IC in cosmological NBS is based on the so-called Zeldovich approximation (ZA), described in section 5.5.2. We will review briefly this approximation in what follows, adapted of the present context. Put simply, it relates the initial position $\mathbf{q}$ of a fluid element to its final position $\mathbf{r}$ through an expression like (5.63) (with $a = 1$)

$$\mathbf{r}(\mathbf{q}, t) = \mathbf{q} + f(t)\mathbf{u}(\mathbf{q}) \,, \tag{7.1}$$

i.e. it expresses the displacement of a particle as a separable function of the initial position $\mathbf{q}$ and the time t. The vector field $\mathbf{u}(\mathbf{q})$ is thus proportional to both the velocity and acceleration of the fluid element, and with a suitable normalization it can thus be taken to satisfy

$$\mathbf{u}(\mathbf{q}) = -\nabla \cdot \Phi(\mathbf{q}) \tag{7.2}$$

[1] One can draw an interesting analogy with, for example, the uncertainty principle in quantum mechanics.

[2] A corrected version of this chapter can be found in the updated paper [JM04].

where $\Phi(\mathbf{q})$ is the gravitational potential at the initial time created by the density fluctuations[3].

The displacements of the fluid elements are associated to density fluctuations, the relation between the two being given, to leading order in the gradient of the displacements, by the continuity equation

$$\delta\rho(\mathbf{r}) = -f(t)\nabla\cdot\mathbf{u}(\mathbf{r}). \tag{7.3}$$

where the density fluctuation $\delta\rho(\mathbf{r})$ is defined by

$$\delta\rho(\mathbf{r}) = \frac{\rho(\mathbf{r})-\rho_0}{\rho_0}, \tag{7.4}$$

$\rho(\mathbf{r})$ is the (continuous) density field and ρ_0 the average density. The PS of density fluctuations is defined as

$$P(\mathbf{k}) = \lim_{V\to\infty}\frac{\left\langle|\delta\hat{\rho}(\mathbf{k})|^2\right\rangle}{V}, \tag{7.5}$$

where $\langle\ldots\rangle$ denotes the average over an ensemble of realizations. It follows then from Eq. (7.3) that

$$P(\mathbf{k}) = f^2(t)k_ik_j\hat{g}_{ij}(\mathbf{k}) \tag{7.6}$$

where

$$g_{ij}(\mathbf{k}) = \lim_{V\to\infty}\frac{\langle\hat{u}_i(\mathbf{k})\hat{u}_j^*(\mathbf{k})\rangle}{V} \tag{7.7}$$

and $\hat{\mathbf{u}}(\mathbf{k})$ is the Fourier transform (FT) of the vector field $\mathbf{u}(\mathbf{q})$. Assuming that the latter is derived from a scalar potential as in Eq. (7.2) we have

$$\hat{g}_{ij}(\mathbf{k}) = \hat{k}_i\hat{k}_j\hat{g}(k) \tag{7.8}$$

where $\hat{g}(\mathbf{k}) = Tr[\hat{g}_{ij}(\mathbf{k})]$ is a function of $k = |\mathbf{k}|$ only because the stochastic process is assumed to be statistically homogeneous and isotropic, and $\hat{\mathbf{k}} = \mathbf{k}/|\mathbf{k}|$. We thus have

$$P(\mathbf{k}) = f^2(t)k^2\hat{g}(k) = f^2(t)k^4P_\Phi(k) \tag{7.9}$$

where $P_\Phi(k)$ is the PS of the potential fluctuation field i.e.

$$P_\Phi(k) = \lim_{V\to\infty}\frac{\langle|\Phi(\mathbf{k})|^2\rangle}{V} \tag{7.10}$$

The basis of the ZA is that Eq. (7.1) implies Eq. (7.9) which describes precisely the evolution of the PS of density fluctuations which follows from the linear theory of perturbations applied to the equations describing a self-gravitating fluid in the Eulerian formalism. The function $f(t)$ can be identified as the factor (see Eq. (4.73)) which describes the amplification of perturbations in this case ($\delta\tilde{\rho}(\mathbf{k},t) \propto f(t)\delta\tilde{\rho}(\mathbf{k},0)$). Usually in cosmological NBS one chooses $f(t)$ to correspond to the function describing the growing mode in the cosmology considered. This fixes then the initial velocities of the particles (which we will not discuss here).

To set up IC for the N particles of a cosmological NBS the procedure is then [EDWF85, Whi94]:

[3]For simplicity we consider here the case of a static universe. In an expanding universe $\mathbf{r}$ corresponds to the comoving position of the particle, and $\mathbf{u}(\mathbf{q})$ is proportional to the peculiar velocity and peculiar gravitational fields. The gravitational potential in Eq. (7.2) is then a solution of a Poisson equation sourced only by the fluctuations in the mass density field.

- to set-up a "pre-initial" configuration of the N particles. This configuration should represent the fluid of uniform density ρ_0. The usual choice is a simple lattice, but a commonly used alternative is an initial "glassy" configuration obtained by evolving the system with negative gravity (i.e. a Coulomb force) with an appropriate damping (see section 5.7.2).

- given an input theoretical PS $P_{th}(k)$, the corresponding displacement field in the ZA is applied to the "pre-initial" point distribution. The cosmological IC are usually taken to be Gaussian, and the displacements are determined by generating a realization of the gravitational potential with independents modes in Fourier space

$$\Phi(\mathbf{q}) = \sum_{\mathbf{k}} a_{\mathbf{k}} \cos(\mathbf{k}\cdot\mathbf{q}) + b_{\mathbf{k}} \sin(\mathbf{k}\cdot\mathbf{q}) \tag{7.11}$$

  with

$$a_{\mathbf{k}} = R_1 \frac{\sqrt{P_{th}(k)}}{k^2}, \quad b_{\mathbf{k}} = R_2 \frac{\sqrt{P_{th}(k)}}{k^2}\,, \tag{7.12}$$

  where R_1 and R_2 are Gaussian random numbers of mean zero and dispersion unity (see also section 5.7.2). From Eq. (7.9) we see that this corresponds to generating a realization of a stochastic displacement field with PS $\hat{g}_{ij}(\mathbf{k})$ as in Eq. (7.8) and

$$\hat{g}(k) = P_{th}(k)/k^2\,, \tag{7.13}$$

  choosing $f(t) = 1$ at the initial time.

7.2 Correlation properties of cosmological IC: general results in k-space

The configuration (or ensemble of configurations) generated by the method outlined in the previous section has PS given through Eq. (7.9), and thus equal to the theoretical PS $P_{th}(k)$, up to the following approximations:

- The system is considered as a continuous fluid. Thus we expect the exact PS of the (discrete) particle distribution to differ by terms which come from the "granularity" (i.e. particle-like) nature of this distribution.

- The calculations are performed at leading order in the gradient of the displacements (cf. Eq. (7.3). We would thus anticipate that the exact PS of the generated configurations will have corrections which are significant for k larger than the inverse of a scale characterising the amplitude of the relative displacements.

The rest of this chapter is principally concerned with the consideration of the resultant differences between the theoretical PS $P_{th}(k)$ and the exact PS (which we will simply denote $P(\mathbf{k})$) of the distribution generated by the algorithm described in the previous section. Note that the latter is assumed to be a function of $\mathbf{k}$ as it will not in general share the statistical isotropy and homogeneity of the theoretical PS (which makes it a function only of $k = |\mathbf{k}|$). We

will be interested in particular in determining how this difference between the theoretical and exact correlation properties is manifested in real space.

The starting point for our analysis is the result (3.113) (we use here the PS instead of the SF, and the function $\xi(r)$ instead of $C_2(r)$):

$$P(\mathbf{k}) = e^{-k_i k_j g_{ij}(\mathbf{0})} \int d^d r e^{-i\mathbf{kr}+k_i k_j g_{ij}(\mathbf{r})} \left(1+\xi_{in}(\mathbf{r})\right) - (2\pi)^d \delta(\mathbf{k})$$

where the integral is extended over all $\mathbb{R}^d$. This expression can be rewritten as

$$P(\mathbf{k}) = P_{in}(\mathbf{k}) + \int d^d r e^{-i\mathbf{kr}} \left(e^{-k_i k_j [g_{ij}(0)-g_{ij}(\mathbf{r})]} - 1\right) . \left(1+\tilde{\xi}_{in}(\mathbf{r})\right) \quad (7.14)$$

Expanding the exponential to linear order in $k_k k_j [g_{ij}(0) - g_{ij}(\mathbf{r})]$, and using Eq. (7.8), we obtain

$$\begin{aligned} P(\mathbf{k}) &= P_{in}(\mathbf{k}) + k^2 \hat{g}(k) \\ &+ \frac{k^2}{(2\pi)^d} \int d^d q (\hat{\mathbf{k}} \cdot \hat{\mathbf{q}})^2 \hat{g}(q) [P_{in}(\mathbf{k}+\mathbf{q}) - P_{in}(\mathbf{k})] \end{aligned} \quad (7.15)$$

In the generation of cosmological IC given an input theoretical PS of density fluctuations $P_{th}(k)$, we have seen in the previous section that one applies a Gaussian displacement field with PS given by Eq. (7.13). Inserting this in Eq. (7.15) we find, at the same order in the expansion of Eq. (7.14), that the PS of density fluctuations in the generated IC is

$$\begin{aligned} P(\mathbf{k}) &= P_{in}(\mathbf{k}) + P_{th}(k) \\ &+ \frac{k^2}{(2\pi)^d} \int d^d q \frac{P_{th}(q)}{q^2} (\hat{\mathbf{k}} \cdot \hat{\mathbf{q}})^2 [P_{in}(\mathbf{k}+\mathbf{q}) - P_{in}(\mathbf{k})] . \end{aligned} \quad (7.16)$$

The full PS is thus a sum of the PS of the "pre-initial" (i.e. lattice or glass) distribution, the input theoretical PS and a term which is a convolution of the two (plus corrections coming from higher order in the expansion leading to Eq. (7.16)). We have anticipated above that the full PS should reduce exactly to the input theoretical one when we neglect (i) granularity of the pre-initial distribution and (ii) corrections at higher than linear order in the gradient of the displacement fields. In keeping with (i) we see that if we set $P_{in}(k) = 0$ in Eq. (7.16), we indeed obtain $P(k) = P_{th}(k)$. For the second point we need to consider more carefully the expansion we have performed in arriving at Eq. (7.16).

We wish to determine both the conditions for the validity of this expansion, and the parameters which characterise the range of k for which the leading term corresponding to Eq. (7.16) is a good approximation. We note first that we have assumed Gaussianity in deriving Eq. (7.14). This is not in fact a necessary condition for the validity of the result Eq. (7.16). We have seen in section 3.3.7 that by starting directly with an expansion of Eq. (7.14), that Eqs. (7.15 and (7.16) can be obtained also only with the weaker assumption that $g_{ij}(\mathbf{0}) - g_{ij}(\mathbf{r})$ is bounded i.e. that the variance of the relative displacements

$$|\langle [u_i(\mathbf{0}) - u_i(\mathbf{r})] \, [u_j(\mathbf{0}) - u_j(\mathbf{r})] \rangle| \quad (7.17)$$

is a bounded function. It is straightforward to show that this condition leads to the following constraint on the small k behaviour[4] of $\hat{g}(k)$:

$$\lim_{k\to 0} k^d \hat{g}(k) = 0 \tag{7.18}$$

which corresponds to the integrability of $\hat{g}(k)$ at small k i.e. to the condition that the one-point variance of the displacement field $\langle u^2 \rangle$ (which is just the integral of $\hat{g}(k)$) be finite. Note that Eq. (7.18) implies

$$\lim_{k\to 0} k^{d-2} P_{th}(k) = 0 \tag{7.19}$$

We will consider here in general the generation of IC for a theoretical model with a PS of the form

$$P_{th}(k) = A k^n f(k/k_c) \tag{7.20}$$

with $f(x)$ is a function which interpolates smoothly between unity for $x \ll 1$ and zero for $x \gg 1$, i.e. which acts as a cut-off (with properties given below) in the PS for $k > k_c$, and A is a constant fixing the amplitude of the PS. As the PS is that of mass fluctuations which are assumed to be Gaussian, its one-point variance must be finite which implies that it must be an integrable function i.e.

$$\lim_{k\to\infty} k^d P_{th}(k) = 0\,, \qquad \lim_{k\to 0} k^d P_{th}(k) = 0 \tag{7.21}$$

i.e. given the assumed properties of the cut-off function f, it must obey

$$\lim_{k\to\infty} k^{n+d} f(k/k_c) = 0 \tag{7.22}$$

i.e. that f decreases faster than the power-law $k^{-(n+d)}$. From the small k constraint we have simply that $n > -d$.

The condition Eq. (7.19) does not, therefore, include the full class of PS we wish to consider, as it excludes the range of exponents $-d < n < -d+2$. We have seen, however, only that Eq. (7.19) is a *sufficient* condition for the validity of the expansion leading to Eq. (7.15). In Appendix D we show in detail, taking a power-law form $\hat{g}(k) \sim k^{n-2}$ (corresponding to $P_{th}(k) \sim k^n$) with $n < -d+2$, that the domain of validity actually extends to $n > -d$. This established that the domain of validity of the expansion coincides precisely with the PS obeying the conditions of Eq. (7.21).

The expansion at linear order Eq. (7.16) is expected then to be a good approximation, for a given k, provided the dimensionless quantity $k^d P_{th}(k)$ is less than unity. This is in fact simply the naive criterion anticipated from Eq. (7.3), as $k^d P_{th}(k)$ is just the dimensionless measure of the amplitude of the density fluctuations at the scale k, which is assumed to be small in the simple derivation of the result. Note that, again consistent with with Eq. (7.3), this condition for the validity of the expansion can be stated equivalently in terms of the boundedness of the dimensionless quantity

$$\frac{|\langle [u_i(\mathbf{0}) - u_i(\mathbf{r})]\,[u_j(\mathbf{0}) - u_j(\mathbf{r})]\rangle|}{r^2} \tag{7.23}$$

[4] We assume all these functions are well behaved at large k because of the intrinsic ultraviolet cut-off always imposed here at the Nyquist frequency.

i.e. of the "gradient" of the displacement fields. We thus find conclude that the expression Eq. (7.16) is indeed valid in the regime anticipated.

Let us now analyse further this expression for the PS of the generated IC. Let us suppose first that the pre-initial distribution is a Poisson distribution of number density n_0. Then $P_{in}(\mathbf{k}) = 1/n_0$, and thus Eq. (7.16) becomes simply

$$P(k) = \frac{1}{n_0} + P_{th}(k)\,. \tag{7.24}$$

Thus for an exponent $n < 0$ in (7.20) one will have $P(k) \approx P_{th}(k)$ for all $k \ll (An_0)^{1/n}$. For $n > 0$, on the other hand, one can have $P(k) \approx P_{th}(k)$ at most in an intermediate range of k: at small k the Poisson variance of the "pre-initial" distribution will always dominate.

In cosmological NBS the "pre-initial" distribution, as we have discussed, is usually taken to be a simple lattice. Its PS is

$$P_{in}(\mathbf{k}) = (2\pi)^d \sum_{\mathbf{h}\neq 0} \delta(\mathbf{k} - \mathbf{h}) \tag{7.25}$$

where the sum over $\mathbf{h}$ is over all the vectors of the reciprocal lattice i.e. $\mathbf{h} = \mathbf{m}(2\pi/a)$, where a is the lattice spacing and $\mathbf{m}$ is a vector of non-zero integers. The minimal value of $|\mathbf{h}| = 2\pi/a$, known as the *Nyquist frequency*. Since $P_{in}(\mathbf{k}) = 0$ for $k < k_N = 2\pi/a$ we therefore have that

$$P(\mathbf{k}) = P_{th}(k) + \frac{k^2}{(2\pi)^d} \int \frac{d\mathbf{q}}{q^2} (\hat{\mathbf{k}} \cdot \hat{\mathbf{q}})^2 P_{th}(q) P_{in}(\mathbf{k} + \mathbf{q}). \tag{7.26}$$

Let us focus briefly on the second term in Eq. (7.26). The coefficient of k^2 is necessarily positive and finite and is given by

$$\sum_{\mathbf{h}\neq 0} (\hat{\mathbf{k}} \cdot \hat{\mathbf{q}})^2 \frac{P_{th}(|\mathbf{h} + \mathbf{k}|)}{|\mathbf{h} + \mathbf{k}|^2} = \sum_{\mathbf{h}\neq 0} (\hat{\mathbf{k}} \cdot \hat{\mathbf{q}})^2 \hat{g}(|\mathbf{h} + \mathbf{k}|) \tag{7.27}$$

where $\mathbf{h}$ are the reciprocal lattice vectors as in Eq. (7.25). This term, which is generically non-zero for the case of cosmological IC, can thus be understood as a manifestation of what is known as "aliasing": an (usually undesired) transfer of power from large wavenumbers (i.e. above the Nyquist frequenecy, which is the characteristic discrete "sampling frequency" of the continuous displacement field) to small wavenumbers. This term is typically[5] of comparable size to $P_{th}(k)$ for $k \sim k_N$ and, we will see, dominates for larger $|\mathbf{k}|$.

We remark also that the appearance of this k^2 term can be understood simply in the following way: any stochastic process which moves matter (even from an exactly uniform initial state) up to a *finite* scale generates such a term at small k[6]. This term can thus be understood as a necessary by-product of the discretisation of the matter distribution which necessarily involves such a "transport" of matter. In principle this term may be made zero if the additional condition is satisfied that the centre of mass of the matter distribution is conserved (i.e. not displaced) locally, but one obtains in this case a term in the PS

[5] If $P_{th}(k)$ is cutoff for scales larger than k_N, if not the aliasing can be important and indeed dominate at scales $k \ll k_N$.

[6] This observation in the context of cosmology was first made by Zeldovich [ZN83]. See [Pee93] and [GJMV03] for discussion of this result and further references.

proportional to k^4 [ZN83, Pee93, GJMV03]. For the method of discretisation under discussion this additional condition is not satisfied.

Let us now return to the implications of the expression given by Eq. (7.26). We can conclude that, for $-d < n < 2$, one has $P(k) \approx P_{th}(k)$ at small k, while for $n > 2$ the k^2 term dominates. Thus the range of exponents for the theoretical PS in which one can obtain generically a PS with the generation algorithm corresponding, at small k (i.e. below the Nyquist frequency), to the input PS is

$$2 > n > -d. \tag{7.28}$$

We have mentioned also that sometimes the "pre-initial" spectrum is taken to be a "glassy" configuration obtained by evolving gravity with a negative sign. This in fact is just the time evolution of what is known as the "one component plasma", i.e. particles interacting through Coulomb potential (see chapters 6 and 8). The small k behaviour of the power spectrum is then expected to be $P_{in}(k) \sim k^2$ at small k [7]. Thus both terms additional to the theoretical PS in (7.16) will generically be small compared to $P_{th}(k)$ for the same range of exponents as in (7.28) i.e. just as for the simple cubic lattice.

7.3 Correlation properties of cosmological IC: general results in real space

We have seen in the previous section that the generation algorithm for cosmological IC, applied to a lattice, will lead, for the range of exponents in the PS given by Eq. (7.28), to an accurate representation of the theoretical PS for wave-numbers k small compared to the Nyquist frequency $2\pi/a$. We have given explicit expressions for the leading corrections to the PS in this range, starting from an exact expression for the PS which allows one, in principle, to calculate the exact PS given both the "pre-initial" PS $P_{in}(k)$ and the PS $P_{th}(k)$ of the input theoretical model. Before using these exact formula to derive results in one dimension which allow us to compare the full correlation properties with the theoretical ones, we discuss now how we expect, in general (in any dimension, and of course in particular for $d = 3$), the real space correlation properties of the IC to reflect those of the theoretical input model and "pre-initial" distribution.

The quantities we will study in real space are the reduced 2-point correlation function $\tilde{\xi}(\mathbf{r})$ and the variance of mass in spheres. In fact we will principally consider the latter for reasons which we will see now.

We recall the asymptotic properties of the mass variance in spheres studied in section 3.2. We have seen that it depends strongly on the value of n:

- for $-d < n < 1$ the integral for $\sigma^2(R)$ is dominated by modes $k \sim 1/R$ and one has
$$\sigma^2(R) \sim k^d P(k)|_{k\sim 1/R} \propto \frac{1}{R^{d+n}} \tag{7.29}$$
- for $n > 1$ the integral is dominated by modes $k \sim k_c^{-1}$ (i.e. by the ultraviolet cut-off) and one has always
$$\sigma^2(R) \propto \frac{1}{R^{d+1}} \tag{7.30}$$

[7] Here "small" means compared to the inverse of the Debye length characterising the screening.

For $n = 1$ one obtains the transition behaviour, in which the integral depends logarithmically on the cut-off k_c. This gives $\sigma^2(R) \propto \ln R/R^{d+1}$. The behaviour in Eq. (7.30) is thus, as we have already seen in chapter 3, a limiting behaviour: the most rapid possible decay of the unnormalized variance of the mass $\langle(\Delta M)^2\rangle_V$ in a volume V is proportional to the *surface* of the volume.

From the expression (7.15), we infer the approximate behaviour

$$\sigma^2(R) \simeq \sigma^2_{in}(R) + \sigma^2_{th}(R) \tag{7.31}$$

$$\tilde{\xi}(r) \simeq \tilde{\xi}_{in}(r) + \tilde{\xi}_{th}(r) \tag{7.32}$$

for normalised mass variance and correlation function of the IC. We have assumed here that all the integrals to be dominated by the k for which Eq. (7.16) is a good approximation i.e. we have assumed that, if the integral of $P_{in}(\mathbf{k})$ or $P_{th}(k)$ is dominated by an UV cut-off scale, this scale is small compared to the k at which the expansion leading to Eq. (7.16) is valid. This will always be true for the case of generation of IC. We have also neglected for simplicity the additional term in k^2 in the expression for the PS: if it does contribute, it follows from what was observed above that it gives a "minimal" contribution to the variance which, for the purposes of the argument which follows, may be absorbed into the "pre-initial" term. There is also a caveat to be noted with respect to Eq. (7.32): it must be taken with caution in the case that $\tilde{\xi}_{in}(r)$ has a singular delta-function structure at the relevant r. This is the case for the perfect lattice which we will discuss further below, and we will return to this point.

Considering the Eqs. (7.31) and (7.32) one can appreciate easily why the problem we consider for most of the rest of this chapter — the question of the representation of real space properties of the IC generated using the ZA — is non-trivial. In k space the PS, approximated at small k by Eq. (7.16), indeed satisfies the condition $P(\mathbf{k}) \approx P_{th}(k)$ for an appropriate choice of $P_{in}(\mathbf{k})$. In particular the choice of a perfect lattice as "pre-initial" configuration is ideal in this respect as $P_{in}(\mathbf{k}) = 0$ for $k < 2\pi/a$. In real space, on the other hand, it is not possible to reduce arbitrarily the "pre-initial" terms in Eqs. (7.31) and (7.32): we have noted above, in particular, that there is a limiting behaviour to the decay with distance of the mass variance.

Let us consider the case of the perfect lattice as "pre-initial"configuration. While the result we cited concerning the variance applies strictly to the case of statistically homogeneous and isotropic distributions, it can be shown (see [SB95, GSLJP05]) that it applies also to the variance measured in a lattice. Thus the localisation of intrinsic "pre-initial" power which is a feature of $P_{in}(\mathbf{k})$ in this case does not extend to real space. And indeed a distribution of points with the analogous property, $\sigma^2_{in}(R) = 0$ for $R \sim a$ does not exist. The "delocalisation" in real space of $P_{in}(k)$, which has compact support in k-space, is even more dramatic: the correlation function of a perfect lattice is a function which oscillates between a delta-function and -1 (see explicit expression below) at all scales. Thus, subject to small relative displacements, one does not expect it to satisfy the condition $\tilde{\xi}(\mathbf{r}) \approx \tilde{\xi}_{th}(r)$, as the highly peaked oscillating structure will not be removed by such a perturbation. Note that one could, however, envisage starting from a distribution with $\xi_{in}(r) = 0$ above some finite scale, and so one might indeed obtain $\tilde{\xi}(\mathbf{r}) \approx \tilde{\xi}_{th}(r)$. An analogous limitation of the variance to a finite region, however, does not apply: it is related to the correlation function

through an integral (Eq. (3.26)), which has the maximal decay rate we have discussed in section 3.2.

We will consider from now on primarily the variance. It is an integrated quantity which has generally a more stable behaviour than the correlation function, and thus it is easier in many cases to study (e.g. evidently in the case of the perfect lattice as initial configuration). We will, however, return to consider the correlation function at the appropriate point below, and we will see that we can ultimately draw the same conclusions about it as for the variance.

Given Eq. (7.31) and the limits we have discussed on the behaviour of the variance we can immediately make a simple classification of the PS of the form (7.20) for what concerns the representation of their variance in real space. The faithfulness of such a representation requires simply

$$\sigma^2_{th}(R) \gtrsim \sigma^2_{in}(R) \tag{7.33}$$

We will assume for simplicity that we are in the "optimal" case that $\sigma^2_{in}(R) \propto 1/R^{d+1}$ (i.e. with the most rapid possible decay of the variance, $\sigma^2_{in}(R)$). Further we will assume that we consider always the case that the full PS approximates well the theoretical PS below the Nyquist frequency i.e. that the expression given by Eq. (7.16) is a good approximation. Given our discussion in the previous section of the validity of the expansion leading to this expression, we expect this to correspond to the criterion that $k^d P_{th}(k) < 1$ for $k < k_N$. Given that we will always consider spectra for which this quantity reaches its maximum value at or close to k_N, this condition will simplify to

$$\delta^2_N = k^d_N P_{th}(k_N) < 1 \tag{7.34}$$

Up to a numerical factor of order unity this is none other that the criterion [8] that $\sigma^2_{th}(R = a) < 1$, and so it is simple to see that we expect the following behaviours:

1. For $2 > n > 1$ we have seen that $\sigma^2_{th}(R) \sim 1/R^{d+1}$ i.e. $\sigma^2_{th}(R)$ has the same functional behaviour as that of the "pre-initial" variance. Given that the former is necessarily smaller at the inter-particle distance, the condition Eq. (7.33) will never be fulfilled, and the full variance will be well approximated by that that of the pre-initial configuration.

2. For $1 > n > -d$ we have that $\sigma^2_{th}(R) \sim 1/R^{d+n}$, which thus decays more slowly than the "pre-initial" term. Thus we expect that there will be a scale R_{min} such that for $R > R_{min}$ one can satisfy the condition Eq. (7.33). Given that $\delta^2_N \sim \sigma^2_{th}(R = a)$ it is easy to infer that, for any d, we have
$$R_{min} \sim a \left(\frac{1}{\delta_N}\right)^{\frac{2}{1-n}} \tag{7.35}$$

In the rest of this paper we verify these qualitative conclusions using both exact analytical calculations and numerical simulations. We will consider the slightly simpler one-dimensional case, but we will see that the results can easily be generalised to three dimensions (which is the case of interest).

[8] For the case $n \geq 1$, this is true provided we assume that $k_N \sim k_c$, which is true in practice here as the input spectrum is always cut at k_N.

7.4 Comparison of reciprocal and real space properties of IC: numerical results in one dimension

To explore further the analytic expression Eq. (7.14) we have given for the full two point correlation properties, and to develop further the qualitative analysis of the corresponding real space properties which we have given in the previous section, we use numerical simulations in one dimension. We work in one dimension because of the numerical feasibility of the study in this case: we can both calculate easily the results obtained from the exact expressions for the correlation properties, and verify these results in detail against those obtained using the generation algorithm applied to a finite number of points. The point is that to make this latter comparison we need to measure the real-space correlation properties on a large ensemble of configurations, which is not numerically feasible (for modest computational power) in three dimensions. We will see that these simulations allow us to verify and develop further the qualitative analysis of the previous sections, and that once we have done this we can easily generalise our results to the three dimensional case which is the case of interest.

We wish to consider theoretical (input) PS of the form given by Eq. (7.20), for the range $-d < n < 2$ in which the method of displacing particles off a lattice using the ZA can in principle produce a configuration with the correct theoretical PS to a very good approximation. We take a simple exponential form for the cut-off in Eq. (7.20) i.e.

$$P_{th}(k) = Ak^n e^{-k/kc}. \tag{7.36}$$

As discussed in the previous section we anticipate a qualitative differences for different ranges of the exponent n. We encompass the two cases with our numerical analyses we have studied the (i) $n = 3/2$, and (ii) $n = -1/2$.

7.4.1 Case $n > 1$ $(n = 3/2)$

For the theoretical PS given by Eq. (7.36) with $n = 3/2$ we have calculated numerically, using Eq. (7.14) and the exact formulae derived in the previous section, the two point correlation properties of the configuration obtained through the procedure used to set up cosmological IC for this PS. We will use units of length in which the interparticle distance a is equal to unity. Note that we are calculating the ensemble average of these quantities (in the infinite volume limit), so the inter-particle distance is the only length scale introduced by the discretisation.

In Figs. 7.1 and 7.2 are shown the PS obtained for two different values of the amplitude A, and a chosen value of the ultra-violet cut-off $k_c = 0.75$. The latter is chosen a little smaller than the Nyquist frequency to minimise the aliasing effects discussed in Sect. 7.2. We see that, in both cases, one obtains at sufficiently small k extremely good agreement between the theoretical PS and that of the distribution which represents its discretisation. For the case $\delta_N^2 \ll 1$ we see that, as anticipated by our treatment in Sect. 7.3, the agreement between the theoretical and real PS is very good up to a scale $k \sim k_N$. Further the corrections for $k \lesssim k_N$ are very well described by the additional convolution term given in Eq. (7.16). For the other case, with $\delta_N^2 \gg 1$, we see that the

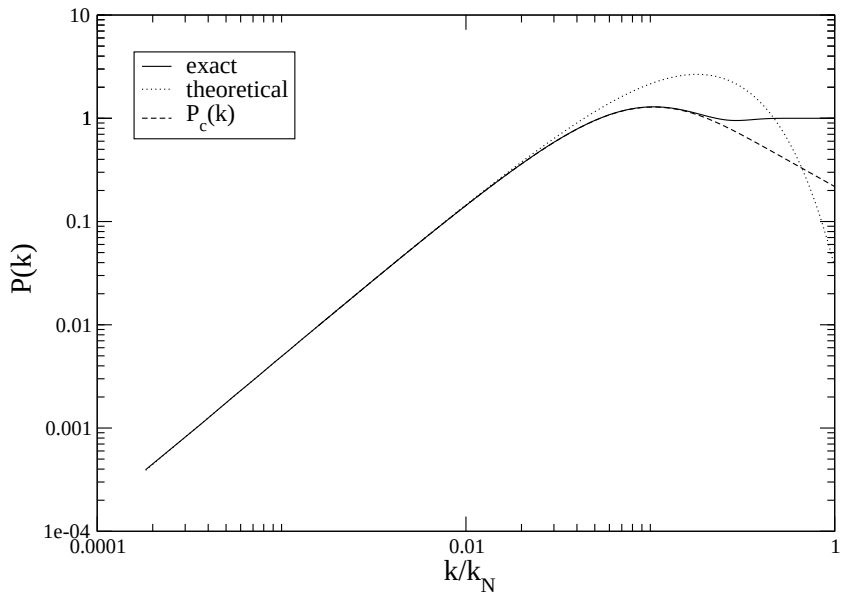

Figure 7.1: The exact PS obtained from the ZA algorithm for the input theoretical PS given in Eq.(7.36) with $n = 3/2$, $k_c = 0.75$, $A = 10$ and $\delta_N^2 = 0.23$. The curve labelled by $P_c(k)$ is the continuous limit of the full expression (7.14), i.e. setting $\xi_{in}(r) = 0$.

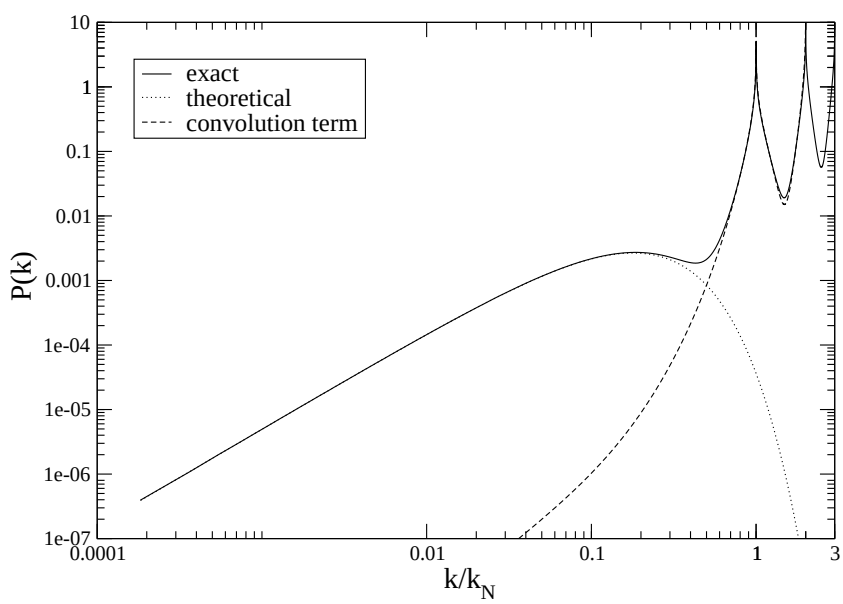

Figure 7.2: The exact PS obtained from the ZA algorithm for the input theoretical PS given in Eq. (7.36) with $n = 3/2$, $k_c = 0.75$, $A = 0.01$ and $\delta_N^2 = 2.4\times10^{-4}$. We have plotted also the second term of Eq. (7.16), which gives the first corrections to discreteness.

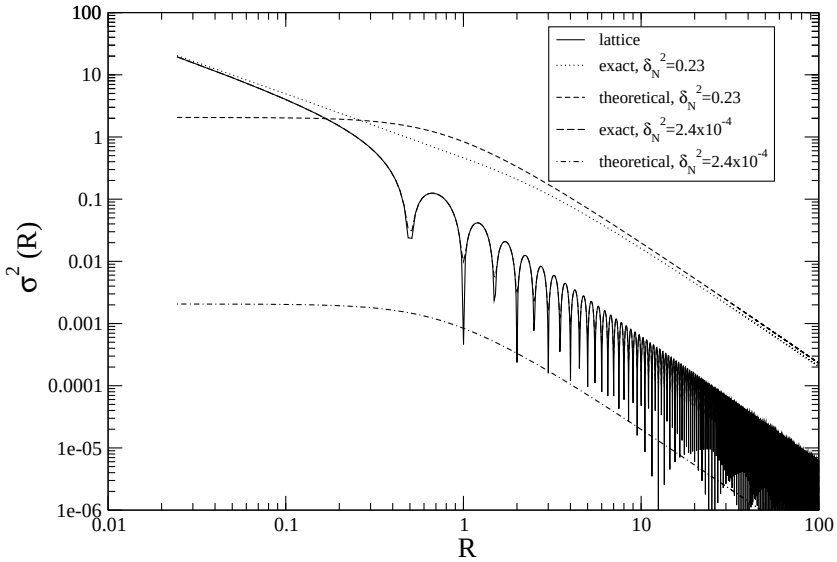

Figure 7.3: The normalised mass variance in spheres as a function of radius R for the same two models as in Figs. 7.1 and 7.2.

theoretical PS and the full PS only coincides up to a smaller k where $k^d P(k) \approx 0.3$. Beyond this scale the full analytic formula given by Eq. (7.14) describes the result perfectly, but the small k expansion is no longer a good approximation. Note that while in the former case, in which the relative displacements at the lattice scale are small compared to the lattice spacing, the peaks of the lattice (at $k = 2\pi, 4\pi$ etc.) are still clearly visible at large k, while in the latter case they have disappeared. Indeed in this case one interpolates directly from the theoretical behaviour to a flat (Poissonian) spectrum, indicating that the particle positions are arranged approximately randomly up to the scale of typical displacement.

In Fig. 7.3 are shown the normalised mass variances in the same two models. Comparing with the variance of the theoretical model, we find very different behaviours in the two cases. For the case $\delta_N^2 \sim 1$ we see that, as anticipated in Sect. 7.3, the total variance is always completely dominated by that of the "pre-initial" lattice configuration, and never approximates the theoretical variance (which is much smaller at all scales). For the other case, with $\delta_N^2 \gg 1$, we see that we observe on the other hand that the total variance does approximate well the theoretical variance from a few times the lattice spacing, while below this scale it does not. These observations correspond precisely to what was anticipated in section 7.3 above for the case $n > 1$.

7.4.2 Case $-d < n < -d + 2$ $(n = -1/2)$

In Figs. 7.4 and 7.5 is shown the PS for two different amplitudes A of the PS given by Eq. (7.36). As in the previous case the values of A have been chosen so that in one case $\delta_N^2 \sim 10^{-3}$ and in the other $\delta_N^2 \sim 1$, which we have noted corresponds roughly to relative displacements at the interparticle distance

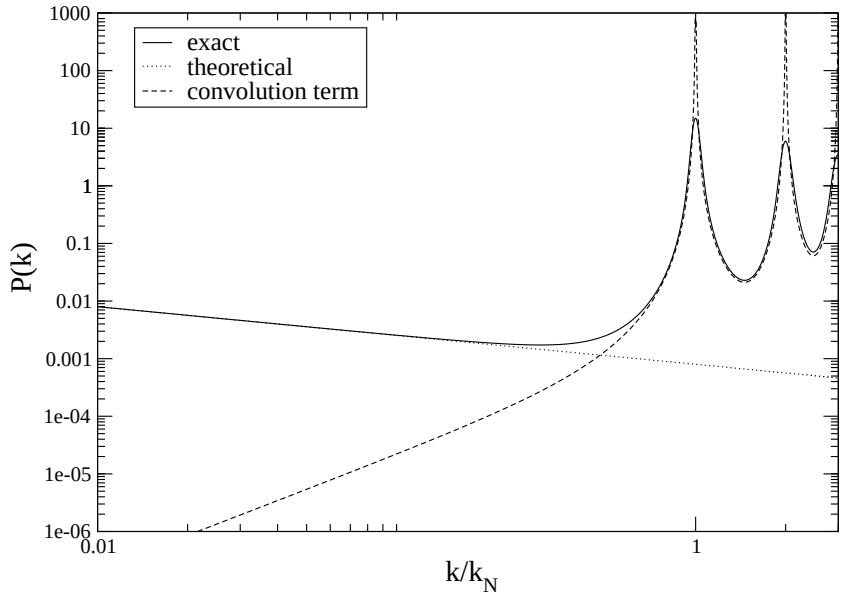

Figure 7.4: The exact PS for the input theoretical model with PS as given in Eq. (7.36) with $n = -1/2$ and $A = 1/500$. We have plotted also the second term of Eq. (7.16), which gives the first corrections to discreteness.

which are, respectively, much smaller or much larger than the lattice spacing. We observe the same qualitative behaviours as for the previous case ($n > 1$). For the first low amplitude case we see that there is very good agreement of the PS with the theoretical PS up to $k \sim k_N$, and excellent agreement over the whole range of k with the full leading order expression Eq. (7.16). For the larger amplitude, we see that there is agreement between the full and theortical PS only for the range s.t. $k^d P(k) \lesssim 1$, and for larger k the expression Eq. (7.16) is no longer valid. Also shown is in this case the exact analytic expression for the PS, but with the granularity contribution of the lattice neglected (i.e. with $P_i n(k) = 0$). We see that the full PS picks up important contributions for $k \gtrsim k_N$ from the discreteness terms, although they are no longer described by the single convolution term in Eq. (7.16).

The real-space variance in spheres of radius R (i.e. intervals of length $2R$) for these same models is shown in Fig. 7.6. For the higher amplitude model we see that the full variance approximates approaches rapidly the theoretical variance (with a behaviour $\sigma^2(R) \propto 1/R^{1/2}$) as soon as $\sigma^2_{th} \lesssim 1$, which in this case is a scale slightly above lattice spacing. In the low amplitude case the agreement between the total variance and the theoretical variance is attained at a considerably larger scale, when the theoretical variance has become sufficiently large to dominate over the lattice variance. These are again precisely the behaviours anticipated above.

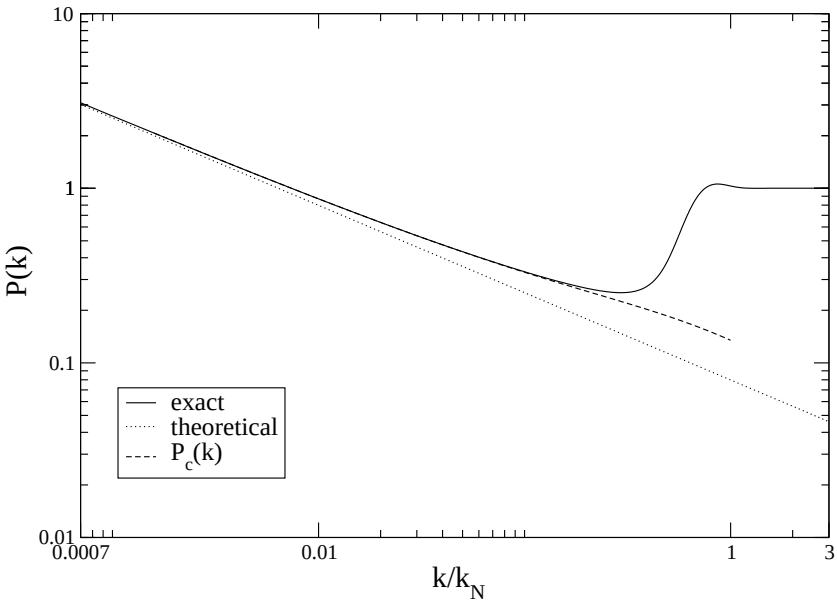

Figure 7.5: The exact PS for the input theoretical model with PS as given in Eq. (7.36) with $n = -1/2$ and $A = 1/5$. The curve labelled by $P_c(k)$ is the continuous limit of the full expression (7.14), i.e. setting $\xi_{in}(r) = 0$.

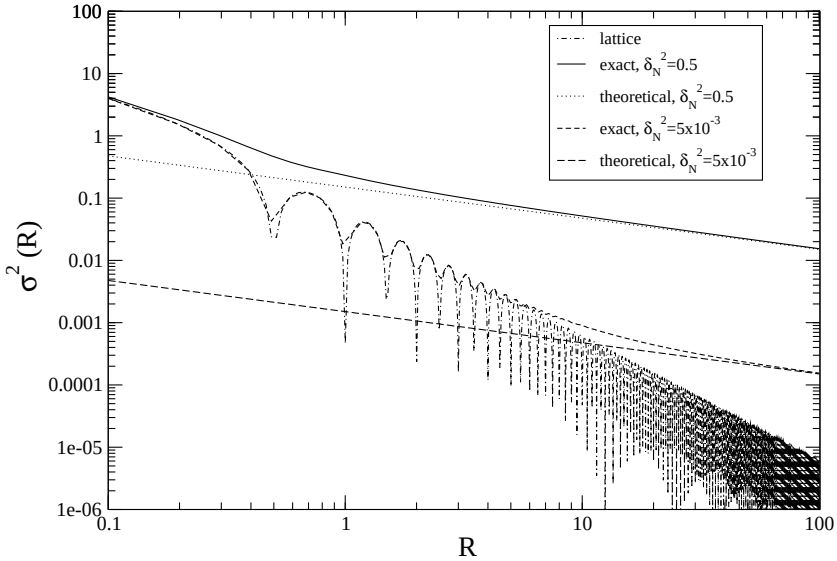

Figure 7.6: The normalised mass variance in spheres as a function of radius R for the same two models as in Figs. 7.4 and 7.5.

7.5 Correlation in real space probed by the two point correlation function

We now turn briefly to consideration of the two point correlation function $\tilde{\xi}(r)$. As discussed in Sect. 7.3 we anticipate that the $\tilde{\xi}(r)$ of a displaced lattice configuration will be, for scales in the relevant regime in which Eq. (7.16) is a good approximation, approximately a linear superposition of the "pre-initial" correlation function $\tilde{\xi}_{in}(r)$ and the theoretical correlation function $\tilde{\xi}_{th}(r)$. The former is that of a perfect lattice, which oscillates between a delta-function at the lattice spacing and -1 at other separations r. Applying, as in the cosmological context, small stochastic displacements we expect that this singular structure will be smoothed out, but that the large amplitude oscillations will persist up to scales very much larger than the lattice spacing. Given that $\tilde{\xi}_{th}(r)$ will generically, in the cosmological context, be a smooth function of small amplitude ($\ll 1$), we therefore expect the full correlation function to approximate, if at all, the theoretical correlation function only at separations very much larger than the lattice spacing.

This considerable difference at zero order between the correlation function of the generated configuration and that of the continuous model is a result of the nature of the discretisation which starts from the highly ordered particle configuration of the perfect lattice. One would anticipate however that the fact that $\tilde{\xi}(r)$ is the correlation function of a discretisation of a continuous model with correlation function $\tilde{\xi}_{th}(r)$ should allow one to extract more directly the latter from the former. Indeed one would expect to be able to recover $\tilde{\xi}_{th}(r)$ by taking the appropriate continuous limit of $\tilde{\xi}(r)$. We will now see that this is the case.

There is in fact no unique prescription for passing from a discrete distribution to a continuous one (for a more discussion, see [G$^+$03b]). We follow the simple prescription described in [G$^+$03b, GSLJP05], and we work with the one dimensional formulae for simplicity. A continuous distribution is given by a convolution of the discrete distribution with a smoothing spatial window function $W_L(x)$

$$\rho_c(x) = \int_{-\infty}^{+\infty} dx W_L(x - x')\rho_d(x'), \tag{7.37}$$

where $\rho_c(x)$ is the density function of the continuous field, $\rho_d(x)$ of the discrete distribution and L is the characteristic scale introduced by the smoothing. One has then that the PS of the continuous distribution $P_c(k)$ is given by

$$P_c(k) = |W_L(k)|^2 P(k), \tag{7.38}$$

where $W_L(k)$ is the FT of $W_L(x)$, and the correlation function $\tilde{\xi}_c(x)$ by

$$\tilde{\xi}_c(x) = \int_{-\infty}^{+\infty} dx' \mathrm{FT}_{x-x'} \left[|W_L(k)|^2\right] \tilde{\xi}_d(x'). \tag{7.39}$$

One can then follow one of two procedures to relate $\tilde{\xi}_c(x)$ to $\tilde{\xi}_{th}(x)$. Firstly one may try to determine the smoothing function $W_L(x)$ which makes the $\tilde{\xi}_c(x) \equiv \tilde{\xi}_{th}(x)$. This can be done most simply, using Eqs. (7.14) and (7.38), by

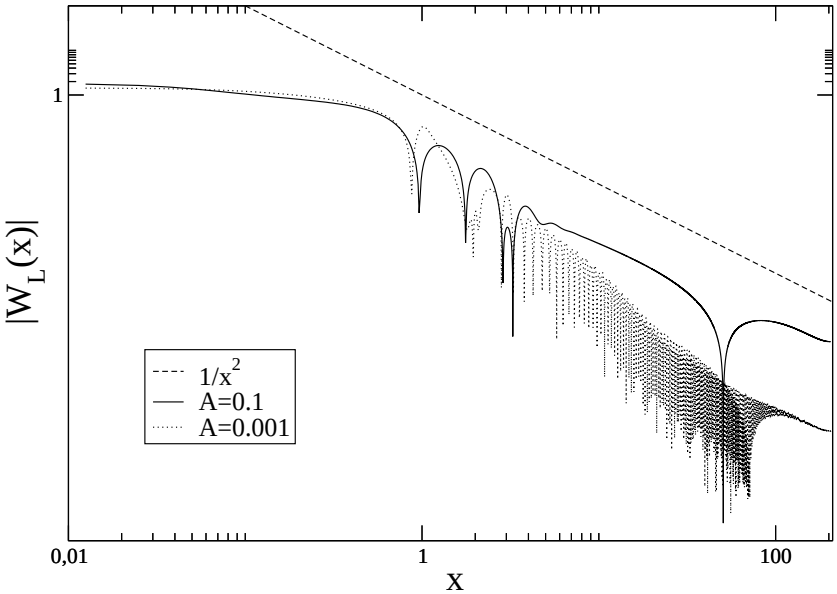

Figure 7.7: The window function calculated in one dimension from Eq. (7.40) for a theoretical model with PS as given in Eq.(7.36), for $n = -1/2$ and $\Lambda = 0.01$ and $k_c = 10$. The two models have $A = 0.1$ and $A = 0.001$.

finding the FT of

$$W_L(k) = \sqrt{\frac{P_{th}(k)}{P(k)}}. \tag{7.40}$$

In Fig. 7.7 is shown the result of such a determination[9] of $W_L(x)$ for the $n = -1/2$ one dimensional model studied in the previous section. We see that this gives a $W_L(x)$ which is a very oscillatory and slowly decaying function. Thus it does not describe what one would desire physically of such a smoothing: that it be localised on the scale of the lattice spacing which is the scale characteristic of the discreteness. The reason for this is that we are requiring that the smoothing remove entirely all trace of the lattice structure in the discretisation: as the lattice is correlated at all scales this leads to a correlation at all scales of the window function to "undo" this correlation in the continuous limit.

We therefore consider a weaker sense for the continuous limit: we apply a more physical smoothing on the scale L and investigate whether $\tilde{\xi}_{th}(x)$ can be recovered approximately from $\tilde{\xi}_c(x)$. We take a simple Gaussian smoothing

$$W_L(k) = e^{-L^2k^2}, \tag{7.41}$$

where the parameter L defines the characteristic width of the smoothing. From

[9] One has in fact evidently the freedom to multiply on the right hand side of Eq. (7.40) by an arbitrary phase factor dependent on k. The $W_L(x)$ determined as described is thus actually just one of a family of smoothing functions which all give the same continuous PS.

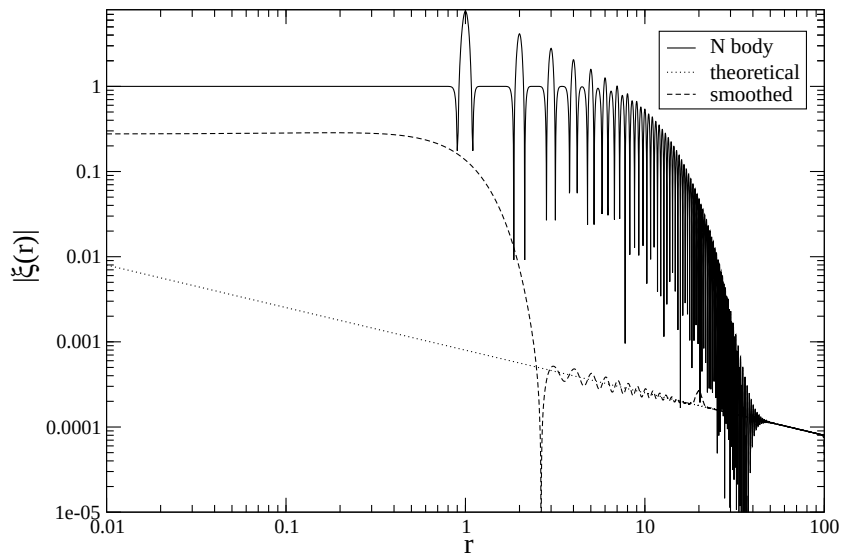

Figure 7.8: The reduced two point correlation function for configurations generated by the ZA algorithm applied to a perfect lattice in one dimension. The theoretical model has $n = -1/2$ and $A = 1/500$. Also shown are the correlation function obtained by applying the smoothing given in Eq. 7.42 with $L = 1$, as well as that of the continuous theoretical input model (given as the Fourier transform of the input PS).

Eq. (7.39) we have

$$\tilde{\xi}_c(x) = \frac{1}{2\sqrt{\pi}L} \int_{-\infty}^{+\infty} dx' e^{-L^2(x-x')^2} \tilde{\xi}(x'). \tag{7.42}$$

In Figs. 7.8 and 7.9 we show the results obtained for the $n = -1/2$ model of the previous section, for the same two amplitudes of the displacement field. In each case is shown the full correlation function $\tilde{\xi}(x)$ of the displaced lattice configuration, that of the theoretical model $\tilde{\xi}_{th}(x)$, and that of the continuous distribution $\tilde{\xi}_c(x)$ obtained by the Gaussian smoothing Eq. (7.42). In the first low amplitude case, with relative displacements smaller than the lattice spacing, we see that the first two are completely different up to a scale of at least one hundred times the lattice spacing. However, from a scale a few times larger than the lattice spacing (also of order the smoothing scale L), we observe that $\tilde{\xi}_c(x)$ approximates extremely accurately $\tilde{\xi}_{th}(x)$. For the larger amplitude case we observe the same behaviour, except that in this case there is a regime at larger separations in which $\tilde{\xi}(x)$ does approximate $\tilde{\xi}_{th}(x)$ well. In this case, therefore, the displacements applied have "erased" the oscillating structure of the underlying lattice correlation function at these scales. Note, however, that the displacements are considerably larger than the lattice spacing and that the oscillating part of the correlation function stills persists to several times the lattice spacing.

The generalisation to three dimensions of these results is less direct and precise than in the case of the mass variance. In the latter case we needed simply

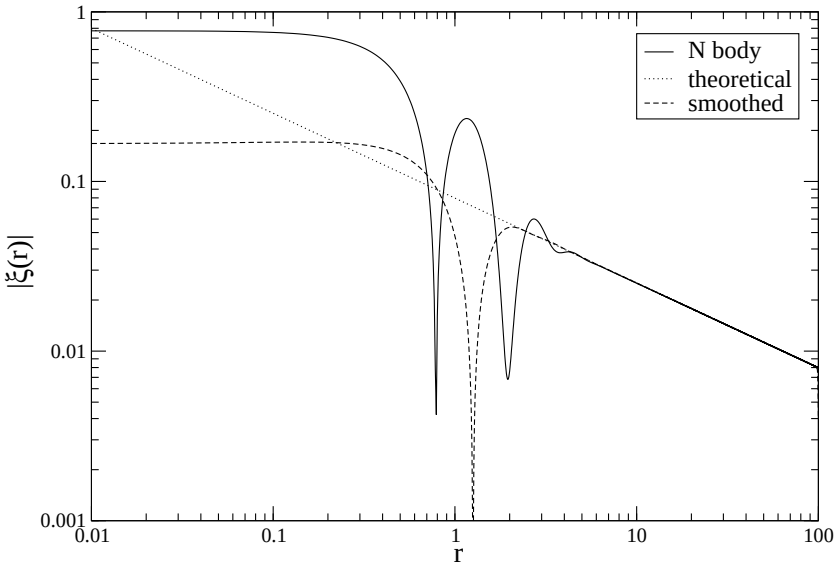

Figure 7.9: The same quantities as in Fig. 7.8 for a larger amplitude of the input PS ($A = 1/5$). The smoothing is again for $L = 1$.

to change appropriately the exponent in the underlying lattice variance. For the correlation function there is an important difference between one and three dimensions: when one averages over angles and estimates a correlation function using a shell of a finite size Δr, the number of oscillations in the underlying lattice correlation function grows in proportion to r^2. Thus there is an intrinsic averaging over directions which will tend to average out the contribution of the underlying variance in a way similar to the smoothing discussed above. The one-dimensional case without smoothing would correspond to $\Delta r \to 0$, in which limit one can recover also in three dimensions the pure oscillating behaviour of the lattice, and thus measure a correlation function with an ensemble average qualitatively different from that of its discretisation. In practice, however, one will typically use a shell thickness which produces a smoothing effect averaging out the underlying lattice, and thus we will find an ensemble average behaviour approaching that of the theoretical model at a scale above the interparticle distnace, which will depend (for given Δr) on the amplitude of the underlying theoretical model.

7.6 Summary and Conclusions

Let us summarize in what follows the main results of this chapter. We consider the case in which the displacements specified by the ZA are applied to a three dimensional lattice, for theoretical models with gaussian fluctuations specified by a PS of the form given in Eq.(7.20) so that the condition (7.17) applies. This is the primary case of interest in the context of the generation of IC for cosmological N-body simulations. Our primary conclusions are that

1. The theoretical PS may be very well represented by the generated config-

urations for $-3 < n < 2$, in the range $k < k_N$ (where k_N is the Nyquist frequency of the lattice).

2. For models with $n > 2$ the PS of the configuration has a leading behaviour $P(k) \sim k^2$ at small k, and the theoretical PS is not represented by it.

3. For models with $2 > n > 1$, the real space variance is dominated by the "pre-initial" variance of the lattice, which is larger at all scales than the theoretical variance.

4. For models with $1 > n > -3$ the real space variance can be well represented by the generated configurations starting from a scale R_{min} as given by (7.35). The lower the amplitude of the model represented, the larger is R_{min}, with $R_{min} \to \infty$ as the amplitude of the theoretical PS goes to zero.

5. The theoretical two-point correlation function (in real space) is generically not approximated by that of the configurations produced by the IC generation algorithm. This is because, in this quantity, the traces of the discrete lattice structure is completely delocalised in real space. A relation to the theoretical correlation function can be recovered at a sufficiently large scale (much larger than the lattice spacing) by performing an appropriate smoothing of the correlation function. In three dimensions the fact that an estimator of the correlation function employs a finite shell thickness would be expected to produce such a smoothing effect, and thus the scale at which the ensemble average of the estimated correlation function will approximate its input theoretical counterpart will depend also on this choice.

Chapter 8

A new method of generating IC for N-body simulations

In chapter 7 we have studied in detail discreteness effects in the IC for comological N-body simulation, in the case of IC generated using a perturbed lattice. We have seen that, despite a good agreement in Fourier space (for scales below the Nyquist frequency k_N corresponding to the discretization scale), the agreement in real space can be very poor. The main reason is that all the discreteness effects are localized in Fourier space at scales $k > k_N$. In real space the discreteness is delocalized and can be actually very high. Moreover, the perturbed lattice is not isotropic, which is a problem when modelizing an isotropic (continuous) medium (for more details about that see chapter 4.4).

It is therefore interesting to develop an alternative method with different discreteness effects. Of course, discreteness will be present in any N-body method to set up IC. It is characterised by the typical sampling scale of the continuous distribution, which is given by the interparticle distance. A priori we do not know which method of discretising to produce IC is appropriate. The method we are going to describe here presents, compared to the standard method we have discussed in the preceding chapter, discreteness effects more distributed between real and Fourier space. It does modelize the theoretical PS up to the Nyquist frequency but, in counterpart, it has approximatly those of the theorerical model in real space. In addition, the initial distribution is statistically isotropic.

The method has similarities to the perturbation of a "glassy" distribution described in chapter 5. It is based also on a kind of "reversed dynamics" but the configuration is obtained directly from the dynamics, without having to perform additional displacements. It uses a modified One Component Plasma (OCP), which has been extensively described in chapter 6. As we have seen, both the OCP and CDM systems are super-homogeneous distributions. The first one has a PS at large scales $P(k \to 0) \sim k^2$ and the latter $P(k \to 0) \sim k$. Using an $1/r^2$ interacting potential, it is possible to obtain a CDM-like spectrum at large scales. Further, we will see how it is possible to compute via an inverted HNC equation (6.103) an adequate potential to obtain a desired CDM spectrum at all scales.

8.1 Representation of continuous spectra with point distributions

8.1.1 Discrete and continuous stochastic density fields

Let us first recall (see chapter 3) some basic properties of the PS, defined in Eq. (3.18). We will use $P_c(\mathbf{k})$ to denote this quantity when we refer to a continuous distribution, $P_d(\mathbf{k})$ for the discrete case. We will also assume[1] statistical homogeneity (i.e. invariance of average quantities under translation). In this case the Fourier transform of the PS, for which we use the convention is the reduced two point correlation $\xi(r)$ function defined with Eqs. (3.8) and (3.11). The intrinsic difference between a continuous and discrete density field $\rho(\mathbf{r})$ manifests itself in a qualitative difference between the mathematical properties of the two-point quantities in each case. In real space the correlation function $\xi(\mathbf{r})$ has, for the class of finite one-point variance continuous fields which we consider, the property (see section 3.1.2)

$$-1 \leq \xi(r) \leq \xi(0) < \infty\,. \tag{8.1}$$

For the discrete case the one-point variance, which is equal to $\xi(0)$, necessarily diverges because of the singular nature of the density field at any point. The correlation function can then be written

$$\xi(r) = \frac{1}{n_0}\delta(\mathbf{r}) + h(r) \tag{8.2}$$

where n_0 is the mean number density, $\delta(\mathbf{r})$ is the (three dimensional) Dirac delta function, and $h(r)$ is a non-singular function for all r which can be taken to have the property analogous to Eq.(8.1).

These properties in real space translate in k space into a difference in the asymptotic properties of the power-spectra at large k. The one-point variance of the density field is also given by the integral of the PS, and so for the continuous case we have

$$\lim_{k\to\infty} k^3 P_c(k) = 0 \tag{8.3}$$

in order that this variance be finite. In the discrete case, on the other hand, we have

$$\lim_{k\to\infty} P_d(k) = \frac{1}{n_0} \tag{8.4}$$

$$\lim_{k\to\infty} k^3 (P_d(k) - \frac{1}{n_0}) = 0\,. \tag{8.5}$$

i.e. the divergence of the one-point variance is entirely associated to the "Poissonian" term in the PS, which is simply the FT of the delta-function singularity in real space explicit in Eq.(8.2). Note that both $P_c(k)$ and $P_d(k)$ are, by definition, positive functions, while $P_d(k) - \frac{1}{n_0}$ is not. There is therefore no bound $P_d(k) \geq 1/n_0$. In particular, one can have $P_d(k) \to 0$ for $k \to 0$, in systems satisfying the constraint

$$\int d^3 r h(r) = -\frac{1}{n_0} \tag{8.6}$$

[1] In assuming statistical homogeneity and isotropy we exclude formally the standard case of a perturbed lattice, which is not in this class. The results which are quoted below for that case are, nevertheless, valid (see [JM04, Gab04]).

i.e. when there is appropriate anti-correlation to balance the contribution to fluctuations at all scales from the Poissonian term associated to any discrete process. As discussed in section 3 these correspond to highly ordered "super-homogeneous" systems.

8.1.2 Smoothing of discrete distributions

The intuitively evident fact that a discrete distribution can only represent the correlation properties of a continuous field above some scale — that characteristic of the "granularity" of the discrete distribution — is reflected mathematically in the differences just discussed between the properties in the two cases of the correlation function at small real space separations, and the PS at large wavenumbers. Let us suppose now that we have a discrete distribution with PS $P_d(k)$, and a continuous distribution with PS $P_c(k)$. What is meant when one says that the former is a discretization of the latter? In what sense can we say that the former represents the correlation properties of the continuous distribution with PS $P_c(k)$? The answer to this question is that there is in fact no unique prescription for passing between a discrete and continuous distribution. In particular taking formally the limit in which the number of particles goes to infinity at fixed mass density, which one might naively think to define the desired continuous limit, does not do so. Consider, for example, the case of an (uncorrelated) Poisson point process: as the number density is taken to infinity the fluctuations also go to zero. Thus the continuous limit is an exactly uniform distribution with $P_c(k) = 0$.

As discussed in [G$^+$03a] the most natural way of defining such a relationship is by an appropriate local smoothing i.e. we assume the represented density field is given by the convolution of the discrete distribution with a spatial window function $W_{R_s}(r)$

$$\rho_c(\mathbf{r}) = \int W_{R_s}(|\mathbf{r} - \mathbf{r}'|)\rho_d(\mathbf{r}')d^3\mathbf{r}' \tag{8.7}$$

where R_s is the (single) characteristic smoothing scale and the realization of the discrete field is a sum over all the particles

$$\rho_d(\mathbf{r}) = \sum_i \delta(\mathbf{r} - \mathbf{r}_i)\,, \tag{8.8}$$

and $\rho_c(\mathbf{r})$ is the corresponding realization of the continuous stochastic density field. We then have that

$$P_c(k) = |\tilde{W}_{R_s}(k)|^2 P_d(k) \tag{8.9}$$

where $\tilde{W}_{R_s}(k)$ is the Fourier transform of $W_{R_s}(r)$. By the assumption that the window function gives a local smoothing, we mean that it is an integrable function. It is naturally normalized to unity (to conserve mass) so that $\tilde{W}_{R_s}(0)$ is equal to unity. Thus the PS of the discrete field must approximate well that of the continuous one for small k (i.e. $k \ll R_s^{-1}$). In real space the smoothing leads to the convolution relation

$$\xi_c(r) = \int W_{R_s}(\mathbf{r}')W_{R_s}(\mathbf{r}'')\xi_d(\mathbf{r} + \mathbf{r}' - \mathbf{r}'')d^3\mathbf{r}'d^3\mathbf{r}'' \tag{8.10}$$

between the continuous correlation function $\xi_c(r)$ and the discrete correlation function $\xi_d(r)$. One sees explicitly how the singularity becomes regularized applying (8.10) to (8.2):

$$\frac{1}{n_0}\delta(\mathbf{r}) \to \frac{1}{n_0}\int W_{R_s}(\mathbf{r}')W_{R_s}(\mathbf{r}+\mathbf{r}')d^3\mathbf{r}'. \tag{8.11}$$

Note that any pair consisting of a discrete and a continuous density field, with PS $P_c(k)$ and $P_d(k)$ respectively, can be related to one another formally by Eq.(8.9), taken simply as a definition of the smoothing function [2]. Whether $P_d(k)$ can be considered to be a physically reasonable discretization of $P_c(k)$ depends then on the mathematical properties of this smoothing function i.e. whether it really represents a physical smoothing. It is useful, for what follows, to express the relation between the two spectra in a slightly different (but equivalent) form:

$$P_d(k) = P_c(k) + \frac{1}{n_0}D(k) \tag{8.12}$$

where n_0 is the number density of the discrete distribution, The function $D(k)$ has then the properties imposed by Eqs.(8.4) and (8.5):

$$\lim_{k\to\infty} D(k) = 1 \tag{8.13}$$

$$\lim_{k\to\infty} k^3(D(k)-1) = 0\,. \tag{8.14}$$

In real space one has analogously

$$h(r) = \xi_c(r) - \frac{1}{n_0}FT[1-D(k)] \tag{8.15}$$

where $\xi_c(r)$ is the Fourier transform of $P_c(k)$ i.e. the reduced two-point correlation function of the continuous model. Expressed in terms of the smoothing we have from Eq.(8.9) that

$$|\tilde{W}_{R_s}(k)|^{-2} = 1 + \frac{D(k)}{n_0 P_c(k)}\,. \tag{8.16}$$

Note that whether the smoothing which is associated to a $D(k)$ is a physical smoothing depends, therefore, not only on its own properties, but also on those of $P_c(k)$.

8.1.3 Determination of the PS of a new discretization

We investigate here a different method than the described one in chapter 7 for discretizing a given input PS $P_c(k)$. The principle is to seek to generate a distribution with an $P_d(k)$ given through Eq.(8.12), where for $D(k)$ we will choose a smooth function of k, characterized by a single scale k_d, and interpolating between zero for $k < k_d$ and unity for $k > k_d$ (and in keeping with the asymptotic properties required Eqs.(8.13) and (8.14)). The scale k_d will be chosen of order the inverse of the mean particle separation a (see below for the exact definition we use). Further the function $D(k)$ will be such that the FT of

[2] This is evidently actually a family of functions as one has the freedom to choose an arbitrary phase factor as a function of k when inverting the expression to obtain a $W_{R_s}(r)$.

$(D(k)-1)$ in Eq.(8.15) is localized strongly in real space on the scale a. Thus, by construction, we will converge to

$$P_d(k) \approx P_c(k) \quad \text{for} \quad k \ll k_d \tag{8.17}$$

$$h(r) \approx \xi_c(r) \quad \text{for} \quad r \gg a \tag{8.18}$$

As we have noted, whether this choice of $D(k)$ corresponds to a physical smoothing, in the sense we have discussed, depends also on the properties of $P_c(k)$. For the well-behaved $P_c(k)$ we will consider we expect this to be the case, but we will check explicitly that the function $W_{R_s}(r)$ is smooth and integrable.

The precise scale $k < k_d$ at which Eq.(8.17) holds will depend both on $D(k)$ and on the form and normalization of the PS. In the cosmological context $P_c(k)$ is generically a monotonically decreasing function over a wide range of k for $k < k_d$, and thus the dimensionless quantity $n_0 P_c(k_d)$ gives a parameterization of the relative amplitudes of the "continuous" and "discrete" parts of the full PS $P_d(k)$. In the simulations of molecular dynamics described below we will take $n_0 P_c(k_d) \sim 1$. Thus we will have in this case Eq.(8.17) for all $k \lesssim k_d$, and (we will verify) Eq.(8.18) from $r \gtrsim a$ [3].

In our explicit examples of the construction of $P_d(k)$ we will make the simple choice $D(k) = 1 - e^{-k^2/2k_d^2}$, which evidently has the required asymptotic properties. It is important to note that we have not shown that the $P_d(k)$ then given by Eq.(8.12) and such a choice of $D(k)$ is necessarily the PS of a real discrete distribution [4]. Indeed it is easy to see that the ansatz for $P_d(k)$ may be unrealizable in a discrete distribution: we have noted that the two-point correlation function $h(r)$ of the discrete distribution must satisfy by definition $h(r) \geq -1$. Taking Eq.(8.15), it is not difficult to verify that this condition places an upper bound on k_d, of order the inverse of the average inter-particle distance[5]. Physically it is very reasonable that such a bound arises: taking k_d larger than the inverse of the inter-particle separation one is requiring the discrete distribution to mimic the correlation properties of the continuous model in a regime where the intrinsic difference in the nature of the distributions is important.

8.2 Modification of the OCP

Studying the standard OCP in chapter 6 we have obtained the expression between the interactive potential and the PS at small k (6.96):

$$P(k \to 0) \sim \frac{1}{\beta n_0^2} \frac{1}{\tilde{v}(k)}, \tag{8.19}$$

[3] The choice $n_0 P_c(k_d) \sim 1$ means that, in real space, the normalized "theoretical" mass variance $\sigma^2(R)$ in spheres of radius R (i.e. that corresponding to the model with PS $P_c(k)$) is of order unity at the inter-particle distance. This follows from the fact that, for these model PS, one has $\sigma^2(R) \sim k^3 P_c(k)$, with $k \sim R^{-1}$. Thus $\sigma^2(a) \sim k_d^3 P_c(k_d) \sim n_0 P_c(k_d)$.

[4] For a continuous SSP with finite variance it suffices that the PS be a positive function with the appropriate convergence properties at small and large k (to make its integral finite). For the discrete case the existence conditions on $P_d(k)$ are, apparently, not known. Note, in particular, that it is not clear whether there are intrinsic limits on the small k behavior of $P_d(k)$. In the case that such limits are established an elegant choice for $D(k)$ would be one giving this limiting small k behavior. One would then have that the "discretization" of a uniform continuous distribution (i.e. $P_c(k) = 0$) would be the (or one of the class of) most uniform possible discrete distributions.

[5] The exact numerical value for the bound in the case $D(k) = 1 - e^{-k^2/2k_d^2}$ will be given at the appropriate point below.

In the case of the standard OCP with Coulombian interaction, the PS at small k is $P(k \to 0) \sim k^2$. As noted in [G$^+$03b], modifying the interactive potential, using $v(r) = 1/r^2$, we obtain a CDM-like spectrum at small k, $P(k \to 0) \sim k$. We can obtain the desired PS at all scales using an inversion of the HNC equation, which we present in what follows.

8.2.1 Semi-analytic determination of the potential

It is simple to use the HNC equation (6.103) in the inverse direction i.e. to determine an interaction potential $v(r)$ which should give at thermal equilibrium desired two-point correlation properties:

$$\beta v(r) = h(r) - c(r) - \ln[h(r) + 1]. \tag{8.20}$$

Starting from an input model specified by a given PS $P_d(k)$ we need just to calculate $h(r)$ and $c(r)$ (using the OZ relation Eq.(6.68)). This can most conveniently be done using FFTs.

As noted above, when we treat the case of a PS with $P_d(k \to 0) = 0$, characteristic of a long-range interaction potential, we have a divergence at $k = 0$ in $\tilde{c}(k)$. Just as in the direct use of the HNC we deal with this numerically by dividing $\tilde{c}(k)$ into two parts. The short-range part, which is regular at $k = 0$, can be taken to be

$$\tilde{c}_s(k) = \frac{1}{n_0}\left(1 - \frac{1}{n_0 P_d(k)} + \frac{\mathrm{erfc}(k\eta)}{n_0 S_0(k)}\right). \tag{8.21}$$

where $S_0(k)$ is the functional form of $P_d(k)$ at small k, and as above, η is a parameter on which the final result does not depend. The subtracted divergent piece is chosen (if possible) so that it can be Fourier transformed analytically, and the full potential can thus be reconstructed easily from a determination of the short-range part of the potential from Eq.(8.20) using $c_s(r)$:

$$\beta v(r) = \beta v_s(r) - \mathrm{FT}[\tilde{c}_l(k)], \tag{8.22}$$

where $\tilde{c}_l(k)$ is the long-range part of $\tilde{c}(k)$, which corresponds to $f(r)$ in section 6.4.

8.2.2 Ewald sum for a $1/r^2$ potential

The Ewald sum (section 6.5.2) needs to be adapted of the new long-range form of the potential. In this case it is convenient to choose the function $f(\mathbf{r};\alpha)$ as [Wu01]:

$$f(\mathbf{r};\alpha) = \exp(-\alpha^2|\mathbf{r} + \mathbf{n}L|^2). \tag{8.23}$$

The short-range part of the energy is

$$\phi^{(s)}_{\mathbf{r}}(\mathbf{r}_i) = \sum_{j=1}^{N}\sum_{\mathbf{n}} q_j \frac{\exp(-\alpha^2|\mathbf{r}_{ij} + \mathbf{n}L|^2)}{|\mathbf{r}_{ij} + \mathbf{n}L|^2} \tag{8.24}$$

and the long-range part

$$\phi^{(l)}_{\mathbf{k}\neq 0}(\mathbf{r}_i) = \frac{2\pi^2}{L^3}\sum_{j=1}^{N}\sum_{\mathbf{k}\neq 0} q_j \frac{1}{k}\mathrm{erfc}\left(\frac{k}{2\alpha}\right)\cos(\mathbf{k}\mathbf{r}_{ij}). \tag{8.25}$$

We will use the same value for α as in the Coulomb case. With this value of α the real part still converges rapidly and the Fourier part is much more rapidly convergent.

8.2.3 Inversion of HNC

In what follows we will wish to simulate the molecular dynamics of particles interacting through the potential determined by the inversion of HNC equation as described in the previous section. As discussed in Sect. 8.1, the small k behavior of cosmological PS (the HZ spectrum of perturbations), requires a long-range $1/r^2$ potential. In the determination of the full potential through the inversion of the HNC, this piece is separated out by construction and the result is written as a sum of it and the short-range part subsequently determined. Taking the long-range part that comes from the subtracted divergence on the r.h.s. of Eq.(8.21), the long-range part is thus in this case

$$\phi^{(l)}_{\mathbf{k}\neq 0}(\mathbf{r}_i) = \frac{1}{n_0 L^3 \beta} \sum_{j=1}^{N} \sum_{\mathbf{k}\neq 0} q_j \frac{1}{n_0 S_0(k)} \mathrm{erfc}\left(\frac{k}{2\alpha}\right) \cos(\mathbf{k}\mathbf{r}_{ij}) \,, \tag{8.26}$$

where $S_0(k) = Nk$ gives the small k behavior of $P_d(k)$. The real part of the potential is then:

$$\phi^{(s)}_{\mathbf{r}}(\mathbf{r}_i) = \frac{\exp(-\alpha^2 r^2)}{2\pi^2 {n_0}^2 N \beta r^2}. \tag{8.27}$$

Note that the parameter α in the Ewald sum needs to have the same numerical value as the parameter η in the HNC.

8.3 Generation of discretizations of cosmological spectra

In chapter 4 and 5 we have seen that N-body simulations of the formation of structure in the distribution of matter at large scales start from an initial time which is "recent" in terms of cosmological history. The universe has entered the phase in which its energy density is dominated by massive particles, and the evolution of perturbations in the distribution of these particles at the scales considered is well approximated by Newtonian gravity. The fluctuations at this initial time are still of small amplitude at the relevant physical scales, and the simulation follows this evolution through to today when very high amplitude fluctuations have formed at scales comparable to those on which they are observed to exist today. These initial conditions for simulations are generically Gaussian in current cosmological models, and thus fully specified by their PS. This PS is the result of the evolution up to this time, which can be calculated precisely in a given model (and depends on the various parameters characterizing it) of the "primordial" fluctuations, which have the unique form given by so-called "scale-invariant" fluctuations. Because the fluctuations evolve in a non-trivial way for a finite time (until the time of "equality", after which matter dominates over radiation) the resultant PS corresponds to the "primordial" spectrum $P_c(k) \sim k$ only up to a characteristic wave-number k_t, above which it "turns over" to a different behavior, with a PS which decreases as a function of k but with a functional behavior which depends on the model. We will

consider here the class of "cold dark matter" (CDM) models which are those currently favored as viable models to explain the diverse observations of large scale structure. We will use as CDM PS the one parametrized in Eq. (4.106).

The PS thus shows the HZ form at small k, reaches a maximum at $k_t \approx 0.2(\mathrm{h}^{-1}\mathrm{Mpc})^{-1}$ and then interpolates between approximate power-law behaviors from $n \approx -1$ to an asymptotic value of $n = -3$ [6]. In practice here we will not work, for our simulations of molecular dynamics, with the full PS described in Eq.(4.106): our simulations are of a size which does not allow us to resolve the numerous different scales in this expression. We use instead a simplified version of this PS which retains its essential qualitative features:

$$P_c(k) = \frac{\mathcal{N}k}{1 + (Ak)^\alpha \exp(k/k_c)}, \tag{8.28}$$

with the maximum k_t chosen well inside the simulation box.

Following the discussion in Sect. 8.1 we seek to produce a discrete distribution with PS $P_d(k)$ given by Eq.(8.12) with

$$D(k) = \left(1 - e^{-k^2/2k_d^2}\right). \tag{8.29}$$

We note that, with this choice for the function $D(k)$, the upper bound on k_d, taking in Eq.(8.15) $\xi_c(r) = 0$ and using the condition $h(r) \geq -1$, is:

$$k_d \leq \sqrt{2\pi}(n_0)^{1/3} \approx 1.55/a, \tag{8.30}$$

where we have used the definition of a given in Eq.(6.72). By increasing n_0 sufficiently one can represent the continuous model up to a desired k.

In the first subsection below we will present an example of a HZ spectrum generated with a simple $1/r^2$ potential. In the following subsection we present the method using the simplified PS of Eq.(8.28), while in the last subsection we give the potential which should allow the generation of the "realistic" cosmological PS of Eq.(4.106).

8.3.1 The HZ spectrum

We consider just the "primordial" part of the PS with the HZ behavior $P_c(k) \sim k$. We have shown in section 8.2, using a simple screening argument explained in chapter 6, that the large scale correlation of a CDM model can be obtained using a modified OCP with $1/r^2$ interaction. To verify this expectation we have used both the HNC and molecular dynamics as described above. In Fig. 8.1 the results for the PS are given for each case, and in Fig. 8.2 the correlation function in real space. Because the potential is still a pure power-law the phase space is, as for the standard OCP, one dimensional and may be characterized by a single dimensionless parameter analogous to that for the OCP. We make the obvious generalization of the definition in Eq.(6.73):

$$\Gamma' = \beta(Ze)^2/a^2. \tag{8.31}$$

[6] To ensure integrability (and the existence of its Fourier transform) it is strictly necessary to add an ultraviolet cutoff. In practice this cut-off is usually not made explicit and the Nyquist frequency acts as the effective cut-off in the discretized model. See sections 3 and 7 for further detail.

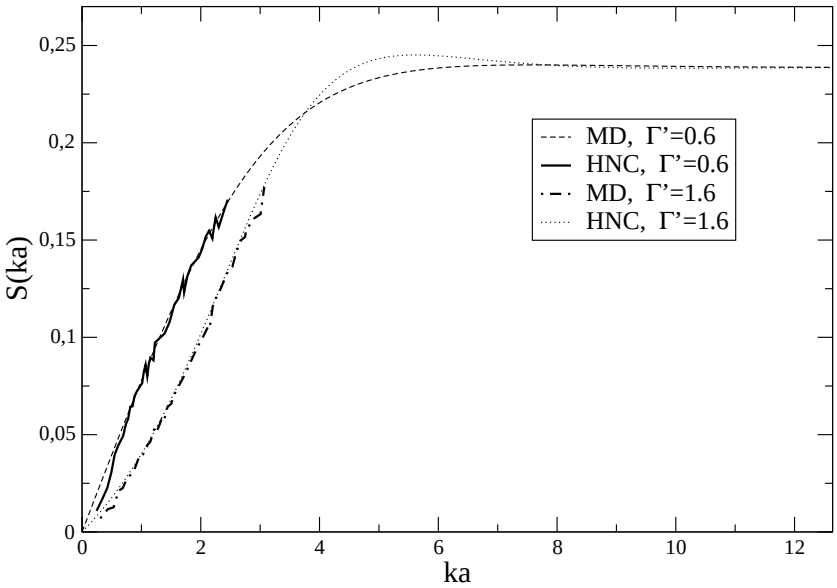

Figure 8.1: The PS of a $1/r^2$ OCP for two different values of the coupling parameter Γ'. Excellent agreement is observed between the predictions from the HNC and MD in the range where they overlap. For the weak coupling case the HZ form for the PS $P_d(k) \propto k$ is clearly evident. The units are normalized to the ionic radius a. Note that the plot is on a linear-linear scale.

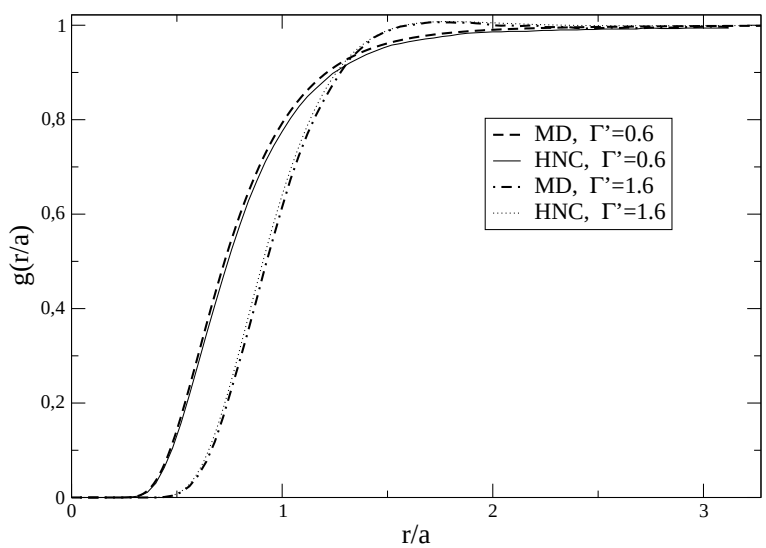

Figure 8.2: The correlation function in real space for the $1/r^2$ OCP for the same cases as in the previous figure. For the smaller coupling one has anti-correlation at all scales ($g(r) < 1$) while for the larger coupling one sees, just as in the standard OCP, the correlation appear with the first neighbor (which becomes more localized as the temperature is lowered).

The results from the HNC are valid in the infinite volume limit and show very good agreement with the prediction of the asymptotic form for both the PS and the correlation function given in Eq. (8.19). The range of these behaviors is, as expected, greater for smaller values of the coupling, and the linearity of the PS in particular is clearly visible in this case. We have checked also that one recovers the characteristic behavior of the correlation function at large scales $(g(r)-1) \sim -1/r^4$, which is also that of cosmological models with this PS (see [GSLJP05, GJSL02]).

The simulations of molecular dynamics were performed in the micro-canonical ensemble with the methods described in Sect. 6.5 above, with 4000 particles [7]. This corresponds to a simulation box with side of length $L = (16000\pi/3)^{1/3} \approx 25.6$ in units of the ionic radius a. Over this limited range very good agreement is seen with the results from the HNC in all cases, with some remaining statistical fluctuations. The units of time used in the simulations is $\tau = \sqrt{3}\omega_p^{-1}$ with $\omega_p^2 = 4\pi n_0 (Ze)^2/m$. To ensure good conservation of energy we have used a time increment of typically $\Delta t \sim 10^{-2}\tau$, which leads to fluctuations of $\sim 10^{-7}$ in the energy. The system evolves for $10^5\tau$ times steps, at which point it has reached thermal equilibrium. Then the PS and correlation functions are computed over many realizations of the system. By the ergodic principle this is equivalent to performing an ensemble average. Each realization is thus a configuration of the system at each time step. We compute the average in all the simulations over 50000 time steps, which leaves only very small fluctuations about the average.

8.3.2 CDM-type spectra: simple model

Let us now consider the spectrum (8.28):

$$P_c(k) = \frac{\mathcal{N} k}{1 + (Ak)^\alpha \exp(k/k_c)} \,. \tag{8.32}$$

We have seen that the small k part of the spectrum can indeed be produced by a repulsive $1/r^2$ potential.

As discussed in Sect. 8.2.3 above, we do the inversion of the HNC by determining the short range potential which needs to be added to modify this simple asymptotic behavior.

We consider the case $\alpha = 3$ in the PS of Eq.(8.28) (i.e. $P_c(k) \sim k^{-2}$ beyond the turn-over) and we choose k_t to have the linear part of the PS inside the simulation box. From now on we work in units of the ionic radius (6.72), in which our simulation box for a 1000 particle simulation corresponds to a cube of side $L \approx 16.1$. We have chosen $k_t = 1$ (corresponding to a inverse real scale of $\sim 2\pi$) so that we have a small range of wavenumbers in which the PS is linear in k inside the box. Choosing this turnover scale is equivalent to fixing A with the relation:

$$A \simeq \frac{1}{(\alpha-1)^{1/\alpha}} \frac{1}{k_t} \,. \tag{8.33}$$

For the value of α and k_t chosen, we have $A \approx 0.69$. The parameter $\mathcal{N}$ can finally be fixed by specifying the amplitude of the mass variance at some scale. The cutoff k_c is not of physical importance, and it can been chosen to ensure

[7] This is the number of particles which can be simulated on an ordinary PC for a reasonable simulation time (a few hours).

the PS to be numerically zero (i.e. $\sim 10^{-10}$) at the edge of the reciprocal space box.

Our determinations of the potential use the HNC equation, which holds only in a regime of weak correlations, and so we choose our parameters always to be in this regime. Ultimately a full simulation of the molecular dynamics is needed to establish that this potential will indeed produce the input correlations. However, one check which we can do on the determination of the potential is to insert it back into the direct HNC equation and check that it gives back the original input PS. In all the examples we have worked with here it is the case that this condition applies and the configuration generated with the molecular dynamics had always the desired spectrum. Note that in the cosmological application we are interested in, we are in always in this regime of weak correlations (i.e. the fluctuations at the starting time of a simulation of structure formation are always of low amplitude, corresponding to a low amplitude in the theoretical correlation function). For the case being discussed we have chosen $\mathcal{N} = 10$ and $k_c = 2.7$.

Once we have determined the theoretical PS it is necessary, as discussed in Sect.8.1, to specify the discrete distribution which is to be sought. Adopting the prescription of Eq.(8.12) with $(D(k) - 1)$ chosen as a simple Gaussian, the discrete and continuous distributions are related by a physical smoothing specified by the smoothing function

$$|W_{k_d,n_0}(k)|^{-2} = 1 + \frac{(1 + (Ak)^\alpha)\,(1 - e^{-k^2/2k_d^2})}{n_0 \mathcal{N} k} \exp(k/k_c). \tag{8.34}$$

We choose the value of k_d determined in Eq.(8.30), to be sure to have a correlation function with the appropriate mathematical properties. The numerically determined smoothing function in real space is shown in Fig. 8.3. It decays at large separation faster than $1/r^4$, and is thus a localized smoothing in the sense we discussed in Sect. 8.1. It has, however, the rather unsatisfactory feature of oscillating through negative values, albeit when the amplitude is already very small. We could, in principle, remedy this by making a slightly different (but more complex) choice of $D(k)$, and we do not anticipate that it should cause any significant change in our results.

Having determined the discretized PS $P_d(k)$ we can use, as described above, the HNC equation (8.20) to determine the required potential. Given the characteristics of the CDM-like PS, we expect a potential which will be attractive at small scales. To ensure equilibrium of the system we add by hand a repulsive core to the potential. We have chosen a core of the form $v_c(r) = 0.2a^{10}/r^{12}$. Using the direct HNC method it is necessary to check that this doesn't modify substantially the original PS. Once this procedure has been performed, a simulation of molecular dynamics with this potential can be performed to obtain configurations of points with the PS desired. Note that the HNC equation give us the potential times the temperature $\beta v(r)$. We choose an arbitrary temperature and we give appropriate initial velocities in the MD to obtain the desired equilibrium temperature. We use the simple choice $\beta = 1$ in our units.

In Fig. 8.4 are shown the different correlation functions and the resulting interaction potential. First of all note that for $r/a > 5$ the potential is $1/r^2$ corresponding, as described above, to the small k-like PS. This behavior comes from the long-range part of the direct correlation function $c_l(r)$ (which is not

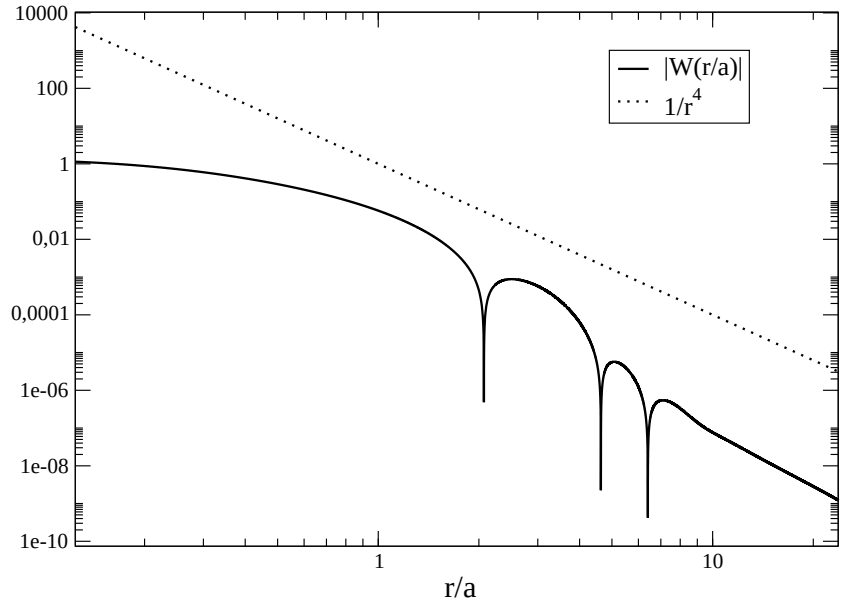

Figure 8.3: The window function in real space $|W_{k_d,n_0}(r)|$.

shown in the figure). For large scales, up to $r \approx 2.2a$, the system is uncorrelated while it becomes correlated for smaller scales. At approximately this scale the potential starts to be attractive to produce such correlation. The scale where the continuous correlation function and the discretized one start to deviate corresponds to k_d^{-1}. At very small scales the potential is dominated by the repulsive core introduced by hand.

In Fig. 8.5 and Fig. 8.6 are shown the results for molecular dynamics simulations with the potential given above.

8.3.3 CDM-type spectra: realistic model

We consider finally the determination of the potential which should reproduce the cosmological PS (4.106), with the parameters of a currently standard cosmological simulation (e.g. like that taken as initial condition in the simulations of the VIRGO consortium [J$^+$98], see Eq. (4.106)). To do so we must choose, in units of physical length, the scale a characterizing the desired discretization. For our example, we choose this scale by supposing we have the same physical density of point n_0 as in some typical simulations of the VIRGO consortium: we suppose that we have the particle density corresponding to 256^3 particles in a cubic box of side 239.5h^{-1}Mpc. The gives $a \approx 0.58$h^{-1}Mpc. We take our initial time to correspond to red-shift $z = 50$, and fix the normalization of the model at this by the prescription that, using the extrapolation of linear theory, one obtain today (at $z = 0$) $\sigma_8 = 1$. This corresponds to a normalization such that $\sigma_8 = 1/(z+1) = 1/51$, and the normalization factor is then $\mathcal{N} = 29381(\mathrm{h}^{-1}\mathrm{Mpc})^4$. As in the previous section we work in units of the "ionic radius" $a \approx 0.58$h^{-1}Mpc. The discretization scale k_d introduced is chosen at

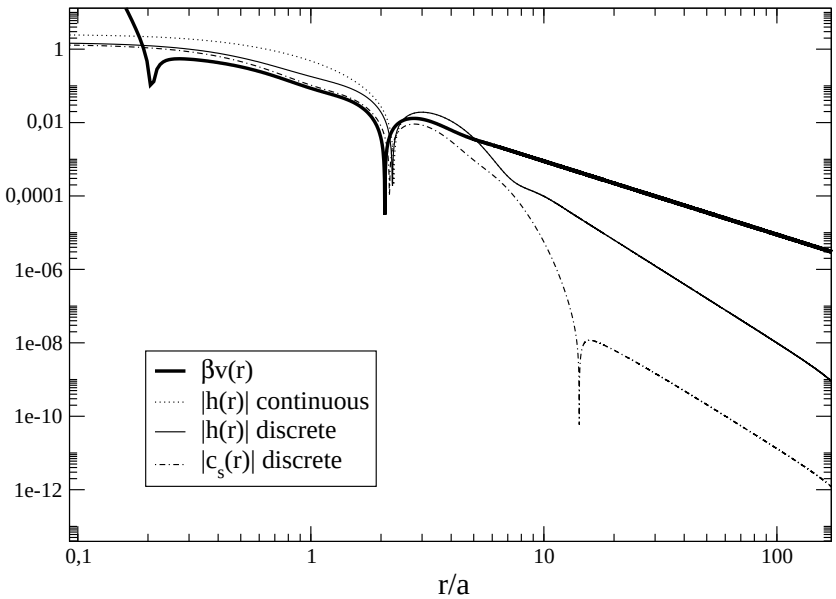

Figure 8.4: The correlation function, discretized correlation function, direct correlation function and interaction potential obtained by the inversion of the HNC for a PS as given in Eq.(8.32), with $\mathcal{N} = 10\,a^4$, $A \approx 69\,a$ $k_c = 2.7/a$ and $k_d = 1.55/a$.

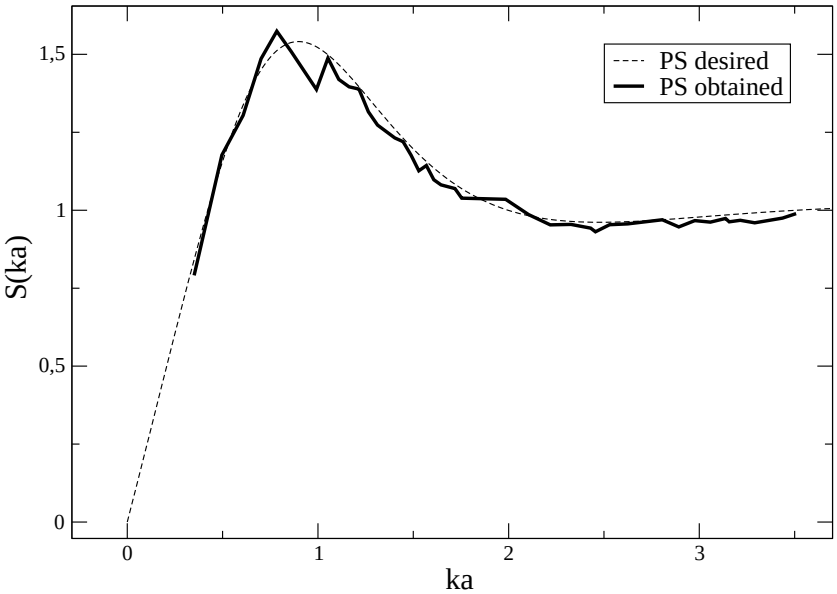

Figure 8.5: The PS measured in a simulation of the molecular dynamics of 1000 particles for the potential shown in the previous figure. Also shown is the input PS i.e. the PS of a system at equilibrium with this potential as calculated in the HNC.

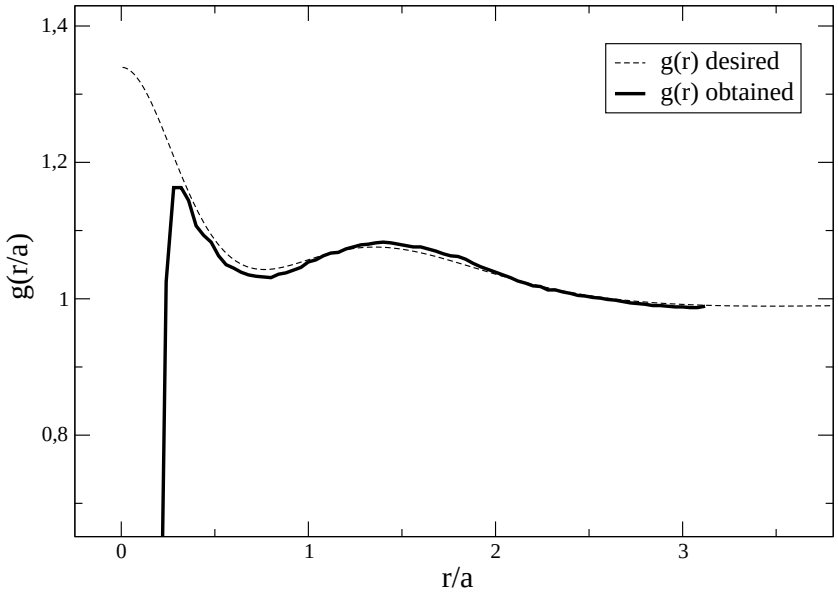

Figure 8.6: The real space correlation function for the same cases as in the previous figure. The abrupt break to anti-correlation below $r/a \approx 0.2$ comes from the hard core introduced to ensure stability of the system.

the bounding value $k_d \approx 1.55$. In Fig. 8.7 are shown the correlation functions and the potential for this case. We note the same $1/r^2$ behavior at large scales, but the potential is more complicated at small scales due to the oscillations in the direct correlation function $c(r)$. By simulating the molecular dynamics with this potential with a sufficiently large number of particles, as we have done for a smaller number of particles for the simpler cases, we should obtain a discretization of the model with the properties Eqs.(8.17) and (8.18).

8.4 Discussion and conclusions

We have presented a new method to generate discrete distributions with desired two-point correlation properties, which could be used in generating initial conditions for N-body simulation in cosmology. It provides a promising alternative to the standard method used in this context, which involves displacing particles in a prescribed manner off a perfect lattice (or, sometimes, "glassy" configuration). As discussed in detail in chapter 7 this method usually represents well the input theoretical PS in Fourier space at wave-numbers below the Nyquist frequency, but produces in real space a system with correlation properties which are a mixture of those of the initial unperturbed lattice configuration and those of the theoretical model. One obtains, in particular, a two-point correlation function which is a rapidly oscillating function up to very large separations, which is a behavior completely different to that of the theoretical model. With respect to this method the interest of this new method is thus that it can give (by construction) a faithful representation of the two-point statistical properties

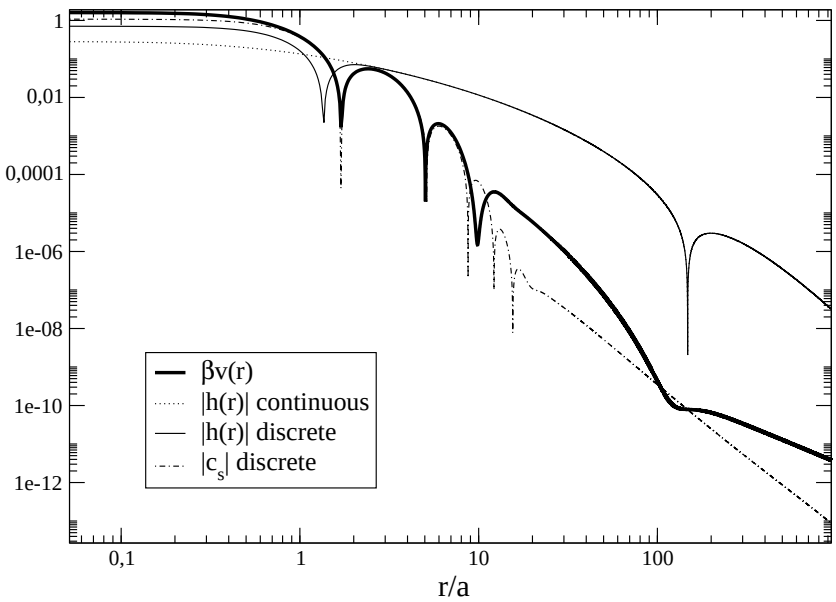

Figure 8.7: Correlation functions and interaction potential obtained for the cosmological CDM spectrum described in the text.

of a CDM-like spectrum in both real and Fourier space. In particular, in the examples we have considered, the correlation function in real space converges very well to the theoretical input correlation function at a scale $r_d \approx 2a$. Increasing the number of particles for the same physical size of the system, the interparticle distance a, and thus this scale, diminishes. In Fourier space the agreement is good (by construction) for wavenumbers less than roughly a factor of two smaller than the inverse of the scale a.

The method we have introduced and studied here (following the proposal of [G$^+$03a]) can be developed and improved in various respects. In particular we draw attention to the fact that we have used here a slow N^2 algorithm in the molecular dynamics (MD) simulations. To apply the method for generating IC for large N-body simulations it will be necessary to use a larger number of particles, and thus to use a faster MD algorithm. In particular particle-mesh methods, widely employed in cosmological N-body simulation, should make it possible to increase greatly the speed of the necessary molecular dynamical simulations (for the thermalization) so that the method can be used to generate much larger initial configurations than those considered here.

One other remark on a possible improvement concerns the choice of initial velocities in our simulations. When introducing the potential calculated with HNC we implicitly choose the equilibrium temperature before performing the MD simulation. Thus, as explained above, we put the initial velocities to get the chosen final temperature. The problem is that we do not know a priori how the system is going to reach equilibrium and it is necessary to do trials with different initial velocities until the desired equilibrium temperature is attained. A solution to this problem would be to modify the MD to work in the canonical

ensemble (in which the temperature is fixed) rather than in the micro-canonical ensemble as we have done here.

Chapter 9

Linearisation of the discrete cosmological N-body problem

We have discussed in section 5.7 that the main approach to understanding discreteness effects in N-body simulations is through numerical studies of convergence, i.e. one studies the stability of the results of simulations as a function of the number of particles in the system. We discussed also that there is no a rigorous understanding of the relation between the N-body method and the underlying fluid theory. This chapter provides a first step towards such rigorous understanding.

A standard way to generate initial conditions (IC) for N-body simulations consists in perturbing a lattice (see chapter 5.7). It is therefore natural to build a perturbative theory –in the same spirit of what we have done studying the initial conditions in chapter 7 – where the perturbed variable is the displacement of each particle about the lattice, which is an equilibrium position. We will therefore have an accurate description of the clustering when the displacements (or, in fact, the relative displacements) are smaller than the interparticle distance. This approach is indeed the discrete counterpart of the Lagrangian fluid theory (see section 5.5). We will show explicitly that the latter is obtained by taking the limit of an infinite number of particles. The essentially analytical treatment of both theories then permit us to understand exhaustively the discreteness effects in their range of validity.

The chapter is organized as follows. In the first section, we introduce the treatment for perturbations of a perfect lattice with gravitational interaction. We will do it at this stage, for simplicity, in a static Euclidean universe. It involves a set of $3N$ coupled differential equations. In the next section we see how it is possible to diagonalize simply this system of equations by exploiting the symmetries of the crystal. We note here that the formalism is totally analogous to the one used in the study in condensed matter physics of the vibrations in a crystal. Then we will study the spectrum of eigenvalues and its physical interpretation, and in particular the fluid limit. In the next section we will explain the modifications introduced by an expanding universe. The last three sections are essentially devoted, on one part, to the comparison of the linearisation with N-body simulations to understand its regime of validity, and on the other part, the comparison with fluid theory to quantify discreteness effects.

9.1 Linearization of gravity on a perturbed lattice

In this section we start by defining and studying some general properties of the gravitational potential and force of an infinite system of point particles. We then consider the particular case of a perturbed infinite lattice in a static Euclidean space, the generalization to an expanding universe being given in Sect. 9.3. Since the force is zero in the unperturbed lattice, the dominant contribution to the force in the perturbed case is linear in the relative displacements of the particles. In the last subsection, we consider the equations of motion resulting from this linearized force.

9.1.1 Definition of the force and the potential

Let us consider carefully first the definition of the gravitational force in an infinite system of point particles of equal mass m. We will assume that this system (either stochastic or deterministic) is characterized by a well defined mean number density $n_0 > 0$, and mass density $\rho_0 = mn_0$. The gravitational potential of a particle, per unit mass, at $\mathbf{r}$, due to the particles in a finite volume V, is:

$$\phi(\mathbf{r}) = -Gm \sum_{\mathbf{r}' \neq \mathbf{r}} \frac{1}{|\mathbf{r} - \mathbf{r}'|} \mathcal{V}(V, \mathbf{r}'), \tag{9.1}$$

where the sum is over all the particles contained in the system, and $\mathcal{V}(V, \mathbf{r})$ is the window function for the volume V, i.e.,

$$\mathcal{V}(V, \mathbf{r}) = \begin{cases} 1 & \text{if } \mathbf{r} \in V, \\ 0, & \text{otherwise.} \end{cases} \tag{9.2}$$

The force per unit of mass (i.e. the acceleration), due to these same particles, is given by the gradient of the potential:

$$\mathbf{F}(\mathbf{r}) = -\nabla \phi(\mathbf{r}). \tag{9.3}$$

Taking the infinite volume limit $V \to \infty$, neither the gravitational potential (9.1), nor the gravitational force (9.3), are well defined. In the first case the result diverges, while in the second it may be finite or infinite, but its value depends on how the limit is taken[1].

In Euclidean spacetime this behaviour in the infinite volume limit may be regulated by the introduction of a negative background — the so-called Jeans swindle (see e.g. [BT87, Kie99]) — so that the potential is defined as

$$\begin{aligned} \phi(\mathbf{r}) &= -G \lim_{V \to \infty} \left[m \sum_{\mathbf{r}' \neq \mathbf{r}} \frac{1}{|\mathbf{r} - \mathbf{r}'|} \mathcal{V}(V, \mathbf{r}') \right. \\ &\quad \left. -\rho_0 \int_{\mathbb{R}^3} d^3 r' \frac{1}{|\mathbf{r} - \mathbf{r}'|} \mathcal{V}(V, \mathbf{r}') \right]. \end{aligned} \tag{9.4}$$

This modifies the usual Poisson equation to

$$\nabla^2 \phi(\mathbf{r}) = 4\pi G(\rho(\mathbf{r}) - \rho_0). \tag{9.5}$$

[1] $\mathbf{F}(\mathbf{r})$ is a conditionally convergent series.

The expression (9.4) is well defined [2], provided (i) that the limit $V \to \infty$ is taken in a physically reasonable way [3], and (ii) that the fluctuations in the system are sufficiently rapidly decaying at large scales [4]. In the cosmological context this negative background appears naturally as a consequence of the expansion of the universe (see Sect. 9.3).

The simulations of self-gravitating systems we are interested in are performed using a *finite* cubic simulation box of side L and volume $V_B = L^3$, subject to periodic boundary conditions. The force on a particle is thus computed not only from all the other particles inside the simulation box, but also from all the copies of the particles contained in the "replicas". The reason for using these boundary conditions is that they introduce the inevitable finite size effects without breaking translational invariance: every particle can be considered to be at the centre of the finite box and therefore sees the boundary in the same way. The infinite system we consider is thus an infinite number of replicas of a finite cubic box, with a negative background as described above to make the force well defined [5]. In this case the gravitational potential may be written as

$$\phi(\mathbf{r}) = \lim_{V\to\infty} \left[\phi_b(\mathbf{r}) + \phi_p(\mathbf{r})\right], \tag{9.6}$$

where

$$\phi_b(\mathbf{r}) = G\rho_0 \int_{\mathbb{R}^3} d^3r' \frac{1}{|\mathbf{r}-\mathbf{r}'|}\mathcal{V}(V,\mathbf{r}') \tag{9.7}$$

is the contribution from the background, and

$$\phi_p(\mathbf{r}) = -Gm \sum_{\mathbf{n},\mathbf{r}'}^{*} \frac{\mathcal{V}(V,\mathbf{r}'+\mathbf{n}L)}{|\mathbf{r}-\mathbf{r}'-\mathbf{n}L|} \tag{9.8}$$

the contribution from the particles. Here the sum over $\mathbf{r}'$ is restricted to the particles in the box, while the other sum, over the three integers $\mathbf{n}$ (i.e. over the images of $\mathbf{r}'$), has a "*" to indicate that the term $\mathbf{r}' = \mathbf{r}$ is excluded when $\mathbf{n} = \mathbf{0}$.

The gravitational force is:

$$\mathbf{F}(\mathbf{r}) = \lim_{V\to\infty} \left[\mathbf{F}_b(\mathbf{r}) + \mathbf{F}_p(\mathbf{r})\right], \tag{9.9}$$

where

$$\mathbf{F}_b(\mathbf{r}) = G\rho_0 \int_{\mathbb{R}^3} d^3r' \frac{\mathbf{r}-\mathbf{r}'}{|\mathbf{r}-\mathbf{r}'|^3}\mathcal{V}(V,\mathbf{r}') \tag{9.10}$$

and

$$\mathbf{F}_p(\mathbf{r}) = -Gm \sum_{\mathbf{n},\mathbf{r}'}^{*} \frac{\mathbf{r}-\mathbf{r}'-\mathbf{n}L}{|\mathbf{r}-\mathbf{r}'-\mathbf{n}L|^3}\mathcal{V}(V,\mathbf{r}'+\mathbf{n}L). \tag{9.11}$$

[2] For a more detailed discussion of the gravitational force in infinite systems see also [G+06].

[3] E.g., taking the infinite volume limit in compact sets.

[4] If $P(k)$ is the power spectrum of density fluctuations, it is simple to show, using the modified Poisson equation Eq. (9.5), that convergence of the fluctuations in the gravitational potential requires $\lim_{k\to 0} k^n P(k) = 0$ for $n > 1$. For finite fluctuations in the force one requires $n > -1$.

[5] Note also that, because the system is just a lattice when considered at scales larger than the box size, the fluctuations are always sufficiently suppressed at large scales so that the gravitational force is well defined. Thus any possible divergence in the fluctuations of force will be regulated by the box size L.

Note that the contribution from the background (9.10) is identically zero if one takes a window function with inversion symmetry in $\mathbf{r}$ (e.g. a sphere or cube centred on $\mathbf{r}$).

9.1.2 Linearization of the gravitational force

We consider the infinite lattice generated by the replication of a sc lattice of volume V_B of side L with N elements, i.e., whose lattice vectors are $\mathbf{R} = (m_1, m_2, m_3)\ell$ with $m_i \in [0, N^{1/3} - 1] \cap \mathbb{N}$ and $\ell = L/N^{1/3}$ is the lattice spacing[6]. This lattice (with a particle at each site) is now perturbed by applying displacements $\mathbf{u}(\mathbf{R})$ to each particle $\mathbf{R}$, so that the new positions of the particles can be written as

$$\mathbf{r} = \mathbf{R} + \mathbf{u}(\mathbf{R}). \tag{9.12}$$

The "particle" term in the gravitational force [i.e. Eq. (9.11)] can then be expanded order by order in Taylor series about its value in the unperturbed lattice. At linear order in the relative displacements $\mathbf{u}(\mathbf{R}) - \mathbf{u}(\mathbf{R}')$ we obtain

$$\begin{aligned}\mathbf{F}_p(\mathbf{r}) \quad = \quad & -Gm \sum_{\mathbf{n},\mathbf{R}'}^{*} \left\{ \frac{\mathbf{R} - \mathbf{R}' + \mathbf{n}L}{|\mathbf{R} - \mathbf{R}' + \mathbf{n}L|^3} + \frac{\mathbf{u}(\mathbf{R}) - \mathbf{u}(\mathbf{R}')}{|\mathbf{R} - \mathbf{R}' + \mathbf{n}L|^3} \right. \\ & \left. -3 \, \frac{[\mathbf{u}(\mathbf{R}) - \mathbf{u}(\mathbf{R}')] \cdot [\mathbf{R} - \mathbf{R}' + \mathbf{n}L]}{|\mathbf{R} - \mathbf{R}' + \mathbf{n}L|^5} (\mathbf{R} - \mathbf{R}' + \mathbf{n}L) \right\} \\ & \times \mathcal{V}(V, \mathbf{R}' + \mathbf{n}L). \end{aligned} \tag{9.13}$$

The first term in this sum

$$- Gm \sum_{\mathbf{n},\mathbf{R}'}^{*} \frac{\mathbf{R} - \mathbf{R}' + \mathbf{n}L}{|\mathbf{R} - \mathbf{R}' + \mathbf{n}L|^3} \mathcal{V}(V, \mathbf{R}' + \mathbf{n}L) \tag{9.14}$$

has the poor infinite volume behaviour which is regulated, as discussed above, by the contribution coming from the background Eq. (9.10). The total linearized force is then also well defined, and given by the infinite volume limit of Eq. (9.13) summed with Eq. (9.10). In the case that we choose to calculate using the infinite volume limit of a volume V with inversion symmetry in $\mathbf{r}$ (i.e. the displaced position of the particle), the full linearized force is thus given by Eq. (9.13). If, however, we choose to sum in a volume with inversion symmetry *in the lattice site* $\mathbf{R}$, it is simple to show that Eq. (9.14) is identically zero. The background term then contributes, with the sum [(9.10) + (9.14)] remaining invariant.

The convergence criterion for *each* term of (9.13) is

$$|\mathbf{R} - \mathbf{R}'| > |\mathbf{u}(\mathbf{R}) - \mathbf{u}(\mathbf{R}')|. \tag{9.15}$$

Note that the validity of the power expansion does not depend on the displacement of the particle $\mathbf{R}$ on which we compute the force, but on *relative* displacements of the particles at the position $\mathbf{R}$ and $\mathbf{R}'$. Under the action of the gravitational interaction, the displacements $\mathbf{u}(\mathbf{R})$ will typically grow so that the condition Eq. (9.15) is violated after some time. However when some pairs

[6] The generalization of all the calculations presented here to any *Bravais* lattice is straightforward (see e.g. [AM76]).

of particles no longer satisfy condition (9.15), it may nevertheless continue to apply for the rest of the particles and (9.13) may remain a sufficiently good approximation to the force. In order to have a precise characterization of the regime of validity of the approximation applied to follow the dynamical evolution of a perturbed lattice, it is necessary to compare the results with those obtained from evolution under full gravity. We will perform such a comparison in Sect. 9.5 using N-body simulations.

It is convenient to write the linearized force just discussed in terms of the so-called *dynamical matrix* $\mathcal{D}(\mathbf{R})$ (see e.g. [Zim72, AM76]):

$$\mathbf{F}(\mathbf{r}) = \sum_{\mathbf{R}'} \mathcal{D}(\mathbf{R} - \mathbf{R}')\mathbf{u}(\mathbf{R}'). \tag{9.16}$$

This matrix has the following properties: it is a complete symmetric operator, i.e., $\mathcal{D}_{\mu\nu}(\mathbf{R}) = \mathcal{D}_{\nu\mu}(-\mathbf{R})$ with inversion symmetry, i.e., $\mathcal{D}_{\mu\nu}(\mathbf{R}) = \mathcal{D}_{\mu\nu}(-\mathbf{R})$. Further, since the same displacement applied to all the particles produces no net force, we have $\sum_{\mathbf{R}} \mathcal{D}_{\mu\nu}(\mathbf{R}) = 0$. For any pair interaction potential $v(\mathbf{r})$ it is straighforward to show that it can be written as [Zim72, AM76]

$$\mathcal{D}_{\mu\nu}(\mathbf{R} \neq \mathbf{0}) = \partial_\mu \partial_\nu w(\mathbf{R}) \tag{9.17a}$$

$$\mathcal{D}_{\mu\nu}(\mathbf{R} = \mathbf{0}) = -\sum_{\mathbf{R}' \neq 0} \partial_\mu \partial_\nu w(\mathbf{R}') \tag{9.17b}$$

where

$$\partial_\mu \partial_\nu w(\mathbf{r}_0) = \left[\frac{\partial^2 w(\mathbf{r})}{\partial r_\mu \partial r_\nu}\right]_{\mathbf{r}=\mathbf{r}_0} \tag{9.18}$$

and $w(\mathbf{r})$ is the periodic function defined as

$$w(\mathbf{r}) = \sum_{\mathbf{n}} v(\mathbf{r} + \mathbf{n}L), \tag{9.19}$$

i.e., the potential due to a single particle and all its copies. For gravity we have $v(\mathbf{r}) = -Gm/r$ and Eq. (9.19) is implicitly understood to be regulated as discussed at length above by the addition of a uniform negative background. We will describe below, and in App. F, how we use the well-known Ewald summation technique to explicitly perform this sum.

Equation (9.17b) gives the force on a particle, at first order in the displacements, when it is displaced and all the others remain unperturbed (see Fig. 9.1). For gravity it is straightforward [G$^+$06] to show that

$$\mathcal{D}_{\mu\nu}(\mathbf{0}) = \frac{4\pi}{3} G\rho_0 \delta_{\mu\nu}, \tag{9.20}$$

i.e., the linearized force $\mathbf{f}_s(\mathbf{r})$ on a particle due only to its own displacement $\mathbf{u}$ with respect to the rest of the lattice is

$$\mathbf{f}_s(\mathbf{r}) = \frac{4\pi}{3} G\rho_0 \mathbf{u}(\mathbf{R}). \tag{9.21}$$

The simplest way to derive this result is by summing the force in spheres centred on the *unperturbed* position of the displaced particle. In this case it is straighforward to show, by symmetry, that the linearized direct particle contribution Eq. (9.13) is zero and the full force is given by the background term Eq. (9.10). The result follows then simply from Gauss' law which gives that the force comes only from the region inside the sphere shown in Fig. 9.1.

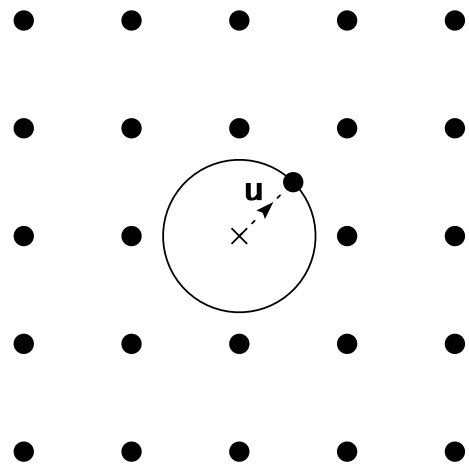

Figure 9.1: Computation of the diagonal terms of the dynamical matrix at $\mathbf{R} = \mathbf{0}$.

9.1.3 Equations of motion in a static Euclidean universe

In this section we derive the equations of motion of the particles in the linear approximation, and then solve them. We treat first a static Euclidean space, giving the generalization to a cosmological expanding universe in Sect. 9.3.

Using Newton's second law and Eqs. (9.12) and (9.16) we can write the equation of motion of the particles as:

$$\ddot{\mathbf{u}}(\mathbf{R}, t) = \sum_{\mathbf{R}'} \mathcal{D}(\mathbf{R} - \mathbf{R}')\mathbf{u}(\mathbf{R}', t), \tag{9.22}$$

where the double dot denotes a double derivative with respect to time. The expression (9.22) is a system of vectorial coupled second order differential equations which can be reduced to an eigenvalue problem, using standard techniques. From Bloch's theorem [AM76] it follows that Eq. (9.22) can be diagonalized by the following combination of plane waves:

$$\mathbf{u}(\mathbf{R}, t) = \frac{1}{N} \sum_{\mathbf{k}} \tilde{\mathbf{u}}(\mathbf{k}, t) e^{i\mathbf{k}\cdot\mathbf{R}}, \tag{9.23}$$

where the sum over $\mathbf{k}$ is restricted to the *first Brillouin zone*, i.e., for a sc lattice to

$$\mathbf{k} = \frac{2\pi}{L}\mathbf{n}, \tag{9.24}$$

with $\mathbf{n} = (n_1, n_2, n_3)$ such that $n_i \in [-N/2, N/2[\cap\mathbb{Z}$. We denote by $\tilde{\mathbf{u}}(\mathbf{k}, t)$ the Fourier transform of $\mathbf{u}(\mathbf{R}, t)$:

$$\tilde{\mathbf{u}}(\mathbf{k}, t) = \sum_{\mathbf{R}} \mathbf{u}(\mathbf{R}, t) e^{-i\mathbf{k}\cdot\mathbf{R}}, \tag{9.25}$$

where the sum is restricted to the simulation box (i.e. without considering the replicas). Inserting Eq. (9.23) in Eq. (9.22), we obtain for each $\mathbf{k}$:

$$\ddot{\tilde{\mathbf{u}}}(\mathbf{k}, t) = \tilde{\mathcal{D}}(\mathbf{k})\mathbf{u}(\mathbf{k}, t), \tag{9.26}$$

where $\tilde{\mathcal{D}}(\mathbf{k})$ is the FT of $\mathcal{D}(\mathbf{R})$, defined analogously to (9.25). From the properties of $\mathcal{D}(\mathbf{R})$ given above, it follows that $\tilde{\mathcal{D}}(\mathbf{k})$ is a real and symmetric operator which satisfies [7]

$$\lim_{\mathbf{k}\to 0} \tilde{\mathcal{D}}_{\mu\nu}(\mathbf{k}) = \frac{4\pi}{3} G\rho_0 \delta_{\mu\nu}. \tag{9.27}$$

We can now solve Eq. (9.26) by diagonalizing the 3×3 matrix $\tilde{\mathcal{D}}(\mathbf{k})$. For each $\mathbf{k}$, this determines three orthonormal eigenvectors $\hat{\mathbf{e}}_n(\mathbf{k})$ with three associated eigenvalues $\omega_n^2(\mathbf{k})$ $(n = 1, 2, 3)$ satisfying the eigenvalue equation:

$$\tilde{\mathcal{D}}(\mathbf{k})\hat{\mathbf{e}}_n(\mathbf{k}) = \omega_n^2(\mathbf{k})\hat{\mathbf{e}}_n(\mathbf{k}). \tag{9.28}$$

We can decompose each mode $\tilde{\mathbf{u}}(\mathbf{k}, t)$ in the basis $\{\hat{\mathbf{e}}_n(\mathbf{k})\}$ as

$$\tilde{\mathbf{u}}(\mathbf{k}, t) = \sum_{n=1}^{3} \hat{\mathbf{e}}_n(\mathbf{k}) f_n(\mathbf{k}, t). \tag{9.29}$$

Using Eqs. (9.26), (9.28) and (9.29) we get the following equation for the coefficients $f_n(\mathbf{k}, t)$:

$$\ddot{f}_n(\mathbf{k}, t) = \omega_n^2(\mathbf{k}) f_n(\mathbf{k}, t). \tag{9.30}$$

Depending on the sign of $\omega_n^2(\mathbf{k})$, we obtain two classes of solutions $U_n(\mathbf{k}, t)$ and $V_n(\mathbf{k}, t)$. We choose them, without any loss of generality, satisfying

$$U_n(\mathbf{k}, t_0) = 1, \qquad \dot{U}_n(\mathbf{k}, t_0) = 0, \tag{9.31a}$$

$$V_n(\mathbf{k}, t_0) = 0, \qquad \dot{V}_n(\mathbf{k}, t_0) = 1. \tag{9.31b}$$

The function $U_n(\mathbf{k}, t)$ is associated with initial displacements and $V_n(\mathbf{k}, t)$ with initial velocities. If $\omega_n^2(\mathbf{k}) \geq 0$ then

$$U_n(\mathbf{k}, t) = \cosh(\omega_n(\mathbf{k})(t - t_0)), \tag{9.32a}$$

$$V_n(\mathbf{k}, t) = \sinh(\omega_n(\mathbf{k})(t - t_0))/\omega_n(\mathbf{k}). \tag{9.32b}$$

If $\omega_n^2(\mathbf{k}) < 0$

$$U_n(\mathbf{k}, t) = \cos(\sqrt{|\omega_n^2(\mathbf{k})|}(t - t_0)), \tag{9.33a}$$

$$V_n(\mathbf{k}, t) = \sin(\sqrt{|\omega_n^2(\mathbf{k})|}(t - t_0))/\sqrt{|\omega_n^2(\mathbf{k})|}. \tag{9.33b}$$

Whereas the modes (9.32) with positive eigenvalues cause an exponential growth of perturbation in the system, the modes (9.33) with negative eigenvalues leads to oscillations. The evolution of the displacement field from any initial state $\mathbf{u}(\mathbf{R}, t_0)$ is then given by the transformation

$$\mathbf{u}(\mathbf{R}, t) = \frac{1}{N} \sum_{\mathbf{k}} \left[\mathcal{P}(\mathbf{k}, t)\tilde{\mathbf{u}}(\mathbf{k}, t_0) + \mathcal{Q}(\mathbf{k}, t)\dot{\tilde{\mathbf{u}}}(\mathbf{k}, t_0) \right] e^{i\mathbf{k}\cdot\mathbf{R}} \tag{9.34}$$

where the matrix elements of the "evolution operators" $\mathcal{P}$ and $\mathcal{Q}$ are

$$\mathcal{P}_{\mu\nu}(\mathbf{k}, t) = \sum_{n=1}^{3} U_n(\mathbf{k}, t)(\hat{\mathbf{e}}_n(\mathbf{k}))_\mu (\hat{\mathbf{e}}_n(\mathbf{k}))_\nu, \tag{9.35a}$$

$$\mathcal{Q}_{\mu\nu}(\mathbf{k}, t) = \sum_{n=1}^{3} V_n(\mathbf{k}, t)(\hat{\mathbf{e}}_n(\mathbf{k}))_\mu (\hat{\mathbf{e}}_n(\mathbf{k}))_\nu. \tag{9.35b}$$

The operator $\mathcal{P}$ thus evolves the initial displacement field and $\mathcal{Q}$ the initial velocity field.

[7] But note that $\tilde{\mathcal{D}}_{\mu\nu}(\mathbf{k} = 0) = \sum_{\mathbf{R}} \mathcal{D}_{\mu\nu}(\mathbf{R}) = 0$, i.e., $\tilde{\mathcal{D}}(\mathbf{k})$ is discontinuous at $\mathbf{k} = \mathbf{0}$.

9.2 Determination and analysis of the spectrum of eigenvalues of $\tilde{\mathcal{D}}(\mathbf{k})$

In this section we describe the determination of the eigenvectors and spectrum of eigenvalues of the dynamical matrix for gravity. We then discuss the physical meaning of the results, notably identifying how the fluid limit is obtained and how corrections to this limit may be calculated. In this discussion we will use extensively the strict analogy between the case we are treating and the Coulomb lattice, or Wigner cystal, studied in condensed matter physics (see e.g. [Pin63]). This is a system of positively charged particles embedded in a negative neutralizing background. The particles interact with a repulsive $1/r$ potential instead of the attractive $-1/r$ potential of Newtonian gravity. Thus all our results are mapped onto those for the corresponding Coulomb lattice by making the formal substitution $Gm^2 \to -e^2$, where e is the electronic charge[8].

9.2.1 Numerical computation of the spectrum of $\tilde{\mathcal{D}}(\mathbf{k})$

The spectrum of the matrix $\tilde{\mathcal{D}}(\mathbf{k})$ must be computed numerically. The matrix $\mathcal{D}(\mathbf{R})$ is constructed using the Ewald sum method [Ewa21, Zim72, AM76, DLPS80] to speed up the convergence of the sum. We continue to work here explicitly, as above, with a sc lattice of side L, with lattice spacing ℓ and N elements[9]. To determine the dynamical matrix we use the Ewald method to evaluate $w(\mathbf{r})$ as given in Eq. (9.19), splitting it into two pieces using an appropriate damping function $\mathcal{C}$:

$$\begin{aligned} w(\mathbf{r}) = &\sum_{\mathbf{n}} v(\mathbf{r}+\mathbf{n}L)\mathcal{C}(|\mathbf{r}+\mathbf{n}L|,\alpha) \\ &+ \sum_{\mathbf{n}} v(\mathbf{r}+\mathbf{n}L)[1-\mathcal{C}(|\mathbf{r}+\mathbf{n}L|,\alpha)], \end{aligned} \tag{9.36}$$

where α is a arbitrary "damping parameter" of which the result is independant. The function $\mathcal{C}(|\mathbf{r}|,\alpha)$ is chosen to be equal to unity at $\mathbf{r} = \mathbf{0}$ and rapidly decaying to zero as $|\mathbf{r}|$ goes to infinity. The first sum is then evaluated in real space and the second one in Fourier space, making use of the Parseval theorem [NDW57], $\mathcal{C}$ being chosen so that the second term in Eq. (9.36) is analytic at $\mathbf{r} = \mathbf{0}$ and thus rapidly convergent in Fourier space. A common choice for a $1/r$ pair potential is

$$\mathcal{C}(|\mathbf{r}|,\alpha) = \mathrm{erfc}(\alpha|\mathbf{r}|). \tag{9.37}$$

The expression for the function w is then:

$$w(\mathbf{r}) = w^{(r)}(\mathbf{r}) + w^{(k)}(\mathbf{r}). \tag{9.38}$$

[8] The potential we have used here for gravity has been defined per unit mass, i.e., in our notation $v(\mathbf{r}) = e^2/mr$ for the Coulomb lattice.

[9] The generalization to a parallelepiped box, and to other Bravais lattices, is straightforward (see e.g. [AM76]).

In the gravitational case

$$w^{(r)}(\mathbf{r}) = -Gm \sum_{\mathbf{n}} \frac{1}{|\mathbf{r}+\mathbf{n}L|} \mathrm{erfc}(\alpha|\mathbf{r}+\mathbf{n}L|), \tag{9.39a}$$

$$w^{(k)}(\mathbf{r}) = -Gm \frac{4\pi}{V_B} \sum_{\mathbf{k}\neq\mathbf{0}} \frac{1}{|\mathbf{k}|^2} \exp\left(-\frac{|\mathbf{k}|^2}{4\alpha^2}\right) \cos\left[\mathbf{k}\cdot\mathbf{r}\right], \tag{9.39b}$$

where V_B is the volume of the box and the wavevectors $\mathbf{k}$ are as in Eq. (9.24), but with $\mathbf{n}$ ranging over all triple integers (i.e. not restricted to the first Brillouin zone). There is no $\mathbf{k}=\mathbf{0}$ term in the sum (9.39) because of the presence of the negative background: when summed over all the particles, this term is equal to

$$\lim_{\mathbf{k}\to 0} \tilde{\phi}_0(\mathbf{k}) = -\lim_{\mathbf{k}\to 0} \frac{4\pi G\rho_0}{k^2}, \tag{9.40}$$

i.e., the $\mathbf{k}=\mathbf{0}$ mode of the potential (calculated from the Poisson equation in Fourier space) which is cancelled by the contribution coming from the negative background.

The Ewald sum for the dynamical matrix can then be calculated directly using Eq. (9.17) and (9.39). The result, as in Eq. (9.38), is divided in two parts:

$$\mathcal{D}(\mathbf{R}) = \mathcal{D}^{(r)}(\mathbf{R}) + \mathcal{D}^{(k)}(\mathbf{R}), \tag{9.41}$$

for which the explicit expressions are given in App. F.

For the results quoted here we have taken $\alpha = 2/L$ [HBS91]. Using this numerical value of α, it is sufficient to sum for

$$|\mathbf{n}| \leq 3 \qquad |\mathbf{k}| \leq \frac{6\pi}{L}. \tag{9.42}$$

to obtain a well converged determination of the dynamical matrix. The diagonalization calculation involves essentially N operations (where N is the number of particles). It is perfectly feasible, with modest computer resources, to perform this diagonalisation for particle numbers as large as those used in the largest current N-body simulations.

9.2.2 Analysis of the spectrum of eigenvalues in a simple cubic lattice

We now describe the spectrum of eigenvalues of the dynamical matrix $\mathcal{D}(\mathbf{R})$ for a sc lattice. As we have discussed in the introduction, this is the lattice which is used very widely in N-body simulations of structure formation in cosmology.

In Fig. 9.2 we plot the spectrum of a sc lattice, for $N = 16^3$, obtained with the method outlined in the previous subsection. We show the normalized eigenvalues

$$\varepsilon_n(\mathbf{k}) = \frac{\omega_n^2(\mathbf{k})}{4\pi G\rho_0} \tag{9.43}$$

as a function of the modulus of the $\mathbf{k}$ vectors, normalized to the Nyquist frequency $k_N = \pi/\ell$. With this normalisation the spectrum remains substantially the same as we increase the number of particles: the only change is that the eigenvalues become denser in the plot, filling out the approximate functional

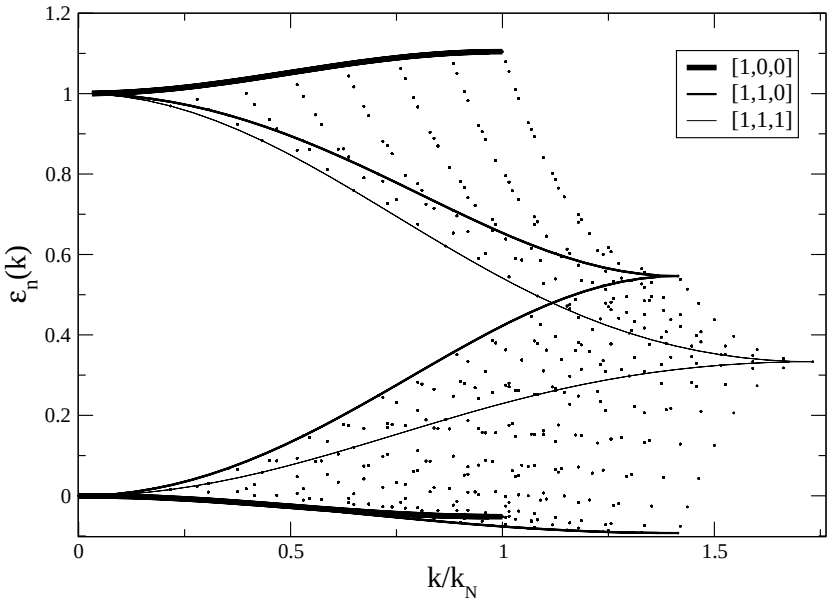

Figure 9.2: Spectrum of eigenvalues for simple cubic lattice with 16^3 particles. The lines correspond to chosen directions in k space.

behaviours with more points. For our discussion here there is no interest in considering a greater number of points than that we have chosen.

For each vector $\mathbf{k}$ there are three eigenvalues $\omega_n^2(\mathbf{k})$, $n = 1, 2, 3$. Each family of eigenvalues (i.e. with same n) defines a surface, corresponding to the three branches of the frequency-wavevector dispersion relation. Sections of these surfaces are plotted for some chosen directions of the vector $\mathbf{k}$ in Fig. 9.2.

An expression for $\tilde{\mathcal{D}}(\mathbf{k})$ and the Kohn sum rule

Before proceeding further it is useful to derive some important results we will employ much in what follows. These are well known in the context of the application of this formalism in condensed matter physics (see e.g. [Pin63]). First of all, we derive an analytical expression for the dynamical matrix in Fourier space. Let us decompose in Fourier modes the function $w(\mathbf{r})$ defined in Eq. (9.19)

$$w(\mathbf{r}) = \frac{1}{V_B} \sum_{\mathbf{k}} \tilde{w}(\mathbf{k}) e^{i\mathbf{k}\cdot\mathbf{r}}, \tag{9.44}$$

where the sum over $\mathbf{k}$ is performed over *all* k space, i.e., not restricted to the first Brillouin zone and

$$\tilde{w}(\mathbf{k}) = \int_{V_B} d^3r\, w(\mathbf{r}) e^{-i\mathbf{k}\cdot\mathbf{r}}. \tag{9.45}$$

The derivatives of the periodic potential are

$$w_{\mu\nu}(\mathbf{r}) = -\frac{1}{V_B} \sum_{\mathbf{k}} k_\mu k_\nu \tilde{w}(\mathbf{k}) e^{i\mathbf{k}\cdot\mathbf{r}}. \tag{9.46}$$

Using the definition of the dynamical matrix

$$\tilde{\mathcal{D}}_{\mu\nu}(\mathbf{k}) = \sum_{\mathbf{R}} \mathcal{D}_{\mu\nu}(\mathbf{R}) e^{-i\mathbf{k}\cdot\mathbf{R}} \tag{9.47}$$

and Eqs. (9.17) and (9.46) we obtain:

$$\tilde{\mathcal{D}}_{\mu\nu}(\mathbf{k}) = -\frac{1}{V_B} \sum_{\mathbf{k}',\mathbf{R}} k'_\mu k'_\nu \tilde{w}(\mathbf{k}') \left(e^{i\mathbf{R}\cdot(\mathbf{k}'-\mathbf{k})} - e^{i\mathbf{k}'\cdot\mathbf{R}} \right) \tag{9.48}$$

where we can include the term $\mathbf{R} = \mathbf{0}$ in the sum because it vanishes. Using the orthogonality relation, we have

$$\sum_{\mathbf{R}} e^{i(\mathbf{k}-\mathbf{k}')\cdot\mathbf{R}} = N \sum_{\mathbf{K}} \delta_{\mathbf{k}',\mathbf{k}+\mathbf{K}}, \tag{9.49}$$

where the $\mathbf{k}$ are restricted to the first Brillouin zone and $\mathbf{K}$ are the reciprocal vectors of $\mathbf{R}$ satisfying

$$\mathbf{K} = 2k_N \mathbf{m}, \tag{9.50}$$

with $\mathbf{m} \in \mathbb{Z}^3$. Substituting Eq. (9.49) in (9.48) we obtain finally the expression [Pin63]:

$$\begin{aligned} \tilde{\mathcal{D}}_{\mu\nu}(\mathbf{k}) &= -n_0 k_\mu k_\nu \tilde{w}(\mathbf{k}) \\ &-n_0 \sum_{\mathbf{K}\neq\mathbf{0}} \left[(k_\mu + K_\mu)(k_\nu + K_\nu) \tilde{w}(\mathbf{k}+\mathbf{K}) - K_\mu K_\nu \tilde{w}(\mathbf{K}) \right], \end{aligned} \tag{9.51}$$

where n_0 is the number density of particles. In the gravitational case, the integral (9.45) cannot be evaluated analytically. However, neglecting finite size effects, this integral can be computed over the whole space and the periodic potential $w(\mathbf{r})$ is approximated by the interaction pair potential $v(\mathbf{r}) = -Gm/r$, so that

$$\tilde{w}(\mathbf{k}) \simeq \tilde{v}(\mathbf{k}) = \int_{\mathbb{R}^3} d^3r\, v(\mathbf{r}) e^{-i\mathbf{k}\cdot\mathbf{r}} = -\frac{4\pi G m}{k^2}. \tag{9.52}$$

Using this it is straightforward to show (see App. G) the following simple result:

$$\sum_{i=1}^{3} \omega_i^2(\mathbf{k}) = -n_0 k^2 \tilde{w}(\mathbf{k}) = 4\pi G \rho_0. \tag{9.53}$$

In the context of the Coulomb lattice this is a well-known result, the so-called *Kohn sum rule*. In this case the quantity which appears on the r.h.s. of the sum, instead of $4\pi G\rho_0$, is $-\omega_p^2 = -4\pi e^2 n_0/m$ where ω_p is the *plasma frequency*. We will discuss further below the significance of this analogy.

We can use these results and the above sum rule to compute — in a different way than in Eqs. (9.20)–(9.21) — the $\mathbf{R} = \mathbf{0}$ term of the dynamical matrix $\mathcal{D}(\mathbf{R})$ (i.e. the term giving the force on a particle, at linear order in the relative displacements, when it alone is perturbed off the lattice). Using the Kohn sum rule (9.53), the trace of the dynamical matrix is:

$$\mathrm{tr}[\mathcal{D}(\mathbf{R})] = 4\pi G \rho_0. \tag{9.54}$$

If the crystal has three equivalent orthogonal directions then the diagonal terms of the dynamical matrix will be equal. In the case of lattices with special

symmetries (like the sc, bcc and fcc) it is simple to show that when a single particle is displaced along the direction of an axis, the force acting on it is parallel to the direction of displacement [10]. This implies that the non-diagonal terms of the dynamical matrix are zero. We can therefore conclude that

$$\mathcal{D}_{\mu\nu}(\mathbf{0}) = \frac{4}{3}\pi G\rho_0\delta_{\mu\nu}. \tag{9.55}$$

The branches of the dispersion relation and the fluid limit

We have noted that the spectrum of eigenvalues has a clear branch structure. To identify the different branches it is useful to consider the $\mathbf{k} \to \mathbf{0}$ limit keeping the interparticle distance ℓ constant. We expect this to correspond to the fluid limit: a plane wave fluctuation $e^{i\mathbf{k}\cdot\mathbf{r}}$ with $\mathbf{k} \ll 1/\ell$ has a variation scale much larger than the interparticle distance, and therefore does not "see" the particles.

From Eq. (9.51) the limit for $\mathbf{k} \to \mathbf{0}$ is straightforward as the contribution of the sum on the r.h.s. vanishes in this limit [11]

$$\lim_{\mathbf{k}\to\mathbf{0}} \tilde{\mathcal{D}}_{\mu\nu}(\mathbf{k}) = -n_0\hat{k}_\mu\hat{k}_\nu\tilde{w}(\mathbf{k}). \tag{9.56}$$

Using the eigenvalue equation (9.28) with Eqs. (9.51) and (9.52), it follows that the solutions in the fluid limit are

1. one *longitudinal* eigenvector polarized parallel to $\mathbf{k}$ with normalized eigenvalue $\varepsilon_1(\mathbf{k} \to \mathbf{0}) = 1$ and

2. two *transverse* eigenvectors polarized in the plane transverse to $\mathbf{k}$ with normalized eigenvalues $\varepsilon_{2,3}(\mathbf{k} \to \mathbf{0}) = 0$.

As the spectrum of eigenvalues $\varepsilon_n(\mathbf{k})$ is exactly the same, up to an overall negative multiplicative constant, to that of the Coulomb lattice, we adapt the same terminology as in this context. The branch of eigenvalues whose associated eigenvectors converges to the longitudinal eigenvector as $\mathbf{k} \to \mathbf{0}$ is called the *optical* or longitudinal branch. The two other branches whose eigenvectors converge to the transverse eigenvectors are called the *acoustic* branches. For finite k, the eigenvectors are not exactly parallel or perpendicular to $\hat{\mathbf{k}}$ for all $\mathbf{k}$ but belong nevertheless to one of the three branches, which define three-dimensional hyper-surfaces in the four-dimensional space $(\omega, \mathbf{k})$ space.

The appearance of an optical branch in a monoatomic crystal is a characteristic feature of the $1/r$ interaction potential (at large r). In the case of a more rapidly decaying potential at large scales, i.e., $1/r^{1+\alpha}$ with $\alpha > 0$, it becomes a third acoustic branch. In the case of a potential that decays slower at large r, i.e., $\alpha < 0$, the optical branch diverges as $\mathbf{k} \to \mathbf{0}$. The physical interpretation of the optical branch is that it represents the coherent excitation of the whole lattice with respect to the background [Cla57]. In a Coulomb crystal, the optical mode is produced by the lattice moving against this background producing a "plasma oscillation", at the plasma frequency ω_p defined above. This mode is, as we have just seen, purely longitudinal, i.e., the perturbations are parallel

[10] This can be explicitly shown e.g. using Eq. (F.2) (taking the limit $\alpha \to 0$ and assuming that the sum over the replicas converges).

[11] We have assumed that the sum in Eq. (9.51) is well defined — which is the case for the gravitational interaction — so that it is possible to take the limit before performing the sum.

to $\mathbf{k}$, while the tranverse modes, i.e., the perturbations orthogonal to $\mathbf{k}$ have zero frequency. The reason for this behaviour of long wavelength density fluctuations can be easily understood. The density fluctuations are related, in this fluid limit, to the displacements through the continuity equation:

$$\delta\rho \sim \nabla \cdot \mathbf{u}, \tag{9.57}$$

which implies in k space that

$$\delta\tilde{\rho} \sim \mathbf{k} \cdot \tilde{\mathbf{u}}. \tag{9.58}$$

Thus tranverse modes do not source density fluctuations, and therefore (by the Poisson equation) they do not produce a force. In the case of gravity, instead of oscillating as in a plasma, the longitudinal mode may be amplified or attenuated (depending on the initial perturbation), in a way which is independent of k. As we will discuss in detail below, this is just the well known linear amplification of density fluctuations in a self-gravitating fluid.

Corrections to the fluid limit

We have just seen that the fluid limit is obtained by taking the dynamical matrix as

$$\tilde{\mathcal{D}}(\mathbf{k}) = \frac{4\pi G\rho_0}{k^2} k_\mu k_\nu. \tag{9.59}$$

We can estimate analytically the corrections to this limit for small k (i.e. for large wavelengths) by expanding the eigenvalues and eigenvectors of the full dynamical matrix about $\mathbf{k} = \mathbf{0}$. We note that this corresponds to calculating the difference, at large wavelengths, between the evolution of the perturbed lattice with a finite number of particles and that of the fluid limit. These are thus what are, in the context of cosmological simulations, "discreteness effects" introduced by the modelling of the fluid by such a system.

When expanding the dynamical matrix in Taylor series about the fluid limit $\mathbf{k} \to 0$, it is simple to show that for $1/r$ interactions this series is in even powers of k, because $\mathcal{D}(\mathbf{R})$ is real and $\tilde{\mathcal{D}}(\mathbf{k})$ analytic for $\mathbf{k} \to \mathbf{0}$ (see [Cla57, CHM60]). It is therefore possible to write the corrections to the eigenvalues of the optical mode as:

$$\omega_1^2(\mathbf{k}) \simeq 4\pi G\rho_0(1 - b_1(\hat{\mathbf{k}})k^2), \tag{9.60}$$

where the expression for $b_1(\hat{\mathbf{k}})$ can be computed by diagonalizing $\tilde{\mathcal{D}}(\mathbf{k})$ expanded up to $\mathcal{O}(k^2)$. The leading correction to the two acoustic modes may be written

$$\omega_2^2(\mathbf{k}) \simeq 2\pi G\rho_0 b_2(\hat{\mathbf{k}})k^2, \tag{9.61a}$$

$$\omega_3^2(\mathbf{k}) \simeq 2\pi G\rho_0 b_3(\hat{\mathbf{k}})k^2. \tag{9.61b}$$

The Kohn sum rule implies that $b_1(\hat{\mathbf{k}}) = (b_2(\hat{\mathbf{k}}) + b_3(\hat{\mathbf{k}}))/2$. In Fig. 9.3 we show the optical branch, in various different chosen directions. The approximation with the leading term in the Taylor expansion is very good up to the Nyquist frequency.

In Fig. 9.4 we show how the anisotropy of the eigenvalues increases as the modulus of the wave vector increases (i.e. when we look at smaller spatial scales). We plot, for three ranges of values of the modulus of $\mathbf{k}$, the value of the normalized eigenvalues as a function of the angle θ between $\mathbf{k}$ and the axis that

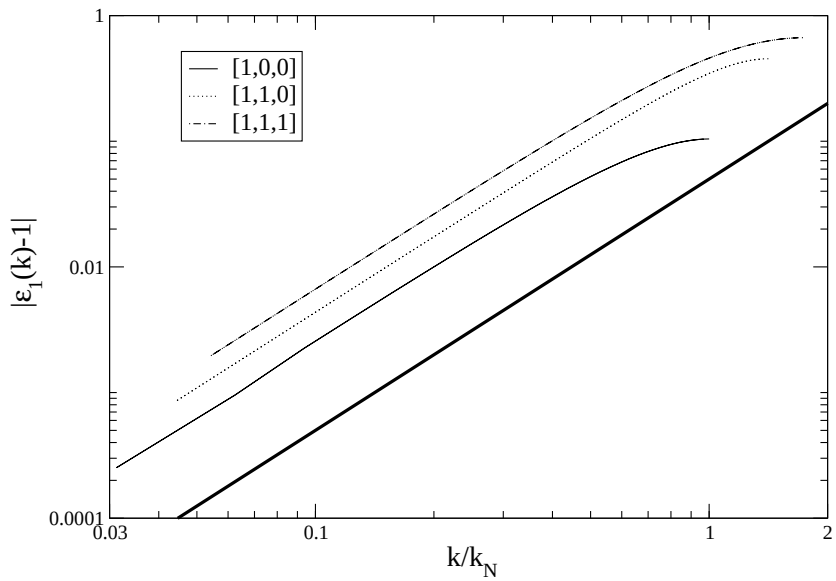

Figure 9.3: Optical branch for different directions of $\mathbf{k}$. The thick line is proportional to k^2.

forms a minimal angle with it. As θ increases (i.e. as $\cos\theta$ decreases with $0 < \theta < \pi/2$) there is a clear trend of decrease in the eigenvalue, in each of the three cases. The difference as a function of orientation of the vector $\mathbf{k}$ is, however, much more marked for larger k, i.e., at scales closer to the Nyquist frequency. This is not unexpected: the effects of anistropy (which is completely absent in the fluid limit, in which the eigenvalues are independent of the orientation $\mathbf{k}$) are naturally strongest for the short wavelength modes.

Oscillatory modes

The spectrum of the sc lattice Fig. 9.2 includes some modes [e.g. for $\mathbf{k} = (k_x, 0, 0)$] with eigenvalues on the optical branch *larger than the fluid limit.* For example, this is the case for modes with initial displacement $\mathbf{u}(\mathbf{r}, 0) \propto \hat{\mathbf{x}} \exp(ik_x x)$, shown in Fig. 9.5-*(i)*. Adjacent planes collapse towards one another, faster than in the fluid limit. The Kohn sum rule Eq. (9.53) states that the sum of the three eigenvalues $\omega_n^2(\mathbf{k})$ is equal to $4\pi G\rho_0$. Therefore, the existence of modes collapsing faster than the fluid limit implies that there are other modes with negative eigenvalues $\omega_n^2(\mathbf{k})$, i.e., which oscillate. This is the case, e.g., of the mode with initial displacement $\mathbf{u}(\mathbf{r}, 0) \sim \hat{\mathbf{y}} \exp(ik_x x)$, shown in the Fig. 9.5-*(ii)*. In this case, contiguous planes oscillate as indicated in the figure.

The existence of oscillating modes in a perturbed and cold *purely* self-gravitating system (i.e. without any additional interaction or velocity dispersion giving rise to a restoring pressure[12]) is an unexpected curiosity, a behaviour qualitatively different to that generically expected based on the analysis of the fluid limit. Translated to the analagous Coulomb system, the result means that

[12] If there is a non negligible velocity dispersion, it known that fluctuations at scales smaller than the Jeans length oscillate [BT87].

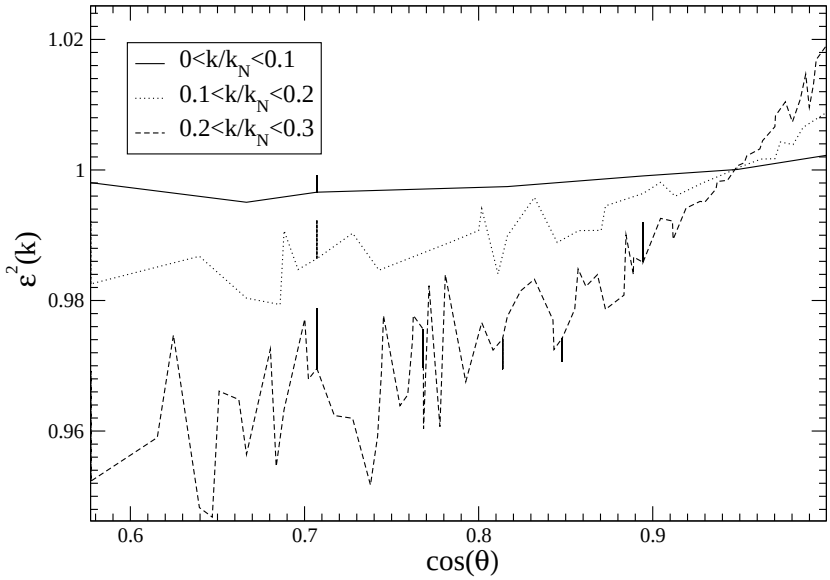

Figure 9.4: Variation of the value of the eigenvalues for various ranges as a function of the cosine of the angle between **k** and the axes of the lattice which forms a minimal angle with it. We see that the effects of anisotropy are strongest for the short-wavelength modes, and decrease as we go towards the fluid limit.

a sc lattice is, in this case, unstable (as there are growing modes). While this result has not apparently been shown in the literature, it is not an unexpected result in this context. It has been established [Fuc35, Car61] that for the (classical) Coulomb lattice that the ground state is the bcc lattice. It has a lower binding energy than the fcc lattice, which in turn is a lower energy configuration than the sc lattice. Our result implies that the latter is not only a higher energy state, but that it is strictly unstable. Indeed we note that the specific modes we have considered above describe a "sliding" of adjacent places in an sc lattice which deform it towards the lower energy configuration represented by the fcc lattice.

9.3 Generalization to an expanding universe

In the previous section, we have described the gravitational evolution of a perturbed lattice in a static Euclidean universe. In the cosmological context, density fluctuations are a perturbation around an homogeneous and isotropic Friedmann-Robertson-Walker (FRW) solution of Einstein's field equations of general relativity. In cosmological N-body simulations, since the regions studied are smaller than the Hubble radius and the velocities are non-relativistic, one considers the limit in which the equations of motion of the particles are strictly Newtonian in physical coordinates **r** [Pee80]. These coordinates are related to the comoving coordinates **x** of the FRW solution by

$$\mathbf{r}(t) = a(t)\mathbf{x}(t), \tag{9.62}$$

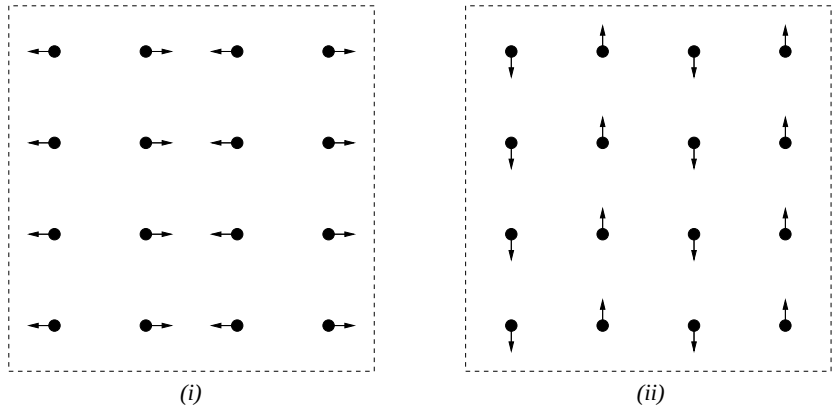

Figure 9.5: Schematic representation of *(i)* a mode collapsing faster than fluid limit and *(ii)* an oscillating mode.

where $a(t)$ is the scale factor describing the expansion of the universe. It satisfies the Friedmann equation

$$\left(\frac{\dot{a}}{a}\right)^2 = \frac{8\pi G}{3}\rho - \frac{\kappa}{a^2}, \tag{9.63}$$

where ρ is the mass density of the universe and κ the curvature. In the unperturbed FRW model the particles are fixed in comoving coordinates, all deviation from these positions arising from perturbations to this model. For this reason it is very natural, and convenient, to work in comoving coordinates. We therefore start by transforming our previous Newtonian equations to these coordinates, the only further difference being that we perturb about a time-dependent solution describing an expanding FRW universe.

Using Eq. (9.62) the acceleration can be written

$$\ddot{\mathbf{r}} = a\ddot{\mathbf{x}} + 2\dot{a}\dot{\mathbf{x}} + \ddot{a}\mathbf{x}. \tag{9.64}$$

The term $\ddot{a}\mathbf{x}$ can be expressed as the background contribution of the gravitational acceleration. For the specific case of an Einstein de Sitter (EdS) Universe, i.e., a universe containing only matter without curvature $[\rho(t) = \rho_0(a(t)/a(t_0))^3$ and $\kappa = 0]$, it is given by

$$\mathbf{g}_0 = \ddot{a}\mathbf{x} = \frac{4\pi}{3a^3}G\rho_0\mathbf{x}, \tag{9.65}$$

which has exactly the same form (for $a = 1$) as the contribution of the negative background of Eq. (9.20). We now write the position of a particle in comoving coordinates in terms of the displacement $\mathbf{u}$ about the lattice position as

$$\mathbf{x}(t) = \mathbf{R} + \mathbf{u}(\mathbf{R}, t). \tag{9.66}$$

The vector $\mathbf{R}$ is now the position of the lattice sites in *comoving coordinates* (i.e. $\mathbf{R}$ does not depend on time) and $\mathbf{u}(\mathbf{R}, t)$ is the displacement of the particle that was originally at $\mathbf{R}$ (in fluid theory, this is a *Lagrangian coordinate*, see e.g.

[Buc92]). By using Eq. (9.64), we can write Eq. (9.22) in an expanding universe as

$$\ddot{\mathbf{u}}(\mathbf{R},t) = -2\frac{\dot{a}}{a}\dot{\mathbf{u}}(\mathbf{R},t) + \frac{1}{a^3}\sum_{\mathbf{R}'}^{N}\mathcal{D}(\mathbf{R}-\mathbf{R}')\mathbf{u}(\mathbf{R}',t), \tag{9.67}$$

where we have implicitly included the background term (9.65) in the dynamical matrix. We emphasize that *the dynamical matrix is identical to that in the static case*: it depends only on the kind of lattice and on the interaction, but not on the dynamics of the background. Therefore all the analysis of this matrix performed in the preceeding section is valid also in this case. From Eq. (9.67), the mode equation (9.30) generalizes simply to

$$\ddot{f}_n(\mathbf{k},t) + 2\frac{\dot{a}}{a}\dot{f}_n(\mathbf{k},t) = \frac{\omega_n^2(\mathbf{k})}{a^3}f_n(\mathbf{k},t). \tag{9.68}$$

This is very similar to the equation of the evolution of a fluid in Lagrangian coordinates [Buc92]. The difference is only in the factor $\omega_n^2(\mathbf{k})$ on the r.h.s., which in the fluid limit is replaced by $4\pi G\rho_0$.

9.3.1 Solution in an Einstein–De Sitter universe

We derive now the solution of the mode equation (9.68) in the case of an EdS universe. The evolution of the scale factor is, from Eq. (9.63):

$$a(t) = \left(\frac{t}{t_0}\right)^{2/3}, \qquad 6\pi G\rho_0 t_0^2 = 1, \tag{9.69}$$

assuming that $a(0) = 0$. Then the mode coefficient equation (9.68) is

$$\ddot{f}_n(\mathbf{k},t) + \frac{4}{3t}\dot{f}_n(\mathbf{k},t) = \frac{2}{3t^2}\varepsilon_n(\mathbf{k})f_n(\mathbf{k},t), \tag{9.70}$$

where we have used again the adimensional quantity $\varepsilon_n(\mathbf{k})$ defined in Eq. (9.43). A set of independent solutions of (9.70) which satisfies the IC (9.31) are:

$$U_n(\mathbf{k},t) = \tilde{\alpha}(\mathbf{k})\left[\alpha_n^+(\mathbf{k})\left(\frac{t}{t_0}\right)^{\alpha_n^-(\mathbf{k})} + \alpha_n^-(\mathbf{k})\left(\frac{t}{t_0}\right)^{-\alpha_n^+(\mathbf{k})}\right], \tag{9.71a}$$

$$V_n(\mathbf{k},t) = \tilde{\alpha}(\mathbf{k})t_0\left[\left(\frac{t}{t_0}\right)^{\alpha_n^-(\mathbf{k})} - \left(\frac{t}{t_0}\right)^{-\alpha_n^+(\mathbf{k})}\right] \tag{9.71b}$$

where

$$\tilde{\alpha}(\mathbf{k}) = \frac{1}{\alpha_n^-(\mathbf{k}) + \alpha_n^+(\mathbf{k})} \tag{9.72}$$

and

$$\alpha_n^-(\mathbf{k}) = \frac{1}{6}\left[\sqrt{1+24\varepsilon_n(\mathbf{k})} - 1\right], \tag{9.73a}$$

$$\alpha_n^+(\mathbf{k}) = \frac{1}{6}\left[\sqrt{1+24\varepsilon_n(\mathbf{k})} + 1\right]. \tag{9.73b}$$

If $\varepsilon_n(\mathbf{k}) > 0$ the solution presents a power-law amplification mode and a power-law decaying mode. If $-1/24 < \varepsilon_n(\mathbf{k}) < 0$, there are two decaying modes. Finally, if $\varepsilon_n(\mathbf{k}) \leq -1/24$, the solution is oscillatory and can be written as

$$U_n(\mathbf{k},t) = \left(\frac{t}{t_0}\right)^{-\frac{1}{6}} \cos\left[\gamma_n(\mathbf{k}) \ln\left(\frac{t}{t_0}\right)\right] + \frac{1}{6\gamma_n(\mathbf{k})}\left(\frac{t}{t_0}\right)^{-\frac{1}{6}} \sin\left[\gamma_n(\mathbf{k}) \ln\left(\frac{t}{t_0}\right)\right], \tag{9.74a}$$

$$V_n(\mathbf{k},t) = \frac{t_0}{\gamma_n(\mathbf{k})}\left(\frac{t}{t_0}\right)^{-\frac{1}{6}} \sin\left[\gamma_n(\mathbf{k}) \ln\left(\frac{t}{t_0}\right)\right] \tag{9.74b}$$

where

$$\gamma_n(\mathbf{k}) = \frac{1}{6}\sqrt{|24\varepsilon_n(\mathbf{k}) + 1|}, \tag{9.75}$$

i.e., the static oscillatory behavior of the static universe survives, but now the oscillation is periodic in the logarithm of time with decreasing amplitude. The evolution of the displacements is computed with Eq. (9.34). The effect of the expansion [through the "viscous" first term of the r.h.s. of Eq. (9.67)] is to slow down the growing and decaying mode of the non-expanding exponential solution into a power-law solution.

9.3.2 Fluid limit and Zeldovich approximation

Let us calculate the fluid limit of the solution given by Eqs. (9.34), (9.35) and (9.71). As explained in Sect. 9.2 this corresponds to taking the limit $\mathbf{k} \to 0$ at fixed ℓ of the dynamical matrix $\tilde{\mathcal{D}}(\mathbf{k})$. In this case, as we have seen in Sect. 9.2 one of the eigenvectors is parallel to $\hat{\mathbf{k}}$, with eigenvalue $4\pi G\rho_0$, and the other two are normal to $\hat{\mathbf{k}}$ with eigenvalue equal to zero. We have then:

$$\hat{\mathbf{e}}_1(\mathbf{k}) = \hat{\mathbf{k}},\ \varepsilon_1(\mathbf{k}) = 1 \longrightarrow \alpha_1^+ = 2/3,\ \alpha_1^- = 1, \tag{9.76a}$$

$$\hat{\mathbf{e}}_2(\mathbf{k}) = \hat{\mathbf{k}}_{2\perp},\ \varepsilon_2(\mathbf{k}) = 0 \longrightarrow \alpha_2^+ = 0,\ \alpha_2^- = 1/3, \tag{9.76b}$$

$$\hat{\mathbf{e}}_3(\mathbf{k}) = \hat{\mathbf{k}}_{3\perp},\ \varepsilon_3(\mathbf{k}) = 0 \longrightarrow \alpha_3^+ = 0,\ \alpha_3^- = 1/3, \tag{9.76c}$$

where $\hat{\mathbf{k}}_{2\perp}$ and $\hat{\mathbf{k}}_{3\perp}$ are orthogonal to $\hat{\mathbf{k}}$ chosen so that $\hat{\mathbf{k}}_{2\perp} \cdot \hat{\mathbf{k}}_{3\perp} = 0$. Using (9.76) in (9.71), we get for the mode parallel to $\hat{\mathbf{k}}$:

$$U_1(\mathbf{k},t) \equiv U_\parallel(t) = \frac{2}{5}\left[\frac{3}{2}\left(\frac{t}{t_0}\right)^{2/3} + \left(\frac{t}{t_0}\right)^{-1}\right], \tag{9.77a}$$

$$V_1(\mathbf{k},t) \equiv V_\parallel(t) = \frac{3}{5}t_0\left[\left(\frac{t}{t_0}\right)^{2/3} - \left(\frac{t}{t_0}\right)^{-1}\right] \tag{9.77b}$$

and for the modes perpendicular to $\hat{\mathbf{k}}$:

$$U_2(\mathbf{k},t) = U_3(\mathbf{k},t) \equiv U_\perp(t) = 1, \tag{9.78a}$$

$$V_2(\mathbf{k},t) = V_3(\mathbf{k},t) \equiv V_\perp(t) = 3t_0\left[1 - \left(\frac{t}{t_0}\right)^{-1/3}\right]. \tag{9.78b}$$

The evolution operators (9.35) are then:

$$\mathcal{P}_{\mu\nu}(\mathbf{k},t) = U_{\parallel}(t)\hat{k}_\mu\hat{k}_\nu \ + (\hat{\mathbf{k}}_{2\perp})_\mu(\hat{\mathbf{k}}_{2\perp})_\nu + (\hat{\mathbf{k}}_{3\perp})_\mu(\hat{\mathbf{k}}_{3\perp})_\nu, \tag{9.79a}$$

$$\begin{aligned}\mathcal{Q}_{\mu\nu}(\mathbf{k},t) &= V_{\parallel}(t)\hat{k}_\mu\hat{k}_\nu + \\ &+ V_{\perp}(t)\left[(\hat{\mathbf{k}}_{2\perp})_\mu(\hat{\mathbf{k}}_{2\perp})_\nu + (\hat{\mathbf{k}}_{3\perp})_\mu(\hat{\mathbf{k}}_{3\perp})_\nu\right],\end{aligned} \tag{9.79b}$$

[where we have used explicitly that $U_\perp(t) = 1$]. Using Eq. (9.34) we write the evolution of the displacements in the fluid limit as:

$$\begin{aligned}\mathbf{u}(\mathbf{R},t) &= \mathbf{u}_\perp(\mathbf{R},t_0) + \mathbf{u}_\parallel(\mathbf{R},t_0)U_\parallel(t) \\ &\quad + \mathbf{v}_\parallel(\mathbf{R},t_0)V_\parallel(t) + \mathbf{v}_\perp(\mathbf{R},t_0)V_\perp(t),\end{aligned} \tag{9.80}$$

where

$$\mathbf{u}_\parallel(\mathbf{R},t_0) = \frac{1}{N}\sum_{\mathbf{k}}(\tilde{\mathbf{u}}(\mathbf{k},t_0)\cdot\hat{\mathbf{k}})\hat{\mathbf{k}}\, e^{i\mathbf{k}\cdot\mathbf{R}}, \tag{9.81a}$$

$$\mathbf{u}_\perp(\mathbf{R},t_0) = \frac{1}{N}\sum_{\mathbf{k}}(\tilde{\mathbf{u}}(\mathbf{k},t_0) - (\tilde{\mathbf{u}}(\mathbf{k},t_0)\cdot\hat{\mathbf{k}})\hat{\mathbf{k}})\, e^{i\mathbf{k}\cdot\mathbf{R}}, \tag{9.81b}$$

and analogously for the velocities $\mathbf{v}$. Using the definition of peculiar gravitational acceleration $\mathbf{g}$ (4.60)

$$\mathbf{g} = \ddot{\mathbf{r}} - \ddot{a}\mathbf{x} = \ddot{\mathbf{r}} - \frac{\ddot{a}}{a}\mathbf{r} = a\left[\ddot{\mathbf{u}} + 2\frac{\dot{a}}{a}\dot{\mathbf{u}}\right], \tag{9.82}$$

we can rewrite Eq. (9.80) [with Eqs. (9.77) and (9.78)] as:

$$\begin{aligned}\mathbf{u}(\mathbf{R},t) &= \mathbf{u}_\perp(\mathbf{R},t_0) \\ &+ \mathbf{g}(\mathbf{R},t_0)t_0^2\left[\frac{9}{10}\left(\frac{t}{t_0}\right)^{2/3} + \frac{3}{5}\left(\frac{t}{t_0}\right)^{-1}\right] \\ &+ \mathbf{v}_\parallel(\mathbf{R},t_0)\frac{3}{5}t_0\left[\left(\frac{t}{t_0}\right)^{2/3} - \left(\frac{t}{t_0}\right)^{-1}\right] \\ &+ \mathbf{v}_\perp(\mathbf{R},t_0)3t_0\left[1 - \left(\frac{t}{t_0}\right)^{-1/3}\right],\end{aligned} \tag{9.83}$$

where $\mathbf{v}$ is the peculiar velocity defined as

$$\mathbf{v}(\mathbf{x},t) = \dot{\mathbf{r}} - \frac{\dot{a}}{a}\mathbf{r} = \dot{\mathbf{r}} - \dot{a}\mathbf{x}. \tag{9.84}$$

The formula (9.83) corresponds precisely to the one (5.83) obtained at leading order in the displacements in the Lagrangian theory of a presureless perfect fluid in an EdS universe.

9.4 Evolution of statistical quantities

In section 9.3 we have computed the evolution of the position $\mathbf{u}(\mathbf{R})$ of each particle. In practice, in cosmology, we are mostly interested in the evolution

of statistical quantities, such as the correlation function or the PS. The PS of displacements is defined as

$$P_D(\mathbf{k},t) = \frac{1}{N}|\tilde{\mathbf{u}}(\mathbf{k},t)\cdot\tilde{\mathbf{u}}(-\mathbf{k},t)|, \tag{9.85}$$

and the correlation function of displacements as

$$\xi_D(\mathbf{R},t) = \langle \mathbf{u}(\mathbf{0})\cdot\mathbf{u}(\mathbf{R})\rangle = \frac{1}{N}\sum_{\mathbf{k}} P_D(\mathbf{k},t)e^{i\mathbf{k}\cdot\mathbf{R}}, \tag{9.86}$$

where in the last step of Eq. (9.86) we have assumed statistical homogeneity. We anticipate that the perturbative treatment we have developed will break down when the *relative* displacements of nearby particles becomes of the order of the lattice spacing ℓ. Therefore a useful quantity to define is the *correlation function of relative displacement of particles at a separation* $\mathbf{R}$:

$$\zeta_D(\mathbf{R},t) = \frac{1}{4}\langle(\mathbf{u}(\mathbf{0})-\mathbf{u}(\mathbf{R}))\cdot(\mathbf{u}(\mathbf{0})-\mathbf{u}(\mathbf{R}))\rangle = \xi_D(0,t)-\xi_D(\mathbf{R},t). \tag{9.87}$$

We expect the that the linear approximation will break down when

$$\zeta_D(\ell,t) \sim \frac{\ell^2}{4}. \tag{9.88}$$

As discussed in section (5.7.2), the standard method to set up initial conditions is using the Zeldovich approximation, i.e. Eqs. (5.86). In this case, using Eq. (9.34), the evolution can be simply written as

$$\mathbf{u}(\mathbf{R},t) = \frac{1}{N}\sum_{\mathbf{k}} \mathcal{A}(\mathbf{k},t)\tilde{\mathbf{u}}(\mathbf{k},t_0)e^{i\mathbf{k}\cdot\mathbf{R}}, \tag{9.89}$$

where

$$\mathcal{A}_{\mu\nu}(\mathbf{k},t) = \mathcal{P}_{\mu\nu}(\mathbf{k},t) + \frac{2}{3t_0}\mathcal{Q}_{\mu\nu}(\mathbf{k},t). \tag{9.90}$$

The evolution of the PS of displacements can be computed inserting Eq. (9.90) in Eq. (9.85). Once the PS of displacements is known it is possible to compute the PS of density fluctuations using the formalism described in chapter 3. However, in the perturbative regime the displacements are small and therefore the naive approximation explained in 3.3.1 is very good. In this approximation the density fluctuations can be approximated by Eq. (3.56). From this expression it follows that

$$P(\mathbf{k},t) = A_P^2(\mathbf{k},t)P(\mathbf{k},t_0), \tag{9.91}$$

where $P(\mathbf{k},t_0)$ is the initial PS of density fluctuations and

$$A_P(\mathbf{k},t) = \sum_{\mu,\nu}\hat{k}_\mu\hat{k}_\nu\mathcal{A}_{\mu\nu}(\mathbf{k},t). \tag{9.92}$$

In the next section we will use this approximation.

9.5 Comparison with N-body simulations

In this section, we compare the linear fluid evolution, the linearized N-body linear evolution and the full gravity N-body evolution. We will consider a shuffled lattice as initial conditions, in a static Euclidean universe. As explained in section (3.77), this is a lattice to which are applied random uncorrelated displacements with uniform probability in a cubic box about each point. As we have seen in chapter 4, these are not realistic initial conditions for cosmology. However, it is a simple starting point to study the physics of gravitational clustering in general (and the discreteness effects in particular). In terms of the PS of the displacement field, the shuffled lattice corresponds to white noise, i.e. equal power in all modes.

We are going to compare *three* different evolutions of the N body system:

1. *Fluid linear evolution* (hereafter FLE): the N-body particles of the shuffled lattice are considered as the "fluid elements" of a fluid theory. The evolution of their position is computed using *Lagrangian fluid theory* at linear order with Eq. (9.83).

2. *N-body linear evolution* (hereafter NBLE): the position of the particles is computed with the formalism developed in this chapter (precisely with Eq. (9.34)).

3. *N-body full evolution* (hereafter NBFE): we use[13] an N-body simulation to compute the evolution of the system under full gravity. We have used the GADGET code, a "tree" based code (see chapter 5). We can safely consider, at the resolution we are interested, in that its results are "exact". We use this simulation for two purposes: to determine the regime of validity of the NBLE and to evaluate its accuracy in comparison with that of FLE.

9.5.1 The system and initial conditions

We consider a system of $N = 16^3$ particles. The initial conditions are a shuffled lattice whose 1-point PDF is given by Eq. (3.77). The initial variance of shuffling is 0.001ℓ. The initial velocity of the particles is zero. The boundary conditions are periodic. We choose a time long enough to observe a discrepancy between NBLE and NBFE, i.e. up to the time when non-linear effects are important and NBLE breaks down. We have chosen units of time in which the dynamical time is[14]:

$$\tau_{dyn} = \frac{1}{\sqrt{4\pi G\rho_0}} = 1092. \tag{9.93}$$

9.5.2 The variance of displacements

To understand better what follows it is useful to start by comparing the evolution of the variance of relative displacements $\zeta_D(\ell, t)$ of the three systems of

[13] These simulations have been performed by Thierry Baertschiger.

[14] This corresponds to the dynamical time in seconds of a system with a density of $1\mathrm{g/cm}^3$.

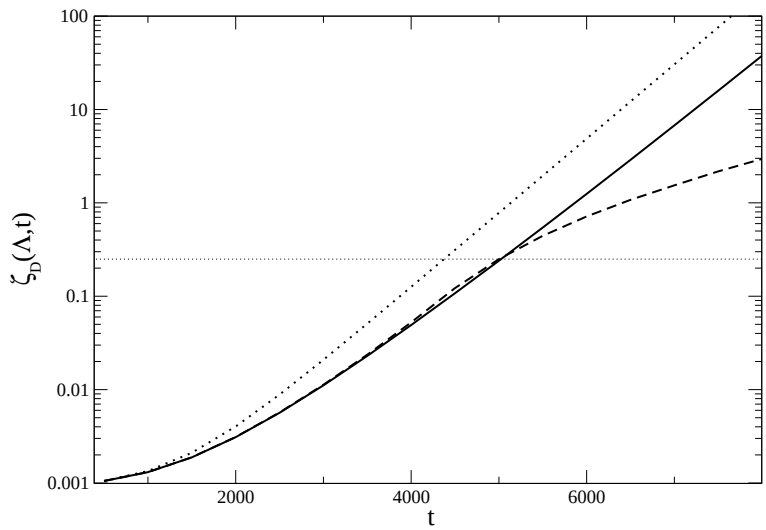

Figure 9.6: Comparison of the evolution of the variance of relative displacements of particles that were initially nearest neighbours, for a shuffled lattice with initial variance of displacements $0.001/\ell$. The solid line is the NBLE, the dashed one NBFE and the dotted one FLE. The thin horizontal line corresponds to $\zeta_D(\ell) = \ell^2/4$.

particles at the scale of the initial interparticle distance ℓ. The variance of the FLE can be simply computed from Eqs. (9.34), (9.85), (9.86) and (9.94) to give

$$\zeta_D(\ell, t) = \cosh^2\left(\sqrt{4\pi G\rho_0}t\right)\zeta_D(\ell, 0), \tag{9.94}$$

where we have taken $t_0 = 0$. This evolution is shown in Fig. 9.6. Note that the scale is log-linear. The case of the NBLE is more complicated, as it is a sum of cosh functions with different eigenvalues $\omega(\mathbf{k})$. However, it is in fact well approximated by a single expression like (9.94) but with an effective eigenvalue smaller than $4\pi G\rho_0$. This is because most of the eigenvalues are smaller than $4\pi G\rho_0$, see Fig. 9.2. We expect, however, that at very large times the eigenvalues larger than the fluid limit will dominate, leading to an evolution faster than that of the fluid (we will see that is indeed the case in section 9.6). Finally, we see clearly the time in which the NBFE diverges from the NBLE. This occurs approximately when the relative variance is (c.f. Eq. (9.87))

$$\zeta_D(\ell, t) \simeq \frac{1}{4}\ell^2. \tag{9.95}$$

It corresponds to an "average shell-crossing" as anticipated.

9.5.3 Comparison of the motion of a single particle

An evident check of the NBLE approximation is to compare the evolution of the position and velocity of a single particle with the same particle in NBFE. We perform this comparison of the evolution of the position of a particle randomly

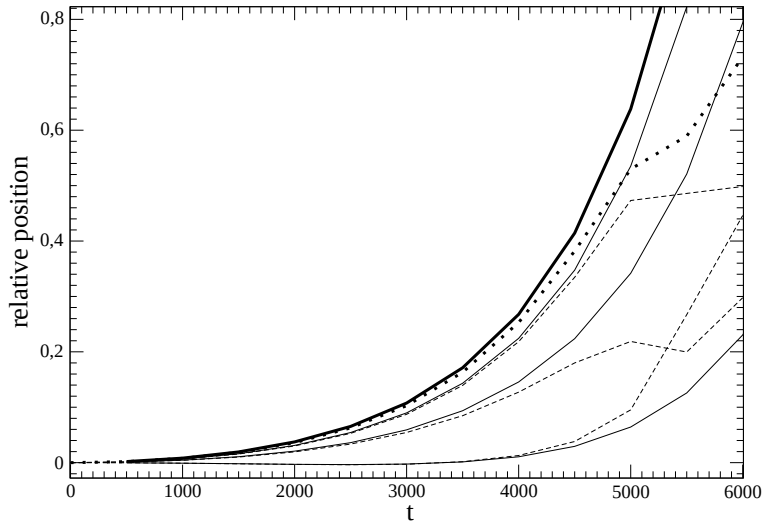

Figure 9.7: Each direction (x, y, z) of displacements of the chosen particle about its initial position. The system is a shuffled lattice with initial variance of displacements $0.001/\ell$. The solid line is the NBLE, the dashed one NBFE and the dotted one FLE. The thick lines corresponds to the modulus of displacements about the initial position for NBLE (solid line) and NBFE (dotted line).

chosen in Fig. 9.7. We see that the agreement is very good up to a little before the "average shell-crossing" computed in section 9.5.2.

We show alsothe evolution of the components of the velocity of the same particle in Fig.9.8, from which we draw the same conclusions.

9.5.4 Evolution of the PS and the correlation function

The comparison of the evolution of the PS and the correlation give similar results. Let us center our attention first on the PS (Fig. 9.9). The different set of curves correspond to different times (with the amplitude increasing as a function of time). At the initial time there is, of course, agreement between the three systems. Then, at $t \approx 2000$ the FLE and the NBLE start to differ at small scales, which is coherent with the variance of displacements given by Fig. 9.6. At $t \approx 6000$ the NBLE and NBFE differ also, which is also compatible with the evolution of the variance.

The correlation function (Fig. 9.10.) is noisier because from $x/L \approx 0.3$ it oscillates around zero. However, it can be seen that, for the selected times, there is a poor agreement between FLE and the other evolutions and a disagreement between the NBLE and NBFE for $t \approx 6000$. This is coherent with all the previous plots.

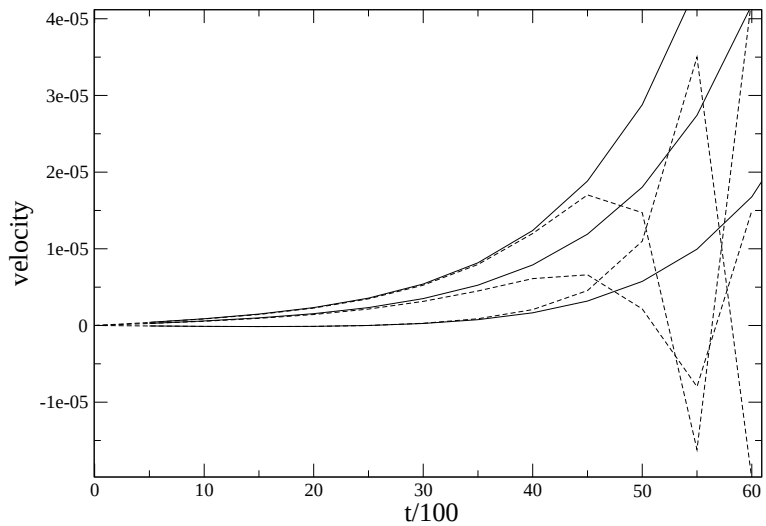

Figure 9.8: Each direction (x, y, z) of velocity of the particles about their initial position for the linearisation (full thin lines) and N-body simulation (thin dotted lines).

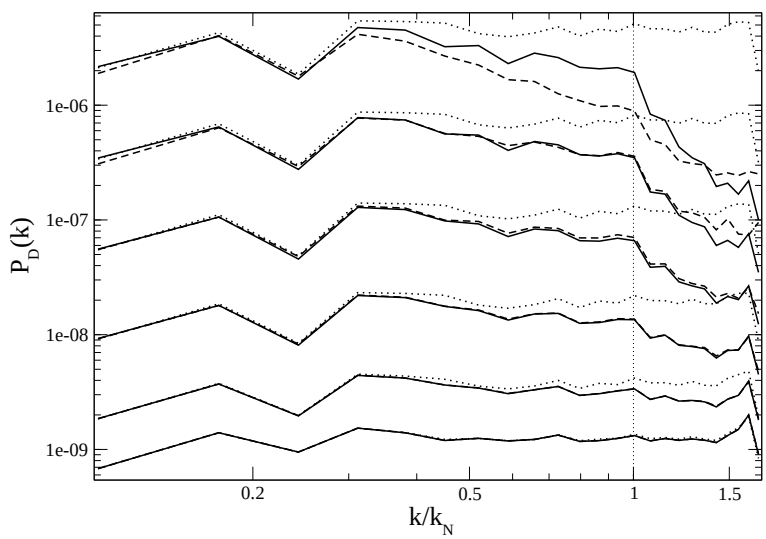

Figure 9.9: Comparison of the evolution of the power spectrum of displacements of a shuffled lattice with initial variance of displacements $0.001/\ell$. The solid lines are the NBLE, the dashed ones NBFE and the dotted ones FLE. The PS are ordered in increasing time from down to up with times from $t = 0$ to $t = 6000$ with increments of $\Delta t = 1000$. The vertical line shows the Nyquist frequency.

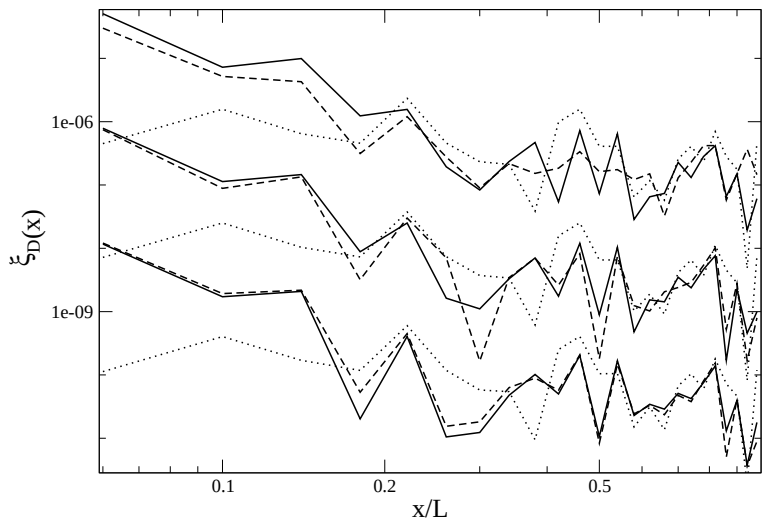

Figure 9.10: Comparison of the evolution of the correlation function in real space of displacements of a shuffled lattice with initial variance of displacements $0.001/\ell$. The solid lines are the NBLE, the dashed ones NBFE and the dotted ones FLE, for $t = 4000$, $t = 5000$ and $t = 6000$.

9.6 Discreteness effects

In this section we study more systematically the discreteness effects in the linear regime.

9.6.1 Parametrisation of the discreteness

In this section we derive the corrections to the fluid evolution due to the discreteness in the evolution of the PS. Given an initial PS, its evolution is given by formulae (9.91) and (9.92). The expression (9.92) is dominated by the optical branch, since the more rapidly growing modes are on this branch. Denoting by $\hat{\mathbf{e}}_1(\mathbf{k})$ the eigenmode corresponding to this branch, we thus have for sufficiently large times:

$$A_P^2(\mathbf{k},t) \simeq \left[U_1(\mathbf{k},t) + \frac{2}{3t_0}V_1(\mathbf{k},t)\right]^2 (\hat{\mathbf{e}}_1(\mathbf{k})\cdot\hat{\mathbf{k}})^2. \tag{9.96}$$

Using this expression with the Eq. (9.60), for the corrections to the eigenvalues on the optical branch, and Eqs. (9.71) we get:

$$A_P^2(\mathbf{k},t) \simeq a^{2+3b(\mathbf{k})k^2/5}, \tag{9.97}$$

where we have neglected terms of order higher than k^2 (and also a prefactor $\sim [1 + b(\mathbf{k})k^2]$). Discreteness in Fourier space can be quantified sucintly by the deviation from the fluid limit of the amplification factor, i.e. by a function defined as

$$D_{A_P}(\mathbf{k},t) = \frac{A_P^2(\mathbf{k},t)}{a^2(t)} = a^{3b(\mathbf{k})k^2/5} \tag{9.98}$$

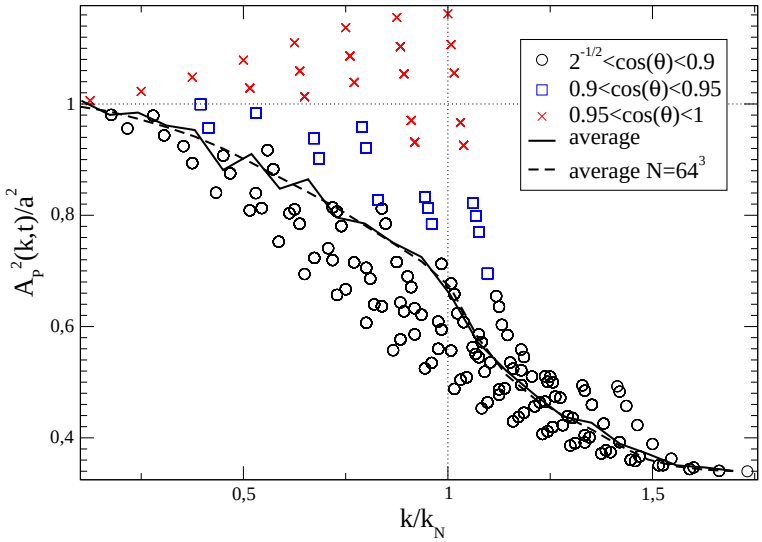

Figure 9.11: Amplification function $A^2(\mathbf{k},t)$ divided by the fluid amplification factor at $a = 5$, for a sc lattice.

In the absence of discreteness effects (i.e. in FLT) $D_{A_P}(\mathbf{k},t) = 1$ (with $a(t_0) = 1$). This function is shown Fig. 9.11. We have chosen a value of $a = 5$ for the scale factor. This is a typical scale factor at which shell crossing occurs in cosmological simulations. Notice the similarity of this figure with the optical branch in Fig. 9.2: the evolution "deforms" the spectrum of eigenvalues through Eq. (9.97). Note how the eigenvalues with $\epsilon > 1$ give rise to $D_{A_P}(\mathbf{k},t) > 1$ for these modes. In the figure, we have classified the modes as a function of the angle subtended by their wave vector $\mathbf{k}$ with the lattice axis that form the minimal angle with it. We see that there is a strong dependence of the value of the eigenvalue on this angle: the closer $\mathbf{k}$ is to parallel to one of the axes, the larger is the eigenvalue of the mode, on average. This is a manifestation of the breaking of isotropy introducing by the N-body discretisation on the lattice.

Even if there are some modes that grow faster than the fluid, averaging over bins with similar $|\mathbf{k}|$ the resultant growth is slower –because we consider sufficiently early times – than the fluid limit. Note that this averaging is generally performed when computing the PS (Eq. (9.91), for example).

If the system is evolved for sufficiently long time, the modes with eigenvalues larger than the fluid will dominate. We can see this situation in the evolution of the variance of the NBLE, normalised to the fluid one, in Fig. 9.12, in which we have taken as initial PS $P_D(k,0) = k^{3/2}$. What it is important to retain in general about the evolution is that at large times the discreteness effects are arbitrary large[15]. As we will discuss below in our conclusions section, it is an important feature that, in an N-body system, discreteness effects are dependent on time, as we will discuss below.

[15] Note that for a lattice without modes larger than the fluid the the normalised variance would be smaller and smaller with time, i.e. discreteness effects also larger and larger.

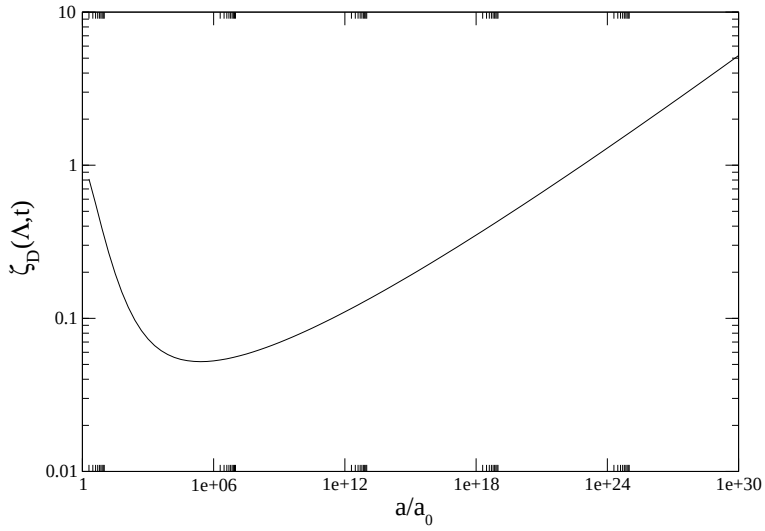

Figure 9.12: Function $\zeta_D(\ell, t)$ for an initial displacements PS $P_D(k, 0) = k^{3/2}$. The ultraviolet cutoff is given by the interparticle distance ℓ.

9.6.2 Effect of smoothing the interaction

In cosmological N-body simulations it is usual to introduce at small scales a smoothing in the potential to reduce discreteness effects. Specifically, for example, it prevents strong two-body collisions (which are characteristic of a discrete dynamics, see chapter 5). In this section we briefly study quantitatively the effects of the introduction of a smoothing in the interaction. We introduce the simple smoothing in the interacting potential:

$$v(r) = \frac{1}{\sqrt{r^2 + \epsilon^2}}. \tag{9.99}$$

We show in Fig.9.13 the effect of the smoothing (9.99) with $\epsilon = \ell$ as well as that of removing the contribution from the first nearest neighbour (NN). Note, however, that in the N-body simulations the smoothing is typically much smaller, in general $\epsilon < 0.1\ell$. We use here a larger smoothing to be able to distinguish a difference with the pure gravitational potential, which is imperceptible for $\epsilon \approx 0.1\ell$. In both cases we see a similar effect, more pronounced in one case than in the other. The effect of anisotropy are very much reduced but, on the other hand, the average growth with respect to the fluid limit is further supressed. Thus, we conclude that the smoothing does not make the system a better approximation to the fluid limit in the range treated by our approximation.

9.7 Extension of perturbative treatment to higher order than linear

In this section we will briefly outline an extension of the linear theory to higher order. This generalisation will be treated extensively in future work. Despite

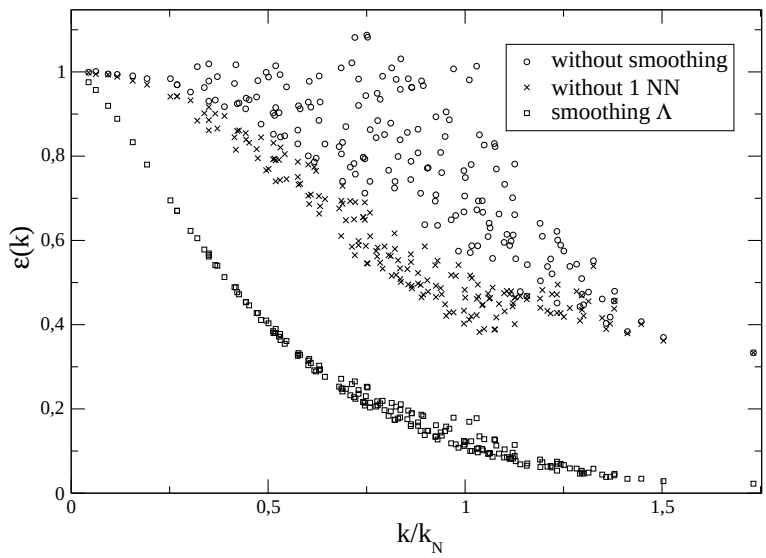

Figure 9.13: Difference in the optical branch for a system without smoothing, smoothing $\epsilon = \ell$ and without considering first NN. The points have been extracted with a probability law $\propto 1/k$ from a 64^3 spectrum.

the fact that the linear order gives a good approximation, higher orders are interesting to consider as they take into account the coupling between different modes and therefore the influence of small scales on large scales and vice-versa. The generalisation of the Taylor expansion of section 9.1 is:

$$F_\mu(\mathbf{R}) = \sum_{n=0}^{\infty} \sum_{\mathbf{R}'} \frac{1}{n!} \mathcal{D}^{(n)}_{\mu,\nu_1\ldots\nu_n}(\mathbf{R}-\mathbf{R}')[u_{\nu_1}(\mathbf{R}') - u_{\nu_1}(\mathbf{R})]\ldots[u_{\nu_n}(\mathbf{R}') - u_{\nu_n}(\mathbf{R})], \tag{9.100}$$

where we have omited for simplicity the sum over replicas. The tensor $\mathcal{D}^{(n)}_{\mu,\nu_1\ldots\nu_n}$ is only a function of the interacting potential $\phi(\mathbf{r})$ and it is equal to:

$$\mathcal{D}^{(n)}_{\mu,\nu_1\ldots\nu_n}(\mathbf{R}) = \frac{\partial^{(n+1)}\phi(\mathbf{R})}{\partial R_\mu \partial R_{\nu_1}\ldots\partial R_{\nu_n}}. \tag{9.101}$$

9.7.1 Second order correction

In the case of the second order correction Eq. (9.101) is

$$\mathcal{D}^{(2)}_{\mu\nu\sigma}(\mathbf{R}) = \frac{-3}{4|\mathbf{R}|^5}\left[R_\mu\delta_{\nu\sigma} - \frac{5R\mu R\nu R\sigma}{3|\mathbf{R}|^2} + \mu \leftrightarrow \nu \leftrightarrow \sigma\right], \tag{9.102}$$

and $\mathcal{D}^{(2)}_{\mu\nu\sigma}(\mathbf{R}=0) = 0$ because the force on a displaced particle, with all the others fixed at the lattice position, is only third order in the displacements (see section 9.1.2). In k-space, following the same procedure as in the section 9.2.2,

we get:

$$\tilde{\mathcal{D}}^{(2)}_{\mu\nu\sigma}(\mathbf{k}) = \frac{i}{2!}\sum_{\mathbf{K}}(k_\mu + K_\mu)(k_\nu + K_\nu)(k_\sigma + K_\sigma)\tilde{\phi}(\mathbf{k}+\mathbf{K}), \tag{9.103}$$

Using (9.100) we obtain two terms, one coming from the term proportional to $\mathbf{u}(\mathbf{R}')\mathbf{u}(\mathbf{R}')$ and the other one from the term proportional to $\mathbf{u}(\mathbf{R})\mathbf{u}(\mathbf{R}')$:

$$\begin{aligned} F^{(2)}_\mu(\mathbf{k}) &= \frac{1}{N}\sum_{\mathbf{k}'}\tilde{\mathcal{D}}^{(2)}_{\mu\nu\sigma}(\mathbf{k})\tilde{u}_\nu(\mathbf{k}')\tilde{u}_\sigma(\mathbf{k}-\mathbf{k}') \\ &- \frac{2}{N}\sum_{\mathbf{k}'}\tilde{\mathcal{D}}^{(2)}_{\mu\nu\sigma}(\mathbf{k}')\tilde{u}_\nu(\mathbf{k}')\tilde{u}_\sigma(\mathbf{k}-\mathbf{k}'). \end{aligned} \tag{9.104}$$

9.7.2 Treatment of corrections in a EdS universe

The corrections at any order can be computed knowing the solution at all the lower orders. We give the example of how to work out the second order correction. The μ-th component of the displacement equation up to second order correction is, in Fourier space, for a EdS universe, :

$$\ddot{\tilde{\mathbf{u}}}_\mu(\mathbf{k},t) + 2H(t)\dot{\tilde{\mathbf{u}}}_\mu(\mathbf{k},t) + \frac{1}{a^3}\mathcal{D}_{\mu\nu}(\mathbf{k})\tilde{\mathbf{u}}_\nu(\mathbf{k},t) = \frac{1}{a^4}F^{(2)}_\mu(\mathbf{k}), \tag{9.105}$$

where the r.h.s. of the last expression is explicitly given in terms of the displacements by Eq. (9.104). Let us expand formally the displacements in a power series:

$$\tilde{\mathbf{u}}(\mathbf{k},t) = \sum_{n=1}^{\infty}\epsilon^n\tilde{\mathbf{u}}^{(n)}(\mathbf{k},t). \tag{9.106}$$

Terms in Eq. (9.106) proportional to ϵ corresponds to the linear solution, proportional to ϵ^2 to the second order correction, and so on. At the end of the calculations the limit $\epsilon \to 1$ is taken. Inserting the expansion of the displacements up to second order in ϵ, i.e. $\epsilon\mathbf{u}^{(1)}(\mathbf{k},t) + \epsilon^2\mathbf{u}^{(2)}(\mathbf{k},t)$ in Eq. (9.105) and dropping terms of order higher of ϵ^2 we get one equation that is just the linear order one (9.67) (proportional to ϵ) and another one with the corrections (proportional to ϵ^2):

$$\begin{aligned} \ddot{\tilde{\mathbf{u}}}^{(2)}_\mu(\mathbf{k},t) &+ 2H(t)\dot{\tilde{\mathbf{u}}}^{(2)}_\mu(\mathbf{k},t) + \frac{1}{a^3}\mathcal{D}_{\mu\nu}(\mathbf{k})\tilde{\mathbf{u}}^{(2)}_\nu(\mathbf{k},t) = \\ &= \frac{1}{a^4 N}\sum_{\mathbf{k}'}\tilde{\mathcal{D}}^{(2)}_{\mu\nu\sigma}(\mathbf{k})\tilde{u}^{(1)}_\nu(\mathbf{k}')\tilde{u}^{(1)}_\sigma(\mathbf{k}-\mathbf{k}') \\ &- \frac{2}{a^4 N}\sum_{\mathbf{k}'}\tilde{\mathcal{D}}^{(2)}_{\mu\nu\sigma}(\mathbf{k}')\tilde{u}^{(1)}_\nu(\mathbf{k}')\tilde{u}^{(1)}_\sigma(\mathbf{k}-\mathbf{k}'). \end{aligned} \tag{9.107}$$

We know from the first order solution $\tilde{u}^{(1)}_\nu(\mathbf{k}')$ that the problem is then reduced to solving an equation like (9.68) but with a source term. We can in principle compute the displacements at any order but it becomes very rapidly numerically unfeasible because of the sum over $\mathbf{k}$ on the r.h.s. of Eq. (9.107).

The fluid limit of Eq. (9.107) is obtained taking the limit $\mathbf{k} \to 0$ of the dynamical matrices $\mathcal{D}^{(1)}(\mathbf{k})$ and $\mathcal{D}^{(2)}(\mathbf{k})$, Eqs. (9.51) and (9.103), respectively.

If we divide the displacements in a part parallel to k, $\tilde{\mathbf{u}}_{\parallel}(\mathbf{k},t)$, and another one perpendicular to k, $\tilde{\mathbf{u}}_{\perp}(\mathbf{k},t)$, Eq. (9.107) multiplied by $(-i\mathbf{k})$ results in the two following equations:

$$\ddot{\tilde{\mathbf{u}}}_{\perp}^{(2)}(\mathbf{k},t) + 2H(t)\dot{\tilde{\mathbf{u}}}_{\perp}^{(2)}(\mathbf{k},t) = 0 \tag{9.108a}$$

$$\ddot{\tilde{S}}^{(2)}(\mathbf{k},t) + 2H(t)\dot{\tilde{S}}^{(2)}(\mathbf{k},t) = \frac{2\pi}{a^4 N}\sum_{\mathbf{k}'}\tilde{S}^{(1)}(\mathbf{k}',t)$$
$$\times\, \tilde{S}^{(1)}(\mathbf{k}-\mathbf{k}',t)(\mathbf{k}\cdot\mathbf{k}')\left[|\mathbf{k}|^2 + 2|\mathbf{k}'|^2 - 3(\mathbf{k}\cdot\mathbf{k}')\right], \tag{9.108b}$$

where $\tilde{\mathbf{u}}_{\parallel}^{(n)}(\mathbf{k},t) = \nabla\cdot\tilde{S}^{(n)}(\mathbf{k},t)$.

Chapter 10

Conclusions and perspectives

In the last chapter of this thesis we have presented a novel formalism to study N-body systems in the perturbative regime, analogous to the Lagrangian perturbative theory in a fluid. It permits to construct an N-body discretization of *separately* each order of the fluid theory. The most immediate application is the study of discreteness effects in the perturbative regime of N-body simulations, *order by order*, by direct comparison with fluid theory.

We have seen that the fluid limit is actually obtained from the N-body system by taking the limit of an infinite number of particles, keeping the interparticle distance ℓ constant. We have also computed analytically the dominant corrections to the fluid limit by expanding in power series the dynamical matrix. This is a first step in the construction of a rigorous theory of the discreteness effects in the N-body systems.

We have shown that, at least in the linear regime, the discreteness effects are a function of time. It means that starting a N-body simulation at higher and higher redshift (i.e. earlier times), can increase arbitrarily the discreteness effects. They are therefore an additive quantity with time. It implies that these effects do not depend only on the new scale introduced as one would expect by the discretization process ℓ, but also on time.

It is instructive to compare this observation with the results of chapter 7 about initial conditions. We found that, when the theoretical PS has a very low amplitude, it can be very well represented by the N-body discretization below the Nyquist frequency. However, this is not the case for the variance in mass (see e.g. Fig. 7.3) or the correlation function (see e.g. Fig. 7.8). According to linear theory, a very low amplitude of fluctuations corresponds to a high redshift, and following the results obtained in the last chapter, the discreteness effects will be very important in this case. This fact suggest strongly that it is indeed important to take into account the real space properties — and not only the Fourier space ones usually considered in the literature — when studying these effects.

This conclusion highlights the interest of developing new methods to generate initial conditions, and specially ones with a better agreement of the real space properties between the N body system and the input theoretical model. We have presented such a method in chapter 8. It would be very interesting to use it with an $N \ln N$ code in order to increase the number of particles. It would permit to generate initial conditions for large N body simulations to be then

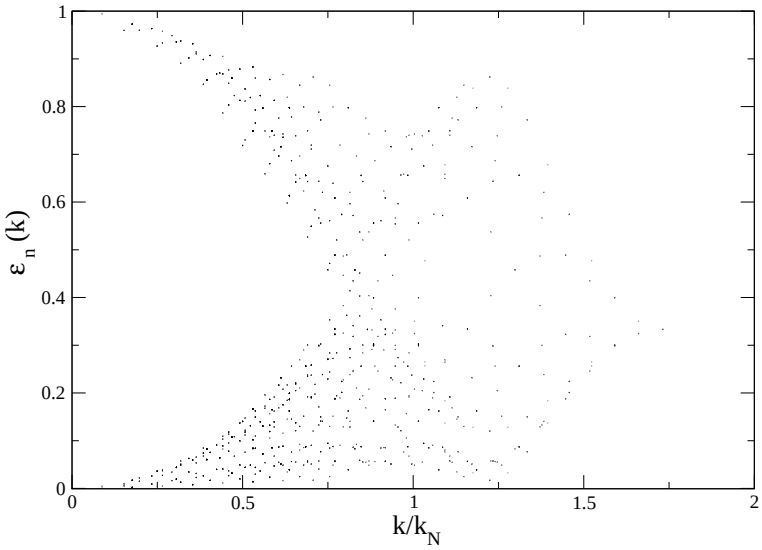

Figure 10.1: Spectrum of eigenvalues of a bcc lattice.

used for dynamical studies of discreteness effects.

We have also seen in chapter 9 that the sc lattice has eigenvalues larger than the fluid limit. It implies – by the Kohn sum rule – that there are some negative ones. In the case of the Wigner crystal (repulsive $1/r$ potential), the modes with negative eigenvalues correspond to growing modes that lead to instabilities. On a other hand, it is known that the Wigner bcc is a stable lattice, which implies that there are no modes with eigenmodes larger than in the fluid. Moreover, it is more densely packed and more isotropic (see Fig. 10.1). This suggests that it could be a better lattice to set up the initial conditions – instead of the sc lattice – in order to minimize discreteness effects.

Another direction will be to study exhaustively the next (second) order in the perturbation theory. It will insights, for example, about the interplay between fluid non-linearities and discreteness effects. Moreover, we hope that the method presented in chapter 9 could contribute more generally to the development of the perturbative theory of the gravitational clustering. The "dust" Lagrangian perturbative theory (see chapter 5) breaks down after shell crossing. The "fluid elements", instead of clustering as would occur in a realistic theory, diffuse. It has the weakness of impossibiliting the formation of structures. To overcome this limitation, the phenomenological adhesion approximation has been introduced [GSS89]. It prevents this problem but it has the inconvenience that it is not a model based on first principle. Some current investigations (e.g. [BD98, Tat04, BD05]) try to obtaining the same effect of "stick" the particles together after shell-crossing by the introduction of an effective pressure. This pressure is justified by the underlying particle structure of the CDM (see chapter 4). However, this pressure is introduced in a unrealistic (but simple) phenomenological way. The perturbative N-body method (where now the N-bodies can be considered for instance CDM particles) permit computing precisely these pressure corrections (see section 9.2.2).

Chapitre 11

Conclusions en français

Dans le dernier chapitre de la thèse nous avons présenté un formalisme novateur pour étudier les systèmes à N-corps dans le régime perturbatif, analogue à la théorie perturbative Lagrangienne dans un fluide. Il permet de construire une discrétisation à N-corps de chaque ordre *séparemment* de la théorie fluide. L'application la plus immédiate est l'étude des effets discrets dans le régime perturbatif des simulations à N-corps, *ordre par ordre*, par comparaison directe avec la théorie du fluide.

Nous avons vu que la limite fluide est effectivement obtenue a partir des simulations à N-corps en prenant la limite d'un nombre infini de particules, en maintenant la distance entre les particules ℓ constante. Nous avons aussi calculé analytiquement les corrections dominantes à la limite fluide en développant en série de puissances la matrice dynamique. Cela est un premier pas dans la construction d'une théorie rigoureuse des effets discrets dans les simulations à N-corps.

Nous avons montré que, au moins dans le régime linéaire, les effets discrets dépendent du temps. Cela implique qu'en commençant les simulations à N-corps à des décalages vers le rouge de plus en plus grands (i.e. de plus en plus tôt), les effets discrets peuvent devenir de plus en plus important. Ce sont donc des effets additifs avec le temps. Cela implique qu'ils ne dépendent pas seulement — comme on pourrait penser dans un premier temps — de la nouvelle échelle introduite ℓ mais aussi du temps.

Il est instructif de comparer cette observation avec les résultats du chapitre 7 sur les conditions initiales. Nous avons trouvé que, lorsque le spectre de puissance théorique présente une très faible amplitude, il peux être très bien représenté par la discrétisation à N-corps en dessous de la fréquence de Nyquist. Cependant, cela n'est pas le cas pour la variance de la masse (Fig. 7.3) ou la fonction de corrélation (Fig. 7.8). Selon la théorie linéaire, une fluctuation de très faible amplitude correspond à un décalage vers le rouge élevé. Les résultats du dernier chapitre de cette thèse prévoient précisément des effets discrets très importants dans ce cas. Cela suggère fortement qu'il soit aussi nécessaire de prendre en compte les propriétés de corrélations dans l'espace réel — et non seulement dans l'espace de Fourier comme il est habituellement fait dans la littérature — lorsque ces effets sont étudiés.

Cette conclusion fait ressortir l'intérêt de développer de nouvelles méthodes pour générer les conditions initiales, et spécialement avec un meilleur accord

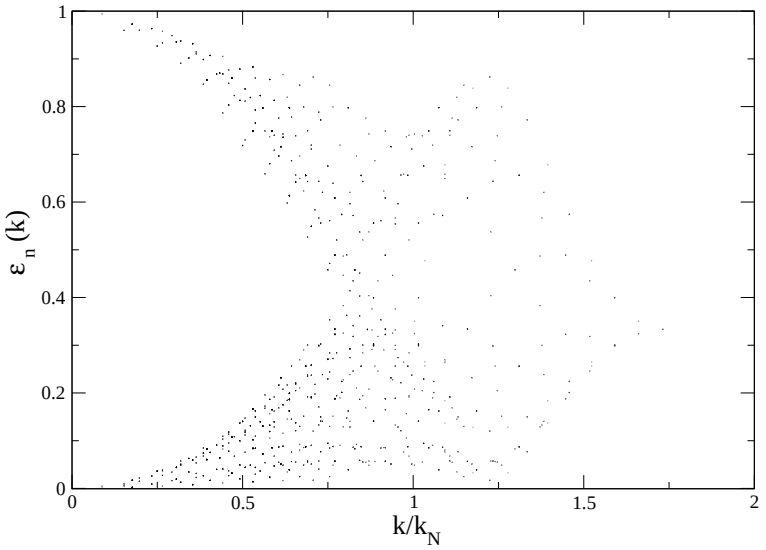

FIG. 11.1 – Spectre de valeurs propres d' un réseau cubique à face centrées.

entre les proprietés de corrélations dans l'espace réel du système à N-corps et celle du modèle théorique. Nous avons présenté une méthode qui a ces propriétés dans le chapitre 8. Il serait très intéressant d'implémenter un code de complexité inférieure à $N \ln N$. Cela permettrait de générer des conditions initiales pour de grandes simulations à N-corps, et d'étudier dynamiquement les effets discrets.

Nous avons aussi étudié dans le chapitre 9 que le réseau cubique simple présente des valeurs propres plus grandes que la limite fluide. Cela implique — selon la règle de somme de Kohn — qu'il y a des valeurs propres négatives. Dans la cas d'un cristal de Wigner (potentiel d'interaction $1/r$), ces modes correspondent à des modes instables. Il est connu que le cristal de Wigner avec une configuration à corp centré est stable, ce qui implique qu'il n'y a pas de modes avec des valeurs propres plus grandes que dans le fluide. De plus, il est empaqueté plus densément et est plus isotrope (Fig. 11.1). Cela suggère qu'il soit peut-être un meilleur réseau pour générer les conditions initiales, au lieu de réseau simple cubique.

Une autre direction de recherche serait l'étude exhaustive de l'ordre suivant de la théorie de perturbation. Cela donnerait, par exemple, de l'information sur la relation entre les non-linéarité et les effets discrets. De plus, nous espérons que les résultats présentés dans le chapitre 9 puissent contribuer plus généralement au développement de la théorie perturbative de l'aggrégation gravitationnelle. Le «dust model» dans la théorie des perturbations Lagrangienne (chapitre 5) ne marche plus après le «shell-crossing». Les «élements de fluide», au lieu de s'aggréger comme cela se passerait dans une théorie réaliste, diffusent, ce qui empêche la formation de structures. Pour outrepasser cette limitation, le modèle phénoménologique de l'«adhésion» a été introduit [GSS89]. Il permet de résoudre ce problème mais a l'inconvénient de ne pas être basé sur des principes premier. Quelques recherches actuelles (par exemple [BD98, Tat04, BD05]) essaient d'obtenir le même effet d'agréger les particules après le «shell-crossing»

par l'introduction d'une pression effective. Cette pression est justifié par la structure sous-jacente des particules de matières noire (chapitre 4). Cependant, cette pression est introduite d 'une façon phénoménologique non réaliste (mais simple). La méthode perturbative présenté dans le chapitre 9 permet de calculer précisément ces corrections de type «pression» (section 9.2.2).

Bibliography

[AM76] N. W. Ashcroft and N. D. Mermin, *Solid state physics*, W.B. Saunders, Philadelphia, 1976.

[ama] `http://www.amara.com/papers/nbody.html`.

[BCHJ95] F. R. Bouchet, S. Colombi, E. Hivon, and R. Juszkiewicz, *Perturbative lagrangian approach to gravitational instability*, Astron. Astrophys. **296** (1995), 575.

[BD98] T. Buchert and A. Domínguez, *Modeling multi-stream flow in collisionless matter*, Astron. Astrophys. **335** (1998), 395.

[BD05] ———, *Adhesive gravitational clustering*, Astronomy & Astrophysics (2005).

[BE84] J. R. Bond and G. Efstathiou, *Cosmic background radiation anisotropies in universes dominated by nonbaryonic dark matter*, Astrophys. J. **285** (1984), L45–L48.

[Ber95] E. Bertschinger, *Cosmics: Cosmological initial conditions and microwave anisotropy codes.*

[BH80] M. Baus and J.-P. Hansen, *Statistical mechanics of the simple coulomb system*, Phys. Rep. **59** (1980), 1.

[BJSL02] T. Baertschiger, M. Joyce, and F. Sylos Labini, *Power-law correlation and discreteness in cosmological n- body simulations*, Astrophys. J. **581** (2002), L63–L66.

[BK02] J. Binney and A. Knebe, *Two-body relaxation in cosmological simulations*, Mon. Not. Roy. Astron. Soc. **333** (2002), 378.

[BKH+94] C. L. Bennett, A. Kogut, G. Hinshaw, A. J. Banday, E. L. Wright, K. M. Gorski, D. T. Wilkinson, R. Weiss, G. F. Smoot, S. S. Meyer, J. C. Mather, P. Lubin, K. Loewenstein, C. Lineweaver, P. Keegstra, E. Kaita, P. D. Jackson, and E. S. Cheng, *Cosmic temperature fluctuations from two years of COBE differential microwave radiometers observations*, Astrophys. J. Suppl. **436** (1994), 423–442.

[BSL02] T. Baertschiger and F. Sylos Labini, *On the problem of initial conditions in cosmological n-body simulations*, Europhys.Lett. **57** (2002), 322.

[BSL03] ———, *Reply to the comment on "on the problem of initial conditions in cosmological n-body simulations"*, Europhys.Lett. **63** (2003), 633.

[BT87] J. Binney and S. Tremaine, *Galactic dynamics*, Princeton Series in Astrophysics, Princeton, 1987.

[Buc89] T. Buchert, *A class of solutions in newtonian cosmology and the pancake theory*, Astron. Astrophys. **223** (1989), 9–24.

[Buc92] ———, *Lagrangian theory of gravitational instability of friedman-lemaître cosmologies and the "zel'dovich approximation"*, Mon. Not. R. astr. Soc. **254** (1992), 729–737.

[Car61] H. Carr, *Energy, specific heat, and magnetic properties of the low-density electron gas*, Phys. Rev. **122** (1961), 1437.

[CHM60] R. A. Coldwell-Horsfall and A. A. Maradunin, *Zero-point energy of an electron lattice*, Journal of Mathematical Physics **1** (1960), 395.

[Cla57] C. B. Clark, *Coulomb interaction in the uniform-background lattice model*, Phys. Rev. **109** (1957), no. 4, 1133.

[Coo73] M. S. Cooper, *Modified hypernetted-chain equation for the screened coulomb potential*, Phys. Rev. A **7** (1973), no. 1, 1.

[DK02] A. Dominguez and A. Knebe, *On the reliability of initial conditions for dissipationless cosmological simulations*, Publ.Astron.Soc.Pac. **20** (2002), 1.

[DK03] ———, *Comment on "on the problem of initial conditions in cosmological n-body simulations" (europhys. lett. 57, 322)*, Europhys. Lett. **63** (2003), 631–632.

[DLPS80] S. W. De Leeuw, J. W. Perram, and E. R. Smith, Proc. R. Soc. Lond. A **373** (1980), 27.

[DMS04] J. Diemand, B. Moore, and J. Stadel, *Convergence and scatter of cluster density profiles*, Mon. Not. Roy. Astron. Soc. **353** (2004), 624.

[DMS05] ———, *Earth-mass dark-matter haloes as the first structures in the early universe*, Nature. **433** (2005), 389–391.

[DMSK04] J. Diemand, B. Moore, J. Stadel, and S. Kazantzidis, *Two body relaxation in cdm simulations*, Mon. Not. Roy. Astron. Soc. **348** (2004), 977.

[E$^+$04] S. Eidelman et al., *Review of particle physics*, Phys. Lett. **B592** (2004).

[EDWF85] G. Efstathiou, M. Davis, S. D. M. White, and C. S. Frenk, *Numerical techniques for large cosmological N-body simulations*, Astrophys. J. Supp. **57** (1985), 241–260.

[Ewa21] P. Ewald, Ann. Phys. **64** (1921), 253–287.

[Fuc35] K. Fuchs, ., Proc. Roy. Soc. **A151** (1935), 585.

[G+03a] A. Gabrielli et al., *Generation of primordial cosmological perturbations from statistical mechanical models*, Phys. Rev. **D67** (2003), 043506.

[G+03b] ———, *Generation of primordial cosmological perturbations from statistical mechanical models*, Phys. Rev. **D67** (2003), 043506.

[G+06] ———, *Graviational force distribution in a randomly perturbed lattice*, In preparation (2006).

[Gab04] A. Gabrielli, *Point processes and stochastic displacement fields*, Phys. Rev. E **70** (2004), 066131.

[GBRW86] M. H. Goroff, Grinstein B., S.-J. Rey, and M. B. Wise, *Coupling of modes of cosmological mass density fluctuations*, The Astrophysical Journal **314** (1986), 6–14.

[GJMV03] A. Gabrielli, M. Joyce, B. Marcos, and P. Viot, *Causality and the superhorizon power spectrum*, Europhys. Lett. **66** (2003), 1.

[GJSL02] A. Gabrielli, M. Joyce, and F. Sylos Labini, *The glass-like universe: Real-space correlation properties of standard cosmological models*, Phys. Rev. D **65** (2002), 083523.

[GSLJP05] A. Gabrielli, F. Sylos Labini, M. Joyce, and L. Pietronero, *Statistical physics for cosmic structures*, Springer-Verlag, Berlin, 2005.

[GSS89] S. N. Gurbatov, A. I. Saichev, and S. F. Shandarin, *The large-scale structure of the universe in the frame of the model equation of non-linear diffusion*, MNRAS **236** (1989), 385–402.

[GT] H. Gould and J. Tobochnik, *Thermal and statistical physics*, `http://stp.clarku.edu/notes/`.

[H+05] D. W. Hogg et al., *Cosmic homogeneity demonstrated with luminous red galaxies*, Astrophys. J. **624** (2005), 54–58.

[HBS91] L. Hernquist, F. R. Bouchet, and Y. Suto, *Application of the Ewald method to cosmological N-body simulations*, Astrophys. J. Supp. **75** (1991), 231–240.

[HM76] J.-P. Hansen and I. R. McDonald, *Theory of simple liquids*, Academic Press, London, 1976.

[HRWH04] K. Heitmann, P. M. Ricker, M. S. Warren, and S. Habib, *Robustness of cosmological simulations i: Large scale structure.*

[Hua87] K. Huang, *Statistical mechanics*, John Wiley & Sons, New York, 1987.

[HYS01] T. Hamana, N. Yoshida, and Y. Suto, *Reliability of the dark matter clustering in cosmological n-body simulation on scales below the mean separation length of particles.*

[I+99] O. Iguchi et al., *Statistical mechanics of self–gravitating system: Cluster expansion method*, Phys. Lett. **A260** (1999), 4–9.

[II83] H. Iyetomi and S. Ichimaru, *Density-functional theory of correlations in dense plasmas: Improvment on the hypernetted-chain scheme*, Phis. Rev. A **27** (1983), no. 6, 3241.

[Isi71] I. Isihara, *Statistical physics*, Academic Press, London, 1971.

[J+98] A. Jenkins et al., *Evolution of structure in cold dark matter universes*, Astrophys. J. **499** (1998), 20.

[JLM05] M. Joyce, D. Levesque, and Bruno Marcos, *A method of generating initial conditions for cosmological n body simulations*, Phys. Rev. D **72** (2005), 103509.

[JM04] M. Joyce and B. Marcos, *Initial conditions of cosmological n-body simulations: a study of their correlation properties in real and reciprocal space.*

[JMG+05] M. Joyce, B. Marcos, A. Gabrielli, T. Baertschiger, and F. Sylos Labini, *Gravitational evolution of a perturbed lattice and its fluid limit*, Phys. Rev. Lett. **95** (2005), 011304.

[Kie99] M. K. H. Kiessling, *Mathematical vindications of the jeans swindle*, `astro-ph/9910247` (1999).

[KMS96] B. Kuhlman, A. L. Melott, and S. F. Shandarin, *A test of the particle paradigm in n-body simulations*, Ap. J. **470** (1996).

[LL59a] L. D. Landau and E. M. Lifshitz, *Mechanics*, Pergamon Press, London, 1959.

[LL59b] ———, *Statistical physics*, Pergamon Press, London, 1959.

[LL66] ———, *Théorie du champ*, Mir, Moscow, 1966.

[LL79] ———, *Fluid mechanics*, Pergamon Press, New York, 1979.

[LP81] E. M. Lifshitz and L. P. Pitaevskii, *Physical kinetics*, Pergamon Press, Oxford, 1981.

[MB04] C.-P. Ma and E. Bertschinger, *A cosmological kinetic theory for the evolution of cold dark matter halos with substucture: quasi-linear theory*, The Astrophysical Journal **612** (2004), 28–49.

[MSS94] D. Munshi, V. Sahni, and A. A. Starobinsky, *Nonlinear approximations to gravitational instability: A comparison in the quasilinear regime*, Astrophys. J. **436** (1994), 517.

[MSS97] A. L. Melott, R. J. Splinter, and S. F. Shandarin, *Demonstrating discreteness and collision error in cosmological n-body simulations of dark matter gravitational clustering*, The Astrophysical Journal **479** (1997), 79–83.

[MT01] M. Morita and T. Tatekawa, *Extending lagrangian perturbation theory to a fluid with velocity dispersion*, Mon. Not. Roy. Astron. Soc. ,328 (2001), 815–828.

[NDW57] B. R. A. Nijboer and F. W. De Wette, *On the calculation of lattice sums*, Physica **XXIII** (1957), 309–321.

[P+03] C. Power et al., *The inner structure of lambdacdm halos i: A numerical convergence study*, Mon. Not. Roy. Astron. Soc. **338** (2003), 14–34.

[PAD88] P. D. Poll, N. W. Ashcroft, and H. E. DeWitt, *One-component plasma bridge function*, Phys. Rev. A **37** (1988), no. 5, 1672.

[Pad93] T. Padmanabhan, *Structure formation in the universe*, Cambridge University Press, Cambridge, 1993.

[Pee80] P. J. E. Peebles, *The large-scale structure of the universe*, Princeton University Press, Princeton, 1980.

[Pee93] ———, *Principles of physical cosmology*, Princeton University Press, Princeton, 1993.

[Pin63] D. Pines, *Elementary excitations in solids*, Benjamin, 1963 (engl.).

[PW65] A. A. Penzias and R. W. Wilson, *A measurement of excess antenna temperature at 4080 mc/s.*, Astrophysical Journal **142** (1965), 419–421.

[Ric01] J. Rich, *Fundamentals of cosmology*, Springer-Verlag, Heidelberg, 2001.

[Sas00] W. C. Saslaw, *The distribution of galaxies*, Cambridge University Press, Cambridge, 2000.

[SB95] P. Schneider and M. Bartelmann, *The power spectrum of density fluctuations in the zel'dovich approximation*, MNRAS **273** (1995), 475–483.

[SC95] V. Sahni and P. Coles, *Approximation methods for nonlinear gravitational clustering*, Phys. Rept. **262** (1995), 1–135.

[SC00] G. Salin and J.-M. Caillol, *Ewald sums for yukawa potentials*, J. Chem. Phys. **113** (2000), no. 23, 10459.

[SDS90] G. S. Strigfellow, H. E. DeWitt, and W. L. Slattery, *Equation of state of the one-component plasma derived from precision monte carlo calculations*, Phys. Rev. A **41** (1990), no. 2, 1105.

[SMSS98] R. J. Splinter, A. L. Melott, S. F. Shandarin, and Y. Suto, *Fundamental limitations on cosmological clustering simulations due to n-bodies*, Astrophys. J. **497** (1998), 38–61.

[SYW01] V. Springel, N. Yoshida, and S. D. M. White, *GADGET: a code for collisionless and gasdynamical cosmological simulations*, New Astronomy **6** (2001), 79–117.

[Tat04] T. Tatekawa, *Correspondence between the adhesion model and the velocity dispersion for the cosmological fluid*, Phys. Rev. **D70** (2004), 064010.

[TSM+02] T. Tatekawa, M. Suda, K.-I. Maeda, M. Morita, and H. Anzai, *Perturbation theory in lagrangian hydrodynamics for a cosmological fluid with velocity dispersion*, Phys. Rev. **D66** (2002), 064014.

[VGM] L. M. Varela, M. García, and V. Mosquera.

[Vio] P. Viot, *Simulation numérique en physique statistique*, `http://www.lptl.jussieu.fr/users/viot/coursPViot.html`.

[Wei72] S. Weinberg, *Gravitation and cosmology*, John Wiley, New York, 1972.

[Whi94] S. D. M. White, *Formation and evolution of galaxies: Lectures given at les houches, august 1993*.

[Wu01] M. G. Wu, *Calculating the r^{-n} interactions, $1 \leq n < 3$, in a periodic system with a neutralizing background charge density*, `cond-mat/0112138v1` (2001).

[WV01] J. A. White and S. Velasco, *The ornstein-zernike equation in the canonical ensemble*, Europhysics Letters **54** (2001), no. 5, 475–481.

[YMGM05] A. Yoshisato, M. Morikawa, N. Gouda, and H. Mouri, *Why is the zel'dovich approximation so accurate?*

[YMM98] A. Yoshisato, T. Matsubara, and M. Morikawa, *Accuracy of nonlinear approximation in spheroidal collapse: why are zeldovich approximations good?*, The Astrophysical Journal **498** (1998), 48–59.

[Zim72] J. M. Ziman, *Theory of solids (2nd ed.)*, Cambridge Univ. Press, 1972.

[ZN83] Ya. B. Zeldovich and I. Novikov, *Relativistic astrophysics*, Univ. Chicago Press, Chicago, 1983.

Part III

Appendixes

Appendix A

Asymptotic behavior of Fourier transforms

We are interested to know the large scale (small k) behavior of the Fourier Transform (FT) of some generic functions $p(\mathbf{r})$, defined as

$$\mathrm{FT}[p(\mathbf{r})](\mathbf{k}) \equiv \tilde{p}(\mathbf{k}) = \int_{\mathcal{R}^d} d^d r\, p(\mathbf{r}) e^{-i\mathbf{k}\cdot\mathbf{r}}. \tag{A.1}$$

We will consider functions which at large $\mathbf{r}$ behaves as a power-law (we do not care about their behavior at small scales):

$$p(\mathbf{r} \to \infty) = \frac{A}{|\mathbf{r}|^{\alpha+d}}, \tag{A.2}$$

where d is the dimension of the space and $\alpha > 0$ is not an integer[1]. We make the hypothesis that the function (A.2)

- depends only in $u = |\mathbf{u}|$ and therefore $\tilde{p}(\mathbf{k}) = \tilde{p}(k)$ and
- it is a real symmetric function, hence $\tilde{p}(k)$ is also a real and symmetric function.

A.1 One-dimensional case

We will consider first the one-dimensional case:

$$\tilde{p}(k) = \int_{-\infty}^{\infty} dx\, p(x) e^{-ikx} = A \int_{\Lambda}^{\infty} dx\, \frac{1}{x^{\alpha+1}} e^{-ikx} \tag{A.3}$$

where we have have relaxed the assumption of symmetry of $p(x)$ and the cutoff Λ is set to zero if the integral converges[2]. For sufficiently small k it is always possible to expand the complex exponential of (A.3) to get:

$$\tilde{p}(k \to 0) = A \sum_{n=0}^{\infty} \frac{(-ik)^n}{n!} \int_{\Lambda}^{\infty} dx \frac{1}{x^{\alpha+1}} x^n, \tag{A.4}$$

[1] It is possible to do the same procedure with α integer. In this case logarithmic corrections will appear.

[2] The cutoff Λ can be introduced because small scales contributions in the integral (A.3) do not affect the final result.

where we have assumed the convergence of in the sum and the integral to permute them. If $p(x)$ decreases as $x \to \infty$ faster than any power law (i.e. $\alpha \to \infty$) then all the terms in the expansion (A.4) are finite. In this case we can write

$$\mathrm{FT}[p(x)](k \to 0) = A \sum_{n=0}^{\infty} (-i)^n C_n k^n \tag{A.5}$$

with

$$C_n = \frac{1}{n!} \int_{-\infty}^{\infty} dx p(x) x^n := \frac{1}{n!} \langle x^n \rangle , \tag{A.6}$$

where $\langle p^n \rangle$ denotes the n-th moment of $p(x)$. The expression (A.5) is a Taylor expansion of an analytical function around $k = 0$.

If $p(x)$ is a power-law then the terms of the sum (A.4) $n > [\alpha]$ (where $[\cdot]$ denotes "integer part") diverges. This is a manifestation that $\tilde{p}(k)$ is not an analytical function around zero and therefore it is not possible to perform a Taylor expansion, i.e. an expansion in integer powers of k. Nevertheless it is possible to expand $\tilde{p}(k)$ in non-integer powers of k. We can split (A.3) into two sums as

$$\begin{aligned} \tilde{p}(k) &= A \int_{\Lambda}^{\infty} dx \frac{1}{x^{\alpha+1}} \left(e^{-ikkx} - \sum_{j=0}^{n} \frac{(-i)^j (kx)^j}{j!} \right) \\ &+ A \sum_{j=0}^{\infty} (-i)^j \int_{\Lambda}^{\infty} dx \frac{1}{x^{\alpha+1}} \frac{(kx)^j}{j!} + \mathcal{O}(k^{n+1}), \end{aligned} \tag{A.7}$$

where $n = [\alpha]$. The first integral (A.7) can be solved using the change of variables $u = kx$. It is then rewritten as:

$$A \int_{\Lambda}^{\infty} dx \frac{1}{x^{\alpha+1}} \left(e^{-ikx} - \sum_{j=0}^{n} \frac{(-i)^j (kx)^j}{j!} \right) = Bk^{\alpha} \tag{A.8}$$

with

$$B = A \int_{\Lambda}^{\infty} du \frac{1}{u^{\alpha+1}} \left(e^{iu} - \sum_{j=0}^{n} \frac{(-i)^j (u)^j}{j!} \right) . \tag{A.9}$$

Note that if $n = [\alpha]$ then A is *finite*. The second integral (A.8) is the standard Taylor expansion up to order n. We write therefore the small k behavior of $\tilde{p}(\mathbf{k})$ as

$$\tilde{p}(k) = A \sum_{j=0}^{n} \frac{(-1)^j}{j!} k^j \langle x^j \rangle + Bk^{\alpha} + \mathcal{O}\left(k^{n+1}\right) . \tag{A.10}$$

We will give in what follows a few worked examples:

Case $0 < \alpha < 1$

The real and imaginary part of $\tilde{p}(k)$ have to be treated separately. For the real part we have:

$$\begin{aligned} \mathrm{Re}[\tilde{p}(k)] &= A \int_0^{\infty} dx \frac{\cos kx}{x^{\alpha+1}} = 1 + A \int_0^{\infty} dx \frac{\cos kx - 1}{x^{\alpha+1}} \\ &= 1 + Ak^{\alpha} \int_0^{\infty} du \frac{\cos u - 1}{u^{\alpha+1}} = 1 + k^{\alpha} \Gamma(-\alpha) \cos\left(\frac{\alpha\pi}{2}\right), \end{aligned} \tag{A.11}$$

where the cutoff Λ has been sent to zero (because it is not necessary) and we have chosen $p(x)$ normalised to one, i.e.,

$$\int_0^\infty dx p(x) = 1. \tag{A.12}$$

The imaginary part is:

$$\mathrm{Im}[\tilde{p}(k)] = A\int_0^\infty dx\,\frac{\sin kx}{x^{\alpha+1}} = Ak^\alpha \int_0^\infty du\,\frac{\sin u}{u^{\alpha+1}} = Ck^\alpha, \tag{A.13}$$

where

$$C = -A\Gamma[-\alpha]\sin\left[\frac{\alpha\pi}{2}\right]. \tag{A.14}$$

Case $1 < \alpha < 2$

The real part is unchanged (because the $\cos(x)$ has only even powers of x). The imaginary part is:

$$\begin{aligned}\mathrm{Im}[\tilde{p}(k)] &= A\int_0^\infty dx\,\frac{\sin kx}{x^{\alpha+1}} = 1 + A\int_0^\infty dx\,\frac{\sin kx - kx}{x^{\alpha+1}} \\ &= 1 + Ak^\alpha \int_0^\infty du\,\frac{\sin u - u}{u^{\alpha+1}} = 1 + Ck^\alpha,\end{aligned} \tag{A.15}$$

where

$$C = -A\Gamma[-\alpha]\sin\left[\frac{\alpha\pi}{2}\right]. \tag{A.16}$$

A.2 Generalisation to any dimension

The generalisation of the Eq. (A.7) to d dimension for the $p(\mathbf{r})$ given in Eq. (A.2) is straigtforward:

$$\tilde{p}(k) = \sum_{j=0}^{n} \frac{(-1)^j}{j!} k^j \left\langle r^j \right\rangle + Ak^\alpha + \mathcal{O}\left(k^{n+1}\right), \tag{A.17}$$

where

$$\left\langle r^j \right\rangle = A\int d^d r p(\mathbf{r})(r\cos\theta)^j \tag{A.18}$$

and

$$B = A\int d^d u \frac{1}{u^{\alpha+d}}\left(e^{iu\cos\theta} - \sum_{j=0}^{n}\frac{(-i)^j(u\cos\theta)^j}{j!}\right), \tag{A.19}$$

where θ is the angle between u and any coordinate axis. Note that if $p(\mathbf{r})$ is a symmetric function, then only even powers of k will appear in the first term of the r.h.s. of (A.17).

Appendix B

Functionals

In this appendix we will give very informal recipes about functional that we need along the text.

We define a functional $\mathcal{F}$ as a single-valued function of a vector space, typically functions. Let us consider for simplicity a functional $\mathcal{F} : \{f\} \longrightarrow \mathcal{R}$ of a single function $f : \mathbb{R} \longrightarrow \mathbb{R}$ defined in the interval $[a, b]$. For example a functional of f can be simply the integral

$$\mathcal{F}[f] = \int_a^b F[f(x)]dx. \tag{B.1}$$

B.1 Functional derivative

We will introduce the notion of *functional derivative* of $\mathcal{F}$ with respect to f looking for the variation $d\mathcal{F}$ due to small variations $\delta f(x)$ in the interval $[a, b]$:

$$d\mathcal{F} = \int \frac{\delta \mathcal{F}}{\delta f(x)} \delta f(x) dx. \tag{B.2}$$

This expression may be better understood if we discretize the continuous variable x into a set of x_i independent variables, with $x_{i+1} - x_i \to 0$. We can write then the function $f(x_i)$ as f_i, because x_i just labels the different functions f. Therefore the functional can be considered a simple function of the variable f_i and its differential is, applying the chain rule:

$$\delta \mathcal{F} = \sum_i \frac{\delta \mathcal{F}}{\delta f_i} \delta f_i. \tag{B.3}$$

Taking the continous limit of (B.3) we obtain Eq. (B.2). We can derive an explicit formula for the functional derivative in the discretized picture. Using the analogy with the partial derivative we can write

$$\frac{\delta \mathcal{F}(f_i)}{\delta f_j} = \lim_{\epsilon \to 0} \frac{\mathcal{F}(f_i + \epsilon \delta_{ij}) - \mathcal{F}(f_i)}{\epsilon}, \tag{B.4}$$

where δ_{ij} is the Kroneker delta function. Taking the continous limit we obtain the expression for the functional derivative

$$\frac{\delta \mathcal{F}[f(x))}{\delta f(y)} = \lim_{\epsilon \to 0} \frac{\mathcal{F}[f(x) + \epsilon \delta(x - y)] - \mathcal{F}[f(x)]}{\epsilon}. \tag{B.5}$$

From what it is explained above it follows that in the particular case in which $\mathcal{F} = f(x)$ then

$$\frac{\delta f(x)}{\delta f(y)} = \delta(x - y). \tag{B.6}$$

A generalization to a functions depending on a vector variable, for example $f : \mathbb{R}^n \longrightarrow \mathbb{R}$, is straightformard and it is left as an "exercise".

B.2 Functional integration

We will denote the functional integral of the functional $\mathcal{F}$ defined above as

$$\int \mathcal{D}[f(x)]\mathcal{F}[f(x)]. \tag{B.7}$$

Discretizing the x variable as before, we obtain:

$$\int \mathcal{D}[f(x)]\mathcal{F}[f(x)] = \lim_{\epsilon \to 0} \int \left[\prod_i d^d f_i\right] \mathcal{F}[f_i], \tag{B.8}$$

where $x_{i+1} - x_i = \epsilon$. In what follow we are going work out the case of gaussian integrals and Fourier transform of multivariate gaussian functions.

B.2.1 Gaussian integrals

Consider the gaussian functional $\mathcal{F} : \mathbf{u} \longrightarrow \mathbb{R}$ of the function $\mathbf{u} : \mathcal{R}^d \longrightarrow \mathcal{R}^d$ defined in the whole space $\mathcal{R}^d$:

$$\mathcal{F}[\mathbf{u}(\mathbf{r})] = \exp\left[-\frac{1}{2}\int_{\mathcal{R}^d} d^d r d^d r' \mathbf{u}(\mathbf{r})\mathcal{K}(|\mathbf{r} - \mathbf{r}'|)\mathbf{u}(\mathbf{r}')\right], \tag{B.9}$$

where $\mathcal{K} : \mathcal{R}^d \longrightarrow \mathcal{R}^d \otimes \mathcal{R}^d$ (i.e. it can be represented by a matrix). Let us compute (as "first exercise") the normalisation of (B.9). Therefore we want to calculate the functional integral

$$N = \int \mathcal{D}[\mathbf{u}(\mathbf{r})]\mathcal{F}[\mathbf{u}(\mathbf{r})] = \lim_{n \to \infty} \sum_{i=1}^{n} \left[\prod_{i=1}^{n} d^d \mathbf{u}_i\right] \mathcal{F}[\mathbf{u}_i] \tag{B.10}$$

where the limit that appears in Eq. (B.8) are now implicit and i are integers. Discretizing Eq. (B.9) and inserting it in Eq. (B.10), we get:

$$\lim_{n \to \infty} \int_{\mathcal{R}^d} \left[\prod_{i=1}^{n} d^d \mathbf{u}_i\right] \prod_{j,k=1}^{n} \exp\left[-\frac{1}{2V}\mathbf{u}_j \mathcal{K}_{jk} \mathbf{u}_k\right]. \tag{B.11}$$

From Eq. (B.9), the matrix $\mathcal{K}$ is symmetric, therefore its eigenvalues will be real. We can therefore always find an *unitary* transformation that makes $\mathcal{K}$ diagonal. Let us denote the eigenvalues of $\mathcal{K}_{jk}$ by λ_j and the vectors $\mathbf{u}$ in this new basis $\mathbf{v}$. Because the transformation is unitary its Jacobian is unity and we can write (B.11) as

$$N = \lim_{n \to \infty} \int_{\mathcal{R}^d} \left[\prod_{i=1}^{n} d^d \mathbf{v}_i\right] \prod_{j=1}^{n} \exp\left[-\frac{1}{2V}\mathbf{v}_j \mathcal{K}_j \mathbf{v}_j\right]. \tag{B.12}$$

It is possible to diagonalize each $\mathcal{K}_j$. Let us write

$$\mathbf{v}_j \mathcal{K}_j \mathbf{v}_j = v_j^\alpha \mathcal{K}_{ij}^{\alpha\beta} v_j^\beta, \tag{B.13}$$

where $\alpha, \beta = 1, \ldots, d$ and let's call $\mathbf{w}_j$ the vectors $\mathbf{u}_j$ in the basis in which $\mathcal{K}_j$ is diagonal. Such transformation is also unitary and then:

$$N = \lim_{n\to\infty} \int_{-\infty}^{+\infty} \left[\prod_{i=1}^{n} \prod_{\beta=1}^{d} dw_i^\beta \right] \prod_{j=1}^{n} \prod_{\alpha=1}^{d} \exp\left[-\frac{1}{2V} w_j^\alpha \lambda_j^\alpha w_j^\alpha \right]. \tag{B.14}$$

It is now strightforward to integrate (B.14) using the well known result:

$$N = \int_{-\infty}^{+\infty} dx \exp\left[-\frac{1}{2V} \lambda x^2 \right] = \left(\frac{2\pi V}{\lambda} \right)^{1/2}, \tag{B.15}$$

we obtain the final result

$$N = \lim_{n\to\infty} \prod_{j=1}^{n} \prod_{\alpha=1}^{d} \left(\frac{2\pi V}{\lambda_j^\alpha} \right)^{1/2}. \tag{B.16}$$

Appendix C

Linear response theory

In this appendix we are going to derive the charge induced in a system when we apply an external field. It is a particular result of *linear response theory* in the case of a perturbation that does not depend on time. For a more general derivation, in the context of liquid physics, read e.g. [HM76]. We are going to derive the result in the canonical ensemble, a generalization to the grand-canonical one is straigtforward.

Let us consider a density of particles at $\mathbf{r}$ as

$$\rho(\mathbf{r}) = \sum_{i=1}^{N} \delta(\mathbf{r} - \mathbf{r}_i). \tag{C.1}$$

The average density of particles at $\mathbf{r}$ is

$$\langle \rho(\mathbf{r}) \rangle = \frac{N}{Z_N} \int e^{-\beta V_N} d\mathbf{r}_2 \dots \mathbf{r}_N = \rho^{(1)}(\mathbf{r}), \tag{C.2}$$

where in the last step we have used (6.14) with $n = 1$:

$$\rho_N^{(1)}(\mathbf{r}) = \frac{N}{Z_N} \int e^{-\beta V_N(\mathbf{r}^N)} d\mathbf{r}_2 \dots d\mathbf{r}_N. \tag{C.3}$$

Let us add a small perturbation δV_N to the potential V_N. Therefore the total potential is:

$$V_N^*(\mathbf{r}^N) = V_N(\mathbf{r}^N) + \delta V_N(\mathbf{r}^N). \tag{C.4}$$

The resulting 1-point density can be obtained inserting the new potential (C.4) in (C.3):

$$\rho_N^{(1)*}(\mathbf{r}) = \frac{N}{Z_N^*} \int e^{-\beta V_N(\mathbf{r}^N) + \delta V_N(\mathbf{r}^N)} d\mathbf{r}_2 \dots d\mathbf{r}_N. \tag{C.5}$$

where Z_N^* denotes the perturbed configurational integral. Expanding to first order in δV_N both Z_N^* and the exponent of the integral we obtain:

$$\rho_N^{(1)*}(\mathbf{r}) \simeq \rho_N^{(1)}(\mathbf{r}) \left(1 - \beta \left\langle \delta V_N(\mathbf{r}^N) \right\rangle\right) - \frac{\beta}{Z_N} \int e^{-\beta V_N(\mathbf{r}^N)} \delta V_N(\mathbf{r}^N) d\mathbf{r}_2 \dots d\mathbf{r}_N. \tag{C.6}$$

We can always set $\left\langle \delta V_N(\mathbf{r}^N) \right\rangle$ to zero redefining the energy. We then obtain the average induced charge:

$$\delta\rho_N^{(1)}(\mathbf{r}) = -\beta \left\langle \rho(\mathbf{r})\delta V(\mathbf{r}) \right\rangle , \tag{C.7}$$

where we have used the definition (C.1) to rewrite the integral and

$$\delta\rho_N^{(1)}(\mathbf{r}) = \rho_N^{(1)*}(\mathbf{r}) - \rho_N^{(1)}(\mathbf{r}). \tag{C.8}$$

Note that the average in (C.7) is over the unperturbed states.

Appendix D

The perturbed lattice with $P_{th}(k) = k^n$

D.1 Properties of the expansion of $P_c(\mathbf{k})$

In this appendix we derive analytically a Taylor expansion in powers of k of the exact result (7.14). We divide first the Eq. (7.14) in two terms[1]:

$$P(k) = P_c(k) + P_d(k) \tag{D.1}$$

where

$$P_c(k) = \int_{\mathcal{R}^d} d^d r e^{-i\mathbf{k}\cdot\mathbf{r}} e^{-k^2 d(r)} - (2\pi)^d \delta(\mathbf{k}) \tag{D.2a}$$

$$P_d(k) = \int_{\mathcal{R}^d} d^d r e^{-i\mathbf{k}\cdot\mathbf{r}} e^{-k^2 d(r)} \xi_{in}(\mathbf{r}), \tag{D.2b}$$

where

$$d(r) = g(0) - g(r). \tag{D.3}$$

The term (D.2a) gives the PS in the continuous limit whereas the second one contains the discreteness. In the case of a lattice as pre-initial configuration we have

$$\xi_{in}(\mathbf{r}) = -1 + \sum_{\mathbf{R}} \delta(\mathbf{r} - \mathbf{R}), \tag{D.4}$$

where $\mathbf{R}$ are the lattice positions.

We expand Eq. (D.2a) in a Taylor series about $\mathbf{k} = 0$:

$$P_c(k) = \sum_{m=1}^{\infty} (-k^2)^m \int_{\mathbb{R}^d} d^d r e^{-i\mathbf{k}\cdot\mathbf{r}} [d(x)]^m - (2\pi)^d \delta(\mathbf{k}). \tag{D.5}$$

We will consider a power-law theoretical PS given by Eq. (7.20). We have therefore to distinguish two different cases in function of the exponent n.

[1] For simplicity — and to be able to obtain simple anlytical results — we assume here that the function $g_{ij}(k)$ is diagonal. This assumption does not change qualitatively the final results.

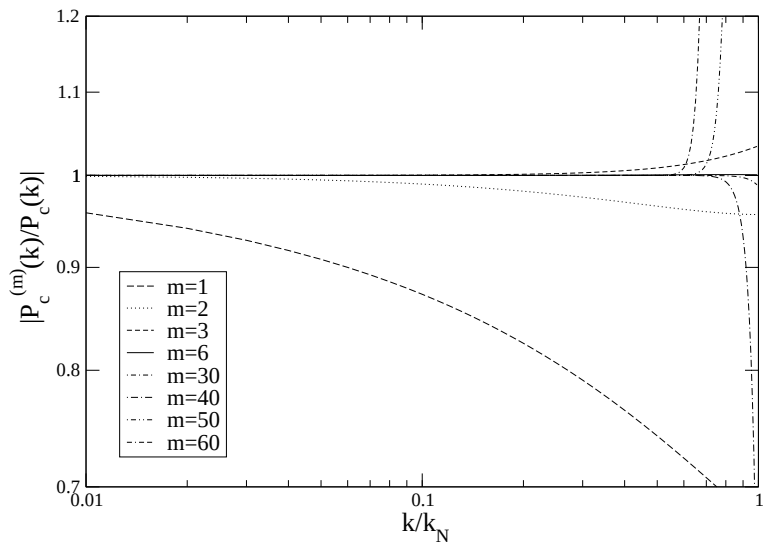

Figure D.1: Ratio of the $m-th$ first terms of the series (D.6) and $P_c(k)$. Observe how the series has converged in the interval considered for $m = 6$ but diverges for $m > 30$.

D.1.1 Case $-d < n < -d + 2$

Because $\tilde{g}(k)$ is a power law, $d(r)$ is also a power law. We have therefore

$$P_c(k) = \sum_{m=1}^{\infty} P_c^{(m)}(k) = \sum_{m=1}^{\infty} A^m a_m k^{m(n+d)-d} - (2\pi)^d \delta(\mathbf{k}), \tag{D.6}$$

where $a_1 = 1$. Note that (D.6) is an *asymptotic expansion*, i.e., its convergence at a given k depends on the number of terms taken in the sum. It means that if an infinite number of terms is taken in Eq. (D.6), the series is *divergent*. However, choosing conveniently, for a given value k, the number of terms gives a very rapidly "convergent" series. This feature can be seen in Fig. D.1, in which is plotted the ratio of the $m - th$ first terms of the series (D.6) and $P_c(k)$. The series converges — in the interval considered — very rapidly to $P_c(k)$ (a feature of asymptotic series) but diverges at smaller and smaller k's for $m > 30$.

It is possible to obtain an analytical expression of the coefficients a_m.

- One dimension:

$$d(x) = -\frac{A}{\pi}\Gamma(n-1)\sin\left(\frac{n\pi}{2}\right)x^{1-n} \tag{D.7}$$

and

$$\begin{aligned} a_m &= -A\frac{2\pi^{-m}}{m!}\sin\left(\frac{1}{2}m\pi(n-1)\right)\Gamma(1+m-mn) \\ &\quad \times\left(\Gamma(n-1)\sin\left(\frac{n\pi}{2}\right)\right)^m. \end{aligned} \tag{D.8}$$

- Three dimension:

$$d(r) = \frac{1}{\pi^2}\Gamma(n)\sin\left(\frac{3n\pi}{2}\right) r^{n-5} \tag{D.9}$$

and

$$\begin{aligned} a_m &= A\frac{2^{2-m}\pi^{1-2m}}{m!}\Gamma(2-m(1+n)) \\ &\times \sin\left(\frac{1}{2}m(n+1)\pi\right)\left(\Gamma(n)\sin\left(\frac{n\pi}{2}\right)\right)^m . \end{aligned} \tag{D.10}$$

Note that for integer values of n the limit of the above expressions has to be taken.

D.1.2 The case $-d+2 < n < 2$

In this case it is not possible to compute simply all the terms of a series like (D.6). However, it is possible to compute very simply the first corrections to $P_{th}(k)$ in the following way. At $\vec{k} \neq \vec{0}$ we have:

$$P_c(k) \simeq k^2\tilde{g}(k) - \frac{k^4}{2!}\int_{\mathbb{R}^d} d^d r[d(r)]^2 e^{-i\mathbf{k}\cdot\mathbf{r}}. \tag{D.11}$$

We are interested in the leading corrections to $P_c(k)$ given by the integral of (D.11). This leading correction is given by the term $-2g(0)g(r)$ of the term $[d(r)]^2$. Doing then the approximation

$$[d(r)]^2 \simeq -2g(0)g(r) \tag{D.12}$$

in Eq. (D.11) we obtain simply:

$$P_c(k) \simeq k^2\tilde{g}(k) - k^4 g(0)\tilde{g}(k). \tag{D.13}$$

The expression g(0) can be simply computed analitically, and gives for the theoretical PS (7.20)

$$g(0) = \frac{Ak_c^{n-1}\Gamma(n-1)}{\pi}, \tag{D.14}$$

in one dimension and

$$g(0) = \frac{Ak_c^{n+1}n\Gamma(n)}{2\pi^2}, \tag{D.15}$$

in three dimensions.

D.2 Corrections to the $P_{th}(k)$ behaviour in the fluid limit

We can write an expression for the scale up to which the theoretical PS $P_{th}(k) = k^2\tilde{g}(k)$ is well represented by the final PS of the discrete distribution.

D.2.1 Case $-d < n < -2 + d$

Using Eq. (D.6), $P_{th}(k)$ is well represented when

$$Ak^n \gg A^2 a_2 k^{2(n+d)-d}, \tag{D.16}$$

i.e., for

$$Aa_2 k^{n+d} \ll 1. \tag{D.17}$$

It can be checked using Eqs. (D.8) or (D.10) that a_m/a_{m-1} is of order unity for small m. We can rewrite Eq. (D.17) in terms of the variance of mass in spheres of the theoretical fluctuations, using the approximation (e.g. [GJSL02, GSLJP05]):

$$\sigma^2(R) = bk^d P_{th}(k)|_{k=R^{-1}}, \tag{D.18}$$

where the coefficient b is of order unity. We can therefore write the condition:

$$\sigma^2(R)|_{k=R^{-1}} \ll 1. \tag{D.19}$$

D.2.2 Case $-2 + d < n < 2$

Using Eq. (D.13) we obtain the condition (in any dimension)

$$g(0)k^2 < 1. \tag{D.20}$$

The PS are generally cut-off at the Nyquist frequency, i.e., $k_c \sim k_N$. If we demand to have the theoretical PS up to the Nyquist frequency, we can rewrite condition (D.20) in function of the variance in mass:

$$\sigma^2(R)|_{k_N=R^{-1}} \ll 1, \tag{D.21}$$

with which we recover condition in real space like in (D.19).

D.3 Discreteness corrections to the PS

It is simple to check also that P_d is subdominant for $|\mathbf{k}| \ll k_N$. Expanding Eq. (D.2b) in powers of k we get:

$$P_d(k) = \sum_{m=0}^{\infty} (-k^2)^m \int_{\mathbb{R}^d} d^d r e^{-i\mathbf{k}\cdot\mathbf{r}} [d(x)]^m \xi_{in}(\mathbf{r}), \tag{D.22}$$

which can be rewritten in function of the PS of the pre-initial distribution as:

$$P_d(k) = \frac{1}{(2\pi)^d} \sum_{m=0}^{\infty} (-k)^{2m} \int_{\mathbb{R}^d} d^d q D^{(m)}(\mathbf{q}) P_{in}(\mathbf{q}+\mathbf{k}), \tag{D.23}$$

where

$$D^{(m)}(\mathbf{k}) := \mathcal{F}[(d(x)^m], \tag{D.24}$$

where $\mathcal{F}$ denotes FT as defined in Eq. (3.12). In the case of a lattice Eq. (D.23) is:

$$P_d(k) = \sum_{m=0}^{\infty} (-k)^{2m} \sum_{\mathbf{q}\neq 0} D^{(m)}(\mathbf{q}+\mathbf{k}), \tag{D.25}$$

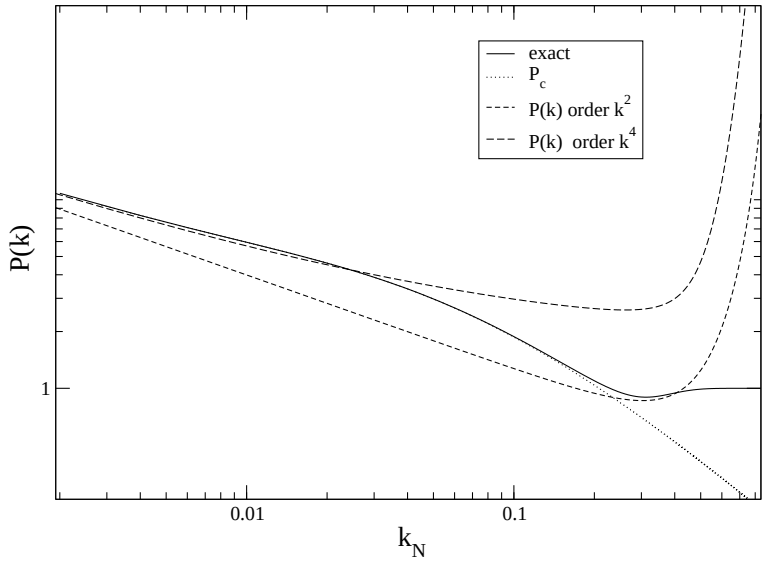

Figure D.2: Comparison of the exact PS, $P_c(k)$, $P_c(k)$ up to order k^2 (i.e. $m = 1$) and $P_c(k)+P_d(k)$ up to the same order, for $n = -1/2$ in one dimansion. Note how the fluid describes well the system up to $k \approx 0.2k_N$. The average relative displacement square at the interparticle scale is $d(\ell) = 0.73$.

where

$$\mathbf{q} = k_N \mathbf{n}, \tag{D.26}$$

where $\mathbf{n}$ are triple integers. The fact that the smallest $\mathbf{q}$ in the sum (D.25) is equal to the Nyquist frequency gives a dominant contribution of the sum as a constant and then

$$P_d(k) \sim k^2. \tag{D.27}$$

It is possible to calculate analytically in one dimension all the terms of the series (D.25). The main dominant contribution at small k is simply:

$$P_d(k) = 2Ak_N^{n-2}\zeta(2-n)k^2 + \mathcal{O}(k^3). \tag{D.28}$$

For example, for $n = -1/2$, $\zeta(5/2) \approx 1.34149$. It is therefore possible to estimate the scale up which the continous limit describe well the system:

$$k \lesssim \left(2k_N^{n-2}\zeta(2-n)\right)^{1/n-2}. \tag{D.29}$$

It is worth to note that the discreteness small k correction does not depend on the amplitude of the PS. For $n = -1/2$, $k \lesssim 4.2$. In three dimensions, the calculations have to be performed numerically.

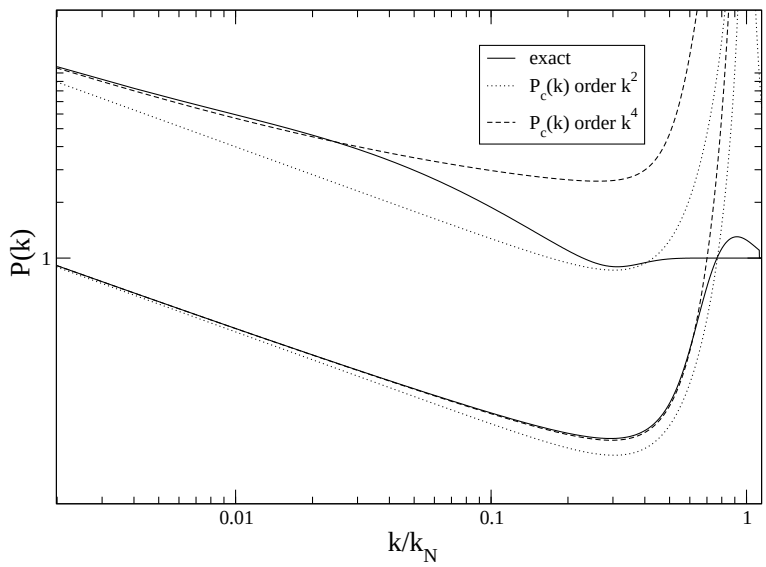

Figure D.3: Comparison of different approximations for $n = -1/2$ and two different amplitudes, with $d(\ell) = 0.73$ and $d(\ell) = 0.23$ respectively.

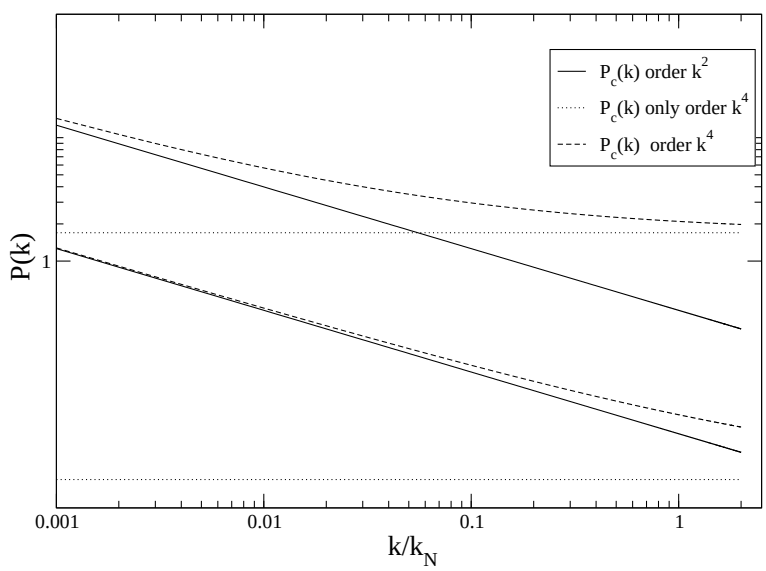

Figure D.4: This plot shows the scale in which the k^4 corrections ($m = 2$) start to be important for $n = -1/2$.

Appendix E

Analytical results in one dimension

In this appendix we present exact results for the PS, variance and correlation function in one dimension.

We recall first the correlation properties of a simple cubic lattice (in d dimensions for generality) which we will take as the "pre-initial" distribution in what follows. For the reduced two point correlation function one has

$$\tilde{\xi}_{lat}(\mathbf{r}_1, \mathbf{r}_2) = \left\langle \overline{\rho(\mathbf{r})\rho(\mathbf{r}')} \right\rangle - 1 = \sum_{\mathbf{l}} \delta\left(\mathbf{r}_1 - \mathbf{r}_2 - \mathbf{l}\right) - 1, \tag{E.1}$$

where $\mathbf{l}$ is a generic displacement vector of the lattice. The expression Eq. (7.25) is simply the Fourier transform of this expression.

Let us now consider the case of one dimension. To compute the variance we use its expression as a function of the PS (see chapter 3):

$$\sigma^2(R) = \frac{1}{2\pi} \int_{-\infty}^{+\infty} dk \left(\frac{\sin(kR)}{kR}\right)^2 P(k) \tag{E.2}$$

or, equivalently, as a function of the correlation function:

$$\begin{aligned} \sigma^2(R) &= \frac{1}{8R^2} \int_{-\infty}^{+\infty} dx\, \tilde{\xi}(x) \times \\ \times \quad & \left[-2x\theta(x) + (x-2R)\theta(x-2R) + (x+2R)\theta(x+2R)\right], \end{aligned} \tag{E.3}$$

where $\theta(x)$ is the Heaviside function. Using Eqs. (E.2) or (E.3) with (7.25) or (E.1) respectively, we obtain the following result for the variance of a lattice with grid spacing equal to unity :

$$\sigma^2_{lat}(R) = \sum_{m=-\infty,\neq 0}^{+\infty} \left(\frac{\sin(2\pi m R)}{2\pi m R}\right)^2. \tag{E.4}$$

As anticipated in section 7.3 we obtain the same limiting behaviour of the variance at large scales as for a homogeneous and isotropic distribution with PS $P(k) \sim k^n$ and $n > 1$ i.e. $\sigma^2(R) \sim 1/R^{d+1}$ with $d = 1$.

We now compute an expression for the PS directly from (7.14), for the case of a one-dimensional system and a "pre-initial" lattice configuration. Using Eq. (E.1) and rearranging terms we obtain:

$$\begin{aligned} P(k) &= \exp(-k^2 g(0)) \sum_{-\infty, l\neq 0}^{+\infty} \delta(k-2\pi l) \\ &+ \sum_{l=-\infty}^{+\infty} e^{-ikl}[\exp(-k^2 d(l))) - \exp(-k^2 g(0))], \end{aligned} \tag{E.5}$$

where $d(x) \equiv g(0) - g(x)$. The first term on the right hand side of Eq. (E.5) contains all the divergent terms in the PS. The second term is a regular function of k which has the behaviour $P(k) \sim k^2 g(k)$ at small k if $g(k) \sim k^\alpha$ with $\alpha < 0$ and $P(k) \sim k^2$ if $\alpha > 0$, unless $\sum_{l=-\infty}^{+\infty} g(l) = 0$, in which case $P(k) \sim k^2 g(k)$ also for $\alpha > 0$.

Performing a Fourier transform of Eq. (7.14) we obtain the correlation function in the form

$$\begin{aligned} \tilde{\xi}(x) &= \frac{1}{2\pi} \int_{-\infty}^{+\infty} dx' \sqrt{\frac{\pi}{d(x')}} e^{-(x-x')^2/4d(x')} \times \\ &\times \left(1 + \tilde{\xi}_{in}(x')\right) - 1. \end{aligned} \tag{E.6}$$

Note that in the limit that no displacements are applied (i.e. $d(x) \to 0$), the argument of the integral is $\delta(x - x')$. Thus we recover explicitly for small displacements $\tilde{\xi}(x) \simeq \tilde{\xi}_{in}(x) + \ldots$. Substituting Eq. (E.1) in Eq. (E.6) we then obtain the result for the specific case of a "pre-initial" lattice configuration:

$$\tilde{\xi}(x) = -1 + \sum_{l=-\infty}^{+\infty} \sqrt{\frac{1}{4\pi d(l)}} e^{-(x-l)^2/4d(l)}. \tag{E.7}$$

To obtain the variance we use the same procedure. Using, for example, Eq. (E.2) with Eq. (7.14) we get:

$$\begin{aligned} \sigma^2(R) &= -1 + \frac{1}{4\sqrt{\pi}R^2} \int_{-\infty}^{+\infty} dx\, (1 + \tilde{\xi}_{in}(x)) \sqrt{d(x)} \times \\ &\times [h(x, 2R) + h(x, -2R) - 2h(x, 0)] \\ &+ \frac{1}{8R^2} \int_{-\infty}^{+\infty} dx\, (1 + \tilde{\xi}_{in}(x)) \times \\ &\times [-2f(x, x) + f(x - 2R, x) + f(x + 2R, x)] \end{aligned} \tag{E.8}$$

where

$$f(x, y) = x \operatorname{erf}\left(\frac{x}{2\sqrt{d(y)}}\right), \; h(x, y) = e^{\frac{-(x+y)^2}{4d(x)}}. \tag{E.9}$$

Expanding at small $d(x)$ it is possible to obtain also explicitly an expression of the form $\sigma^2(R) = \sigma^2_{lat}(R) + \ldots$. In the specific case of an initial lattice distribution the variance can be written:

$$
\begin{aligned}
& \sigma^2(R) = -1 + \frac{1}{4\sqrt{\pi}R^2} \sum_{l=-\infty}^{+\infty} \sqrt{d(l)} \times \\
\times \quad & [h(l,2R) + h(l,-2R) - 2h(l,0)] \qquad \text{(E.10)} \\
+ \quad & \frac{1}{8R^2} \sum_{l=-\infty}^{+\infty} \left[-2f(l,l) + f(l-2R,l) + f(l+2R,l)\right].
\end{aligned}
$$

Appendix F

Ewald sum of the dynamical matrix $\mathcal{D}(\mathbf{R})$

The Ewald sum for the dynamical matrix is given from (9.17) using the Ewald sum for the potential (9.39):

$$\mathcal{D}(\mathbf{R}) = \mathcal{D}^{(r)}(\mathbf{R}) + \mathcal{D}^{(k)}(\mathbf{R}) \tag{F.1}$$

with

$$\begin{aligned}
\mathcal{D}^{(r)}_{\mu\nu}(\mathbf{R} \neq \mathbf{0}) &= -Gm \sum_{\mathbf{n}} \left[\frac{(\mathbf{R} - \mathbf{n}L)_\mu (\mathbf{R} - \mathbf{n}L)_\nu}{|\mathbf{R} - \mathbf{n}L|^2} \right] \\
&\times \frac{4\alpha^3}{\sqrt{\pi}} \exp(-\alpha^2 |\mathbf{R} - \mathbf{n}L|^2) \\
&+ Gm \sum_{\mathbf{n}} \left[\frac{\delta_{\mu\nu}}{|\mathbf{R} - \mathbf{n}L|^3} - 3 \frac{(\mathbf{R} - \mathbf{n}L)_\mu (\mathbf{R} - \mathbf{n}L)_\nu}{|\mathbf{R} - \mathbf{n}L|^5} \right] \\
&\times \left[\mathrm{erfc}(\alpha |\mathbf{R} - \mathbf{n}L|) + \frac{2\alpha}{\sqrt{\pi}} \exp(-\alpha^2 |\mathbf{R} - \mathbf{n}L|^2) |\mathbf{R} - \mathbf{n}L| \right]
\end{aligned} \tag{F.2}$$

and

$$\mathcal{D}^{(k)}_{\mu\nu}(\mathbf{R}) = \frac{4\pi Gm}{V_B} \sum_{\mathbf{k} \neq 0} \frac{1}{|\mathbf{k}|^2} \exp\left(-\frac{|\mathbf{k}|^2}{4\alpha^2} \right) \cos(\mathbf{k} \cdot \mathbf{R})\, k_\mu k_\nu. \tag{F.3}$$

The $\mathbf{R} = 0$ term is

$$\mathcal{D}(\mathbf{R} = \mathbf{0}) = -\sum_{\mathbf{R} \neq \mathbf{0}} \mathcal{D}(\mathbf{R}). \tag{F.4}$$

Note that, by symmetry, only the first term of the r.h.s. of (F.2) and Eq. (F.3) contribute in the sum of Eq. (F.4). In the case of pure gravity the result of the sum (F.4) is given by Eq. (9.20).

Appendix G

Kohn sum rule

We derive here the Kohn sum rule (9.53). Multiplying Eq. (9.51) by $(\hat{\mathbf{e}}_n(\mathbf{k}))_\mu(\hat{\mathbf{e}}_n(\mathbf{k}))_\nu$ and summing over n, μ and ν we obtain, with Eq. (9.28):

$$\begin{aligned}\sum_{n=1}^{3}\omega_n^2(\mathbf{k}) &= -n_0\sum_{n=1}^{3}\Bigg\{\tilde{w}(\mathbf{k})(\mathbf{k}\cdot\hat{\mathbf{e}}_n(\mathbf{k}))^2+\sum_{\mathbf{K}\neq 0}\tilde{w}(\mathbf{k}+\mathbf{K})\left[(\mathbf{k}+\mathbf{K})\cdot\hat{\mathbf{e}}_n(\mathbf{k})\right]^2 \\ &\quad -\sum_{\mathbf{K}\neq 0}\tilde{w}(\mathbf{K})\left[\mathbf{K}\cdot\hat{\mathbf{e}}_n(\mathbf{k})\right]^2\Bigg\}. \qquad \text{(G.1)}\end{aligned}$$

Using the orthogonality relation

$$\sum_{n=1}^{3}(\hat{\mathbf{e}}_n(\mathbf{k}))_\mu(\hat{\mathbf{e}}_n(\mathbf{k}))_\nu=\delta_{\mu\nu}, \qquad \text{(G.2)}$$

we get finally [Pin63]

$$\sum_{i=1}^{3}\omega_n^2(\mathbf{k})=-n_0k^2\tilde{w}(\mathbf{k})-n_0\sum_{\mathbf{K}\neq 0}\left(|\mathbf{k}+\mathbf{K}|^2\tilde{w}(\mathbf{k}+\mathbf{K})-K^2\tilde{w}(\mathbf{K})\right). \qquad \text{(G.3)}$$

In the case of gravity, using the same approximation as in Eq. (9.52) we conclude that

$$\sum_{n=1}^{3}\omega_n^2(\mathbf{k})=-n_0k^2\tilde{w}(\mathbf{k})=4\pi G\rho_0. \qquad \text{(G.4)}$$

Appendix H

Small k expansion of the dynamical matrix

Expanding Eq. (9.51) in Taylor series, up to order $(k/K)^2$, for a potential $v(\mathbf{r}) = -Gm/r$, with the approximation (9.52), we get:

$$\begin{aligned}\tilde{\mathcal{D}}_{\mu\nu}(\mathbf{k}) &= 4\pi G\rho_0 \frac{k_\mu k_\nu}{k^2} \\ &+ 4\pi G\rho_0 \sum_{\mathbf{K}\neq\mathbf{0}} \frac{1}{K^2}\left[k_\mu k_\nu - 2(k_\mu K_\nu + k_\nu K_\mu)\frac{\mathbf{k}\cdot\mathbf{K}}{K^2}\right. \\ &\qquad \left. + K_\mu K_\nu \left(-\frac{k^2}{K^2} + 4\frac{(\mathbf{k}\cdot\mathbf{K})^2}{K^4}\right)\right],\end{aligned} \tag{H.1}$$

where the terms linear in k cancel by symmetry. The expression (H.1) can be written for elements $\mu = \nu = 1$, for example, as

$$\tilde{\mathcal{D}}_{11}(\mathbf{k}) = 4\pi G\rho_0 \frac{k_1^2}{k^2} + 4\pi G\rho_0 k^2 \left(c_a + c_b \frac{k_1^2}{k^2} + c_c \frac{k_2^2 + k_3^2}{k^2}\right), \tag{H.2}$$

where

$$c_a = -\sum_{\mathbf{K}\neq 0} \frac{K_1^2}{K^4} \tag{H.3a}$$

$$c_b = \sum_{\mathbf{K}\neq 0} \frac{1}{K^2}\left(1 - 4\frac{K_1^2}{K^2} + 4\frac{K_1^4}{K^4}\right) \tag{H.3b}$$

$$c_c = 4\sum_{\mathbf{K}\neq 0} \frac{K_1^2 K_2^2}{K^4} = 4\sum_{\mathbf{K}\neq 0} \frac{K_1^2 K_3^2}{K^4}. \tag{H.3c}$$

The coefficients c_i depend on the lattice considered and have to be computed numerically. To ensure numerical convergence, it is necessary to write an Ewald sum for the Eq. (H.2). The non-diagonal elements of the dynamical matrix are:

$$\tilde{\mathcal{D}}_{12}(\mathbf{k}) = 4\pi G\rho_0 \frac{k_1 k_2}{k^2} + 4\pi G\rho_0 c_d k^2 \frac{k_1 k_2}{k^2}, \tag{H.4}$$

where

$$c_d = \sum_{\mathbf{K}\neq 0} \frac{1}{K^2}\left(1 - \frac{2}{K^2}(K_1^2 + K_2^2) + 8\frac{K_1^2 K_2^2}{K^4}\right). \tag{H.5}$$

From this derivation we see that the exact expression for the small k behavior of the dynamical matrix is very complicated in general and has to be computed numerically. In addition, it depends on the kind of lattice considered.

Appendix I

Gravitational Evolution of a Perturbed Lattice and its Fluid Limit

Gravitational Evolution of a Perturbed Lattice and its Fluid Limit

M. Joyce
Laboratoire de Physique Nucléaire et de Hautes Energies, Université de Paris VI, 4, Place Jussieu, Tour 33 -RdC, 75252 Paris Cedex 05, France

B. Marcos
Laboratoire de Physique Théorique, Université de Paris XI, Bâtiment 210, 91405 Orsay, France

A. Gabrielli
SMC-INFM & ISC-CNR, Dipartimento di Fisica, Università "La Sapienza", P.le A. Moro 2, I-00185 Rome, Italy

T. Baertschiger
Dipartimento di Fisica, Università "La Sapienza", P.le A. Moro 2, I-00185 Rome, Italy

F. Sylos Labini
"E. Fermi" Center, Via Panisperna 89 A, Compendio del Viminale, 00184 - Rome, Italy
(Received 8 April 2005; published 30 June 2005)

We apply a simple linearization, well known in solid state physics, to approximate the evolution at early times of cosmological N-body simulations of gravity. In the limit that the initial perturbations, applied to an infinite perfect lattice, are at wavelengths much greater than the lattice spacing l, the evolution is exactly that of a pressureless self-gravitating fluid treated in the analogous (Lagrangian) linearization, with the Zeldovich approximation as a subclass of asymptotic solutions. Our less restricted approximation allows one to trace the evolution of the *discrete* distribution until the time when particles approach one another (i.e., "shell crossing"). We calculate modifications of the fluid evolution, explicitly dependent on l, i.e., discreteness effects in the N-body simulations. We note that these effects become increasingly important as the initial redshift is increased at fixed l.

DOI: 10.1103/PhysRevLett.95.011304 PACS numbers: 98.80.−k, 95.10.Ce

In current cosmological theories the physics of structure formation in the universe reduces, over a large range of scales, to understanding the evolution of clustering under Newtonian gravity, with only a simple modification of the dynamical equations due to the expansion of the Universe. The primary instrument for solving this problem is numerical N-body simulation (NBS, see, e.g., [1]). These simulations are very widely started from configurations which are simple cubic (sc) lattices perturbed in a manner prescribed by a theoretical cosmological model. In this Letter we observe that, up to a change in sign in the force, this initial configuration is identical to the Coulomb lattice (or Wigner crystal) in solid state physics (see, e.g., [2]), and we exploit this analogy to develop an approximation to the evolution of these simulations. We show that one obtains, for long-wavelength perturbations, the evolution predicted by an analogous fluid description of the self-gravitating system, and, in particular, as a special case, the Zeldovich approximation [3]. Further, we can study precisely the deviations from this fluidlike behavior at shorter wavelengths arising from the discrete nature of the system. This analysis should be a useful step towards a precise quantitative understanding, which is currently lacking, of the role of discreteness in cosmological NBS (see, e.g., [4–6]). One simple conclusion, for example, is that a body centered cubic (bcc) lattice may be a better choice of discretization, as its spectrum has only growing modes with exponents bounded above by fluid linear theory.

The equation of motion of particles moving under their mutual self-gravity is [1]

$$\ddot{\mathbf{x}}_i + 2H(t)\dot{\mathbf{x}}_i = -\frac{1}{a^3}\sum_{i\neq j}\frac{Gm_j(\mathbf{x}_i - \mathbf{x}_j)}{|\mathbf{x}_i - \mathbf{x}_j|^3}. \qquad (1)$$

Here dots denote derivatives with respect to time t, $\mathbf{x}_i$ is the comoving position of the ith particle, of mass m_i, related to the physical coordinate by $\mathbf{r}_i = a(t)\mathbf{x}_i$, where $a(t)$ is the scale factor of the background cosmology with Hubble constant $H(t) = \frac{\dot{a}}{a}$. We treat a system of N point particles, of equal mass m, initially placed on a Bravais lattice, with periodic boundary conditions. Perturbations from the Coulomb lattice are described simply by Eq. (1), with $a(t) = 1$ and $Gm^2 \to -e^2$ (where e is the electronic charge). As written in Eq. (1), the infinite sum giving the force on a particle is not explicitly well defined. It is calculated by solving the Poisson equation for the potential, with the mean mass density subtracted in the source term. In the cosmological case this is appropriate as the effect of the mean density is absorbed in the Hubble expansion; in the case of the Coulomb lattice it corresponds to the assumed presence of an oppositely charged neutralizing background.

We consider now perturbations about the perfect lattice. It is convenient to adopt the notation $\mathbf{x}_i(t) = \mathbf{R} + \mathbf{u}(\mathbf{R}, t)$ where $\mathbf{R}$ is the lattice vector of the ith particle (which we can consider as its Lagrangian coordinate), and $\mathbf{u}(\mathbf{R}, t)$ is the displacement of the particle from $\mathbf{R}$. Expanding to linear order in $\mathbf{u}(\mathbf{R}, t)$ about the equilibrium lattice configuration (in which the force on each particle is exactly zero), we obtain

$$\ddot{\mathbf{u}}(\mathbf{R}, t) + 2H\dot{\mathbf{u}}(\mathbf{R}, t) = -\frac{1}{a^3}\sum_{\mathbf{R}'}\mathcal{D}(\mathbf{R} - \mathbf{R}')\mathbf{u}(\mathbf{R}', t). \quad (2)$$

The matrix $\mathcal{D}$ is known in solid state physics, for any interaction, as the *dynamical matrix* (see, e.g., [2]). For gravity we have $\mathcal{D}_{\mu\nu}(\mathbf{R} \neq \mathbf{0}) = Gm(\frac{\delta_{\mu\nu}}{R^3} - 3\frac{R_\mu R_\nu}{R^5})$ (where $\delta_{\mu\nu}$ is the Kronecker delta), and $\mathcal{D}_{\mu\nu}(\mathbf{0}) = -\Sigma_{\mathbf{R}\neq\mathbf{0}}\mathcal{D}_{\mu\nu}(\mathbf{R})$ [7].

From the Bloch theorem for lattices it follows that $\mathcal{D}$ is diagonalized by plane waves in reciprocal space. Defining the Fourier transform by $\tilde{\mathbf{u}}(\mathbf{k}, t) = \Sigma_{\mathbf{R}} e^{-i\mathbf{k}\cdot\mathbf{R}}\mathbf{u}(\mathbf{R}, t)$ and its inverse as $\mathbf{u}(\mathbf{R}, t) = \frac{1}{N}\Sigma_{\mathbf{k}} e^{i\mathbf{k}\cdot\mathbf{R}}\tilde{\mathbf{u}}(\mathbf{k}, t)$ (where the sum is over the first Brillouin zone), Eq. (2) gives

$$\ddot{\tilde{\mathbf{u}}}(\mathbf{k}, t) + 2H(t)\dot{\tilde{\mathbf{u}}}(\mathbf{k}, t) = -\frac{1}{a^3}\tilde{\mathcal{D}}(\mathbf{k})\tilde{\mathbf{u}}(\mathbf{k}, t) \quad (3)$$

where $\tilde{\mathcal{D}}(\mathbf{k})$, the Fourier transform (FT) of $\mathcal{D}(\mathbf{R})$, is a symmetric 3×3 matrix for each $\mathbf{k}$. Diagonalizing it, one can determine, for each $\mathbf{k}$, three orthonormal eigenvectors $\mathbf{e}_n(\mathbf{k})$ and their eigenvalues $\omega_n^2(\mathbf{k})$ ($n = 1, 2, 3$), which obey [2] the Kohn sum rule $\Sigma_n \omega_n^2(\mathbf{k}) = -4\pi G\rho_0$, where ρ_0 is the mean mass density.

Given the initial displacements and velocities at a time $t = t_0$, the dynamical evolution is then given as

$$\mathbf{u}(\mathbf{R}, t) = \frac{1}{N}\Sigma_{\mathbf{k}}\Sigma_n[\tilde{\mathbf{u}}(\mathbf{k}, t_0)\cdot\hat{\mathbf{e}}_n(\mathbf{k})U_n(\mathbf{k}, t) + \dot{\tilde{\mathbf{u}}}(\mathbf{k}, t_0)\cdot\hat{\mathbf{e}}_n(\mathbf{k})V_n(\mathbf{k}, t)]\hat{\mathbf{e}}_n(\mathbf{k})e^{i\mathbf{k}\cdot\mathbf{R}} \quad (4)$$

where $U_n(\mathbf{k}, t)$ and $V_n(\mathbf{k}, t)$ are a set of linearly independent solutions of the mode equations

$$\ddot{f} + 2H\dot{f} = -\frac{\omega_n^2(\mathbf{k})}{a^3}f, \quad (5)$$

chosen so that $U_n(\mathbf{k}, t_0) = 1$, $\dot{U}_n(\mathbf{k}, t_0) = 0$, $V_n(\mathbf{k}, t_0) = 0$, $\dot{V}_n(\mathbf{k}, t_0) = 1$.

Shown in Fig. 1 are the eigenvalues of the dynamical matrix for gravity, on a 16^3 sc lattice, determined numerically by applying the linearization to a standard Ewald summation of the gravitational force (see, e.g., [8]). For convenience, the eigenvalues have been normalized, with $\epsilon_n(\mathbf{k}) = -\frac{\omega_n^2(\mathbf{k})}{4\pi G\rho_0}$, and they are plotted, as a function of the modulus $k \equiv |\mathbf{k}|$, normalized to the Nyquist frequency $k_N = \pi/l$, where l is the lattice spacing. This diagonalization can be performed rapidly even for the largest lattices used in current cosmological NBS, but the figure remains essentially unchanged except for an increase in the density

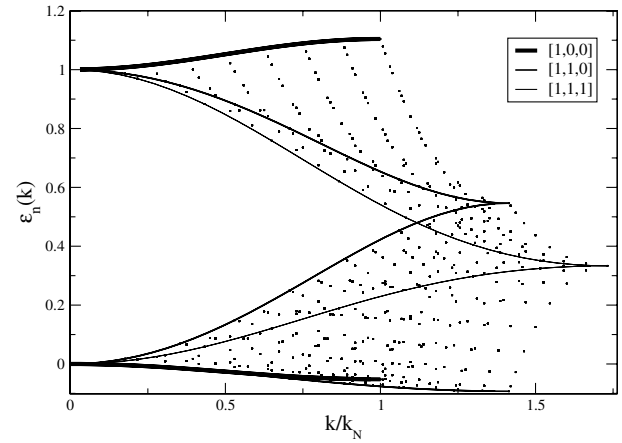

FIG. 1. Eigenvalues $\epsilon_n(\mathbf{k})$ for a sc lattice. The lines connect eigenvectors with $\mathbf{k}$ in the specific directions indicated. Note that the two acoustic branches are degenerate in the $[1, 0, 0]$ and $[1, 1, 1]$ directions.

of the eigenvalues. The lines in the figure connect the eigenvectors along some specific chosen directions, making the characteristic branch structure of the eigenvectors evident. It can be shown [2] that $\mathcal{D}_{\mu\nu}(\mathbf{k} \to 0) = -\hat{k}_\mu\hat{k}_\nu 4\pi G\rho_0$ (where $\hat{\mathbf{k}} = \mathbf{k}/k$), so the branch with the eigenvalue tending to $-4\pi G\rho_0$ is longitudinal (in this limit). In the Coulomb lattice this is the *optical* branch, describing oscillations with plasma frequency $\omega_p^2 = 4\pi e^2 n_0/m$ (where n_0 is the electronic number density). There are then also two *acoustic* branches with eigenvalues tending to zero as $k \to 0$ and which become purely transverse in this limit. A striking feature of Fig. 1 is that there are eigenvectors with $\epsilon_n(\mathbf{k}) < 0$, which correspond to negative eigenvalues $\omega_n^2(\mathbf{k})$, i.e., unstable modes for the Coulomb system, with solutions to Eq. (5) $U_n(\mathbf{k}, t) = \cosh(|\omega_n(\mathbf{k})|t)$ and $V_n(\mathbf{k}, t) = (1/|\omega_n(\mathbf{k})|)\sinh(|\omega_n(\mathbf{k})|t)$ (taking $a = 1$ and $t_0 = 0$). Thus the sc Coulomb lattice is unstable to perturbations, which is not an unexpected result: the ground state of this classical system is known to be the bcc lattice [9], and these unstable modes in the sc lattice correspond to instabilities towards such lower energy configurations. For the case of gravity, in a static universe, these modes are sinusoidally oscillating, while the modes $\epsilon_n(\mathbf{k}) > 0$ describe the expected exponential instabilities. Note further that, since the Kohn sum rule can be written $\Sigma_n \epsilon_n(\mathbf{k}) = 1$, the appearance of modes with $\epsilon_n(\mathbf{k}) > 1$ is only possible when there are modes with $\epsilon_n(\mathbf{k}) < 0$. We can thus conclude that a bcc lattice will have only unstable modes in the case of gravity, and that $\epsilon_n(\mathbf{k}) \leq 1$. We will return to this point below.

The damping term coming from the expansion of the universe modifies these solutions to Eq. (5). For the case of an Einstein–de Sitter (EdS, flat matter dominated) universe, for which $H^2(t) = \frac{8\pi G\rho_0}{3a^3}$ and thus $a = (t/t_0)^{2/3}$, we find

$$U_n(\mathbf{k}, t) = \frac{\alpha_n^+(\mathbf{k})(t/t_0)^{\alpha_n^-(\mathbf{k})} + \alpha_n^-(\mathbf{k})(t/t_0)^{-\alpha_n^+(\mathbf{k})}}{\alpha_n^+(\mathbf{k}) + \alpha_n^-(\mathbf{k})},$$
$$V_n(\mathbf{k}, t) = t_0 \frac{(t/t_0)^{\alpha_n^-(\mathbf{k})} - (t/t_0)^{-\alpha_n^+(\mathbf{k})}}{\alpha_n^+(\mathbf{k}) + \alpha_n^-(\mathbf{k})}, \tag{6}$$

where $\alpha_n^\pm(\mathbf{k}) = \frac{1}{6}[\sqrt{1 + 24\epsilon_n(\mathbf{k})} \pm 1]$. Thus for $\epsilon_n(\mathbf{k}) > 0$ there are, as in the static case, both a growing and a decaying solution. For $\epsilon_n(\mathbf{k}) < 0$ the solutions are all power-law decaying. For $\epsilon_n(\mathbf{k}) < -\frac{1}{24}$, there is a weak remnant of the static universe oscillating behavior: $\alpha_n^\pm(\mathbf{k})$ are then complex, and it is simple to show that the mode functions are a product of a power law $(t/t_0)^{-1/6}$ and a sinusoidal oscillation periodic in the logarithm of the evolution time $\ln(t/t_0)$.

Let us now consider the case that the initial fluctuations contain only modes such that $kl \ll 1$. We have then simply for each $\mathbf{k}$ the longitudinal mode $\mathbf{e}_1(\mathbf{k}) = \hat{\mathbf{k}}$, with $\epsilon_1(\mathbf{k}) = 1$, and two transverse modes with zero eigenvalues. Using the corresponding mode functions from Eq. (6) and (4), a simple calculation shows that

$$\mathbf{u}(\mathbf{R}, t) = \mathbf{u}_\perp(\mathbf{R}, t_0) + \mathbf{u}_\parallel(\mathbf{R}, t_0)\left[\frac{3}{5}\left(\frac{t}{t_0}\right)^{2/3} + \frac{2}{5}\left(\frac{t}{t_0}\right)^{-1}\right] + \mathbf{v}_\parallel(\mathbf{R}, t_0)t_0\left[\frac{3}{5}\left(\frac{t}{t_0}\right)^{2/3} - \frac{3}{5}\left(\frac{t}{t_0}\right)^{-1}\right] + \mathbf{v}_\perp(\mathbf{R}, t_0)3t_0\left[1 - \left(\frac{t}{t_0}\right)^{-1/3}\right] \tag{7}$$

where we have decomposed the particle displacements and peculiar velocities $[\mathbf{v}(\mathbf{R}, t) \equiv \dot{\mathbf{r}}_i - H\mathbf{r}_i = a\dot{\mathbf{u}}(\mathbf{R}, t)]$ into an irrotational (curl-free) part $\mathbf{a}_\parallel(\mathbf{R}) = \frac{1}{N}\Sigma_\mathbf{k}[\mathbf{a}(\mathbf{R}) \cdot \hat{\mathbf{k}}]\hat{\mathbf{k}}e^{i\mathbf{k}\cdot\mathbf{R}}$, and a rotational part $\mathbf{a}_\perp = \mathbf{a} - \mathbf{a}_\parallel$. Using the definition of the peculiar gravitational acceleration $\mathbf{g}(\mathbf{R}, t) \equiv \ddot{\mathbf{r}}_i - \frac{\ddot{a}}{a}\mathbf{r}_i = a[\ddot{\mathbf{u}} + 2H\dot{\mathbf{u}}]$, it is simple to show, using Eq. (2), that $\mathbf{g}(\mathbf{R}, t_0) = 4\pi G\rho_0\mathbf{u}_\parallel(\mathbf{R}, t_0) = \frac{2}{3t_0^2}\mathbf{u}_\parallel(\mathbf{R}, t_0)$. Using this expression in Eq. (7), the displacement of each particle with respect to its initial position [i.e., $\mathbf{u}(\mathbf{R}, t) - \mathbf{u}(\mathbf{R}, t_0)$] can be written solely in terms of the initial gravitational field $\mathbf{g}(\mathbf{R}, t_0)$ and the components of the initial peculiar velocity, $\mathbf{v}_\perp(\mathbf{R}, t_0)$ and $\mathbf{v}_\parallel(\mathbf{R}, t_0)$. It is then easy to verify that the solution in Eq. (7) corresponds exactly to that derived in [10], from a linearization of the Lagrangian equations for a self-gravitating fluid, for the displacements of fluid elements with respect to their Lagrangian coordinates [11]. As discussed in [10] there are several limits of this expression which correspond to the so-called Zeldovich approximation (ZA), which assumes [3] a decomposition of $\mathbf{u}(\mathbf{R}, t)$ into a product of a function of time and a single vector field defined at $\mathbf{R}$. The most commonly used form of this approximation takes $\mathbf{u}_\perp(\mathbf{R}, t_0) = 0 = \mathbf{v}_\perp(\mathbf{R}, t)$ and $\mathbf{u}_\parallel(\mathbf{R}, t_0) = \frac{3}{2}\mathbf{v}_\parallel(\mathbf{R}, t_0)t_0$. This corresponds to setting the coefficients of all but the growing mode in Eq. (7) to zero, i.e., it imposes directly the asymptotic behavior of the general solution. We then have simply $\mathbf{u}(\mathbf{R}, t) = \frac{3}{2}\mathbf{g}(\mathbf{R}, t_0)t_0^2(t/t_0)^{2/3}$ which is precisely the solution used standardly in setting up initial conditions for cosmological NBS (e.g., [1]).

This result provides a direct analytical derivation explaining precisely the well documented success (see, e.g., [12]) of the ZA in describing the evolution of cosmological NBS, in particular, in "truncated" forms of the approximation in which initial short wavelength power is filtered [13]. The eigenvectors and the spectrum of eigenvalues contain, however, much more than this fluid limit. The expression Eq. (4) gives an approximation to the full early time evolution of any perturbed lattice, treated as a full discrete N-body system. It therefore includes *all* modifications of the theoretical fluid evolution in its regime of validity, which extends up to the time when particles approach one another (i.e., up to close to shell crossing). We will report elsewhere detailed comparisons in numerical simulations of this approximation with the ZA and its improvements. In the rest of this Letter we consider the quantification of the discreteness corrections to the pure fluid limit described by our approximation.

Assuming still an EdS universe, and that the initial perturbations are set up in the standard manner using the ZA, as described above, it follows directly from Eq. (4) that $\tilde{u}_\mu(\mathbf{k}, t) = \Sigma_\nu \mathcal{A}_{\mu\nu}(\mathbf{k}, t)\tilde{u}_\nu(\mathbf{k}, t_0)$, where $\mathcal{A}_{\mu\nu}(\mathbf{k}, t) = \Sigma_n[U_n(t) + \frac{2}{3t_0}V_n(t)](\hat{\mathbf{e}}_n)_\mu(\hat{\mathbf{e}}_n)_\nu$ ($\mathbf{k}$ dependences implicit). The full linearized evolution is encoded in this matrix, which can be calculated straightforwardly for any given lattice once the eigenvalues and eigenvectors have been found. One can then determine directly, e.g., the power spectrum (PS) of the displacement fields $S_{\mu\nu}(\mathbf{k}, t) \equiv \tilde{u}_\mu(\mathbf{k}, t)\tilde{u}_\nu^*(\mathbf{k}, t)$. Given S one can then calculate, by the method developed in [14], the PS of the density field for the full point distribution. For small displacements (compared to l), and neglecting the terms describing the discreteness of the lattice, it is a good approximation to use the continuity equation which gives $\delta\tilde{\rho}(\mathbf{k}, t) \approx -i\mathbf{k} \cdot \tilde{\mathbf{u}}(\mathbf{k}, t)$, where $\delta\tilde{\rho}(\mathbf{k}, t)$ is the FT of the density fluctuation field. It follows that $P(\mathbf{k}, t) \approx A_P^2(\mathbf{k}, t)P(\mathbf{k}, t_0)$ where $A_P(\mathbf{k}, t) = \Sigma_{\mu,\nu}\hat{k}_\mu\hat{k}_\nu\mathcal{A}_{\mu\nu}(\mathbf{k}, t)$ and $P(\mathbf{k}, t) \propto |\delta\tilde{\rho}(\mathbf{k}, t)|^2$ is the PS of the density fluctuations. It is simple to verify that in the fluid limit discussed above ($kl \to 0$) one obtains, as expected, $A_P^2(\mathbf{k}, t) = a^2(t)$.

In Fig. 2 is shown this amplification factor $A_P^2(\mathbf{k}, t)$, divided by a^2. The scale factor chosen is $a = 5$, a value at which typical NBS reach shell crossing. Deviations from unity are a direct measure of the modification of the theoretical evolution introduced by the discretization. Note that $A_P^2(\mathbf{k}, a)$ is plotted as a function of k, each point corresponding to a different value of $\mathbf{k}$. The fact that the evolution depends on the orientation of the vector $\mathbf{k}$ is a manifestation of the breaking of rotational invariance by the lattice discretization. The three different symbols for

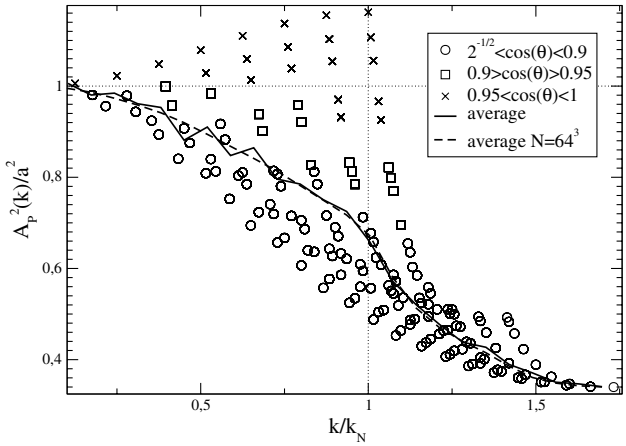

FIG. 2. Amplification function $A_P^2(\mathbf{k}, t)$ for the power spectrum, divided by the fluid limit amplification (a^2), at $a = 5$, for a sc lattice. See text for details.

the points correspond to three different intervals of the cosine of the minimum angle θ between the vector $\mathbf{k}$ and one of the axes of the lattice. We thus see that the largest eigenvalues correspond to modes describing motion parallel to one of the axes of the lattice. For a N^3 lattice and N even, for instance, the largest eigenvalue, with a growth law $\propto a^{1.06}$, is a longitudinal mode with $k = k_N$ and $\mathbf{k}$ parallel to the axes of the lattice, which describes the motion of pairs of adjacent infinite planes towards one another. Also shown in the figure is an average of $A_P^2(\mathbf{k}, a)$ over 25 bins of equal width in k, both for the 16^3 lattice from which the points have been calculated, and for a larger 64^3 lattice.

We thus see that there are qualitatively two kinds of effects introduced by the discretization: (i) an average slowing down of the growth of the modes relative to the theoretical fluid evolution, and (ii) a pronounced anistropy in k space. There are notably a small fraction of modes (approximately 2.5%) with growth exponents larger than in linear fluid theory (which, for sufficiently large a, will always dominate the evolution). We can conclude, however, as foreshadowed in the discussion above, that this evidently undesirable feature of the sc lattice discretization can be circumvented by employing a bcc lattice. The known stability of this configuration of the Coulomb lattice [9] implies that the fluid exponent is in this case an upper bound for all modes (and that there are no oscillating modes for the case of gravity). Further, the bcc crystal is more isotropic (and indeed more compact [15]), than the sc lattice, and thus we would expect the effects of breaking of isotropy to be less pronounced. The average slowing down of the growth of the modes, by an amount which depends on the time and the dimensionless product kl (at $a = 5$, as seen in Fig. 2, a 10% effect at half the Nyquist frequency), on the other hand, would be expected to be a common feature of any discretization (e.g., using "glassy" configurations [16], or the discretization developed in [17]).

One important implication which we highlight is the following: the discrepancy between the fluid and full evolution grows, up to shell crossing, with time. *Thus, for a given physical scale, discreteness effects increase when the starting time of the simulation is decreased*. This implies that at least one of the conditions for keeping discreteness effects under control in an NBS will be, for a fixed discretization scale, that the starting redshift be greater than some value. We note that the initial redshift is not a parameter considered in discussions of discreteness effects in NBS in the literature (e.g., [4,6]).

We can extend our treatment easily to incorporate a smoothing of the gravitational force up to a scale ϵ. Here we have taken pure gravity (i.e., $\epsilon = 0$) as in most cosmological NBS $\epsilon \ll l$, which gives negligible modification of our results. Just as in the analogous condensed matter system, the method can also be extended to higher order. It would be interesting, in particular, to map at higher order this description of the discrete system onto the corresponding order of fluid Lagrangian theory, which has been explored extensively in the cosmological literature (see, e.g., [18], and references therein). Further, it should be possible to use the approach presented here to understand better the nature of existing approximations which go beyond the simple fluid limit, for example, those involving pressure terms associated to velocity dispersion (see, e.g., [18,19] and references therein).

[1] G. Efstathiou *et al.*, Astrophys. J. Suppl. Ser. **57**, 241 (1985).
[2] D. Pines, *Elementary Excitations in Solids* (Benjamin, New York, 1963).
[3] Ya. Zeldovich, Astron. Astrophys. **5**, 84 (1970).
[4] A. Melott and S. Shandarin, Astrophys. J. **410**, 469 (1993); A. Melott *et al.*, Astrophys. J. Lett. **479**, L79 (1997); R. Splinter *et al.*, Astrophys. J. **497**, 38 (1998).
[5] T. Baertschiger *et al.*, Astrophys. J. Lett. **581**, L63 (2002).
[6] T. Hamana *et al.*, Astrophys. J. **568**, 455 (2002).
[7] For conciseness of notation we have left implicit in these expressions the sum over the copies which results from the periodic boundary conditions.
[8] L. Hernquist *et al.*, Astrophys. J. Suppl. Ser. **75**, 231 (1991).
[9] R. R. Sari *et al.*, J. Phys. A: Math. Gen. **9**, 1539 (1976).
[10] T. Buchert, Mon. Not. R. Astron. Soc. **254**, 729 (1992).
[11] The Lagrangian coordinate $\mathbf{x}$ used in [10] is the position of the particle at $t = t_0$, i.e., $\mathbf{x} = \mathbf{R} + \mathbf{u}(\mathbf{R}, t_0)$.
[12] A. Melott, Astrophys. J. **426**, L19 (1994).
[13] P. Coles *et al.*, Mon. Not. R. Astron. Soc. **260**, 765 (1993).
[14] A. Gabrielli, Phys. Rev. E **70**, 066131 (2004).
[15] S. Torquato and F. H. Stillinger, Phys. Rev. E **68**, 041113 (2003).
[16] S. D. M. White, astro-ph/9410043.
[17] M. Joyce, D. Levesque, and B. Marcos, astro-ph/0411607.
[18] T. Tatekawa, astro-ph/0412025.
[19] T. Buchert and A. Dominguez, astro-ph/0502318.